UNIVERSITY OF BIRMINGHAM



OPTIMISING THE MYOCARDIAL HOMING AND THERAPEUTIC EFFICACY OF MESENCHYMAL STEM CELLS USING 3D CULTURE AND SPECIFIC SUB-POPULATIONS OF BONE MARROW-DERIVED CELLS

By

Kobkaew Bumroongthai

A thesis submitted to the University of Birmingham for the degree of

DOCTOR OF PHILOSOPHY

College of Medical and Dental Sciences

School of Clinical and Experimental Medicine

The University of Birmingham

September 2020

UNIVERSITY OF
BIRMINGHAM

University of Birmingham Research Archive

e-theses repository

This unpublished thesis/dissertation is copyright of the author and/or third parties. The intellectual property rights of the author or third parties in respect of this work are as defined by The Copyright Designs and Patents Act 1988 or as modified by any successor legislation.

Any use made of information contained in this thesis/dissertation must be in accordance with that legislation and must be properly acknowledged. Further distribution or reproduction in any format is prohibited without the permission of the copyright holder.

Abstract

Myocardial infarction (MI) results from ischemia and reperfusion (IR) injury and is the significant cause of death worldwide. Bone marrow mesenchymal stem cell (BM-MSC) transplantation has been identified as having the most potential to treat a broad range of diseases due to their unique ability to evade the host immune system. However, clinical success is limited due to poor homing and survival of MSCs in the injured heart. There is still no consensus on which stem cell population confers the most therapeutic capacity to treat heart disease. Furthermore, the cellular targets of MSC actions and the mechanisms explaining their therapeutic effects are still not fully understood. This current study used two subpopulations of human BM-MSCs (hBM-MSCs) originally derived from the same bone marrow site called hBM-MSCs Y201 and hBM-MSCs Y202. The hBM-MSCs Y201 were a highly tri-lineage differentiating, $CD317^{neg}$ MSC subset, with the expression of genes consistent with perivascular interactions in the BM. hBM-MSCs Y202 were a sub-population that included non-differentiating $CD317^{pos}$ BM resident MSCs, which did not express genes associated with vascular interactions. We are the first group to image in real-time the kinetics of MSC recruitment and their impact on microvascular events at a cellular level in a mouse beating injured heart model. This current study provides novel pieces of evidence to show that subpopulations of hBM-MSCs possessed different retention potential to mouse beating heart and anti-inflammatory capacities to ameliorate myocardial IR injury. 3D culture technique improved hBM-MSCs Y201 vasculoprotective benefits in reducing the thromboinflammatory response within the coronary microcirculation. hBM-MSCs derived from 3D spheroid were much smaller, which may reduce their pulmonary microvascular entrapment, leading to increased trafficking through the heart, which enhanced their therapeutic effect. The mechanism of vasculoprotective benefits of 3D cultured hBM-MSCs Y201 may have been accomplished by lowering coronary endothelial cells oxidative stress and reducing the levels of plasma pro-inflammatory cytokines. Combination therapy of 3D cultured hBM-MSCs Y201 with unfractionated heparin reduced neutrophils and platelets' recruitment within the coronary microcirculation following IR injury.

Publications Arising from this Thesis:

Poster Presentation:

- 68th British Microcirculation Society Conference, University of Nottingham 2018, UK.
  K. Bumroongthai, D.P.J. Kavanagh, P. Genever, N. Kalia. Investigating the impact of 2D vs 3D culture and tissue of origin on the adhesive capacity of mesenchymal stem cells in vitro and to the beating mouse heart in vivo.

- Institute of Cardiovascular Sciences Away Day 2018, University of Birmingham, UK
  K. Bumroongthai, A. Lokman, D.P.J. Kavanagh, N. Kalia. Expansion in 3D culture alters the morphology and adhesive capability to the injured heart of mesenchymal and haematopoietic stem cells.

- 67 th British Microcirculation Society Conference, University of Birmingham 2017, UK.
  K. Bumroongthai, A. Lokman, D.P.J. Kavanagh, N. Kalia. Expansion in 3D culture alters the morphology and adhesive capability to the injured heart of mesenchymal and haematopoietic stem cells.

- Institute of Cardiovascular Sciences Away Day 2017, University of Birmingham, UK
  K. Bumroongthai, A. Lokman, D.P.J. Kavanagh, N. Kalia. Investigating the homing and vasculoprotective effects of different mesenchymal stem cells (MSCs) in the injured beating murine heart in vivo – a comparison of 2D vs 3D culture.

Oral Presentation:

- Samaggi Academic Conference and Careers Fair 2020, London, UK.
  K. Bumroongthai, D.P.J. Kavanagh, P. Genever, N. Kalia. 3D Culture and Co-administration of Heparin Enhances the Homing and Therapeutic Efficacy of Mesenchymal Stem Cells in Murine Myocardial Infarction.

  HIGHLY RECOMMENDED

- 69 th British Microcirculation Society Conference, University of Exeter 2019, UK.
  K. Bumroongthai, D.P.J. Kavanagh, P. Genever, N. Kalia. Optimising the myocardial homing and therapeutic efficacy of mesenchymal stem cells using 3D culture and specific sub-populations of bone marrow-derived cells.

- Health Challenge Thailand 2019, the Academic Conference. London, UK.
  K. Bumroongthai, D.P.J. Kavanagh, P. Genever, N. Kalia. Optimising the myocardial homing and therapeutic efficacy of mesenchymal stem cells using 3D culture and specific sub-populations of bone marrow-derived cells.

  ORAL PRIZE WINNER

- 3 Minutes Thesis College Gala 2019, University of Birmingham, UK.
  K. Bumroongthai, D.P.J. Kavanagh, P. Genever, N. Kalia. Optimising the myocardial homing and therapeutic efficacy of mesenchymal stem cells using 3D culture and specific sub-populations of bone marrow-derived cells.

- Anglo-Thai Society Educational Award 2017. London, UK.
  K. Bumroongthai, D.P.J. Kavanagh, P. Genever, N. Kalia. Investigating the homing and vasculoprotective effects of different mesenchymal stem cells (MSCs) in the injured beating murine heart in vivo – a comparison of 2D vs 3D culture.

  ORAL PRIZE WINNER

แด่พ่อกับแม่ที่รักและผู้คนที่แสนดีที่ผ่านพบมาเจอกัน

Acknowledgement

I would like to express my sincere gratitude to my supervisor, Dr. Neena Kalia, for the invaluable suggestions and patience throughout my PhD study at the University of Birmingham. I am very thankful for your kind words that encouraged me to finish this thesis when I lost my way during the COVID-19 lockdown. Without your knowledgeable and consistent guidance, my research would never come this far, and this thesis would never be successfully completed. You are the best supervisor I could ever ask for. I also thank Dr. Dean Kavanagh, my mentor, who taught me many valuable lab skills especially the exciting IVM experiments. Moreover, thank you so much for the funny Youtube videos on Friday afternoon in the office. They were so funny I had good laughs for so many times. Many thanks to Adam, Juma and Giorgiana; you are good lab partners/friends. Also the people at ICVS, thank you so much for helping me with lab works.

Many thanks to all the people I met during this PhD; Katrina for inviting me to join your fun trips on vacation, Thai friends and others for good food, great times and shelter, Jiahuan for the deep and meaningful conversations on the couch until 5 AM in the house number 3 at the Spinney. I am glad that I met you and you are my favorite person I met in the UK! I had great times and memories during this wonderful 4-years PhD journey in UK thanks to all these people.

To mom, dad, sis and family, thank you so much for greatest support. This PhD is not only my achievements but it is also yours. I felt good every morning when I saw your messages asking me have I eaten anything or not. Without you guys, I would never have made it to this far.

I would like to extend my gratitude to Thai government for providing me the scholarship throughout this PhD study. I will go back to Thailand and make a good use of this invaluable knowledge I received to develop the stem cells research in Thailand.

“There is so much strength in all of us.

Every woman, child, and man.

It is the moment that you think you can’t.

You will discover that you can.”

The Power of Dream

By

Celine Dion

Table of Contents

1. General Introduction 1-53

1.1. Myocardial Ischaemia-Reperfusion (IR) Injury 2-11

1.1.1. Injury after ischaemia 3-5

1.1.2. Injury after reperfusion 5-11

1.1.2.1. The pH paradox 7

1.1.2.2. Ca^{2+} overload 7-8

1.1.2.3. Mitochondrial dysfunction 8

1.1.2.4. Reactive oxygen species production 9

1.1.2.5. Initiation of inflammatory process 11

1.2. Clinical Manifestations of Myocardial IR Injury 11-17

1.2.1. Myocardial stunning - flow-contractility mismatch 12

1.2.2. Reperfusion arrhythmias 12-13

1.2.3. The no-eflow paradox 13-14

1.2.4. Lethal reperfusion injury 14-17

1.3. The Role of the Coronary Microcirculation in Myocardial IR Injury – an Important Determinant of Infarct Size 17-23

1.3.1. Extravascular compression of the coronary microcirculation 19-20

1.3.2. Coronary microembolization 22

1.3.3. Tonal changes to vessels 22

1.3.4. Intraluminal cellular plugging 23

1.4. Thromboinflammatory Responses during Myocardial IR Injury 24-30

1.4.1. The thrombogenic response 24-25

1.4.2. The inflammatory response 25-26

1.4.2.1. Leukocyte recruitment – rolling, adhesion and transmigration 26-30

1.5. Mesenchymal stem cells 31-41

1.5.1. Anti-inflammatory and immunomodulatory properties of MSCs 32-33

1.5.2. Multiple populations and sub-populations of MSC 34-36

1.5.3. Distribution of exogenous MSC following systemic administration 36-37

1.5.4. Adhesive mechanisms governing MSC homing to sites of injury 39-41

1.6. Three-dimensional (3D) culturing techniques 41-44

1.7. Imaging the beating mouse heart *in vivo* –

Intravital microscopy (IVM) 44-46

1.8. Summary 48-50

1.9. Aims and hypothesis 51-53

2. Materials and Methods 55-104

2.1. Materials 55-57

2.1.1. Antibodies 55

2.1.2. Standard materials and chemical substances 56-57

2.2. Methods 58-104

2.2.1. Cell culture, cell preparation and cell labelling 58-59

2.2.1.1. Culture medium 58

2.2.1.2. Cell counting 58-59

2.2.1.3. Culturing of murine vena cava endothelial cells 59

2.2.1.4. 2D culture of hematopoietic stem cells (HSCs) 60

2.2.1.5. 2D culture of mesenchymal stem cells (MSCs) 61-62

2.2.1.6. 3D culture of HSCs and MSCs 63

2.2.1.7. Preparation of CFSE-labelled fluorescent stem cells 65-66

2.2.2. Investigation of stem cell adhesion to various substrates *in vitro* 66-70

2.2.2.1. Tissue preparation and cryosection of frozen murine hearts 66-67

2.2.2.2. Stamper-Woodruff (SW) heart tissue section *in vitro* adhesion assay 67-68

2.2.2.3. Endothelial cell *in vitro* adhesion assay 68-69

2.2.2.4. Immobilised ICAM-1 and VCAM-1 protein*in vitro* adhesion assay 70

2.2.3. Flow cytometry and confocal studies to investigate surface adhesion molecules and chemokine receptors on 2D and 3D cultured hBM-MSCs 70-72

2.2.3.1 Flow cytometry studies of 2D and 3D cultured hBM-MSCs 70-72

2.2.3.2. Confocal microscopy imaging of 2D and 3D cultured hBM-MSCs 72

2.2.4. Murine endothelial cells + hBM-MSCs co-culture experiments *in vitro* 73-76

2.2.4.1. Endothelial cells + hBM-MSCs co-culture 73

2.2.4.2. Quantification of reactive oxygen species using Dihydroethidium in endothelial cells + hBM-MSCs co-culture experiments *in vitro* 73-74

2.2.4.3. Quantification of oxidative stress using 8-OHdG labelling in endothelial cells + hBM-MSCs co-culture experiments *in vitro* 74-76

2.2.4.4. Analysis of endothelial cell + hBM-MSC co-culture experiments *in vitro* 76

2.2.5. Intravital microscopy studies of the IR injured beating mouse heart to image hBM-MSC trafficking and their vasculoprotective effects *in vivo* 77-86

2.2.5.1. Animals 77

2.2.5.2. Pre-surgical preparation 78

2.2.5.3. Induction of myocardial ischaemia-reperfusion injury 80-81

2.2.5.4. Intravital imaging of beating mouse heart *in vivo* 82-83

2.2.5.5. Imaging and quantification of hBM-MSC trafficking to the IR injured beating heart *in vivo* 83-86

2.2.5.6. Imaging and quantification of neutrophils and platelets in the IR injured beating heart *in vivo* after hBM-MSC therapy 86-88

2.2.5.7. Imaging functional capillary density in the IR injured beating heart *in vivo* 88

2.2.5.8. Dual therapy with hBM-MSC administration and heparin 88-89

2.2.6. Mulitphoton microscopy studies to image vasculoprotective Effects of hBM-MSCs in deeper layers of the IR injured heart muscle – *ex vivo* studies 89-93

2.2.6.1. Preparing the excised hearts for multiphoton imaging 89-91

2.2.6.2. Imaging and quantification of neutrophils and platelets in IR injured hearts after hBM-MSC ± heparin therapy using multiphoton microscope *ex vivo* 92

2.2.6.3. Reconstruction, image display and rendering of Image stacks from multiphoton experiments 93

2.2.7. Flow cytometry experiments to analyse hBM-MSC recruitment, coronary endothelial and cardiomyocyte oxidative damage and endothelial adhesion molecule expression in whole excised digested hearts *ex vivo* 96-99

2.2.7.1. Digestion of whole hearts and lungs 96

2.2.7.2. Quantification of hBM-MSC recruitment in excised whole hearts and lungs of mice following myocardial IR injury 97

2.2.7.3. Determination of coronary endothelial cell and cardiomyocyte oxidative damage in excised whole hearts and lungs of mice following myocardial IR injury 97-98

2.2.7.4. Determination of endothelial cell adhesion molecules expression in excised whole hearts and lungs of mice following myocardial IR injury 99

2.2.8. Quantification of inflammatory cytokines in the serum of IR injured hearts after hBM-MSC therapy using multiplex immunoassays 99-100

2.2.9. Quantification of infarct size in IR injured hearts after hBM-MSC ± heparin therapy using the Triphenyl Tetrazolium Chloride (TTC) staining assay 101-102

2.3. Statistical analysis 104

3. Developing strategies to improve mesenchymal stem cell adhesion to the ischaemia-reperfusion Injured heart – *in vitro* studies 106-140

3.1. Introduction and Hypothesis 106-109

3.1.1. Introduction 106-107

3.1.3. Specific aims 108-109

3.2. Methods 1109-110

3.3 Results 110-122

3.3.1. 3D cultured MSCs were smaller than 2D cultured cells and formed spheroids 110-111

3.3.2. 3D culture increased HSC and MSC adhesion to injured mouse heart sections 112-115

3.3.3. 3D culture only increased hBM-MSCs Y201 adhesion to TNFα stimulated vena cava ECs 115

3.3.4. 3D culture only increased MSC adhesion to ICAM-1 and VCAM-1 116

3.3.5. 3D cultured increased surface expression of various cells molecules on MSCs – notable increases in CXCR4 on hBM-MSCs Y201 120-121

3.3.6. 3D cultured MSCs exhibited more uniform adhesion molecule distribution on their cell surface 122-123

3.4. Discussion 124-138

3.4.1. 3D cultured MSCs formed spheroids and were smaller in size 128

3.4.2. 3D cultured stem cells were more adherent *in vitro* 129-133

3.4.3. 3D culture increased expression primarily of CXCR4 on hBM-MSCs Y201 137-138

3.4.4. 3D cultured hBM-MSCs Y201 increased ICAM-1 expression which was more evenly distributed on its surface 138-139

3.5. Conclusion 139-140

4. Developing strategies to improve mesenchymal stem cell adhesion to the IR Injured heart – *in vitro* studies 142-206

4.1. Introduction and Hypothesis 142-146

4.1.1. Introduction 142-144

4.1.2. Hypothesis 145

4.1.3. Specific aims 145-146

4.2. Methods 146-147

4.3. Results 148-188

4.3.1. Increased 3D cultured MSC adhesion within injured coronary microcirculation 148-149

4.3.2. 3D culture technique increases free flowing and adherent hBM-MSCs Y201 in the healthy sham heart 150-152

4.3.3. Increased myocardial recruitment of 3D cultured hBM-MSCs confirmed *ex vivo* using EVOS microscopy with significant entrapment within lungs of All MSCs 152-156

4.3.4. 3D culture increases both free flowing and adherent hBM-MSCs Y201, but only adhesion of hBM-MSCs Y202, to the IR injured heart 156-160

4.3.5. Increased myocardial recruitment of 3D cultured hBM-MSCs Y201 confirmed *ex vivo* using flow cytometry, but the same effect is not seen with hBM-MSCs Y202 161-165

4.3.6. Only 3D cutured hBM-MSCs Y201 reduce neutrophil recruitment within the IR Injured coronary microcirculation *in vivo* 166

4.3.7. hBM-MSCs Y201 and hBM-MSCs Y202 marginally reduce platelet presence within the IR Injured coronary microcirculation *in vivo* 166-170

4.3.8. Heparin slightly increases the presence of adherent 3D cultured hBM-MSCs Y201 following myocardial IR injury 171-172

4.3.9. Dual therapy with heparin induces an earlier onset of 3D hBM-MSCs Y201 mediated anti-inflammatory effects following myocardial IR injury.....173-174

4.3.10. Multiphoton microscopy visualised neutrophil adhesion and platelet aggregation within deeper layers of the myocardium in IR injured hearts 174-175

4.3.11. Multiphoton microscopy demonstrated that co-administration of heparin with 3D cultured hBM-MSCs Y201 was vasculoprotective even within the deep layers of the heart.....181-182

4.3.12. Myocardial IR injury reduces functional capillary density which is restored by pre-treatment with 3D hBM-MSCs Y201.....182-183

4.3.13. 3D cultured hBM-MSCs Y201 therapy decreases infarct size following myocardial IR injury which is further decreased when combined with heparin.....183

4.4. Discussion 188-194

4.4.1. IR injured coronary vasculature targeted by systemically delivered MSCs.....190-193

4.4.2. 3D culture enhances myocardial hBM-MSCs Y201 recruitment *in vivo* 193-196

4.4.3. 3D culture enhances hBM-MSCs Y201 recruitment – Supporting evidence.....196-197

4.4.4. Extensive neutrophil and platelet presence throughout the ventricular wall prevented by a combination therapy of heparin and 3D cultured hBM-MSCs Y201.....197-198

4.4.5. 3D cultured hBM-MSCs Y201 are vasculoprotective in the injured heart 198-201

4.4.6. Combination therapy with heparin? 202-205

4.5. Conclusion 205-206

5. Mechanisms by which MSCs may confer vasculoprotection following myocardial IR Injury – *in vitro* and *in vivo* Studies 207-242

5.1. Introduction and Hypotheses 208-204

5.1.1. Introduction 208-211

5.1.2. Hypothesis 211

5.1.3. Specific aims 211-213

5.2. Methods 213-214

5.3. Results 215-218

5.3.1. hBM-MSCs did not reduce ROS generation from injured VCECs *in vitro* 215

5.3.2. Only 2D and 3D cultured hBM-MSCs Y201 reduced oxidative damage of H_2O_2 injured VCECs cells *in vitro* 215-216

5.3.3. Coronary endothelial cells are more susceptible to oxidative stress than cardiomyocytes following myocardial IR injury – all hBM-MSCs reduce endothelial oxidative damage 216-221

5.3.4. ICAM-1 and VCAM-1 expression increases on coronary endothelial cells following myocardial IR injury – all hBM-MSCs reduce endothelial adhesion molecule expression 221-222

5.3.5. 3D cultured hBM-MSCs Y201 are most potent at reducing serum levels of multiple circulating Pro-inflammatory factors *in vivo* 226-226

5.3.6. Circulating peripheral blood cell panel following myocardial IR injury 226-227

5.4. Discussion 227-240

5.4.1. hBM-MSCs do not reduce endothelial ROS generation 230-232

5.4.2. hBM-MSCs Y201 co-culture protects endothelial cells from oxidative damage 232-234

5.4.3. Coronary endothelium is an early target for oxidative damage but protected by hBM-MSCs 234-236

5.4.4. Reducing endothelial ICAM-1 / VCAM-1 – another therapeutic mechanism 236-237

5.4.5. 3D cultured hBM- MSCs Y201 are most potent at reducing circulating serum levels of pro-inflammatory factors *in vivo* 238-240

5.5. Conclusion..... 241-242

6. General discussion 244-243

6.1. Summary of the main findings and general discussion 244-252

6.2. Future work 253-254

6.3. Concluding remarks..... 254-255

7. References..... 256-286

List of Figures

Figure 1.1. Contributions of ischaemia and reperfusion to the final myocardial infarction size……6

Figure 1.2. Schematic of the mechanism of myocardial IR injury……10

Figure 1.3. Four clinical manifestations of myocardial reperfusion injury……16

Figure 1.4. The Role of the Coronary Microcirculation in Myocardial IR Injury……21

Figure 1.5. The Leukocyte Adhesion Cascade Mediates Neutrophil Recruitment during Myocardial IR Injury……30

Figure 1.6. MSC Sub-Populations Identified Within Different Bone Marrow Niches……39

Figure 1.7. The Mesenchymal Stem Cell Adhesion Cascade Showing Key Players in Mediating their Rolling, Activation, Adhesion and Transmigration within Inflamed Sites……42

Figure 1.8. MSCs Cultured as Spheroids Using 3D Culture Methods Have Greater Therapeutic Effectiveness……47

Figure 2.1. Illustration of the hanging drop method used for generating 3D spheroid cultures of HSCs, WJ-MSCs, hBM-MSCs Y201 and hBM-MSCs Y202……64

Figure 2.2. Selection criteria used for quantitative and qualitative analysis of stem cell adhesion to frozen heart tissue sections *in vitro*……69

Figure 2.3. Murine endothelial cell + hBM-MSC co-culutre assay……75

Figure 2.4. Protocols for quantification of ROS (Superoxide) generation using dihydroethidium and VCEC oxidative stress using 8-OHdG labelling……79

Figure 2.5. Surgical preparation of the anaesthetised male C57Bl/6 mouse for intravital imaging of the exposed beating heart in vivo……84

Figure 2.6. Preparation of the anaesthetised CB7Bl/6 mouse beating heart for novel intravital imaging *in vivo*……85

Figure 2.7. Analysis of platelet aggregation within the beating heart coronary microcirculation using Image J software……90

Figure 2.8. Timeline for intravital experiments of the beating mouse heart to image hBM-MSC trafficking and the vasculoprotective effects of delivering them alone or as a dual therapy with heparin……94

Figure 2.9. Preparing the murine left ventricle for multiphoton imaging following myocardial ischaemia reperfusion injury *ex vivo*……95

Figure 2.10. Timeline for infarct size experiments to assess whether 3D cultured hBM-MSCs Y201 heparin is effective at reducing myocardial infarction following IR injury……103
Figure 3.1. Morphology of HSCs and different populations of MSCs cultured using conventional 2D or 3D hanging drop methods……113
Figure 3.2. Size distribution of HSCs and different populations of MSCs cultured using conventional 2D or 3D hanging drop methods……114
Figure 3.3. Adhesion capacity of HSCs and different populations of MSCs cultured using conventional 2D or 3D hanging drop methods to sham and IR injured frozen heart sections and assessed using the modified Stamper-Woodruff (S-W) adhesion assay……117
Figure 3.4. Adhesion capacity of HSCs and different populations of MSCs cultured using conventional 2D or 3D hanging drop methods to vena cava endothelial cells (VCECs) and assessed using static adhesion assays……..118
Figure 3.5. Adhesion capacity of HSCs and different populations of MSCs cultured using conventional 2D or 3D hanging drop methods to immobilised substrate proteins ICAM-1 and VCAM-1 and assessed using static adhesion assays……119
Figure 3.6. Cell surface expression of the SDF-1 receptor and CD44/ICAM-1/VCAM-1 adhesion molecules on different populations of MSCs cultured using conventional 2D or 3D hanging drop methods as assessed by flow cytometry at 2 days of cultivation……121
Figure 3.7. Cell expression of the integrin β7 subunit, CD54/ICAM-1 and CD44 on different populations of MSCs cultured using conventional 2D or hanging drop 3D methods and assessed confocally at 2 days of cultivation……123
Figure 3.8. Proposed mechanism for mesenchymal stem cell (MSC) aggregation……130
Figure 4.1 Survival rate of hBM-MSCs transplanted mice following myocardial IR injury……151
Figure 4.2. Intravital microscopy demonstrated an increased adhesion of both CFSE-labelled MSC subpopulations within the IR Injured heart with 3D cultured cells most adhesive……153

Figure 4.3. Intravital microscopy demonstrated that 3D culture improved numbers of hBM-MSCs Y201 trafficking through the healthy sham beating heart after systemic infusion and their adhesion within the coronary microcirculation *in vivo*……154
Figure 4.4. Intravital microscopy demonstrated that 3D culture improved numbers of hBM-MSCs Y202 trafficking through the healthy sham beating heart after systemic infusion and their adhesion within the coronary microcirculation *in vivo*……...155
Figure 4.5. Increased myocardial recruitment of 3D cultured hBM-MSCs Y201 in healthy sham hearts confirmed *ex vivo* with significant entrapment within lungs of all MSCs……..157
Figure 4.6. Increased myocardial recruitment of 3D cultured hBM-MSCs Y202 in healthy sham hearts confirmed *ex vivo* with significant entrapment within lungs of all MSCs……...158
Figure 4.7. Intravital microscopy demonstrated that 3D culture improved numbers of hBM-MSCs Y201 trafficking through the IR injured beating heart after systemic infusion and their adhesion within the coronary microcirculation *in vivo*……..160
Figure 4.8. Intravital microscopy demonstrated that 3D culture does not increase numbers of hBM-MSCs Y202 trafficking through the IR injured beating heart after systemic infusion but does increase their adhesion within the coronary microcirculation *in vivo*……..162
Figure 4.9. Intravital microscopy demonstrated that 3D culture increases adhesion of both hBM-MSCs Y201 and hBM-MSCs Y202 to a similar level within the sham and IR injured coronary microcirculation *in vivo*……163
Figure 4.10. The presence of 3D cultured hBM-MSCs Y201 in the heart and lungs of mice undergoing myocardial IR injury was also determined *ex vivo* using flow cytometry……..164
Figure 4.11. Increased myocardial recruitment of 3D cultured hBM-MSC Y201 confirmed *ex vivo* using flow cytometry, but the same effect is not seen with hBM-MSCs Y202……165
Figure 4.12. Intravital microscopy demonstrated a high burden of adherent neutrophils and platelet microthrombi in the IR injured heart……..168
Figure 4.13. Intravital microscopy demonstrated that 3D culture of hBM-MSCs Y201 decreased endogenous neutrophil adhesion in the IR injured beating heart *in vivo*……169

Figure 4.14. Intravital microscopy demonstrated that 3D culture of hBM-MSCs Y201 decreased endogenous neutrophil adhesion in the IR injured beating heart *in vivo*……..170
Figure 4.15. Intravital microscopy demonstrated that heparin infusion 30 minutes post-reperfusion did not increase adhesion of 3D cultured hBM-MSCs Y201 within the IR injured beating heart *in vivo*……172
Figure 4.16. Intravital microscopy demonstrated that heparin infusion 30 minutes post-reperfusion marginally increased neutrophil recruitment within the IR injured beating heart *in vivo*……..176
Figure 4.17. Intravital microscopy demonstrated that dual therapy with heparin induced an earlier onset of 3D hBM-MSCs Y201 mediated anti-inflammatory effects following myocardial IR injury…….177
Figure 4.18. Preparing the murine left ventricle for multiphoton imaging following myocardial ischaemia-reperfusion injury *ex vivo*……178
Figure 4.19. Multiphoton *ex vivo* imaging revealed the accumulation of platelet and neutrophil within the coronary microcirculation even within the deeper layers of the left ventricular muscle wall……..179
Figure 4.20. Multiphoton *ex* vivo imaging revealed the accumulation of mixed platelet-neutrophil aggregates within the coronary microcirculation even within the deeper layers of the left ventricular muscle wall……..180
Figure 4.21. Multiphoton microscopy demonstrated that co-administration of heparin with 3D cultured hBM-MSCs Y201 was vasculoprotective even within the deep layers of the heart following myocardial IR injury……184
Figure 4.22. Multiphoton microscopy demonstrated that co-administration of heparin with 3D cultured hBM-MSCs Y201 was vasculoprotective even within the deep layers of the heart following myocardial IR injury……185
Figure 4.23. Intravital microscopy demonstrated that 3D cultured hBM-MSCs Y201 was able to improve functional capillary density following myocardial IR injury. FITC-BSA was injected after 2 hours of reperfusion……186
Figure 4.24. 3D cultured hBM-MSCs Y201 therapy decreases infarct size following myocardial IR injury which is further decreased when combined with heparin……..187
Figure 5.1. Representative images from co-culture assays of murine vena cava endothelial cells (VCECs) with 2D and 3D cultured hBM-MSCs Y201 and hBM-MSCs Y202 taken at 72 hours……217

Figure 5.2. Neither 2D or 3D cultured hBM-MSCs Y201 or hBM-MSCs Y202 decreased the generation of ROS by H_2O_2 injured VCECs *in vitro* at 72 hours……218

Figure 5.3. Both 2D and 3D cultured hBM-MSCs Y201 significantly decrease oxidative damage of H2O2 injured VCECs *in vitro* at 72 hours……219

Figure 5.4. Flow cytometric analysis of whole digested hearts in sham, IR injured and IR + hBM-MSCs mice……223

Figure 5.5. Coronary endothelial cells (ECs) are more susceptible to oxidative stress than cardiomyocytes following IR injury, but all populations of 2D and 3D cultured hBM-MSCs are able to protect the ECs (and cardiomyocytes) from oxidative damage……224

Figure 5.6. ICAM-1 and VCAM-1 expression increases on coronary endothelial cells (ECs) following myocardial IR injury, but all populations of 2D and 3D cultured hBM-MSCs are able to reduce their expression……225

Figure 5.7. Increased vascular and non-vascular production of reactive oxygen species (ROS) within the IR injured heart leads to local tissue oxidative stress and ultimately damage to the vital yet delicate coronary microvessels……242

Figure 6.1. Proposed mechanism explaining how 3D culture may enhance the homing and recruitment of hBM-MSCs Y201 within coronary microvessels following myocardial IR injury……252

List of tables

Table 2.1. List of antibodies used in endothelial & *in vitro* assay, flow cytometry and intravital experiments……55

Table 2.2. Materials frequently used in experiments……56

Table 3.1. Multiparameter analysis of human bone marrow stem / stromal cells identifies distinct subtypes……134

Table 5.1. 3D cultured hBM-MSCs Y201 is the most effective at reducing serum levels of multiple pro-inflammatory cytokines……228

Table 5.2. Circulating cell profile in murine blood following myocardial IR injury……229

List of Abbreviations

2D culture	Two dimensional culture
3D culture	Three dimensional culture
8-OHdG	8-Hydroxy-2'-Deoxyguanosine
AAR	Area at risk
Ab	Antibody
ACD	Acid citrate dextrose
AF488	Alexa fluor 488
ANG-1	Angiopoeitin-1
ANOVA	Analysis of variance
APC	Allophycocyanin
ASPA	Animals scientific procedures act
ATP	Adenosine triphosphate
BM	Bone marrow
BSA	Bovine serum albumin
Ca2+	Calcium ion
CAT	Catalase
CCR	C-C Chemokine Receptor
CVD	Cardiovascular diseases
CFDA-SE	Carboxyfluorescein diacetate duccinimidyl ester
CFSE	Carboxyfluorescein succinimidyl ester
CMR	Cardiac magnetic resonance
cTnT	Cardiac troponin T
DAMP	Damage-associated molecular patterns
DC	Dendritic cell
DHE	Dihydroethidium
DMEM	Dulbecco's MEM
DMSO	Dimethyl sulphoxide
EC	Endothelial sell
ECG	Electrocardiographic
eNOS	Endothelial nitric oxide synthase
ER	Endoplasmic reticulum
ESC	Embryonic SC
ET-1	endothelin-1
FITC	Fluorescein isothiocyanate
FBS	Foetal bovine serum
FCD	Functional capillary density
FGF-2	Fibroblast growth factor-2
H+	Hydrogen ion
H2O2	Hydrogen peroxide
HGF	Hepatocyte growth factor
hMSC	Human mesenchymal stem cell
HPC	Haematopoietic progenitor cell
HSC	Haematopoietic stem cell
ICAM-1	Intercellular adhesion molecule-1
ISCT MSC	International society for cell and gene therapy mesenchymal stromal cell

IFN-γ	Interferon-gamma
IgG	Immunoglobulin G
IHC	Immunohistochemistry
IL	Interleukin
IL-1RA	Interleukin-1 receptor antagonist
IMR	Index of microcirculatory resistance
IR	Ischaemia/reperfusion
IVIS	In vivo imaging system
IVM	Intravital microscopy
JAM-A/C	Junctional adhesion molecule-A/C
K^+	Potassium
LAD	Left anterior descending
LFA-1	Lymphocyte function-associated antigen 1
LSCI	Laser speckle contrast imaging
LTB4	Lipid mediator leukotriene B4
Ly6	Lymphocyte antigen 6
MAO	Monoamine oxidase
MAP	Mitogen-activated protein
MCP-1	monocyte chemoattractant protein 1
MEM	Modified Eagle's media
Mg2+	Magnesium ion
MI	Myocardial infarction
MMP	Matrix metalloprotease
MP	Microparticle
MPO	Myeloperoxidase
mPTP	Mitochondrial permeability transition pores
MSC	Mesenchymal stem cell
Na^+	Sodium
NADPH	Nicotinamide adenine dinucleotide phosphate
NCE	Sodium-calcium exchanger
NF-kB	Nuclear factor kappa-light-chain-enhancer of activated B cells
NHE	Sodium-hydrogen exchanger
NO3-	Nitrate NOX NADPH oxidase
O2-	Superoxide
OH	Hydroxyl radical
OCT	Optimal cutting temperature
P/S	Penicillin/streptomycin
PBMC	Primary bone marrow cell
PBS	Phosphate buffer solution
PCA	Percutaneous coronary angioplasty
PDGFR- α	Platelet-derived growth factor receptor alpha
PECAM-1	Platelet-endothelial cell adhesion molecule-1
PET	Positron emission tomography
PGE2	Prostaglandin E2
PPCI	Primary percutaneous coronary intervention
PRP	Platelet-rich plasma
PSGL-1	P-selectin glycoprotein ligand-1

ROS	Reactive oxygen species
SC	Stem cell
Sca-1	Stem cell antigen-1
SCF	Stem cell factor
SDF-1	Stromal cell derived factor 1
SEM	Standard error of the mean
SOD	Superoxide dismutase
TGF-β	Transforming growth factor-beta
TNF-α	Tumour necrosis factor-alpha
TSG-6	TNFα stimulated gene/protein 6
TTC	Triphenyl tetrazolium chloride
TXA_2	Thromboxane 2
VCAM-1	Vascular cell adhesion molecule-1
VCEC	Vena Cava EC
VE-Cadherin	Vascular endothelial cadherin
VEGF-A	Vascular endothelial growth factor-A
VLA-4	Very late antigen-4
WJ-MSC	Wharton's Jelly mesenchymal stem cell
XO	Xanthine oxidase

CHAPTER 1

General Introduction

1.0 General Introduction

1.1 Myocardial ischaemia-reperfusion (IR) injury

Myocardial infarction (MI), commonly known as a heart attack, develops when the heart muscle is damaged following blockage of one or more of the epicardial coronary arteries. The symptoms of an MI include chest pain, sweating, anxiety, shortness of breath and abnormal heart beating (Valensi et al., 2011). Risk factors are smoking, high blood pressure, advanced age, obesity and diabetes. Ischaemic heart diseases and strokes are the leading causes of death globally. Indeed, an estimated 13 million people globally died from these two conditions in 2010 (Mc Namara et al., 2019). Treatment focuses on rapidly restoring blood flow to the heart using either thrombolytic or fibrinolytic drugs, coronary angioplasty or primary percutaneous coronary interventions (PPCI). The latter involves placement of a stent to open the culprit artery and has been shown to be very effective at decreasing the morbidity and mortality linked with MI.

Despite these interventions, a significant proportion of MI patients still incur extensive muscle damage. This loss of functioning cardiomyocytes reduces pumping efficiency and subsequently leads to the development of heart failure, a major driver of morbidity, mortality and healthcare cost (Cahill & Kharbanda, 2017). Indeed, mortality rates in hospitalized MI patients is high, ranging between 6% and 14%, but have been shown to be as high as 20% in some studies (Frohlich et al., 2013). This damage is partly due to PPCI-induced reperfusion, which is the only way to salvage the ischaemic myocardium, paradoxically leading to additional tissue damage, a condition termed ischaemia-reperfusion (IR) injury (Yellon & Hausenloy, 2007). Indeed, it is estimated that the process of

reperfusing the heart following an ischaemic episode is responsible for approximately 50% of the final necrotic infarct size (**Figure 1.1**). This limits the full benefit of reperfusion therapy in terms of infarct size and is therefore an area of significant interest as interventions administered at the point of reperfusion have the potential to improve the prognosis of many patients following an MI. However, successful therapies that can prevent reperfusion-related myocardial injury have not been identified and thus remain one of the top 10 unmet clinical needs in cardiology (Ziegler et al., 2019).

1.1.1. Injury after ischaemia

During the ischaemic phase, myocardial cells lack both oxygen and nutrition and also endure rising levels of carbon dioxide and metabolic waste products. Ultimately, the local rate of energy production is unable to meet the demands of the actively working heart. Many metabolic functions are disturbed during this phase as cells switch from performing aerobic to anaerobic metabolism (Wu et al., 2018). In the early stages of ischaemia, stored glycogen is converted to glucose to drive mitochondrial energy production anaerobically. However, this process generates 2 molecules of adenosine triphosphate (ATP), which is much reduced compared to up to 38 produced from each glucose during oxygen availability (Stanley et al. 2004). Pyruvate and hydrogen ions (H^+) are also formed during this process, with the latter lowering cell pH. Lactate, formed as a result of pyruvate and H^+ ions combining, also accumulates in the myocardium and has been associated with contractile dysfunction during and immediately after ischaemia (Li et al., 2016).

As the duration of ischaemia increases, mitochondrial oxidative phosphorylation stops, leading to a cessation of ATP production. This, along with the fall in intracellular pH, has several negative effects on the contractile activity of cardiomyocytes through profound disturbances in the ionic homeostasis of sodium (Na^+), potassium (K^+) and calcium (Ca^{2+}) ions (Wu et al., 2018). Without ATP, energy dependent exchangers such as the membrane Na^+K^+ATPase and Ca^{2+} ATPase become inactivated. Disruption of the former leads to increased intracellular Na^+ and decreased potassium K^+ within cardiac cells. In order to compensate for the fall in intracellular pH, H^+ are transported out of the cell via the Na^+/H^+ exchanger, again resulting in increased intracellular Na^+. This accumulation of intracellular Na^+ drives water entry into the cells ultimately leading to cellular swelling, plasma membrane rupture and leakage of intracellular content (Kalogeris et al., 2012).

The large influx of Na^+ also leads to an influx of Ca^{2+} which induces further Ca^{2+} release from intracellular stores. Furthermore, its re-uptake by the sarcoplasmic reticulum storage sites is reduced. The alteration of the transport system in sarcoplasmic reticulum and sarcolemma causes an increased influx of Ca^{2+}, which leads to Ca^{2+} overload in the cells (Allen and Xiao, 2000). The overabundant presence of Ca^{2+} also destroys cell structure by directly activating phospholipases, mainly phospholipase A and protein kinase C, which disintegrates membrane lipids (Hausenloy et al., 2016). Indirect cellular damage occurs as Ca^{2+} overload triggers the release of pro-inflammatory cytokines such as tumour necrosis factor-α (TNFα) (Sanada et al., 2011). Ultimately, ischaemia results in energy-starved, Ca^{2+} overloaded, acidotic myocytes which collectively disrupt the activity of contractile proteins and induce arrhythmia and cell death.

Excessive intracellular Ca^{2+} and ATP depletion also precipitates the opening of large conductance channels located on the inner mitochondrial membrane called mitochondrial permeability transition pores (mPTP) (Kalogeris et al., 2012). During reperfusion, these open channels lead to mitochondrial and then cardiomyocyte death and, as a result of this, initiation of an inflammatory response as detailed in **Section 1.1.2.5** and **Section 1.4**.

1.1.2. Injury after reperfusion

Reperfusion aims to recover the supply of substrates and oxygen for ATP production and normalise extracellular pH by flushing out the accumulated H^+. However, although cells undergo specific damage during ischaemia, paradoxically, the major damage to cells comes from the re-introduction of oxygen during reperfusion and is known as reperfusion injury. This was first noted by Robert Jenning and colleagues in his seminal study in 1960 as adverse structural and electrical changes in reperfused canine hearts (Jenning et al., 1960). Later studies demonstrated that reperfusion induced further ionic and histological differences that were not present during ischemia, particularly the swollen appearance of mitochondria and cardiac cells. A plethora of studies have since established reperfusion injury as a multifactorial and complex process leading to further heart injury that had not occurred during the ischaemic period (Kalogeris et al., 2012). Some important pathological processes that underlie reperfusion mediated injury are listed below (**Figure 1.2**).

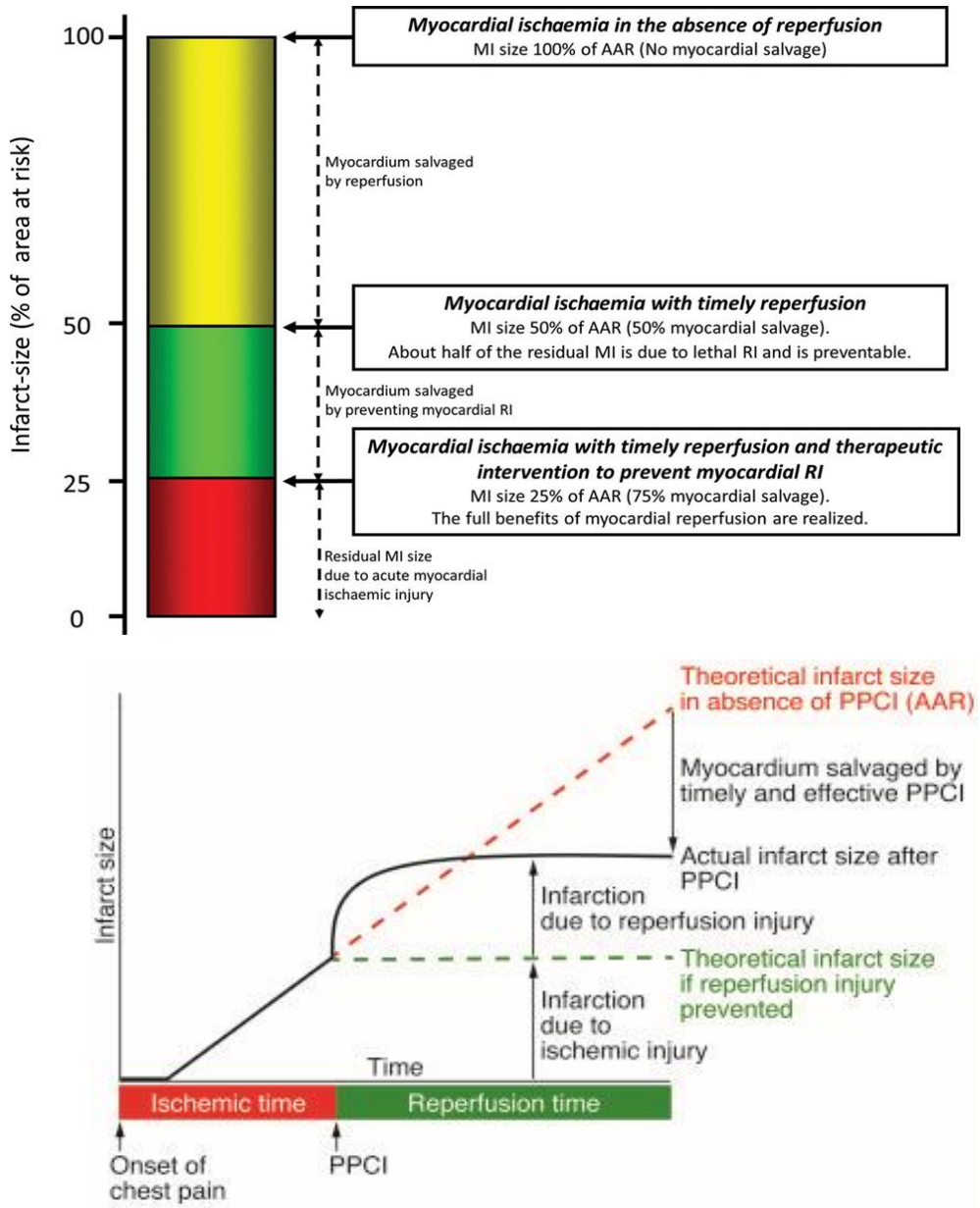


Figure 1.1. Contributions of Ischaemia and Reperfusion to the Final Myocardial Infarction Size. In the top panel, red depicts that the theoretical infarct size is upto 25% of the area at risk if timely reperfusion using PPCI does not in itself cause any reperfusion injury – green dashed line in the lower panel. Hence this 25% infarction is a direct result of the ischaemia alone. This is the ideal situation as the full benefits of myocardial reperfusion have been realised. This is clearly better than not reperfusing the ischaemic heart at all, as is shown in yellow in the top panel, and highlights how a timely reperfusion can salvage the heart and reduce infarct size – red dashed line in the lower panel. Timely reperfusion does indeed salvage the myocardium, but not to a point where just ischaemia causes tissue damage. Paradoxically, reperfusion itself causes tissue damage in its own right as shown in green in the top panel – curved solid black line in the lower panel. Indeed, a theoretical 50% of the final myocardial infarct size is due to lethal myocardial reperfusion mediated injury (RI). This is preventable, yet remains an unmet need in cardiology and needs to be reduced in order to maximize the benefits of myocardial reperfusion. Source: Frohlich et al., 2013 and Yellon & Hausenloy, 2007.

1.1.2.1. The pH Paradox

The accumulation of intracellular Na^{2+} and Ca^{2+} leads to an increase in intracellular H^+ (which is transported out of the cells) and thus development of acidosis during ischaemia (Sezer et al., 2018). After the restoration of blood flow, the acidosis is amended rapidly by the Na^+-H^+ exchanger and Na^+-HCO_3^- transporter (Lemasters et al., 1996). However, Leamasters and colleagues demonstrated that the acidosis actually 'protected' against cell death during ischaemia and that the rapid return to normal pH after reperfusion caused the cardiomyocytes to lose viability and accelerated their death (Lemasters et al., 1996). Worsening of the post-ischaemic injury as a result of normalising cellular pH was coined the 'pH paradox'. A number of mechanisms may explain this phenomenon including the fact that the rapid return to normal pH led to the opening of the MPTPs and generated reactive oxygen species (ROS) (Yang, 2018).

1.1.2.2. Ca^{2+} Overload

Intracellular and mitochondrial Ca^{2+} overload, initiated during the early stage of ischaemia, becomes intensified during reperfusion (Li et al., 2016). With re-introduction of blood flow, the aforementioned Na^+-H^+ exchanger and Na^+-HCO_3^- transporter are activated, resulting in the accumulation of Na^+ inside the cells in an attempt to remove intracellular H^+. In turn, Na^+ becomes exchanged for Ca^{2+} which is greatly exacerbated during reperfusion. The lack of ATP production during the IR process enhances the intracellular Ca^{2+} accumulation (Kalogeris et al., 2012). In an attempt to remove this high cytosolic Ca^{2+}, the mitochondria become involved. However, elevation in mitochondrial Ca^{2+} triggers MPTP opening and thus

mitochondrial damage. Furthermore, this increased cytosolic Ca^{2+} also stimulates an inflammatory response, myofibrillar hypercontractility and myocardial stunning (Yang, 2018).

1.1.2.3. Mitochondrial Dysfunction

The density of mitochondria in cardiomyocytes is high in order to meet the high demand for energy of the heart in order to keep constantly pumping blood (Sezer et al., 2018). Under normal conditions, Ca^{2+} in mitochondria acts as a supportive effector which induces the mitochondria to produce ATP (Kalogeris et al., 2012). However, during IR injury, the accumulation of Ca^{2+} in the cells induces the overload of Ca^{2+} inside the mitochondria, which then destroys the ability of mitochondria to function. This is primarily mediated through the opening of MPTPs that become permeable to and allow free movement of ions and other solutes with a molecular mass of less than 1500 Da across the inner mitochondria membrane (Bernardi and Di Lisa, 2015). As a result, the mitochondria swell, eventually resulting in rupture of the outer mitochondrial membrane. This is a major determinant of mitochondrial death, which further reduces ATP production, and leads to cardiomyocyte death (Kalogeris et al., 2012, Webster, 2012). Necrotic myocytes generate inflammatory responses which, as will be seen later in **Section 1.1.2.5**, perpetuate myocardial IR injury. Additionally, mitochondria are key players in the production of ROS. Although they produce a small but steady amount as by-products of cellular respiration, the re-introduction of O_2 during reperfusion not only lowers mitochondrial anti-oxidants such as mitochondrial superoxide dismutase, but also increases ROS production (Murphy, 2009).

1.1.2.4. Reactive Oxygen Species Production

ROS are critical mediators of reperfusion injury in the heart capable of damaging proteins, lipids and DNA, and further impairing mitochondrial function such that cell death ensues. The increase of ROS can be detected in tissues within a few minutes after reperfusion (Andrienko et al., 2017). There are various potential enzymatic sources of ROS in the heart capable of reducing oxygen to form ROS, such as superoxide ($O_2\bullet^-$), hydroxyl radical (•OH), and hydrogen peroxide (H_2O_2) and also include those that arise from xanthine oxidase (XO), the mitochondrial electron transport chain, nicotinamide adenosine dinucleotide phosphate (NADPH) oxidase, cytochrome P450, lipoxygenase/cyclooxygenase and nitric oxide synthase (Raedschelders et al., 2012). During ischaemia, ATP is catabolised to hypoxanthine, and at the same time, XO accumulates in the ischaemic tissue. Reperfusion of previously ischaemic sites allows for the return of aerobic respiration as oxygen supply is re-established. Paradoxically, however, O_2 reacts with hypoxanthine and XO to generate both $O_2\bullet^-$ and H_2O_2 (Granger, 1988, Raedschelders et al., 2012). These free radicals rapidly and severely damage the cells free radical scavenging system causing injury to cell membranes and proteins directly and also induce injury indirectly by MPTP opening, which activates programmed cell death (Yang, 2018). Similar to the pH paradox phenomenon, this 'oxygen paradox' also leads to further intracellular Ca^{2+} overload as damage to membrane structures promotes Ca^{2+} accumulation within the cell (Kalogeris et al., 2016).

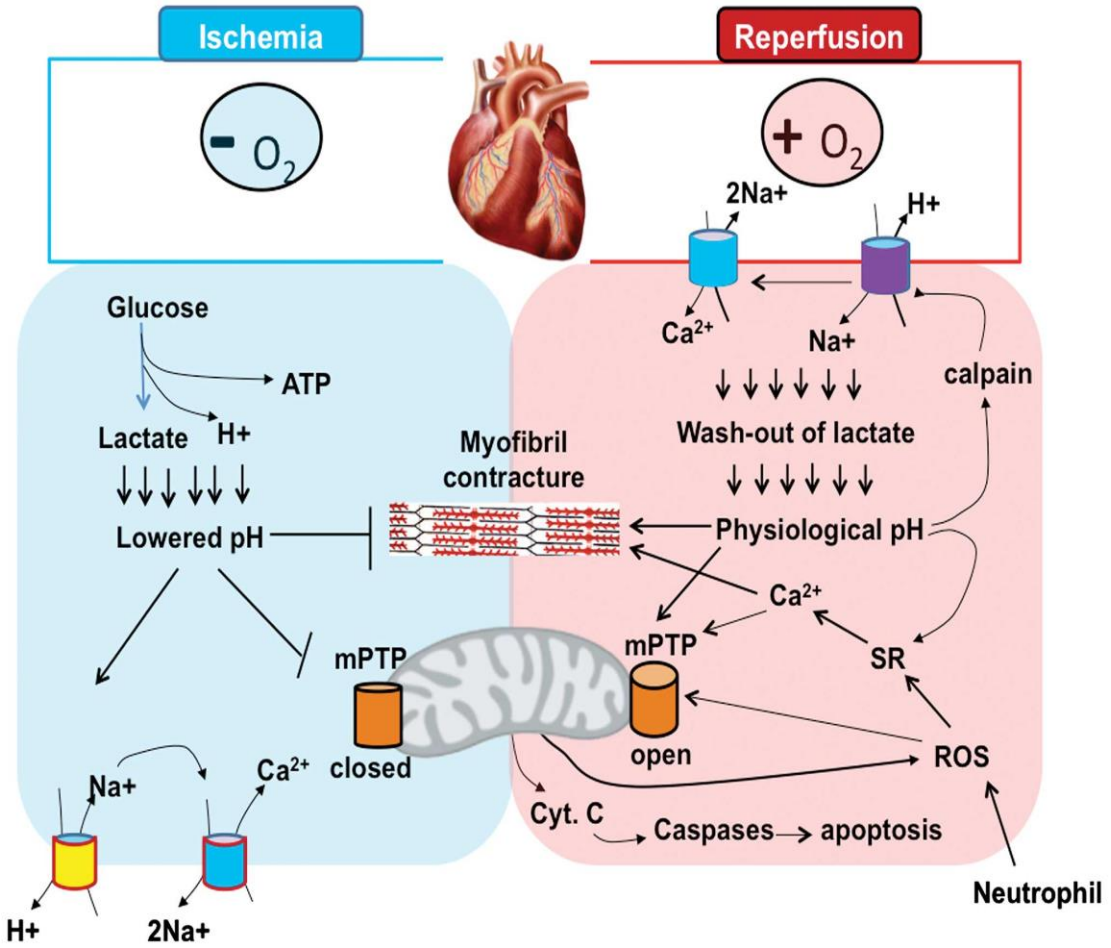


Figure 1.2. Schematic of the mechanism of myocardial IR injury. During ischaemia, cells switch to anaerobic metabolism in order to generate ATP. However, this results in a decrease in cellular pH or acidosis and insufficient ATP generation to meet the metabolic demands of a busy pumping heart. ATPases become inactivated such that Na^+/K^+ATPase pumps stop working leading to Na^+ accumulation within the cell. Ca^{2+} uptake by the endoplasmic reticulum is also reduced leading to Ca^{2+} overload in the cell. With the establishment of reperfusion, oxygen is re-introduced, as are the substrates required for aerobic ATP generation. Furthermore, both lactate and H^+ are washed out. However, the washout of H^+ encourages more Ca^{2+} influx, known as the pH paradox. Re-introduction of O_2 also drives reactive oxygen species (ROS) generation. ROS, also delivered by infiltrating neutrophils, leads to excessive cellular damage, mediating through the opening of mitochondrial permeability transition pores (MPTPs) and initiation of thromboinflammatory cascades. Source: Li et al., 2016.

1.1.2.5. Initiation of Inflammatory Process

Reperfusion also leads to the production of pro-inflammatory agents, chemokines and cytokines which culminate in the recruitment of circulating inflammatory cells, especially neutrophils, and an increase in microvascular permeability (Kvietys and Granger, 2012). In the absence of activation by pathogens, this inflammation is called sterile inflammation (Shen et al., 2013). The main mediators are ROS and the Ca^{2+} overload described earlier. Injured endothelial cells (ECs) start to express a higher level of cellular adhesion molecules (e.g. E-selectin, VCAM-1, ICAM-1), which subsequently leads to recruitment of inflammatory cells and their tissue invasion (Jaakkola et al., 2000). Activated neutrophils produce proteolytic enzymes, pore-forming molecules and further ROS, cytokines and chemokines resulting in adverse effects on myocardial cells(Kalogeris et al., 2012). This inflammatory process initiated post-reperfusion is described in more detail in **Section 1.4**.

1.2 Clinical manifestations of myocardial IR injury

Myocardial IR injury ultimately leads to the clinical manifestation of 4 different types of dysfunction in the heart, varying in range from reperfusion arrhythmias to fatal multi-organ dysfunction syndrome (Sirotkovic-Skerlev et al., 2006). These 4 disturbances include (i) myocardial stunning, which is a mechanical dysfunction that persists despite the fact the heart has been successfully reperfused, (ii) reperfusion arrhythmias, (iii) no-reflow phenomenon, which is an inability to reperfuse the ischaemic myocardium region after opening the culprit coronary artery due to a high impedance to the flow of blood through the microvasculature and, (v) lethal reperfusion injury (**Figure 1.3**).

1.2.1. Myocardial stunning - flow-contractility mismatch

Myocardial stunning is a term coined to describe the prolonged, reversible contractile dysfunction which occurs following a short period of non-lethal ischaemia (Kalogeris et al., 2016). It is associated with normal perfusion of the heart after PPCI but depressed myocardial function that can last for hours or weeks after the ischaemic insult (Kalogeris et al., 2012). Myocardial stunning occurs after unstable angina, myocardial intervention, acute MI and cardiac surgery (Papadakis et al., 2018). A short duration of ischaemia that is rapidly reversed is not long enough to cause significant necrosis of myocardial cells (Kloner, 2020). The mechanism of myocardial stunning is not fully understood but appears to be linked primarily to dysfunctional calcium cycling and homeostasis in the heart. As described earlier, ROS interferes with ion transport activity via abnormalities in the Ca^{2+} ATPase, $Na^{+}Ca^{2+}$ ATPase and $Na^{+}K^{+}$ ATPase channels which leads to an increased level of intracellular Ca^{2+} (Kloner et al., 1998). Additionally, ROS can lower the myofilament response to Ca^{2+} and decrease sarcolemma reticulum function. These events eventually lead to a decrease in the maximal force of contraction but can be helped by using inotropic drugs (Hasenfuss and teerlink, 2011).

1.2.2. Reperfusion arrhythmias

Myocardial reperfusion injury can result in serious electrophysiological and metabolic alterations which trigger arrhythmias, particularly if the period of ischaemia is long (Gorenek et al., 2015). Reperfusion arrhythmias can be life threatening if they cause ventricular tachycardia and ventricular fibrillation which are one of the main causes of sudden death in

patients relieved from coronary ischaemia (Kalogeris et al., 2012). The most common type of arrhythmias noted after PPCI in patients with acute MI are accelerated idioventricular rhythm, sinus tachycardia, sinus bradycardia and atrial fibrillation (Yang, 2018). Again, anaerobic glycolysis metabolism with lactic acid production, ROS generation and abnormal changes in Ca^{2+}, Na^{+} and K^{+} inside and outside of contractile cells contributes to shorter action potentials and reduction of contractile forces which ultimately generates reperfusion arrhythmias (Gorenek et al., 2014). Numerous factors enhance the sensitivity of the myocardium to reperfusion arrhythmias, such as acidosis, angiotensin II release and α-adrenergic stimulation. The management of arrhythmias is based on anti-arrhythmia drugs designed to reduce advancement to a more severe condition and to restore normal conduction and rhythm.

1.2.3. The no-reflow paradox

Removal of the occlusion within one or more epicardial coronary artery does not always lead to resumption of blood flow in the downstream microvasculature of the ischaemic myocardium, leading to an event called the 'no-reflow paradox' (Ito, 2006). Indeed, no re-flow is often noted post-PPCI, likely bought about by targeted damage of the tiniest blood vessels of the heart as a result of the ischaemic insult. After reperfusion, thromboemboli break away from the obstructing plaque resulting in blockage of downstream coronary microvessels (Gupta and Gupta, 2016). However, as well as being a 'victim', the reperfused coronary microcirculation itself can also act as a 'culprit' and contribute to tissue damage (Jaffe et al., 2008). After reperfusion, the small thromboemboli release from the large

plaques and move downstream the microvessels, resulting in the blockage of microcirculation. In addition, the reperfusion also causes the recruitment of inflammatory cells and accumulation of free radical to injure the vascular endothelial cells which intensify the damage of the organ (Rezkalla et al., 2017). This can be mediated by multiple microcirculatory perturbations, including EC damage, loss of EC integrity, activation and adhesion of inflammatory cells and platelets to inflamed endothelium, microvascular red blood cell congestion, capillary hemorrhage, reduction of EC associated vasorelaxation and interstitial fluid accumulation and oedema formation to list but a few (**Figure 1.4**). Again ROS generation has a key part in mediating this vascular damage. These events lead to the obstruction of smaller blood vessels, resulting in the limitation of blood flow and exacerbation of injury, and thus determine infarct size (Collard and Gelman, 2001, Hausenloy and Yellon, 2013). It is therefore clear that myocardial IR injury can also be considered multi-faceted microvascular pathology. As such the coronary microcirculation, a 'culprit and victim' of MI, has been identified as a prime target for cardioprotection (Hausenloy *et al.,* 2019). Pharmacological therapy such as intracoronary nitroprusside, veramilor and nicardioine improves the coronary blood flow and prognosis in the patients who suffer from the no-reflow phenomenon, indicating the importance of suitable management of the condition. However, there is currently no specific therapy to actually prevent this condition (Rezkalla et al., 2017).

1.2.4. Lethal reperfusion injury

The term 'lethal reperfusion injury' specifically refers to the death of viable cells that occurs specifically as a consequence of reperfusion (Garcia-Dorado et al., 2009). Indeed,

immediate death of cardiomyocytes can be observed within minutes of reperfusion. It is the most severe consequence of IR injury and the most important cause of contemporary treatment failure. During both ischaemia and reperfusion, activation of programmed cell death occurs including apoptosis, necroptosis, necrosis and autophagy of dead cells (Sezer et al., 2018). Apoptosis is defined by the breakdown of deoxyribonucleic acid, which leads to alterations in cell morphology such as cell shrinkage and blebbing. Necrosis is defined by organelle and cell swelling resulting in rupture of the cell membrane (Yang et al., 2015). The death of cells is a strong stimulus for immune cell activation and leads to excessive pro-inflammatory cytokine production and recruitment of inflammatory cells (Slegtenhorst et al., 2014). Once again, the main mechanism of cardiomyocyte death involves Ca^{2+} overload and production of ROS. Ca^{2+} overload induces cardiomyocyte damage through various mechanisms such as calpain-dependent cytoskeleton fragility, excessive contraction and Na^{2+} pump dysfunction. Additionally, ROS-induced increases in mitochondrial permeability leads to their rupture and subsequent cell death (Garcia-Dorado et al., 2009).

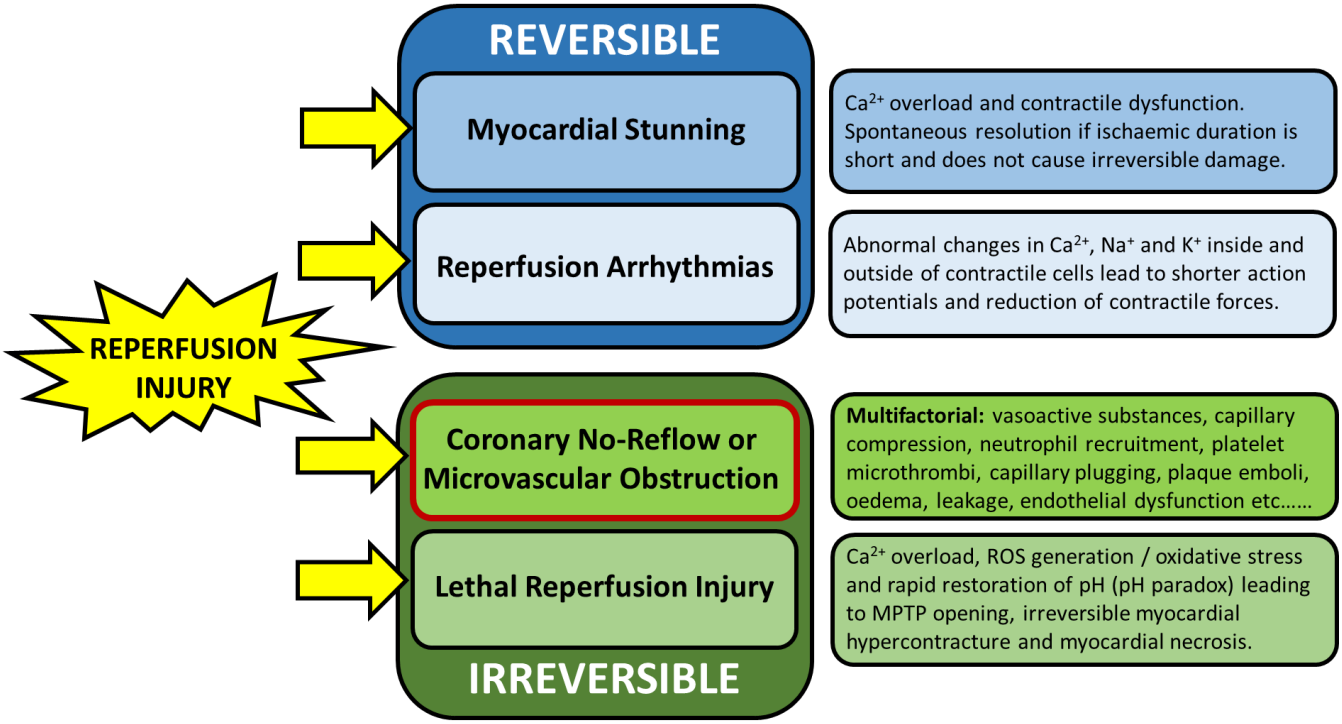


Figure 1.3. Four Clinical Manifestations of Myocardial Reperfusion Injury. Myocardial stunning and reperfusion arrhythmias are either transient or can be easily treated. However, coronary no-reflow, which is associated with microvascular obstruction, and lethal myocardial reperfusion injury are not reversible. Currently, there are no viable treatment options for these two clinical manifestations that contribute up to 50% of the final myocardial infarct size. This thesis will focus on identifying strategies that can protect against the microvascular complications (outlined in red). Source: courtesy of Dr Neena Kalia, University of Birmingham.

There is a golden-window of opportunity to reduce lethal reperfusion injury which appears within 2-3 hours of the onset of MI symptoms (Gloekler et al., 2014). The development of a pharmacological and non-pharmacological intervention to reduce the injury of vascular ECs, cardiomyocytes and smooth muscle cells has been studied for almost 50 years (Sezer et al., 2018). However, a suitable and specific treatment still needs to be discovered.

1.3 The role of the coronary microcirculation in myocardial IR injury – an important determinant of infarct size

Clinically, restoration of normal epicardial coronary artery blood vessel flow, but with sub-optimal myocardial perfusion, can be observed in as many as 50% of PPCI patients, leading to worse outcomes than in patients with full perfusion recovery (Bolognese et al., 2004; Camici & Crea 2007; De Maria et al., 2015; (Niccoli et al., 2016). This suggests myocardial tissue damage likely occurs subsequent to inadequate perfusion at the level of the coronary microcirculation (Bolognese et al., 2004; McAlindon et al., 2018). Indeed, the 'no reflow' phenomenon described in **Section 1.2.3** is often noted post-PPCI, likely brought about by targeted damage of the tiniest blood vessels of the heart as a result of both the ischaemic and reperfusion insults. This increased clinical recognition of the importance of the coronary microcirculation has meant identifying effective strategies to improve perturbations and restore microvascular integrity has gained recent attention (Sambuceti et al., 2000; Crea et al., 2014; Pries and Reglin 2016; Luscher 2017).

Surprisingly, however, clinical research into the role of the coronary microcirculation in cardiovascular diseases (CVD) has been limited. Several challenges present themselves making it difficult to investigate dynamic events within the coronary microcirculation clinically. Primarily, the microvessels of interest are small, at less than 200µm in diameter, making imaging modalities such as cardiac magnetic resonance (CMR) and positron emission tomography (PET) unsuitable due to their limited spatial resolution (Thackeray et al., 2015). This inability to directly image coronary microvessels has led to cardiologists focusing their efforts on improving flow post-MI within the angiographically visible part of the coronary circulation. Hence, little is known about the full range of coronary microcirculatory responses to reperfusion-mediated injury in the clinical setting (Kavanagh et al., 2019).

Nevertheless, progressive loss of distal microvessel perfusion has been clinically demonstrated recently in post-MI patients using PET scanning (Thackeray et al., 2015). Furthermore, CMR imaging has demonstrated a dark hypointense core within the infarct zone representing microvascular obstruction in MI patients, which when persistent was indicative of patients more likely to develop adverse ventricular remodeling (Bulluck et al., 2018). Functional readouts, such as local blood flow and pressure, determined clinically using a Doppler flow wire inserted into the coronary artery, have also indicated a lack of perfusion in microvessels downstream of an opened epicardial artery (Fearon and Kobayashi, 2017). The index of microcirculatory resistance (IMR), a pressure-temperature sensor guidewire-based measurement, has also been proposed for quantitatively assessing coronary microvessel functional status indirectly post-PPCI in the territory surrounding the artery from which the measurement is made (Fearon and Kobayashi, 2017). However, these various anatomical and functional assessments are mainly the larger coronary vessels.

Hence, actual visualisation of the coronary microcirculation, let alone any perturbations within them or the vasculoprotective effects of novel therapies, remains impossible to ascertain with current clinical imaging tools.

The microcirculation is the critical link between the cardiomyocytes and epicardial blood vessels (Sambuceti et al., 2002). Most of our knowledge of what may be happening within the coronary microvessels post-IR injury has been obtained primarily from experimental studies in experimental models of IR injury in which the heart tissue has been interrogated histologically and biochemically for morphological deterioration, inflammatory cell infiltration and infarct size (Ibanez et al., 2015). These various microvascular perturbations are summarised in the sections below, with mechanistic insights provided, and include the presence of: (i) swollen and injured ECs compressed by oedematous fluid and surrounding cardiomyocytes that are themselves swollen ; (ii) microthromboembolization released from the breakdown of atherosclerotic plaque that travel downstream and appear to obstruct microvessels ; (iii) vasoconstriction triggered by soluble vasoactive factors and ; (iv) thromboinflammation as evidenced by the presence of a high number of intraluminal leukocytes, platelet-platelet and platelet-leukocyte aggregates interacting with injury-activated endothelium (Ibanez et al., 2015).

1.3.1. Extravascular compression of the coronary microcirculation

A number of factors can cause the coronary microvasculature to become compressed from the outside during IR injury. As described earlier, osmotic water movement into cardiomyocytes as a direct consequence of ionic changes leads to these cells becoming

swollen. This can lead to extravascular compression of coronary capillaries and a substantial reduction, if not total prevention, of blood flow through the heart upon reperfusion. Furthermore, the microcirculation has been reported to be very sensitive to extravascular compression by interstitial oedema which occurs as a result of inflammatory responses taking place as detailed later in **Section 1.3.4** and **Section 1.4** (Kloner et al., 1980). The lack of blood flow during the ischaemic phase leads to hypoxia which induces endothelial dysfunction and loss of the microvascular barrier function, which again leads to fluid leakage from microvessels which accumulates in the interstitial spaces surrounding blood vessels. This myocardial oedema is exacerbated after the restoration of blood flow (Sezer et al., 2018). IR injury also damages the endothelial glycocalyx leading to an increase in vascular permeability and capillary leakage. During IR injury, ROS and proinflammatory cytokines TNF-α and IL-1β released from activated neutrophil responsible for the activation of enzyme such as Heparanase and Metalloproteinase, which induce the degradation of endothelial glycocalyx (Yu et al., 2019). Activated neutrophils also release Myeloperoxidase enzyme which further the degradation of glycocalyx by cleaving the SYND-1 glycocalyx protein (Manchanda et al., 2018). In the hypoxic and postischemic heart, the degradation of ATP/ADP causes the accumulation of Inosine, which stimulates mast cells via A3-type receptor activation (Becker et al., 2011). Degranulation and releasing of tryptase β and heparanase from mast cells induce the shedding of endothelial glycocalyx (Vlodavsky et al., 2013). Also, in MI patients, increased filling of the heart chambers takes places during the relaxation phase of the cardiac cycle. This can also contribute to an increase in the compression of muscle capillaries that limits coronary blood flow particularly during heart relaxation (Sezer et al., 2018). Collectively, these external compression forces induce a reduction of the capillary diameters resulting in a decreased myocardial perfusion.

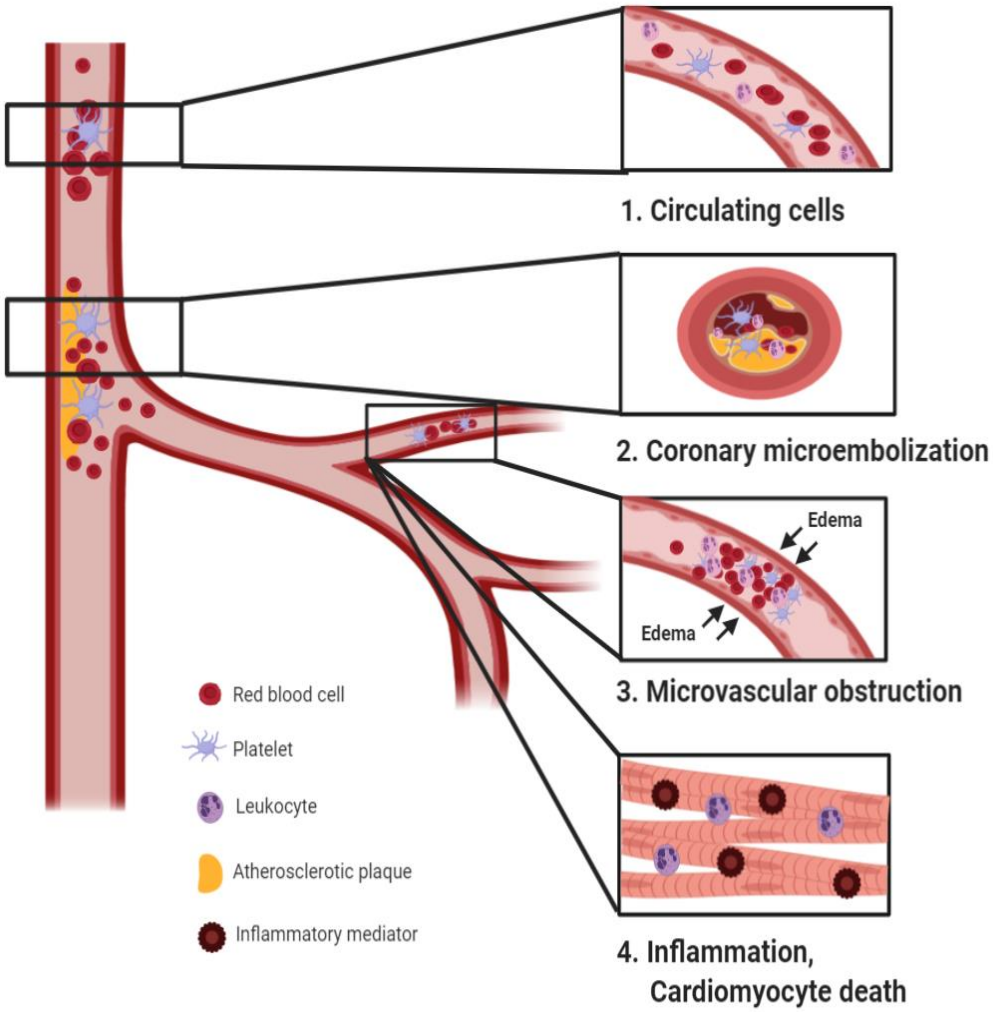


Figure 1.4. The Role of the Coronary Microcirculation in Myocardial IR Injury. Various microvascular perturbations take place in the IR injured heart. **(1)** Circulating thromboinflammatory cells, primarily activated platelets and neutrophils, contribute to a local inflammatory response, microthrombus formation and capillary plugging. **(2)** During clinical procedures designed to induce reperfusion such as PPCI, thromboemboli and plaque debris from the culprit artery can distribute in downstream microvessels. **(3)** Oedema from surrounding swollen cardiomyocytes and from fluid lost from leaky microvessels results in the external compression of coronary microvessels, which leads to a reduction of blood perfusion within them. **(4)** The increased vascular permeability permits the transmigration of inflammatory cells into the interstitial space. Significant inflammation can also lead to the death of cardiomyocytes. Source - adapted from Ibanez et al, 2015.

1.3.2. Coronary microembolization

Coronary microembolization occurs as a result of some portion of the atherosclerotic plaque in the occluded epicardial artery breaking away as a result of PPCI and lodging in the downstream microvasculature. Coronary vascular microembolization can cause contractility dysfunction and infarction in the heart. Patients who have the largest myocardial infarcts have been identified as those who have a substantially higher amount of distal coronary vascular microemboli within the 'larger microvessels' that can be imaged during angiography (Napodano et al., 2012).

1.3.3. Tonal changes to vessels

Although ischaemia is a powerful stimulus for vasodilation, during IR injury the significant damage to coronary ECs means that this ability is lost (Ibanez et al., 2015). This is primarily due to the fact that the damaged endothelium stops generating nitric oxide (NO), which would normally elicit vasodilation and prevent platelet-leukocyte-endothelial interactions (Sezer et al., 2018). Furthermore, powerful vasoconstrictors such as endothelin-1 (ET-1) and thromboxane 2 (TXA_2) are released which act on coronary arteries and arterioles to decrease their diameters and further reduce downstream blood flow (Ibanez et al., 2015). Indeed, ET-1 is one of the most potent endogenous vasoconstrictors known and is synthesized and released from both vascular cells and cardiomyocytes following IR injury. Patients who demonstrate coronary vasospasm present with high plasma circulating levels of ET-1 and this is strongly linked to poorer prognostic outcomes post-MI (Skovsted et al., 2017).

1.3.4. Intraluminal cellular plugging

In addition to extravascular compression of the coronary microcirculation, further reductions in blood flow post-reperfusion can be mediated by intraluminal microvascular obstruction (Yellon and Hausenloy, 2007). The major perturbations that contribute to luminal obstruction include inflammatory cell plugging whereby neutrophils in particular become adherent to activated endothelium, microthrombosis and vasospasm (Sezer et al., 2018). Proteolytic digestion of the endothelial basement membrane by these adherent and transmigrating neutrophils also contributes to EC detachment, loss of vascular integrity and increased vascular permeability (Mutgan et al., 2020). Indeed the detached cells and cellular debris can also contribute to microvascular obstruction. Hypoxia also promotes a pro-coagulant response in ECs which leads to platelet activation and subsequent aggregation (Boyle et al., 1996). Hence, cellular plugging is not just restricted to neutrophil events. Platelet-neutrophil aggregates and platelet-platelet aggregates can exacerbate the microcirculatory obstruction. Additionally, leukocyte plugging may contribute to red blood cell rouleaux formation and packing upstream of areas of cellular plugging from mechanical obstruction which again limits the number of capillaries effectively perfusing the heart (Sezer et al., 2018). The impairment of the glycocalyx layer on the abluminal surface of ECs also makes the capillaries more susceptible to leukocyte plugging by reducing the endothelial surface layer lubricity, which make the endothelial surface more slippery and less permeable leading to more obstruction of microvessels (Weinbaum et al., 2007).

1.4 Thromboinflammatory responses during myocardial IR injury

Both inflammation and thrombotic events play key roles in the pathophysiology of myocardial IR injury. Although platelets appear to have a critical role, it is argued that inflammation accounts for a large portion of injury that occurs during reperfusion, ultimately affecting final infarct size (Kalogeris et al., 2016, Yellon and Hausenloy, 2007). As such, there may be a potential therapeutic benefit in limiting the inflammatory response in myocardial IR injury. Previous study demonstrated that when nanoparticle – delivered small interfering ribonucleic acid to silence macrophage polarization regulating factor IRF5 in macropage in skin woud of mice (Courties et al., 2014). Decreasing of IRF5 expression decreased the expression of inflammatory M1 macrophage marker resulting in increased the infarct healing (Courties et al., 2014, Arai et al., 1996). This indicated that attenuation of inflammatory cell subsets has shown a reduction in final infarct size. Whilst some inflammatory infiltration may occur during the period of ischaemia, the majority of infiltration occurs during the period of reperfusion (Nourshargh and Alon, 2014, Kalogeris et al., 2016). These events provide the exact conditions for activation of inflammatory cells and initiation of the leukocyte adhesion cascade (**See Section 1.4.2.1**).

1.4.1. The thrombogenic response

Accumulation and aggregation of platelets in myocardial IR injury is a well-documented event and shown to be extremely damaging in nature (Rodrigues and Granger, 2010). Platelets mediated direct tissue damage by releasing adhesion proteins (e.g., VWF, fibronectin, fibrinogen, thrombospodin), chemokines (e.g., platelet factor 4 and RANTES),

coagulation factors (factor V, plasminogen, factor XI) and cytokine- like mediators (e.g. β-thromglobolin and IL-1 β) that induce the activation of inflammatory cells and hampering blood flow (Barrabes et al., 2010). Using a Langendorff rat heart model of IR injury perfused with human platelets isolated from healthy or MI patients, they found that glycoprotein IIb/lla receptor blocker acciximab drug reduced infarct size and improved functional contractile readouts induced by MI patient platelets (Barrabes et al., 2010). Others have shown that the 'sticky' nature of activated platelets not only promotes platelet-platelet and platelet-EC adhesion, but also platelet-leukocyte adhesion (Lam et al., 2015). This interaction can be damaging to the microenvironment as it promotes inflammation in the tissue. Hussain and colleagues demonstrated release of potent vasoconstrictors such as serotonin and TXA_2 from activated platelets that lead to more tissue damage (Husain et al., 1998). Recruitment appears to be mediated by damaged ECs exposing underlying collagen which creates a pro-thrombogenic environment (Massberg et al., 1999). Collectively, these studies show that the presence of activated platelets in myocardial IR injury is detrimental and promotes more damage to cardiac tissue.

1.4.2. The inflammatory response

Myocardial IR injury triggers the release of various pro-inflammatory cytokines such as TNFα, platelet activation factor (PAF), interleukin (IL)-1, IL-6 and IL-8 as well as the transcription factor nuclear factor kappa B (NF-KB) (van Zuylen et al., 2015). These pro-inflammatory cytokines play an important role in mediating the progressive systemic inflammatory response in the IR injured heart. TNFα is one of the more potent pro-inflammatory cytokines released by ECs, monocytes, macrophages, T-cells, neutrophils and

natural killer cells (Xia et al., 1998). It has many functions which include acting as a strong chemoattractant, triggering the expression of other cytokines including IL-1, IL-6 and IL-8, inducing production of ROS and activating the expression of adhesion molecules on the surface of ECs (Couffinhal et al., 1993). These adhesion molecules include ICAM-1 and VCAM-1. IL-1α and IL-1β are also generated during IR injury by similar cells and induce the expression of endothelial ICAM-1/VCAM-1 leading to adhesive interactions of neutrophils with ECs (Bonaventura et al., 2016). Recently, studies have suggested targeting the IL-1 receptor as a novel target against myocardial IR injury (Zhu et al., 2019). IL-6 induces a neutrophil respiratory burst, triggers endothelial expression of adhesion molecules and enhances vascular endothelial permeability. Elevation of IL-6 level in systemic blood is correlated with acute coronary syndrome, indicating that IL-6 also plays a crucial role in the progression of myocardial injury (Ikeda et al., 1999). IL-6 has also been reported to be associated with the activation of microvascular thrombosis (Jong et al., 2016). MI is also associated with the release of IL-8, a potent neutrophil chemotactic factor released from activated ECs and leukocytes following ischaemia-induced IL-1 and TNFα generation. IL-8 stimulates the diapedesis of activated neutrophils through ECs (Oz et al., 1995).

1.4.2.1. Leukocyte Recruitment – Rolling, Adhesion and Transmigration

Neutrophils are the first cells to infiltrate the heart following myocardial IR injury following activation of the inflammatory process (Sezer et al., 2018). IR injury leads to the release of inflammatory cytokines as described earlier, with IL-1β and TNFα triggering the local production of chemokines. Activated neutrophils roll along the IR and ROS activated

microvascular endothelium before becoming firmly adherent and then transmigrating out of the vessel (van Zuylen et al., 2015). This multi-step process is called the leukocyte adhesion cascade (**Figure 1.5**). The initial rolling step is facilitated primarily by L-selectin, expressed on leukocytes, and P-selectin and E-selectin, expressed by inflamed ECs. Selectins bind to either sialyl Lewis^{X}-like glycans or P-selectin glycoprotein ligand-1 (PSGL-1) expressed on leukocytes and ECs to mediate the tethering of leukocytes (Ulbrich et al., 2003).

The presence of pro-inflammatory cytokines such as TNFα and IL-1β increases selectin expression rapidly thus leading to neutrophil rolling. P-selectin is present in specific granules of endothelial cells and platelets, which mobilized to surface of the cells within 3 to 10 minutes after stimulation (McEver, 1991). After stimulated by TNF-α, e-selectin can be detected rapidly and reach the maximal level of expression at 2-6 hours and return to basal levels after 24 hours (Bevilacqua et al., 1989). Rolling leukocytes come in close contact with the activated endothelium which produces chemoattractants such as IL-8 and PAF. IL-8 is one of the most important endogenous neutrophil chemoattractants and, after binding to its chemokine receptor, activates rolling neutrophils to activate integrins expression on their surface (Gonzalez-Aparicio and Alfaro, 2019).

IL-8 is a heparin-binding protein which presented on rolling leukocyte and attaches to glycosaminoglycans on the endothelial surface. As the rolling leukocyte binds IL-8 via CXCR1 or CXCR2, the reaction initiated by the leukocyte starts a signal cascade inside the leukocyte that stimulates the integrin via its cytoplasmic tail (Muller, 2013). This effect is also termed "inside-out" signalling since signals trigger the integrin from the inside resulting in improved external adhesion (Hynes, 1992). Inside-out signalling activities cause a drastic transformation of integrin from bent low-affinity conformation to stretched

intermediate-affinity to high-affinity arrangement (Luo et al., 2017). Neutrophil firm adhesion to ECs is triggered by these integrins which are heterodimers comprised of a large α-subunit and a smaller β-subunit (Muller, 2013). Integrins are important players in leukocyte migration cascade, mediating leukocyte firm arrest on inflamed endothelium and organizing transmigration across the basement membrane to facilitate homing to the infection or inflammation location (Abram and Lowell, 2009). The specific integrins involved in neutrophils making firm adhesive interactions with inflamed ECs are: (i) lymphocyte function-associated antigen- 1 (LFA-1) which is also known as CD11a/CD18 and αLβ2; (ii) macrophage-1 antigen (MAC-1) which is also known as as CD11b/CD18 and αMβ2 and; (iii) very late antigen-4 (VLA-4) also known as CD49d/CD29 (Muller, 2013). These integrins bind with their respective counterligands that become expressed on ECs after being stimulated with TNFα and IL-1β. Ligands expressed on ECs for LFA-1 and MAC-1 includes ICAM-1 and ICAM-2. VCAM-1 is the major ligand for the integrin VLA4 (Muller, 2013).

After arrest, leukocyte adhesion is reinforced by integrin clustering and outside-in signalling involving SRC kinases, spleen tyosine kinase and PI3K (Ley et al., 2007). Interaction between ligands and integrins triggers "outside-in" signals on the cell membrane, which allow the leukocyte to sense and react to extracellular environment. Integrin outside-in signalling activates cell migration, spreading, survival, and proliferation (Shen et al., 2012). Guanine nucleotide-binding proteins (G protein) mediate integrins inside-out and outside-in signalling (Shen et al., 2012).

Cytoskeleton rearrangement of leukocytes plays importence part in leukocyte recruitment in injured site. It reduces leukocytes ability to alter their shape from spherical to elliptical, which inhibits them from squeezing through the capillary segment and causing the

leukocytes to stop at the inflammatory organs (Vicente-Manzanares and Sanchez-Madrid, 2004). The alterations include the F-actin rim formation of plasma membrane within 10 seconds after the stimulation by mediators (Yoshida et al., 2006). Lipid mediator leukotriene B4 (LTB4) activates leukocytes and triggers the alteration of their shape and inducing leukocyte binding to endothelial cells via promoting cell-adhesion molecules expression. In postischemic kidney, LTB4 alone causes the neutrophils to migrate into the damaged organs in mice model (Noiri et al., 2000). After fiminly attachment to endothelial cells, neutrophils polarize and flatten which facilitate them to crawl on the endothelial lumen surface in order to find the suitable site for endothelial transmigration (Filippi, 2019).

Transendothelial migration or diapedesis is considered the final step of the leukocyte adhesion cascade (Choi et al., 2009). The junction between ECs consists of adhesion molecules, such as vascular endothelial cadherin (VE-cadherin), holding the ECs together. These inter-endothelial contacts become loose in the presence of adherent leukocytes. Endothelial cells extend the membrane structures which swamp the adhered neutrophils. These structures are called transmigratory cup or docking structure and enriched with ICAM-1 and VCAM-1 (Schnoor, 2015). Carman and colleagues provide the evidence of TEM images suggested that the transmigratory cup helps facilitate the neutrophil transendothelial migration and diapedesis (Carman and Springer, 2004). A number of adhesion molecules that favour leukocyte transmigration, such as platelet-EC adhesion molecule-1 (PECAM-1) and junctional adhesion molecule-A (JAM-A), also play a pivotal role in this process (Ley et al., 2007).

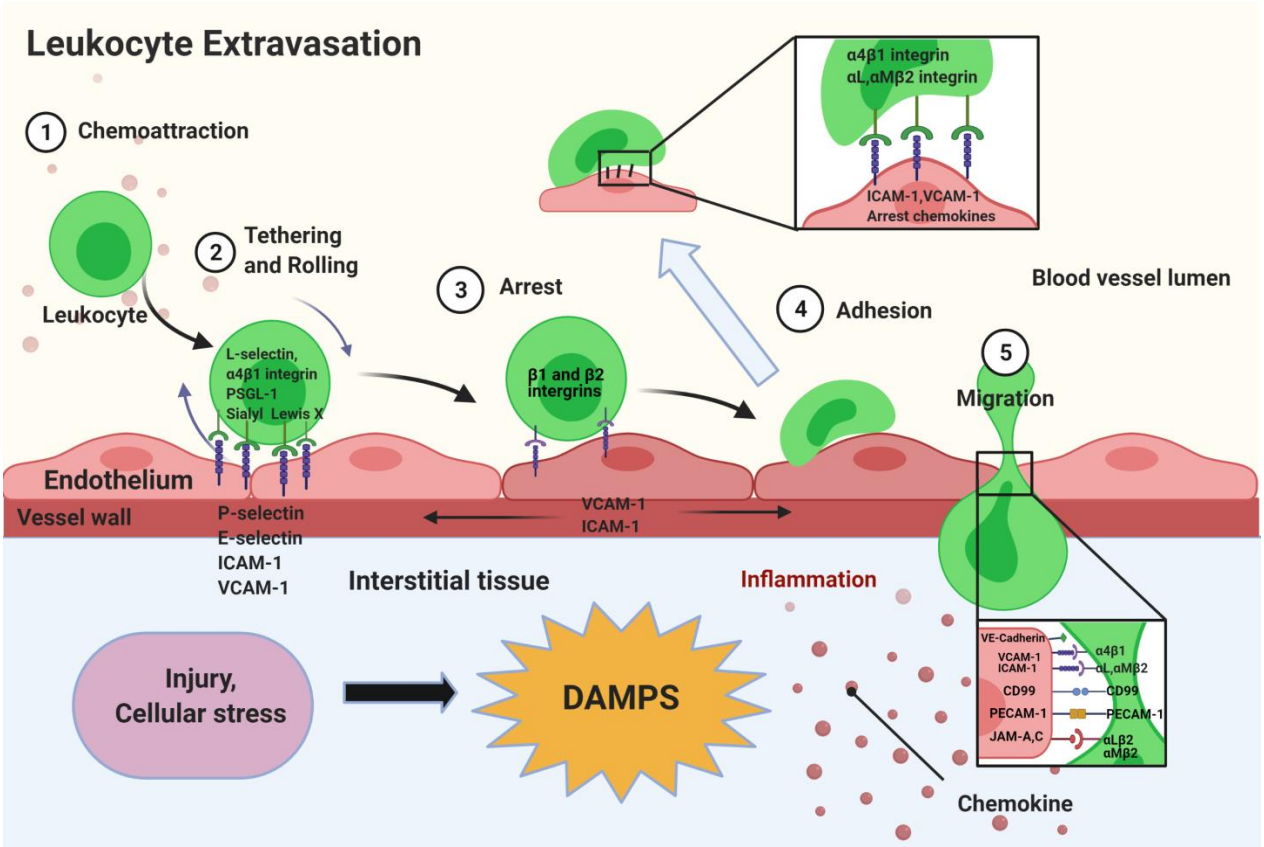


Figure 1.5. The Leukocyte Adhesion Cascade Mediates Neutrophil Recruitment During Myocardial IR Injury. Multiple cytokines, chemokines and adhesion molecules are involved in this process. IR injury leads to the local release of potent inflammatory cytokines including TNFα and IL-1β. These lead to the subsequent release of chemokines that attract passing neutrophils to the injured tissue microvasculature. The initial step of leukocyte rolling is facilitated by L-selectin, expressed by leukocytes, and P-selectin and E-selectin expressed on activated ECs. These selectins then interact with ether sialyl Lewis^X-like glycans or PSGL-1 expressed on leukocytes and ECs to mediate the tethering of leukocytes. Thereafter, chemokines activate leukocytes to express integrins on their surface. Neutrophils firmly adhere to ECs using LFA-1 or MAC-1 integrins binding to endothelial ICAM-1. Additionally, the VLA-4 integrin can mediate firm interactions after binding to endothelial VCAM-1. Transendothelial migration is the final stem of the leukocyte adhesion cascade and leads to the infiltration of these inflammatory cells into the myocardial tissue. It involves a host of adhesion molecules including JAM-A,C , CD99 and PECAM-1. **Abbreviations:** IR – ischaemia-reperfusion; ECs- endothelial cells; IL-1β – interleukin-1β; TNFα - tumour necrosis factor-α; PSGL-1 – P-selectin glycoprotein ligand-1; LFA-1 – lymphocyte function-associated antigen-1 (CD11a/CD18; αLβ2); MAC-1 – macrophage-1 antigen (CD11b/CD18; αMβ2); VLA-4 – very late antigen-4 (CD49d/CD29; α4β1); ICAM-1 – intercellular adhesion molecule-1; VCAM-1 – vascular cell adhesion molecule-1; PECAM-1 – platelet-EC adhesion molecule-1 ; JAM-A – junctional adhesion molecule-A; DAMPS – danger associated molecular patterns.

1.5 Mesenchymal stomal cells

Mesenchymal stromal cells (MSCs) are spindle-shaped non-haematopoietic, multipotent progenitor cells that can differentiate themselves into mesodermal lineages, such as bone, cartilage, adipose tissue and muscle. They were first described by Friendenstein, and later by others, as supportive stromal cells that maintained the bone marrow (BM) microenvironment as the hematopoietic stem cells (HSCs) worked to maintain hematopoiesis (Friendenstein et al., 1968). Although originally isolated from BM, MSCs can also be found in many adult tissues including dental pulp, lung, liver, heart, gut, periodontal ligament, connective tissue, cord blood, placenta, adipose tissues and skeletal muscle (Robey, 2017). In 2019, International Society for Cell and Gene Therapy mesenchymal stromal cell (ISCT MSC) offers a statement to clarify the nomenclature of MSCs. The ISCT MSC committee supports the use of acronym MSCs with the: (i) supplement by origin of the tissue source of cells which highlight the tissue-specific properties; (ii) propose as MSCs unless evidences with both *in vitro* and *in vivo* data for stemness; (iii) relate with evidences of functional assays to show the MSCs properties with appropriate controls (Viswanathan et al., 2019).

In the absence of a specific or unique cell surface marker, the ISCT set the essential requirements for the classification of MSCs which were that they should: (i) demonstrate adhesion to a plastic surface in standard culture conditions; (ii) express cell surface molecules CD73, CD90, and CD105 and lack haematopoietic cell markers CD11b or CD14, CD19 or CD79a, CD34, CD45, HLA-DR surface molecules; (iii) be able to tri-differentiate into adipocytes, chondrocytes and osteoblasts *in vitro* (Horwitz et al., 2005; Dominici et al.,

2006). These criteria can be applied only to human MSCs (hMSCs). MScs express a very low level of HLA class I and no HLA class II molecules which allow them to escape from host immune responses. This interesting feature makes MSCs hypoimmunogenic or 'immune-privileged', which makes them exceptionally suited for both allogeneic and autologous transplantation (Puglisi et al., 2011).

1.5.1. Anti-inflammatory and immunomodulatory properties of MSC

The anti-inflammatory and immunomodulatory capabilities of MSC are now well accepted and have been described by many researchers (Weiss and Dahlke, 2019). This fact, in addition to them being easy to isolate and expand in culture, has led to MSCs being at the forefront as candidates for cellular therapy to treat CVD including the reperfusion injury that occurs post-MI (Rowart et al., 2015). Several studies have demonstrated that exogenously administered MSCs 'home' or traffic via the circulation to the injured tissue and once there can modulate inflammation through release of a secretome containing a number of soluble cytoprotective, growth and anti-inflammatory factors which may mechanistically explain their beneficial effects. For example, the growth factor TNFα stimulated gene/protein 6 (TSG-6), vasoactive prostaglandin E2 (PGE_2) and the interleukin-1 receptor antagonist (IL-1RA) have all been shown to be increased in IR injured murine hearts treated with an exogenous infusion of human MSCs (Eleuteri and Fierabracci, 2019). Additional factors produced by MSCs include growth factors, such as hepatocyte growth factor (HGF), vascular endothelial growth factor (VEGF), basic fibroblast growth factor (bFGF), IL-6, transforming growth factor beta (TGF-β) and stromal cell derived factor 1α (SDF-1α) (Jimenez-Puerta et al., 2020). MSCs can drive macrophage polarization from the

M1 pro-inflammatory phenotype towards the M2 anti-inflammatory phenotype by releasing PGE_2, TGF-β and HGF (Faulknor et al., 2017). Macrophages are also key players in inflammation, and can contribute to it as well as help resolve it. As such they can exist as a pro-inflammatory M1-like phenotype or an anti-inflammatory M2-like phenotype. M1 macrophages produce high levels of pro-inflammatory cytokines and are involved in the early stages of inflammation (Martinez and Gordon, 2014). In contrast, M2 macrophages, with lower pro-inflammatory cytokine production, are associated with the resolution of inflammation and tissue repair (Ley, 2017). Indeed, PGE_2 is one of the important anti-inflammatory factors in the MSCs immunomodulatory activity, produced from arachidonic acid metabolism by cyclooxygenase – 2 (Kota et al., 2017). TGF-β is one of the major cytokines not only responsible for the induction and resolution of inflammation but also the initiation of tolerance to the immune cells (Kyurkchiev et al., 2014). MSCs also secrete HGF which suppresses the expansion of several immune cells (Madrigal et al., 2014). The M2 anti-inflammatory macrophage secretes IL-10 which is an immunosuppressive cytokine that reduces proliferation of immune cells such as lymphocytes. Additionally, IL-10 stimulates the production of regulatory T-cells (Treg) while concurrently decreasing tissue migration of neutrophils (Karantalis and Hare, 2015). MSCs can also perform immunomodulatory effects by suppressing maturation and proliferation of pro-inflammatory immune cells such as T-lymphocytes, dendritic cells, and natural killer cells, and also triggering anti-inflammatory subsets such as Tregs. Moreover, MSCs can drive T-cell development towards the regulatory phenotype (Karantalis and Hare, 2015). Collectively, secretion of these various factors from MSCS can inhibit inflammatory responses.

1.5.2. Multiple populations and sub-populations of MSCs

Although Friedenstein and colleagues discovered MSCs in BM, MSCs have since been isolated from various tissues such as fat, umbilical cords and heart (Fridenshtein et al., 1968). Recent reports showed that these different tissue isolates of MSCs have varying abilities to tri-differentiate into adipocytes, osteocytes and chondrocytes (Kang et al., 2012). Additionally, some but not all MSC populations can also differentiate into endodermal lineage cells such as hepatocytes (Ju et al., 2010) as well as cells of endodermal lineage including keratinocytes and neurons (Chen et al., 2011, Lynch and Ahearne, 2017). More importantly, it has been shown that chemokines or chemical signals from local tissues can also varyingly affect the cytokine secretions and immunomodulatory properties of MSCs (Weiss and dahlke, 2019). From a therapeutic perspective, this has an important impact on their tissue regenerative and restorative potential. It has also been shown that the therapeutic capacity of MSCs can be influenced by donor age with a higher donor age decreasing MSC vitality and differentiation capacity (Zarychta Wisniews et al., 2019). Choudhery and colleaques show evidences suggested that MSCs obtained from donors under 35 years old demonstrate faster growth in vitro, viability, and stronger differentiation capacity than MSCs obtained from donors at the age over 60 years old (Choudhery et al., 2014).

Interestingly, MSCs derived from the same site can also vary structurally and functionally. This has been demonstrated by expanding subpopulation of MSCs obtained from same organ *in vitro* and identifying different proteins expressed on their surface, such as Stro-1, CD 271, CD 105 and CD 106 (Mo et al., 2016, Bensidhoum et al., 2004, Busser et al., 2015,

Mabushi et al., 2013). For example, BM-derived MSC cultures, even from the same donor, can present as a heterogeneous population that show differing morphology, differentiation and migratory capacity (Phinney et al., 2012). Using a process of cell cloning and telomerase-based immortalization, the Genever group recently generated 4 distinct sub-populations of human BM-derived MSCs which possessed differing phenotype but also functionality (James et al., 2015). They showed that the smaller MSCs exhibited potent tri-lineage differentiation capabilities and had a higher expression set of genes that were related to interactions with the BM vasculature and in playing a role in vascular processes such blood vessel remodeling, blood vessel morphogenesis, development and patterning of vessels. This distinct sub-type of BM-MSCs was also CD317 negative and was called Y201 cells. The larger and more rare MSC sub-population were poorly or non-differentiating and rarely associated with $CD31^{+}$ vascular cells in the BM when imaged using immunohistological staining and did not co-localise with perivascular stroma. This distinct sub-type of BM-MSCs was CD317 positive and was called Y202 cells (**Figure 1.6** – also see **Chapter 3, Table 3.1** which highlights the distinct differences between these sub-populations). This novel study suggests single cells are unlikely to possess all properties commonly ascribed to MSCs and that specific functional attributes, such as differentiation or immunomodulatory competency, are found within distinct sub-populations.

In order for MSCs to be utilised clinically, there is a preference in delivering these cells systemically. Hence, there is a reliance on the local injured tissue microvasculature to capture circulating exogenously infused MSCs as they traffic through or 'home' to the tissue or organ. Therefore, it is very important to determine whether differences between the types, population and sources of MSCs impacts on their migration and homing ability.

Any inter- and intra-tissue MSC heterogeneity may be associated with a varying homing potential and therapeutic efficacy in the injured heart, which may explain the poor clinical success to date. However, this has not been extensively studied in any injured organ. Indeed data from *in vivo* studies specifically comparing the efficacy of intra-tissue MSC sub-populations are limited (An et al., 2018).

1.5.3. Distribution of exogenous MSC following systemic administration

The ability of MSCs to modify inflammation and also have potent regenerative properties led to an explosion of small-scale clinical studies in patients with CVD, particularly in patients with MI (Sanina et al., 2015). There are various techniques to study the distribution and homing of MSCs after transplantation such as histology, real-time PCR, fluorescence *in situ* hybridization, fluorescent protein labeling (Zhao et al., 2014). Nevertheless, these techniques are invasive and cannot track the kinetics of circulating cells in real-time and *in vivo*. However, despite major advances in optimising the protocols, the clinical outcome of MSC-based therapy remains poor particularly when larger randomised controlled clinical trials are performed. Obstacles to success include the fact that following intravenous injection, exogenous MSCs can be found at very low levels in the heart (Barbash et al., 2003). High numbers of systemically administered cells were found mostly entrapped within pulmonary capillaries and less so in the liver, kidney and gastrointestinal tissues 24 hours after the administration. Indeed, engraftment in non-pulmonary tissues was very low ranging from 0.1% - 3% of the delivered cells (Deak et al., 2010). Gamma camera imaging and isolated organ counting were used to study the distribution of systemically infused 99mTC-labelled MSCs. After 4 hours,

most MSCs were found in the lung, and only a small number were found in liver, spleen, and heart (Barbash et al., 2013). Infrared imaging was used to detect Qtracker655 and Qtracker 800 labelled MSCs in the heart, lung, kidney, and liver of the Sprague-Dawley rats model. Infrared imaging demonstrated most of infused exogenous MSCs were trapped and distributed evenly over the lung (Fischer et al., 2009). A recent intravital study demonstrated that intravascularly transplanted MSCs physically trapped in the pulmonary vascular bifurcation due to MSC size (Masterson et al., 2021). The MSC physical entrapment is due to the average size of infused MSCs are bigger than the pulmonary microvascular diameter (Toma et al., 2019). However, Intra-arterial infusion is preferred over intravenous to avoid immediate pulmonary entrapment on first pass and in order to image the first instance of MSCs trafficking through the coronary microcirculation, before the cells completed their first pass through the systemic circulation (Kean et al., 2013). Eggenhofer and colleagues suggested that escape of lung entrappment may improve MSC survival and may affect MSC distribution to injured organ after transplantation (Eggenhofer et al., 2017).

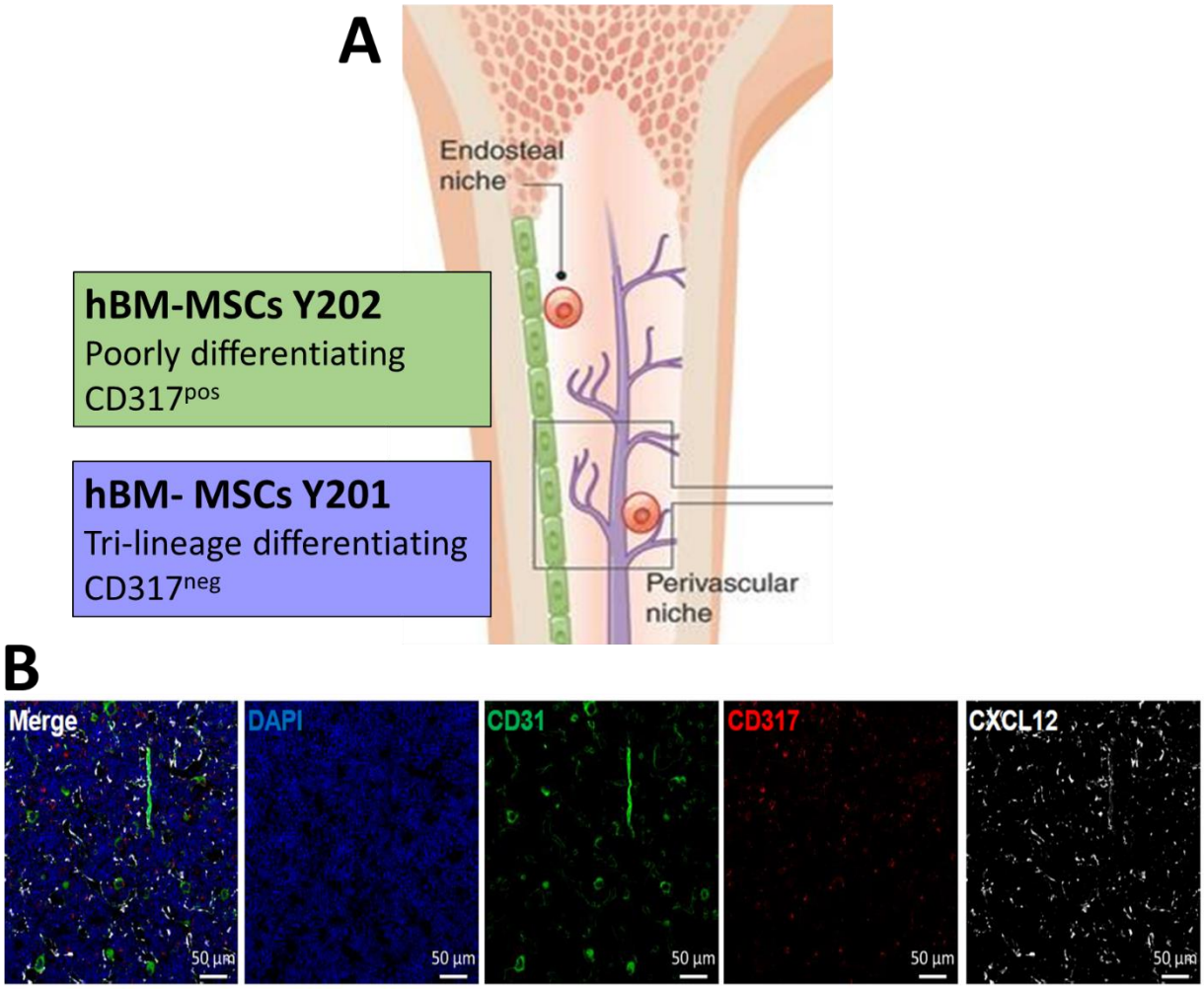


Figure 1.6. MSC Sub-Populations Identified Within Different Bone Marrow Niches. (A) The perivascular niche is the inner core of the BM and contains actively dividing HSCs and sinusoidal endothelium. The endosteal niche is the outer edge of the BM that contains osteocytes, bone matrix and quiescent HSCs. Recent work from the Genever group (University of York) identified that even MSCs residing in the same BM site possess distinct structural and functional characteristics. MSCs that had a higher expression set of genes that were related to interactions with the BM vasculature showed great tri-lineage differentiation capacity, were $CD317^{neg}$ and were called hBM-MSCs Y201. MSCs which rarely associated with the vasculature and were more endosteal in presence exhibited poor differentiation capacity, were $CD317^{pos}$ and were called hBM-MSCs Y202. **(B)** The images from published work by the Genever group show that in mouse tissue sections, CD317 (red) was expressed sporadically throughout the BM. $CD317^{pos}$ cells rarely associated with $CD31^{+}$ vascular cells (green) or with *Cxcl12*-$DsRed^{+}$perivascular stromal and endothelial cells (white) (James et al., 2015).

1.5.4. Adhesive mechanisms governing MSC homing to sites of injury

The exact mechanisms governing MSC trafficking to injured sites have not been fully understood, especially for all the different MSC populations. It is inferred that these MSCs follow the same adhesion cascade that was described for leukocyte migration and homing to sites of inflammation (**Section 1.4.2.1**; De Becker and Riet, 2016). Indeed, the trafficking process of MSCs also includes their tethering, activation, adhesion and transendothelial migration or diapedesis (**Figure 1.7**). In the initial step, immune signals, chemokines, and homing receptors are secreted in response to injury. Similar to neutrophils, these activate MSCs to tether and roll on the endothelium (Zhao et al., 2014). The tethering step is initially expedited by the expression of selectins on the endothelial surface. Interestingly, MSCs have been found to be negative for PSGL-1 (Suila et al., 2014). In the absence of PSGL-1, MSCs utilise the non-integrin CD44 which is compatible with selectins, leading to their rolling on the endothelium (Sackstein et al., 2008). Immobilized P-selectin triggers MSC binding to ECs as evidenced by the observation that anti-P-selectin antibodies inhibit MSC rolling (Ruster et al., 2006). Galectin-1 expressed on human umbilical cord MSCs has also been reported to play an important role as an MSC ligand that can interact with P-selectin on ECs. These selectins activate MSCs to tether and roll on the endothelium causing them to come into close contact with the vessel lining which subsequently leads to stagnation of MSCs in the blood circulation.

In the second process, MSCs are activated by G-protein coupled chemokine receptors in response to the signals from the injured site. For this activation step, SDF-1α expressed on ECs interacts with its receptor CXCR4 expressed on MSCs and is a critical pathway for

gradient-guided cell homing to sites of injury (Honczarenko et al., 2006). However, CXCR4 expression has not been detected by all groups (De Becker and Riet, 2016). MSCs also express CXCR7 and it has been shown that this can also bind to SDF-1α to expedite MSC homing to the injured lungs (Shao et al., 2019). Recent work has shown that chemokines such as monocyte chemoattractant protein 1 (MCP-1) and MCP-3 expressed on myocardium interacts with their receptors including CCR2 to mediate MSC activation (Ullah et al., 2019).

Similarly to inflammatory neutrophils, several studies have confirmed the importance of the VLA-4 / VCAM-1 pathway in mediating MSC firm adhesion to endothelium after activation by SDF-1α. This has been demonstrated by the use of neutralizing antibodies against the β1 sub-unit of the VLA4 integrin which inhibited MSC homing to ischaemic myocardium (Ip et al., 2007). MSCs also express ICAM-1 and VCAM-1, traditionally found on ECs, although their role is somewhat unclear (Krampera et al., 2005).

In the final transendothelial migration step, matrix metalloproteases (MMPs) secreted by MSCs play an essential role in cleaving basement membrane components. MMPs are proteolytic enzymes which degrade collagen and gelatin in the basement membrane. Inflammatory cytokines stimulate MMP production leading to a substantial induction of chemotactic migration of MSCs (Kang et al., 2012). Additionally, growth factors such as PDGF and HGF also stimulate MSC migration and homing (Deak et al., 2010).

Clinical applications of MSC cytotherapy are very much based on the ability of these exogenous cells to successfully migrate or home to the injured tissue such the ischaemic heart after their systemic administration and become retained by the local microcirculation (Ullah et al., 2019). However, as stated earlier, this process is inefficient with only a small percentage of MSCs reaching the target tissue following systemic administration. This limits

the ability to realise the full therapeutic potential of MSC-based therapies and so there is a need to develop strategies to improve MSC recruitment (Ullah et al., 2019). It is anticipated that this will allow greater anti-inflammatory effects to be mediated once within the injured microvasculature.

1.6 Three-dimensional (3D) culturing techniques

One of the more recent and exciting strategies being considered to improve the therapeutic effectiveness of MSCs for various ischaemic diseases is to culture them in a way that can enhance their anti-inflammatory potential (Silva et al., 2018). Cell culture traditionally relies on culturing cells as two-dimensional (2D) monolayers on plastic surfaces. However, the growth of cells using conventional 2D culture methods does not mimic the complexity of the microenvironment surrounding them in real tissues or organs *in vivo*. Cells grown on plastic surfaces leads to cell flattening and changes to their internal cytoskeleton (Knight and Przyborski, 2015). These changes affect the shape of the nucleus which results in alterations in gene expression and protein synthesis. This has a significant impact on how they subsequently behave in various experimental *in vitro* and *in vivo* assays. For example, cell culture on a flat polystyrene flask decreases the differentiation ability of cells (Cukierman et al., 2002).

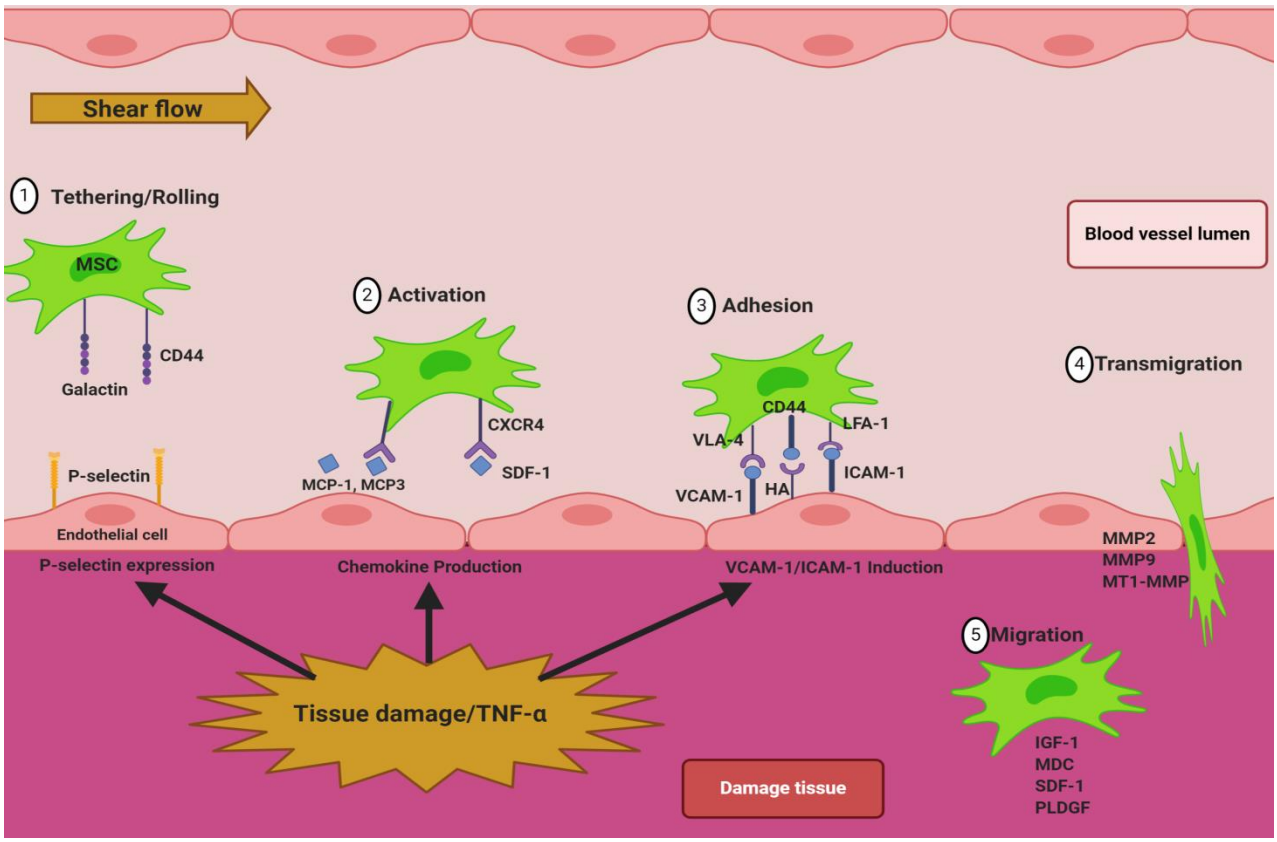


Figure 1.7. The Mesenchymal Stem Cell Adhesion Cascade Showing Key Players in Mediating their Rolling, Activation, Adhesion and Transmigration within Inflamed Sites. MSCs express various molecules such as CD44 and galectin which interact with selectins expressed on inflamed endothelial cells. BM-MSCs also express the chemokine receptor CXCR4 which binds to its ligand SDF-1 located on the endothelium. This leads to activation of the MSCs. There are other chemokine receptors on MSCs which can interact with chemokines such as MCP-1 and MCP-3. Next, MSCs arrest and adhere firmly to endothelial cells primarily using their VLA-4/ $\alpha 4\beta 1$ surface integrin which cooperates with endothelial VCAM-1. Firm adhesion can also be mediated through interactions of LFA-1/$\alpha 4\beta 2$ and CD44 on MSCs binding with endothelial endothelial ICAM-1 and HA respectively. In the transmigration step, matrix metalloproteases (MMPs) play an essential role in cleaving basement membrane components. MMP is a lytic enzyme which degrades collagen and gelatin in the basement membrane allowing MSC diapedesis.

More recently, there has been a gradual increase in the development of three-dimensional (3D) culturing technologies to overcome these problems and help cells to preserve their natural physiological properties, architecture and function (Knight and Przyborski, 2015). These culturing techniques help increase cell-to-cell contact and interaction which allow cells to form more complex structures and lead to enhancement of intercellular signaling (Bartosh et al., 2010). Many techniques have been developed to meet the growing demand for 3D cell culture and can be basically classified into 2 types, namely scaffold-free and scaffold-based cell culture. 3D culture methods utilize non-adherent dishes, cell sheets, micro-fluidics and the hanging drop cell culture method (Page et al., 2013).

The MSC hanging drop culture method leads to the development of cell spheres rather than monolayers and is considered to have many benefits over other 3D methods (Ryu et al., 2019). First, this method is inexpensive and does not require specialized or expensive equipment. Cell spheroids can be generated easily by simple cell culture dishes and collected by pipettes. Secondly, the final size of the cells is simply manipulated by altering the cell concentration or the size of cell suspension droplets (Bartosh and Ylostalo, 2014). This technique allows the cells being cultured to aggregate or compress tightly within 48-96 hours at the apex of the suspension droplets and form a sphere (Bartosh et al., 2010).

Recent studies show that 3D culture of MSCs can improve their therapeutic capacities (**Figure 1.8**) (Jaukovic et al., 2020b, Petrenko et al., 2017). Indeed, 3D cultured MSCs exhibit higher anti-inflammatory potential, stemness, angiogenic properties and survival rates following cell administration (Petrenko et al., 2017). This may be linked to the fact that 3D cultured MSCs secrete higher level of TSG-6 than cells dissociated from a monolayer (Xu et al., 2016). TSG-6 plays an important role in inhibiting neutrophil migration by down-

regulating pro-inflammatory IL-1β production from macrophages (Jaukovic et al., 2020a). Importantly, MSCs derived from 3D spheroids have been reported to be more effective in reducing hepatic inflammation by lowing plasma aminotransferase levels, neutrophil infiltration, liver damage score and hepatic apoptosis in rat model with hepatic IR when compared to rat transplanted with cells derived from conventional 2D culture (Sun et al., 2018). Anti-inflammatory IL-10 levels have also been shown to be higher in macrophages co-cultured with spheroid MSCs (Ylostalo et al., 2012). MSC spheroids also secrete more HGF and PGE_2 which suppresses macrophage cytokine production more so than cells grown in 2D monolayers (Follin et al., 2016). 3D spheroid culture has also been shown to enhance the immunomodulatory capacity of MSCs by significantly increasing TGF-β1 and IL-6 production (Zimmermann and McDevitt, 2014).

1.7 Imaging the beating mouse heart in vivo – intravital microscopy (IVM)

The importance of the role of the coronary microcirculation in MI has increased clinically (Pries et al., 2017). Therefore, imaging the multitude of dynamic thromboinflammatory and vasoactive events that take place in the coronary microcirculation in real-time is key to understanding the mechanisms that underpin myocardial IR injury (Kavanagh et al., 2019). Furthermore, identifying whether novel therapeutic interventions, such as MSC therapy, are beneficial through direct vasculoprotective actions on coronary microvessels is important. The lack of clinical methodologies capable of visualising coronary microcirculation has contributed to a research 'black box' with regards our understanding of the dynamic changes that occur in the microcirculation of the IR injured heart (Pries and Reglin, 2017). This gap in

our current knowledge can be met through experimental studies. Indeed, as stated earlier in **Section 1.3** most of our understanding of microvascular dysfunction post-reperfusion injury has been obtained from heart tissue imaged histologically for morphological deterioration, inflammatory cell infiltration and infarct size (Sezer et al., 2018). However, these static snapshots provide no indication of the real-time kinetics of deleterious thromboinflammatory cell recruitment in the presence of pathophysiological flow, nor information on microvessel integrity post-injury.

Recently, the cardiovascular research community suggested creating an international 'coronary microcirculatory observatory', an EU-wide virtual facility, utilising *in vivo* imaging techniques such as intravital microscopy (IVM) to properly interrogate coronary microvascular dysfunction (Pries and Reglin, 2017). IVM is used extensively to experimentally image in real-time the microcirculation of solid organs (e.g. liver, kidney, gut) or transparent tissues (e.g. mesentery, cremaster muscle) in anaesthetised rodents. It has been used to investigate cellular events in various areas such as immunology, tumour biology and neurology. Indeed, much of our existing knowledge of the impact of IR injury on the microcirculation has been obtained using transparent preparations such as the cremaster muscle or gut mesentery (Gavins and Chatterjee, 2004, Kozhura et al., 2005, Yago et al., 2015). The advantage of IVM is the ability to image a single cell and track its movement in real-time *in vivo* (Matsuura et al., 2018). However, application of this powerful technique to the beating heart in rodents has been challenging primarily due to cardiac cycle and respiratory related movement of the heart in all three dimensions, thus imposing a practical limitation on the imaging resolution of the coronary microvasculature. As such, other surrogate tissue beds, particularly the cremaster, have been used as models of the cardiac

microcirculation (Pries and Reglin, 2016). However, the coronary microcirculation is unique in both its anatomical design and physical properties, particularly its contractile activity which compresses coronary capillaries during systole reducing their diameter up to 20% (Yada et al., 1993, Toyota et al., 2002). As such, the impact of IR injury, and the mechanisms by which therapeutic vasculoprotective strategies act, may vary in a site specific manner. It is only over the last 10 years that suitable techniques capable of imaging cellular trafficking have been developed and combined with ECG gating (Lee et al., 2012), pacing (Aguirre et al., 2014), stabilisers (Jones et al., 2018, Vinegoni et al., 2015, Kavanagh et al., 2019b) and advanced software tools (Kavanagh et al., 2019a, Soulet et al., 2013, Gómez-Conde et al., 2015). The main commonality between these studies is the use of a tissue stabiliser which is attached to the heart using an appropriate veterinary glue (Kavanagh et al., 2019b, Lee et al., 2012, Jones et al., 2018) or is held in place by suction (Vinegoni et al., 2012, Jung et al., 2013). The stabiliser secures a small portion of the heart ventricle in space and permits imaging of the epicardial surface through a central ring and, importantly, without impeding its physiological role in blood circulation. As a result of this developmental work, recent studies have started to investigate cellular trafficking in the context of pathological cardiac microcirculatory conditions (Jung et al., 2013, Matsuura et al., 2018, Kavanagh et al., 2019b, Allan-Rahill et al., 2020).

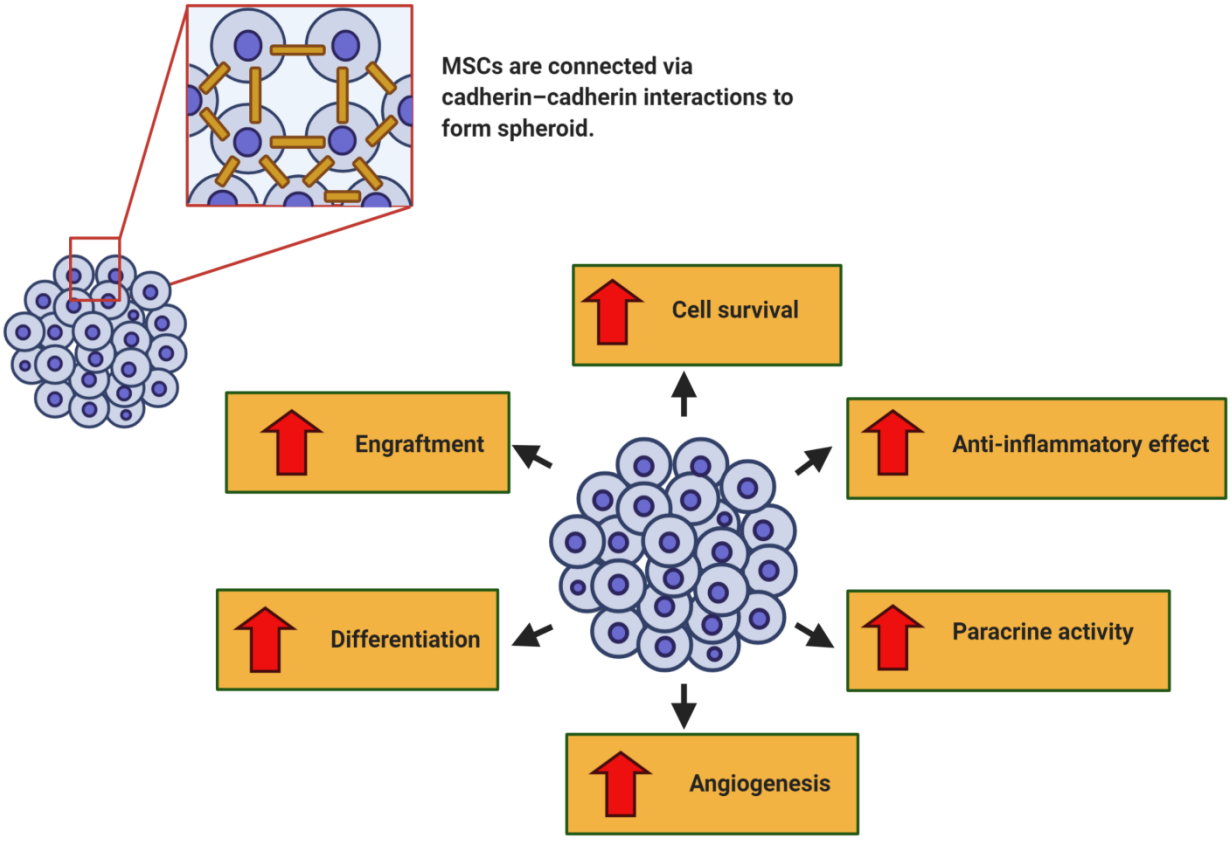


Figure 1.8. MSCs Cultured as Spheroids Using 3D Culture Methods Have Greater Therapeutic Effectiveness. Culturing MSCs as spheroids promotes their paracrine secretion, anti-inflammatory activity, cell survival after transplantation, differentiation capacity and angiogenesis.

1.8 Summary

Despite experimental and clinical studies providing strong evidence that MSCs are beneficial in models of ischaemic heart injury, just as many clinical trials have either failed to replicate these findings or have shown minor or temporary benefit (Madigan and Atoui, 2018). This may in part be due to the fact that there is no consistency amongst the various studies with regards to the phenotypic nature of the cells used, route of delivery, number of cells injected, timing of delivery post-MI etc. Since coronary microcirculatory dysfunction is increasingly identified as a critical pathological component in ischaemic heart disease (Pries et al., 2017), understanding whether MSCs, or indeed any form of cellular therapy, can protect these delicate structures is important. However, this has received very little attention with pertinent questions remaining unanswered. For example, do systemically infused MSCs actually traffick to the injured heart and subsequently make firm adhesive interactions with the coronary microvasculature in the presence of pathological flow, or do they simply passage through? Which anatomical branches of the microcirculation mediate this capture – arterioles, capillaries, post-capillary venules – and are these interactions short-lived? Most importantly, does MSC therapy preserve the integrity of the coronary microvessels and ensure flow is maintained through the heart – do they only modify one or the many different microvascular disturbances?

This inter- and intra-tissue MSC heterogeneity may be associated with varying homing potential and therapeutic efficacy in the injured heart, which may explain the poor clinical success of MSCs in clinical trials to date (Mastrolia et al., 2019). However, this has not been

extensively studied in any injured organ, and data from comparative *in vivo* studies, particularly of intra-tissue MSC subpopulations, are limited. For MSCs to be utilized clinically, there is a significant interest in delivering these cells systemically. Hence there is a reliance on the local injured tissue microvasculature to capture circulating MSCs as they traffic through or 'home' to that organ. Therefore, it is important to determine whether differences between the types, population and sources of MSCs impacts on their migration and homing ability. Recent studies also suggest that 3D spheroid culture enhances the beneficial properties of MSCs treatment for cardiovascular disease. The cytokines and growth factors derived from MSCs spheroids can ameliorate post-infarct inflammation, promote myocardial metabolism and contractility and reduce myocardial fibrosis. However, information on the therapeutic effects of cells derived from 3D spheroids in the heart is still scarce with nothing known about whether 3D cultured MSCs confer enhanced vasculoprotective effects in the reperfused coronary microvessels compared to cells cultured as 2D monolayers.

Research using conventional immunohistochemistry of tissue sections has tried to answer some of these questions but the information they provide is limited as the assays used simply provide a 'static' snapshot of events at a particular moment in time. Indeed, such studies do not inform us whether MSCs are genuinely adherent in the heart or simply caught in time passing through it. Ultimately, restoration of blood flow and ventricular muscle perfusion is a key to the survival of the myocardium, yet static assays cannot 'show' dynamic events such as blood flow. As such, they provide no indication of whether injected stem cells themselves can occlude blood flow within the tiny coronary vessels. If this does occur, and it is a significant event, it may cause more damage than good and impact negatively on their therapeutic effectiveness. It is noteworthy that clinical studies have monitored therapeutic

effectiveness of MSCs many weeks or months after their administration, focusing on functional improvements or changes in infarct size. However, damage to the coronary vasculature post-reperfusion injury is usually mediated within minutes, with the development of tissue infarction observed experimentally within hours. Whether MScs have the potential to modify these rapid microvascular perturbations has not previously been investigated but may prove critical to improving outcomes for MI patients in the acute period post-PPCI.

However, to even begin understanding the potential vasculoprotective efficacy of MSCs, a detailed understanding of the exact damage the coronary microcirculation undergoes following IR injury *in vivo* is needed. Currently, little is known about the full range of dynamic microcirculatory responses to MI. The Kalia Group has been the first to apply powerful spinning Nipkow-based confocal intravital imaging to the beating mouse heart (Kavanagh et al., 2019b). They used a stabilisation method, which involved vet-bonding 3D printed in-house designed stabiliser to the left ventricle, which sufficiently reduced motion in a small region of the beating heart to permit intravital imaging of the coronary microcirculation. Multiple thromboinflammatory events were identified in the coronary capillaries which led to an overall decrease in the density of perfused capillaries in the myocardium within 30 minutes of IR injury. Whether MSCs can confer vasculoprotection and prevent these disturbances is not known.

1.9 Aims and Hypothesis

MSCs have been broadly studied for their therapeutic capacity for MI for several decades (Madigan and Atoui, 2018, Levy et al., 2020). They show therapeutic potential to reduce inflammation and promote tissue healing depends on the quantity of administered cells homed to the injured organ (Ullah et al., 2019). However, only a small number of systematically transplanted MSCs can effectively recruit to the target tissue, which dramatically decreases exogenous cytotherapy effectiveness (De Becker and Riet, 2016). Therefore, enhancing the homing of exogenous MSCs would significantly improve their beneficial capacity (Li et al., 2017). Moreover, MSCs are heterogeneous with distinct characteristics and therapeutic potential, affecting their therapeutic ability (James et al., 2015). Therefore, it is essential to determine whether differences between the types, population and sources of MSCs impact their migration, homing and therapeutic ability (An et al., 2018).

The overall aim of this thesis is to develop a method to improve the ability of MSCs to protect the coronary microcirculation of the heart following IR injury. Two strategies will be employed which include: (i) infusing MSCs derived from spheroids grown using a 3D culture method and comparing them with MSCs cultured using a conventional 2D method; (ii) testing the vasculoprotective ability of MSC populations derived from different tissues sources and heterogeneous sub-populations derived from the same tissue source. The mechanisms governing any potential improvement in vasculoprotective capability will also be determined. For example, do 3D culture and/or use of a particular sub-population of MSC have increased adhesive interactions with the inflamed IR injured coronary microcirculation *in vivo*. This would allow us to identify an MSC sub-population that is most

adhesive and which may therefore have a more therapeutic effect due to their increased local presence in the injured heart. The coronary microcirculation of the beating mouse heart, that has undergone myocardial IR injury, will be imaged *in vivo* using confocal-based IVM. Heart tissue will also be interrogated *ex vivo* using multiphoton microscopy, to elucidate events taking place in the deeper layers of the myocardium, and also using flow cytometry to assess the impact of injury and MSC therapy specifically on coronary ECs. Therefore, we hypothesise that 3D culture technique can improve MSC homing within IR injured heart and increase of their vasculoprotective effect. Moreoever, these abilities may differ between MSC from different sub-populations.

The overall aims and hypotheses of this study are to:

1. **Aim:** The general morphology and surface expression of critical adhesion molecules and chemokine receptors of three different populations of MSCs will be compared microscopically and using flow cytometrically. The impact of culturing MSCs in a 3D hanging drop method on these characteristics will also be determined. The three different populations of MSCs tested will be human WJ-MSCs and two immortalised human BM-derived MSC sub-populations, namely hBM-MSCs Y201 and hBM-MSCs Y202 obtained from the Genever group. The adhesive ability of MSCs derived from 3D spheroids will be compared with 2D cultured MSCs to different substrates *in vitro*.

   Hypothesis: Adhesion of 3D cultured MSCs to various substrates *in vitro* will be greater than 2D cultured MSCs.
2. **Aim:** Intravitally image the homing kinetics and retention capabilities of 2D and 3D cultured MSCs within the IR injured beating mouse heart coronary microcirculation *in*

vivo. **Hypothesis:** 3D cultured MSCs will have a greater ability to home to, and become adherent within, the IR injured beating heart *in vivo*.

3. **Aim:** Intravitally image the ability of 2D and 3D cultured MSCs to modify thromboinflammatory responses and improve perfusion within the IR injured beating mouse heart *in vivo*. Specifically, the recruitment of endogenous neutrophils and platelets and changes in functional capillary density will be assessed. Infarct size will also be determined. **Hypothesis:** 3D cultured MSCs will reduce infarct size more so by having a greater potency to inhibit thromboinflammatory events, protect the structural integrity of the microvessels and increase regional blood flow perfusion through the heart.
4. **Aim:** Determine the mechanisms by which MSCs may confer vasculoprotection. **Hypothesis:** 3D cultured MSCs will greatly reduce endothelial ROS production, endothelial oxidative damage, and endothelial adhesion molecule expression and/or modify circulating plasma inflammatory cytokine levels.

CHAPTER 2

Materials and Methods

2.0 Materials and Methods

2.1 Materials

2.1.1. Antibodies

Table 2.1. List of antibodies used in *in vitro* assay, flow cytometry and intravital experiments.

Experiments	Antibody	Conj.	Clone	Origin	Target	Company	Conc.
Blocking Antibodies	Anti-CD16/CD32	-	93	Rat	Mouse	Biolegend	0.5 mg/ml
Endothelial & *In Vitro* Assay	Anti-VCAM-1	AF647	NS	Rat	Mouse	Biolegend	0.5mg/ml
	Anti-ICAM-1	FITC	YN1/1.7.4	Rat	Mouse	Biolegend	0.5mg/ml
	Anti-CD31	FITC	390	Rat	Mouse	Biolegend	0.5mg/ml
	Anti-8-OHdG	-	NS	Goat	SI	Abcam	NS
	IgG control	-	NS	Goat	SI	Abcam	5 mg/ml
	Anti-goat IgG	AF488	NS	Donkey	Goat	Abcam	2 mg/ml
	Anti-goat IgG	AF647	NS	Donkey	Goat	Abcam	2 mg/ml
Flow Cytometry Experiments	Anti-CD18	PE	GAME-46	Rat	Human	eBiosciences	80 µg/ml
	Anti-CXCR4	FITC	247506	Mouse	Human	eBiosciences	80 µg/ml
	Anti-CD44	FITC	IM7	Rat	Mouse	eBiosciences	1:50
	Anti-VCAM-1	FITC	429	Mouse	Human	eBiosciences	0.2
	Anti-ICAM-1	FITC	HCD54	Mouse	Human	eBiosciences	0.2 mg/ml
	Anti-CD31	PE	390	Rat	Mouse	Biolegend	0.2 mg/ml
	IgG Control	PE	RTK2758	Rat	Mouse	Biolegend	0.2 mg/ml
	Anti-Troponin (cTnT)	PE	REA400	NS	Mouse	Miltenyi Biotech	NS
	REA Control	PE	REA400	NS	Mouse	Miltenyi Biotech	NS
	Anti-8-OHdG	-	NS	Goat	SI	Abcam	NS
	IgG Control	-	NS	Goat	SI	Abcam	NS
	Anti-Goat IgG	AF488	NS	Donkey	Goat	Abcam	5 mg/ml
	Anti-ICAM-1	FITC	YN1/1.7.4	Rat	Mouse	Biolegend	0.5 mg/ml
	IgG Control	FITC	RTK4530	Rat	Mouse	Biolegend	0.5 mg/ml
	Anti-VCAM-1	PE-Cy7	429	Rat	Mouse	Biolegend	0.2 mg/ml
	IgG Control	FITC	RTK2758	Rat	Mouse	Biolegend	0.5 mg/ml
Intravital Experiments	Anti-Ly6G (Gr-1)	PE	RB6-8C5	Rat	Mouse	Thermo Fisher	0.2 mg/ml
	Anti-CD41	APC	MWReg30	Rat	Mouse	Biolegend	0.2 mg/ml

* NS = Not Specified; SI = Species Independent.

2.1.2. Standard materials and chemical substances

Table 2.2. Materials frequently used in experiments.

Material	Abbreviation	Manufacturer	Location
24-Well Plates	-	Nunc, Rochester	New York, USA
96-Well Pplates	-	Nunc, Rochester	New York, USA
5-0 Suture	-	Ethicon	New Jersey, USA
8-0 Suture	-	Ethicon	New Jersey, USA
Acetone	-	Thermo Fisher Scientific	Leicestershire, UK
Accutase® Enzyme	-	STEMCELL Technologies	Cambridge, UK
Bovine Serum Albumin	BSA	Sigma	Poole, UK
Carboxyfluorescein Succinimidyl Ester	CFSE	Molecular Probes (Invitrogen)	Paisley, UK
Chlorhexidine	-	Medipal	Leicestershire, UK
Collagenase Type 2	-	Sigma	Poole, UK
Dihydroethidium	DHE	Thermo Fisher Scientific	
Dimethyl Sulphoxide	DMSO	Sigma	Poole, UK
DMEM-High Glucose	-	Sigma	Poole, UK
DMEM-Low Glucose	-	Sigma	Poole, UK
DMEM+ High Glucose + Sodium Pyruvate	DMEM	Fisher Scientific	Leicestershire, UK
D-Valium	-	US Biological	Leicestershire, UK
Ethanol	-	YYY	
Evans Blue	-	MP Biomedical	California, USA
Fluorescein Isothiocyanate - Bovine Serum Albumin	FITC-BSA	Sigma	Poole, UK
Formalin – 10%	-	Sigma	Poole, UK
Gelatin - Type 1 from Porcine Skin	-	Sigma	Poole, UK
Glucose	-	Sigma	Poole, UK
Glutaraldehyde	-	Sigma	Poole, UK
Heat Inactivated Foetal Bovine Serum	FBS	Sigma	Poole, UK
Heparin Sodium Salt	-	Sigma	Poole, UK
Hydrogen Peroxide	H_2O_2	Sigma	Poole, UK
Hydromount	-	National Diagnostics	Hessle, UK

Material	Abbreviation	Manufacturer	Location
Interferon Gamma	IFN-γ	Creative Biolabs	New York, USA
Ketamine/ Medetomidine	Ket/Med	Vetoquinol	Northamptonshire, UK
L-Glutamine	-	Sigma	Poole, UK
Low Glucose Dulbecco's Modified Eagle Medium	-	BIOSERA	East Sussex, UK
Non-Essential Amino Acids	-	Invitrogen	Paisley, UK
Normal Saline	-	Sigma	Poole, UK
Magnesium Chloride	$MgCl_2$	Sigma	Poole, UK
MEM Alpha Modification	-	Sigma	Poole, UK
Modified Eagle Medium	MEM	Sigma	Poole, UK
Optimal Cutting Temperature Compound	OTC	Thermo Fisher Scientific	Leicestershire, UK
Petri Dish - 92 mm	-	Thermo Fisher Scientific	Leicestershire, UK
Penicillin/Streptomycin	P/S	Invitrogen	Paisley, UK
Phosphate Buffer saline	PBS	Invitrogen	Paisley, UK
Propidium Iodide	PI	eBiosciences	UK
Sodium Azide	-	Sigma	Poole, UK
Sodium Bicarbonate	$NaHCO_3$	Sigma	Poole, UK
Sodium Citrate	-	Sigma	Poole, UK
Sodium Phosphate Diphasic	Na_2HPO_4	Sigma	Poole, UK
Sodium Phosphate Monophasic	NaH_2PO_4	Sigma	Poole, UK
Sodium EDTA	Na. EDTA	Sigma	Poole, UK
Stem Cell Factor	SCF	Thermo Fisher Scientific	Leicestershire, UK
StemPro Supplement	-	Thermo Fisher Scientific	Leicestershire, UK
Tissue Culture Flask - 75 mm	-	Sigma	Poole, UK
Trypan Blue	-	Sigma	Poole, UK
Trypsin-EDTA	-	Invitrogen	Paisley, UK
Tumour Necrosis Factor - alpha	TNF-α	Life Technologies	Poole, UK
VetBond® Glue	-	3M	Minnesota, USA
Veet® Hair Removal cream	-	Reckitt Benckiser	Slough, UK
Vitamin Mix	-	Sigma	Poole, UK

2.2 Methods

2.2.1. Cell culture, cell preparation and cell labelling

2.2.1.1. Culture medium

The cell types used in this study that needed cultivation were murine vena cava endothelial cells (VCECs), human BM-derived MSCs Y201 (hBM-MSCs Y201), human BM-derived MSCs Y202 (hBM-MSCs Y202), human Wharton's jelly-derived MSCs (WJ-MSCs) and a murine embryonic-derived HSC line, HPC-7 (More details were stated later in this chapter). These cell types required their own specific media and were cultured using different methods as described below.

2.2.1.2. Cell counting

A standard Neubauer haemocytometer was used for cell counting. Cell suspensions were centrifuged and supernatants were removed. Cell pellets were re-suspended in 1ml of media. Trypan blue was added to the cell suspension in a ratio of 1:1 before counting to eliminate dead cells from the final count. Counting was assessed microscopically using an inverted light microscope with a x10 objective magnification. Viable cells were those that had not absorbed the blue dye and were counted in the four large corner squares of the haemocytometer (1x1 mm^2 fields). Dead cells were those that had taken up the blue dye and were therefore excluded from counting (Strober, 2015). Once total cell counts were obtained, the cell concentration was calculated using the following formula:

$$Total\ cell/ml = Total\ cells\ count \times \frac{Dilution\ Factor}{N\ of\ square} \times 10{,}000\ cells/ml$$

2.2.1.3. Culturing of murine vena cava endothelial cells

Immortalised murine VCECs were kindly provided by Dr. Jonathan S Alexander (Health Science Centre, Louisiana State University, USA). VCECs were thawed from a cryopreserved stock when required and cultured using an endothelial 'expansion media' containing 85.8% v/v deionised water, 0.96% w/v modified eagle media (MEM) D-valine powder, 0.22% w/v sodium bicarbonate, 10% v/v heat inactivated foetal bovine serum (FBS), 1% v/v penicillin/streptomycin, 1% v/v of MEM non-essential amino acids, 1% v/v of vitamin mix and 10 unit/ml interferon-γ (IFNγ). This endothelial expansion media was adjusted to pH 7.4. Cells were transferred into T75 culture flasks and incubated at 33.5°C in a 5% CO_2 humidified incubator to allow the cells to expand as previously described (Langley et al., 2003). Cells were split at a ratio of 1:3 when confluent which required them to be centrifuged at 400g for 5 minutes at room temperature. When actual experiments were to be conducted using the VCECs, they were cultured using a different 'experimental media' which was used instead of the expanding media. VCECs were cultured in high glucose (4,500 mg/L) Dulbecco's MEM (DMEM) combined with 10% v/v heat-inactivated FBS and 1% v/v penicillin/streptomycin and incubated at 37 in a 5% CO_2 humidified incubator to allow the cells to be in quiescent state as previously described (Langley et al., 2003). All cell culturing procedures were performed in a class II biological laminar flow hood using sterile techniques.

2.2.1.4. 2D culture of hematopoietic Stem Cells (HSCs)

The haematopoietic stem/precursor cells used in this study were an immortalised murine BM-derived hematopoietic precursor cell line called HPC-7s. They were kindly obtained from Professor Leif Carlsson (Umea Centre for Molecular Medicine, Umea University, Sweden). HPC-7 cells were originally generated by transfecting murine embryonic SCs with the LIM-Homeobox gene LHx2 (Pinto do et al., 1998). HPC-7s display many characteristics of primary HSCs, including early haematopoietic transcription markers such as SCL, c-myb, GATA-1 and PU.1, express common cell surface markers and are lineage negative (negatively expressed mature cell line markers such as CD4, CD8 for T lymphocytes and CD11b/CD18 for macrophages as previously described (Pinto do et al., 1998). In addition, the Kalia lab has demonstrated previously that HPC-7s express adhesion molecules known to be present on primary HSCs and have previously used HPC-7s to model hepatic, renal and myocardial HSC recruitment (Kavanagh et al., 2010). These cells were thawed from stock as required and cultured in StemPro-34 serum free media, topped with 10% v/v heat-inactivated FBS, 1% v/v P/S, 2mM L-glutamine, 2.5% v/v StemPro supplement and 0.02% v/v stem cell factor (White et al., 2013). Cells were seeded in T25 tissue culture flasks at a density of 1 x 10^6 cells/ml in suspension and maintained as such on a daily basis. They were centrifuged at 400g for 5 minutes at room temperature during the sub-culturing or passaging process and cultured at 37^{o}C in a humidified, 5% CO_2 controlled incubator. Cell culturing procedures were performed in class II biological laminar flow hood using sterile techniques.

2.2.1.5. 2D culture of mesenchymal stomal cells (MSCs)

Two different types of MSCs were used in this study namely human bone marrow (BM)-derived MSCs (hBM-MSCs) and human WJ-derived MSCs (WJ-MSCs). The hBM-MSCs used were an immortalised cell line that consisted of two MSC sub-populations, namely hBM-MSCs Y201 and hBM-MSCs Y202. These were kindly obtained from Professor Paul Genever (University of York, UK; please refer to https://web.expasy.org/cellosaurus/CVCLVG68 for further details on these cells). These sub-populations have been demonstrated, using multiparameter analysis, to be two distinct MSC sub-types despite both originating from the BM. The Genever group had isolated a heterogeneous population of hBM-MSCs (also called marrow stromal cells) and generated 4 phenotypically different immortalised clones (James et al., 2015).

Two of these clones, namely hBM-MSCs Y201 and hBM-MSCs Y202, were used in the current study and expressed typical MSC surface markers and were also negative for vascular markers. However, The Genever group had identified a number of differences between these two sub-populations. hBM-MSCs Y201 were a highly tri-lineage differentiating, $CD317^{neg}$ MSC subset, with expression of genes consistent with perivascular interactions in the BM. hBM-MSCs Y202 were a sub-population that included non-differentiating, $CD317^{pos}$ BM resident MSCs, which did not express genes associated with vascular interactions (James et al., 2015). The same group later demonstrated that hBM-MSCs Y202 cells were less effective at suppressing $CD4^{+}$ T cell proliferation and polarised more of these lymphocytes after 5 days co-culture into a sub-population of T helper cells with a more pro-inflammatory profile when compared to Y201 cells (Kay et al., 2018). These two sub-types were therefore used in the current study as they were both BM-derived MSCs, yet possessed remarkably different

structural and functional characteristics. These details have been summarised later in **Chapter 3, Table 3.1**. Both types of hBM-MSCs were cultured using 500ml of DMEM topped with 0.9% v/v L D-glucose, pyruvate, L-glutamine, 10% v/v FBS and 1% v/v penicillin/streptomycin.

WJ-MSCs obtained from the umbilical cord of humans which were kindly provided by the research group of Professor Gerard Nash (Institute of Cardiovascular Sciences, University of Birmingham) and used in compliance with the ethical standards subscribed to by this group. The study was conducted in compliance with the Declaration of Helsinki. All human samples were obtained with written, informed consent and approval from the North East – Tyne and West South Research Ethics Committee (REC 15-NE-0285). Umbilical cords were collected from anonymous donors with the assistance of the Birmingham Women's Health Care NHS Trust and Sandwell and West Birmingham Hospitals NHS Trust. They were cultured in media contained 500ml of low glucose (1g/L) DMEM, with L-glutamine, 10% v/v heat inactivated FBS, and 1% v/v penicillin/streptomycin. Cells were seeded in tissue culture T75 flasks and cultured at 37^{o}C in a humidified, 5% CO_2 controlled incubator.

To sub-culture WJ-MSCs, hBM-MSCs Y201 and hBM-MSCs Y202, the cell suspension was centrifuged at 400g for 5 minutes at room temperature, transferred into T25 culture flasks and incubated at 37˚C in a 5% CO_2 humidified incubator. To measure the cell size, MSCs were dissociated from the flasks with the Accutase® enzyme. After that, 1 ml of cell suspension was transferred onto the glass slide. A total of 50 cells were counted from 5 randomly selected fields of view and imaged microscopically using an x20 magnification with an EVOS microscope. Experiments for each kind of cell were repeated two times with two different cell donors. The size of these various stem cells was measured and analysed using ImageJ software. The data were presented as the average cell diameter±SEM.

2.2.1.6. 3D culture of HSCs and MSCs

MSCs and HSCs were cultured in a 3D, sphere forming system using a hanging drop method, that did not required the addition of exogenous chemicals, as previously described (Bartosh and Ylostalo, 2014). Firstly, all stem cells were proliferated using the conventional 2D culture method, until they reached 80% confluency, after which 3D cultures were set up. Cell suspensions of HSCs, WJ-MSCs, hBM-MSCs Y201, and hBM-MSCs Y202 were then produced to yield a concentration of $1.5x10^6$ cells/ml (sufficient to produce 40-60 spheres if needed). This was then diluted using culture media for each type of cells to yield 714 cells/µl. Using a pipette, 35µl droplets of this suspension which finally consisted of 25,000 cells were dispensed onto the inverted lid of a 150mm petri dish. Many droplets could be comfortably added to each petri dish lid. 10ml of PBS was added to the bottom of the petri dish to create a water chamber. The lid on which the stem cell droplets were added was then carefully flipped so as to cover the petri dish, allowing the pinnacle of the droplets to face downward. Petri dishes were incubated at 37˚C in a 5% CO_2 humidified incubator for 1-2 days (**Figure 2.1A**). The hanging drop technique allowed cells to aggregate and form homogenous 3D spheres at the apex of the droplet suspension (**Figure 2.1B**). The size of the cells was measured as previously described in **section 2.2.1.5.** The data were presented as the average of cell diameter±SEM.

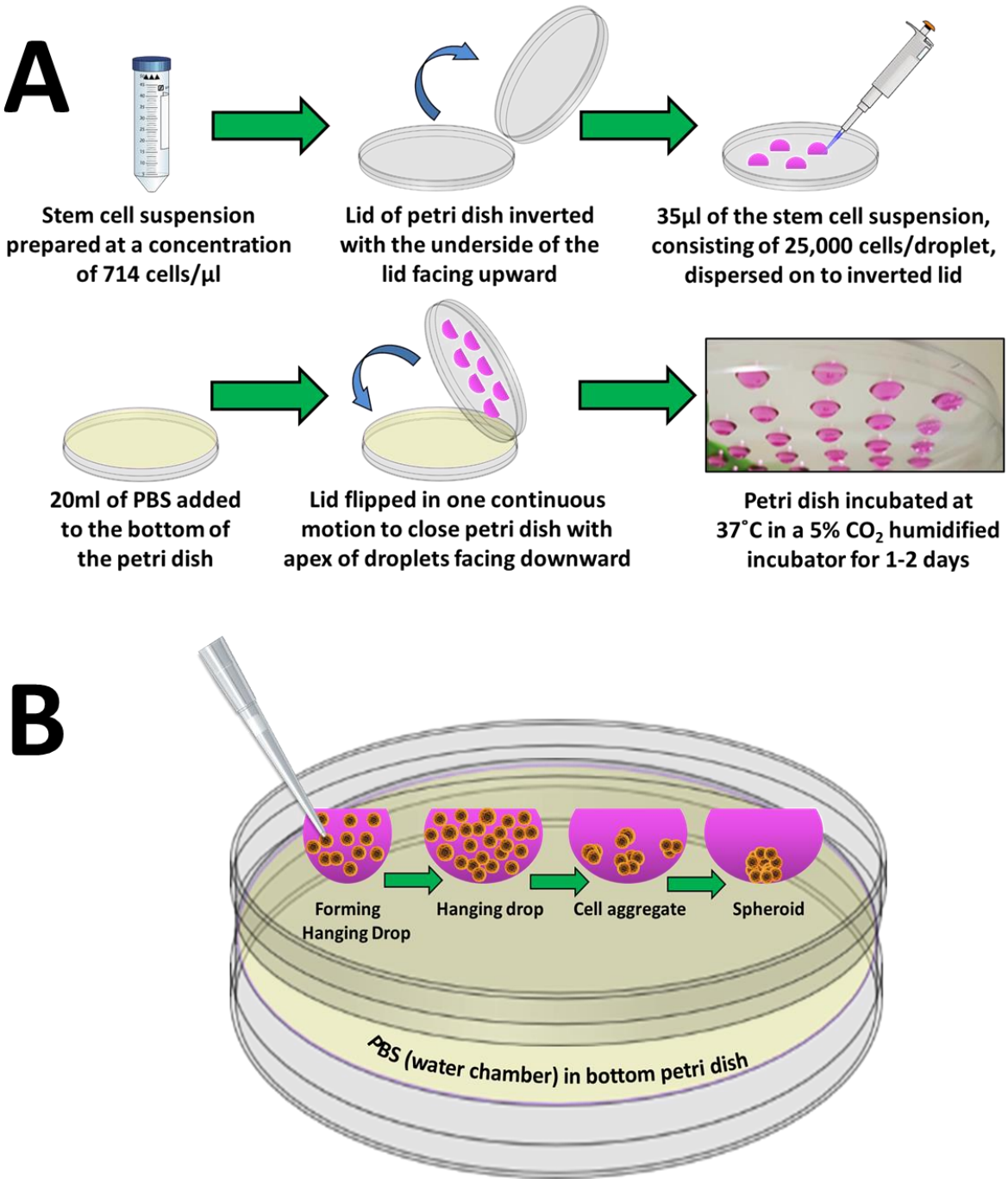


Figure 2.1. Illustration of the hanging drop method used for generating 3D spheroid cultures of HSCs, WJ-MSCs, hBM-MSCs Y201 and hBM-MSCs Y202. (A) The schematic outlines the various steps required for performing the hanging drop method in which each drop had a stem cell concentration of 25,000cells/droplet. **(B)** Following incubation, the stem cells within the droplets began to aggregate until 3D spheres formed at the apex of the cell suspension droplets.

2.2.1.7. Preparation of CFSE-labelled fluorescent stem cells

Fluorescent labelling of stem cells was carried out using the 5,6-carboxyfluorescein diacetate succinimidyl ester (CFDA-SE). This chemical substance is a non-fluorescent, highly cell-permeable fluorescein, It is altered by intracellular esterase enzymes and converted into the fluorescent carboxyfluorescein succinimidyl ester (CFSE), which is impermeable to the cell membrane, locking it within the cell. CFSE is a very useful fluorescent intracellular dye which can be used for staining numerous types of cells including stem cells and leukocytes (Hsu et al., 2015).

To prepare stem cells for labelling, the desired number of HPC-7s, WJ-MSCs, or 2D and 3D cultured hBM-MSCs Y201 or Y202 MSCs were centrifuged at 400g at room temperature for 7 minutes and then washed with 2ml of PBS. This process was repeated twice. Stock CFDA-SE was diluted in DMSO to obtain a concentration of 10mM and aliquoted in micro-Eppendorf tubes for future use. Whilst waiting for the cells to spin down, aliquoted CFDA-SE was thawed at room temperature and kept away from the light. 2µl of 10mM CFDA-SE was added to 2ml of PBS to obtain the final staining solution at 10µM. 2ml of this prepared CFDA-SE solution was added to 2ml of the cell suspension, leading to a total volume of 4ml at 5µM of concentration of CFDA-SE. The labelled cell solution was then incubated for 15 minutes at 37°C in the dark. After incubation, 6ml of culture media was added to stop the binding of excess CFDA-SE and cells were again centrifuged 400g for 5 minutes at 37°C. The resultant supernatant was removed, and the pellet re-suspended with 2ml culture medium and centrifuged again at 400g. This process was repeated twice with culture medium to remove excess CFDA-SE. Cells were suspended at the desired concentration and ready for

the experiments. CFDA-SE labelled cells were visible as bright green cells using a 488nm emission wavelength.

2.2.2. Investigation of stem cell adhesion to various substrates *in vitro*

Studies were performed to assess the adhesive capacity of stem cells to various substrates *in vitro*. These included testing adhesion to snap frozen sections of heart tissue obtained from mice undergoing sham or myocardial IR injury, TNFα-stimulated or non-stimulated VCECs and also to immobilised endothelial counterligand proteins, ICAM-1 and VCAM-1.

2.2.2.1. Tissue preparation and cryosection of frozen murine hearts

Details on the surgical procedures performed on mice can be found later in **Section 2.2.5.1**, **2.2.5.2, 2.2.5.3** and **2.2.5.4** as previously described (Kavanagh et al., 2018). Briefly, hearts were obtained from male C57BL/6 mice (Harlan, Oxfordshire, UK) that underwent either sham surgery or myocardial IR injury. Mice were anaesthetised with 100 mg/kg ketamine hydrochloride (Zoetis UK, UK) and 10mg/kg xylazine hydrochloride (Chanelle Animal Health, UK) intraperitoneally. Myocardial IR injury was induced in the beating left ventricle by reversible ligation of the left anterior descending (LAD) coronary artery for 45 minutes followed by reperfusion for 2 hours. After sacrifice, hearts were removed and mounted on a small volume of optimal cutting temperature (OCT) compound added to corkboard and immediately snap frozen in liquid nitrogen and stored at -80^{o}C until use. 8µm tissue sections were sliced from the sham or injured left ventricle, incorporating the area of injury, using a

microtome-cryostat (Bright Instrument, UK) and transferred onto glass slides which were then air-dried and fixed in acetone for 10 minutes. To store the slides, samples were wrapped in research grade aluminium foil and stored at -20^{o}C until use.

2.2.2.2. Stamper-Woodruff (SW) heart tissue section *in vitro* adhesion assay

Modified SW adhesion assays allowed quantification of stem cell adhesion to frozen tissue sections *in vitro* (Stamper and Woodruff, 1976). For 2D cultured MSCs, 1ml of 0.25% w/v Trypsin/EDTA was added to the flask to detach cells from the plastic bottom. For 3D cultured MSCs, the spheres were collected from the petri dish lids and aspirated into a 15ml corning tube and washed with PBS. To dissociate the spheres into single cells, 2ml Stem pro Accutase® enzyme was added to the tube and incubated at room temperature for 10 minutes. After the incubation, the suspension was pipetted up and down until the spheres dissociated into single cells. Cells were then labelled with CFDA-SE following the protocol mentioned in **Section 2.2.1.7**. The number of fluorescently labelled cells was counted as described in **Section 2.2.1.2** to obtain the desired concentration.

Slides of frozen heart sections were thawed at room temperature for 20 minutes and then placed in a humidified chamber. 1x10^{5} CFSE-labelled cells / 100µl culture media was carefully added to each tissue section and incubated for 1 hour on an orbital shaker at room temperature. After this incubation, slides were submerged in PBS to remove non-adherent stem cells and media, fixed with 100% v/v acetone for 5 minutes and washed with PBS again to remove the excess acetone. Finally, once dry, slides were mounted using non-fluorescein Hydromount. The numbers of adherent cells were counted from 5 randomly selected fields

of view imaged microscopically using an x20 objective of an EVOS fluorescent cell imaging system microscope (Thermo Fisher Scientific). Firstly, the centremost field of view was imaged and then 4 additional regions above, below and to the left and right of this field were imaged. This allowed for the avoidance of bias (**Figure 2.2**).

2.2.2.3. Endothelial cell *in vitro* adhesion assay

The protocol was used as previously described (Kavanagh et al., 2013). VCECs were expanded on gelatin-coated plates at 33.5^{o}C using the expansion media described earlier in **Section 2.2.1.3**. For experiments, 25,000 VCECs were added to gelatin coated 24 wells plate and incubated until confluent at 37°C in experimental DMEM. To activate VCECs, 100ng/ml of TNF-α was added to each well and incubated at 37°C for 4 hours. For control experiments, the vehicle PBS was added. Single cell suspensions at a concentration of 5x10^{4} cells of either 2D or 3D cultured HPC-7s, WJ-MSCs, hBM-MSCs Y201 and hBM-MSCs Y202 MSCs were incubated with VCECs for 20 minutes at 37°C as shown in **figure 2.3**. Plates were washed 3 times with PBS to remove non-adherent cells prior to imaging. Experiments for each group were repeated in triplicate. The average number of adherent cells from 10 random fields of view per well was determined after imaging microscopically using a x20 magnification and an EVOS microscope.

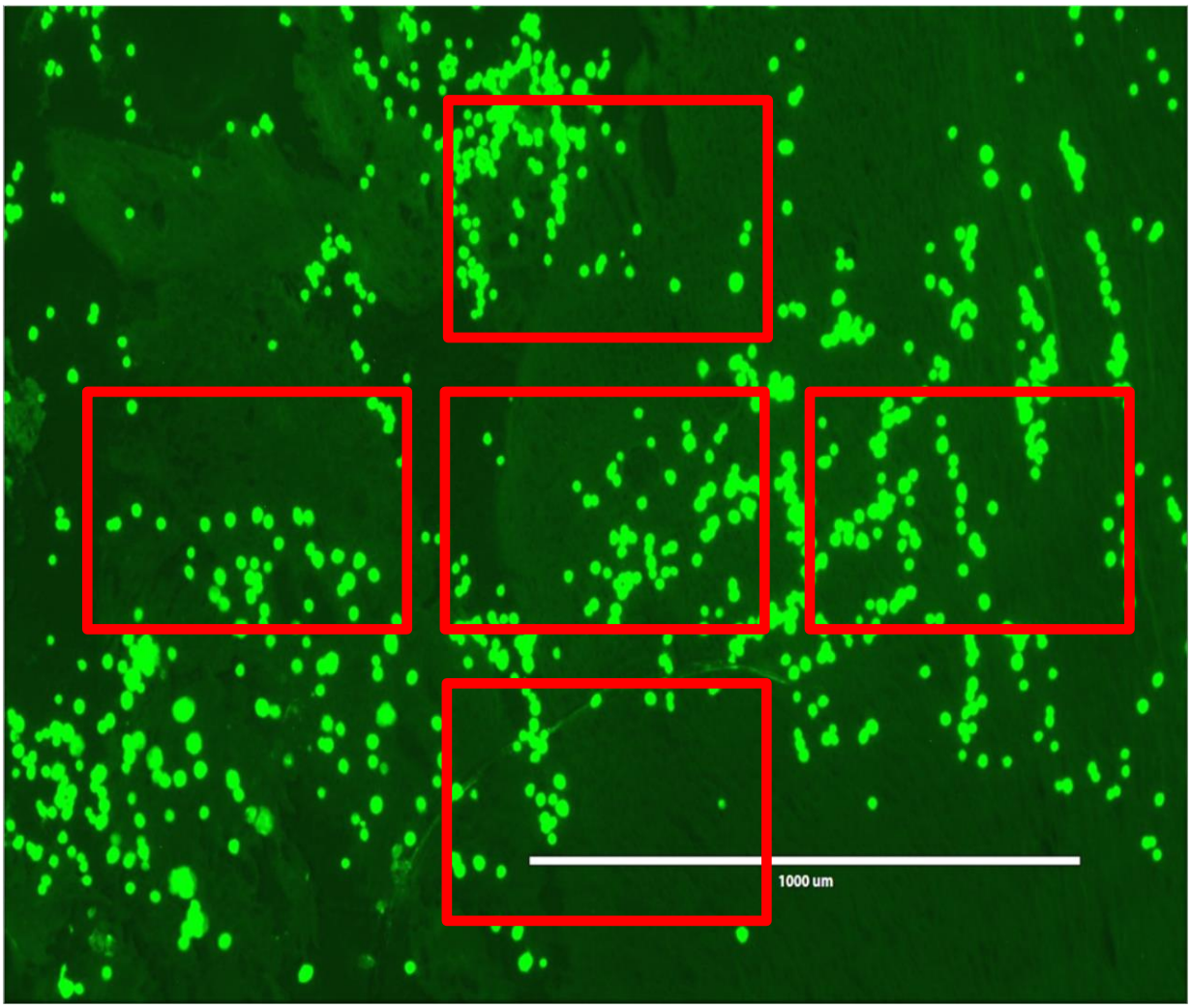


Figure 2.2. Selection criteria used for quantitative and qualitative analysis of stem cell adhesion to frozen heart tissue sections *in vitro*. Adherent cells within 5 randomly selected fields of view (red squares) were counted to quantitate their adhesion using the *in vitro* Stamper-Woodruff frozen tissue adhesion assay. The area in the middle of the tissue was chosen as the first selected area and imaged. 4 additional regions on the left, right, above and below of the first region were also chosen to quantitate cell adhesion within. The same criteria were used to quantitate cell adhesion on vena cava endothelial cells and on immobilised ICAM-1/VCAM-1 protein in vitro. The image is a representative frozen heart tissue section showing CFSE-labelled stem cells adherent on it and was captured using an EVOS microscope at 4X magnification. Scale bar = 1000 µm.

2.2.2.4. Immobilised ICAM-1 and VCAM-1 protein *in vitro* adhesion assay

96-well plates were coated with 10 µg/ml of recombinant murine intercellular adhesion molecule-1 (ICAM-1) or 10 µg/ml of recombinant murine vascular cell adhesion molecule-1 (VCAM-1) for 1 hour at room temperature (Kavanagh et al., 2015). Wells with 1% v/v bovine serum albumin (BSA) were set as a negative control. Plates were washed with PBS 3 times and the non-coated area of the well base blocked with 1% v/v BSA for 5 minutes. Wells were then washed 3 times with PBS and $5x10^4$ of either 2D or 3D cultured HPC-7s, WJ-MSCs, hBM-MSCs Y201 and hBM-MSCs Y202 were added to each well and incubated with the coated plate for 20 minutes at 37°C. After incubation, the plate was washed with PBS three times and the cells fixed to the immobilised proteins using 2% v/v glutaraldehyde at 37°C for 15 minutes. Plates were rewashed after which 100µl of PBS was added to the wells prior to imaging. Again, experiments for each group were performed in triplicate. The average number of adherent cells from 3 random fields of view per well was determined after imaging microscopically using a x20 magnification and an EVOS microscope. Adherent cells were quantified and represented as a proportion of the cell adhesion on negative controls.

2.2.3. Flow cytometry and confocal studies to investigate surface adhesion molecules and chemokine receptors on 2D and 3D cultured hBM-MSCs

2.2.3.1 Flow cytometry studies of 2D and 3D cultured hBM-MSCs

Flow cytometry was used to assess the surface expression of CD18 (integrin sub-unit β2)), integrin sub-unit β7, CD44, ICAM-1 (CD54), VCAM-1 (CD106) and CXCR4 (receptor for the

chemokine SDF-1α) on 2D and 3D cultured MSCs. Cells were dissociated from monolayers grown in conventional 2D culture plates or from spheres grown in 3D cultured, washed twice with PBS and then centrifuged at 300g for 5 minutes. Pellets were re-suspended in cold FACs buffer to reach a concentration of $1x10^5$ cell/ml (PBS, 5% v/v FBS, 0.1% v/v NaN_3) and incubated for 15 minutes on ice to block the Fc receptor to reduce non-specific binding. After blocking, 200µl of the cell suspension was transferred to eppendorf and incubated with a fluorochrome-conjugated primary antibody (dilution 1:100) for 30 minutes in darkness and on ice before performing flow cytometry analysis (Ise et al., 2019). Cells were stained with propidium iodide (PI).

Antibodies used were mouse anti-human PE-conjugated anti-CD18, mouse anti-human FITC conjugated integrin sub-unit β7, rat anti-human FITC conjugated anti-CD44, mouse anti-human FITC conjugated anti-ICAM-1, mouse anti-human FITC conjugated anti-VCAM and mouse anti-human FITC conjugated anti-CXCR4. After incubation, cells were washed two times with FACS buffer and then re-suspended in 300µl of FACS buffer solution. Samples were analysed using a FACSCalibur flow cytometer with analysis conducted on 10,000 cells/events. Flowing software 2.5.1 (University of Turku, Finland) was used to visualise the data. Cells were gated using side scatter (SSC) vs forward scatter (FS). Individual populations were then gated on before identifying and eliminating cells that have joined together using pulse width vs FS. Live cells (PI-) were gated and shown by FS and SSC. These viable cells were gated on FL-1+ or FL-2+ events to evaluate the presence of molecules assessed in this study. Histograms were generated, representing the negative control and the positive test allowing for quantification of cell adhesion molecules. The expression of cell adhesion molecule were quantified and presented as the percentage of total number of cell count.

The percentage of cells expressing cell adhesion molecules was determined by calculating those with adhesion molecule expression compared to the total number of cells.

2.2.3.2. Confocal microscopy imaging of 2D and 3D cultured hBM-MSCs

The pattern of expression of these same molecules was assessed confocally on 2D and 3D cultured MSCs fixed with 5% v/v formalin solution for 30 minutes. After fixation, cells were washed 3 times with 2% v/v PBSA and then incubated in PBSA for 30 minutes at room temperature to reduce unspecific binding. Following incubation, cells were suspended in cold mouse anti-human PE-conjugated anti-CD18, mouse anti-human FITC conjugated integrin β7**,** rat anti-human FITC conjugated anti-CD44, mouse anti-human FITC conjugated anti-ICAM-1, mouse anti-human FITC conjugated anti-VCAM and mouse anti-human FITC conjugated anti-CXCR4 antibody at 1:50 dilution in the dark on ice for 60 minutes (Kavanagh et al., 2013). After antibody incubation, cell suspensions were washed 3 times with 2% v/v PBSA. Labelled cells were allowed to settle onto gelatin-coated coverslips overnight at 4^{o}C and then mounted with Hydromount agent. Glass coverslips were coated with gelatin to increase cell adhesion onto their surface prior to confocal microscopic analysis. 22mm^2 glass coverslips (Pearl, UK) were placed in the 24 well plates. 400µl of 0.1% w/v gelatin was added to each well to coat the surface of the coverslips and then incubated for 10 minutes at the room temperature. Coated coverslips were air-dried and stored at room temperature before use. Slides were imaged using the Zeiss 780 Zen Laser scanning confocal microscope (Zeiss, US) with 40x magnification water immersion lens. All images were captured using LSM Zen 2009 software (Zeiss, US) and were analysed off-line using the ImageJ program (NIH, US).

2.2.4. Murine endothelial cells + hBM-MSCs co-culture experiments *in vitro*

2.2.4.1. Endothelial cells + hBM-MSCs co-culture

These experiments were conducted to investigate the ability of 2D and 3D cultured hBM-MSCs Y201 and hBM-MSCs Y202 to reduce hydrogen peroxide (H_2O_2) mediated oxidative damage of VCECs *in vitro* as previously described (Kavanagh et al., 2019). To set up the assay, immortalised mouse VCECs were seeded in 24 well plates with 1 ml of high glucose DMEM media and incubated at 37°C in a humidified, 5% CO_2 incubator. Once confluent, the culture media was removed, the wells were washed three times with PBS and 1ml of fresh media was added. In some wells, $5x10^4$ of either 2D or 3D cultured hBM-MSCs Y201 or hBM-MSCs Y202 were seeded with the VCECs. 110µl of 100µM H_2O_2 was added to all wells to form a final concentration of 10µM H_2O_2 to induce oxidative damage of the VCECs (Liu et al., 2010). The last three steps were repeated every 24 hours, with the experiments lasting 72 hours overall. At 72 hours, VCECs were stained to determine how much ROS had been generated (using dihydroethidium) and the degree of VCEC oxidative damage (using 8-OHdG staining) and whether the stem cells were able to reduce these events (**Figure 2.3**).

2.2.4.2. Quantification of reactive oxygen species using Dihydroethidium in endothelial cells + hBM-MSCs co-culture experiments *in vitro*

These experiments were conducted to assess the ability of 2D and 3D cultured hBM-MSCs Y201 and hBM-MSCs Y201 to modify ROS generation from H_2O_2 injured VCECs using the

superoxide sensitive dye dihydroethidium (DHE). DHE is a cell permeable, fluorescent probe commonly used to detect intracellular superoxide. In the presence of superoxide in living cells, DHE is oxidised to 2-hydroethidium which is further converted to ethidium, that intercalates with nucleic acids staining them a bright fluorescent red (Chen et al., 2013). DHE is specifically used to detect superoxide since other types of ROS, (such as the hydroxyl radical, singlet oxygen, and alpha-oxygen) do not oxidise DHE. Following the co-culture method described in **Section 2.2.4.1**, the culture media containing the hBM-MSCs was once again removed, wells were washed with PBS and then 500µl of 10 µM of DHE solution was added as previously described (Kavanagh et al., 2019). Plates were incubated at 37°C, 5% CO_2 in the dark for 30 minutes. The wells were then washed thoroughly with PBS and 500µl of PBS was added to all wells. This experiment was repeated three times. Images were taken with an EVOS fluorescence microscope with a x20 objective lens. Five images per field were taken for each well as shown in **Figure 2.4A**.

2.2.4.3. Quantification of oxidative stress using 8-OHdG labelling in endothelial cells + hBM-MSCs co-culture experiments *in vitro*

These experiments were carried out to investigate the ability of 2D and 3D cultured hBM-MSCs Y201 and hBM-MSCs Y201 to protect H_2O_2 injured VCECs from oxidative damage by staining for 8-hydroxygaunine (8-OHdG). 8-OHdG is a specific marker for oxidative damage of DNA and RNA. Following the co-culture method described in **Section 2.2.4.1**, the culture media containing the hBM-MSCs was once again removed and wells were washed with PBS.

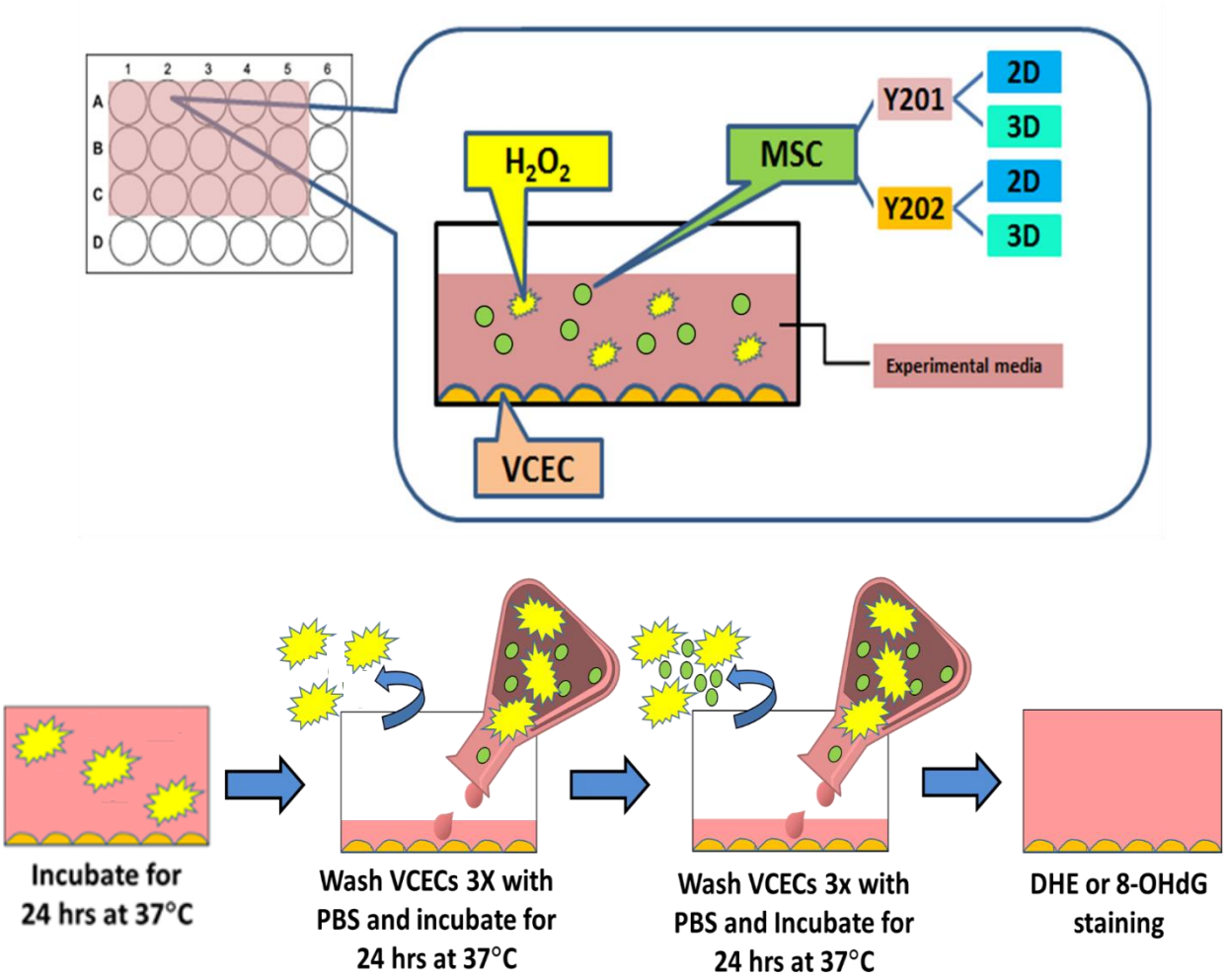


Figure 2.3. Murine endothelial cell + hBM-MSC co-culture assay. VCECs (orange) were seeded in 24 well plates with 1ml high glucose DMEM media topped with 1% v/v penicillin/streptomycin and 10% v/v FBS and incubated at 37˚C in a humidified, 5% CO_2 incubator. Once confluent, culture media (pink) was removed, the wells were washed three times with PBS and 1ml of fresh media was added to each well. In some wells, $5x10^4$ of either 2D or 3D cultured hBM-MSCs Y201 or hBM-MSCs Y202 (green) were seeded with the VCECs. 500µl of 10µm H_2O_2 (yellow) was added to all wells to induce oxidative damage of the VCECs. The last three steps were repeated every 24 hours, with the experiments lasting 72 hours overall. After 72 hours, VCECs were stained to determine how much ROS had been generated (using dihydroethidium) and the degree of VCEC oxidative damage (using 8-OHdG staining) and whether the stem cells were able to reduce these events.

Following the protocol described by Kavanagh and colleagues, VCECs were fixed and permeabilised with 300µl of 70% v/v ethanol and incubated for 1 hour at -20°C (Kavanagh et al., 2019). After cell fixation, the alcohol was removed and the plates were washed in PBS. To block non-specific binding of IgG to Fc receptors, 300µl of the blocking agent (anti-CD16/CD32 diluted to a ratio of 1:500) was added to the wells and incubated at room temperature for 30 minutes. The blocking solution was then removed and the plates were washed thoroughly with PBS. The wells were incubated with 1:500 dilution of the primary anti-8-OHdG antibody for 1 hour in the dark at room temperature. Wells were again washed with PBS and incubated with 1:250 dilution of the secondary Alexa Fluor 488 donkey anti-goat antibody in the dark at room temperature for 1 hour (Kavanagh et al., 2019) (**Figure 2.4B**).

2.2.4.4. Analysis of endothelial cell + hBM-MSC co-culture experiments *in vitro*

Images were taken using an EVOS fluorescence microscope with the 20x objective lens. Five images per field were taken for each well. Images analysis was conducted using ImageJ software. The area of absent and low-intensity colour was excluded from the analysis using the threshold modifier function. The formula used to calculate the mean fluorescence intensity was the area of intensity multiplied with mean intensity. The fluorescence intensity of the experimental groups containing 2D and 3D cultured hBM-MSCs MSCs Y201 and hBM-MSCs Y202 was compared to the control group of VCECs in which no stem cells were added. The data are expressed as mean fluorescence intensity±SEM.

2.2.5. Intravital microscopy studies of the IR injured beating mouse heart to image hBM-MSC trafficking and their vasculoprotective effects *in vivo*

State-of-the-art confocal-based intravital microscopy (IVM) was used to image the kinetics of hBM-MSC trafficking to and through the beating heart coronary microcirculation in anaesthetised sham and IR injured mice *in vivo*. Specifically, the impact of 2D and 3D culture on the numbers of hBM-MSCs free flowing through or becoming firmly adherent within the heart microvasculature was assessed. Furthermore, novel beating heart intravital imaging was also used to assess whether hBM-MSCs could prevent the thromboinflammatory disturbances previously described by us intravitally to take place in the IR injured heart *in vivo* (Kavanagh et al., 2019). Specifically the ability of 2D and 3D cultured hBM-MSCs to prevent neutrophil recruitment and platelet aggregation and restore coronary capillary perfusion was assessed.

2.2.5.1. Animals

All animals studies were approved by the University of Birmingham Ethics Committee and the United Kingdom Home Office, in accordance with the Animals (Scientific Procedures) Act of 1986 (ASPA 1986) under Project Licences P552D4447 and P95F9B96 (held by Dr Neena Kalia). 8-12 week old male C57BL/6 mice, housed at the Biomedical Services Unit (University of Birmingham) were used at a body weight ranging between 25-32g. All mice were provided with food and water *ad libitum.*

2.2.5.2. Pre-surgical preparation

All surgical instruments were sterilised using a hot air autoclave before use. Furthermore, the downdraft surgical table and surgical stereomicroscope was also disinfected using chlorhexidine. General anaesthesia was induced by an intraperitoneal injection of a combination of Ketamine hydrochloride (100mg/kg) and Medetomidine hydrochloride (100mg/kg). The depth of surgical anaesthesia was monitored every 10 minutes throughout surgery by checking the pedal reflex (firm toe pinch). Maintenance anaesthesia was introduced intra-peritoneally as and when required. Prior to surgery, the hair over the neck and left thoracic regions of the mouse was removed using a surgical hair clipper and Veet® hair removal cream. Once exposed, the underlying skin was disinfected using chlorhexidine. The mouse was then placed on a specially designed surgical board which contained a heating pad linked to a temperature monitor which was adjusted to maintain the mouse body temperature at around 37°C. Body temperature was measured using a rectal probe (**Figure 2.6**). The surgical board was designed so that the mouse could easily transfer from the surgical area to the intravital microscope stage.

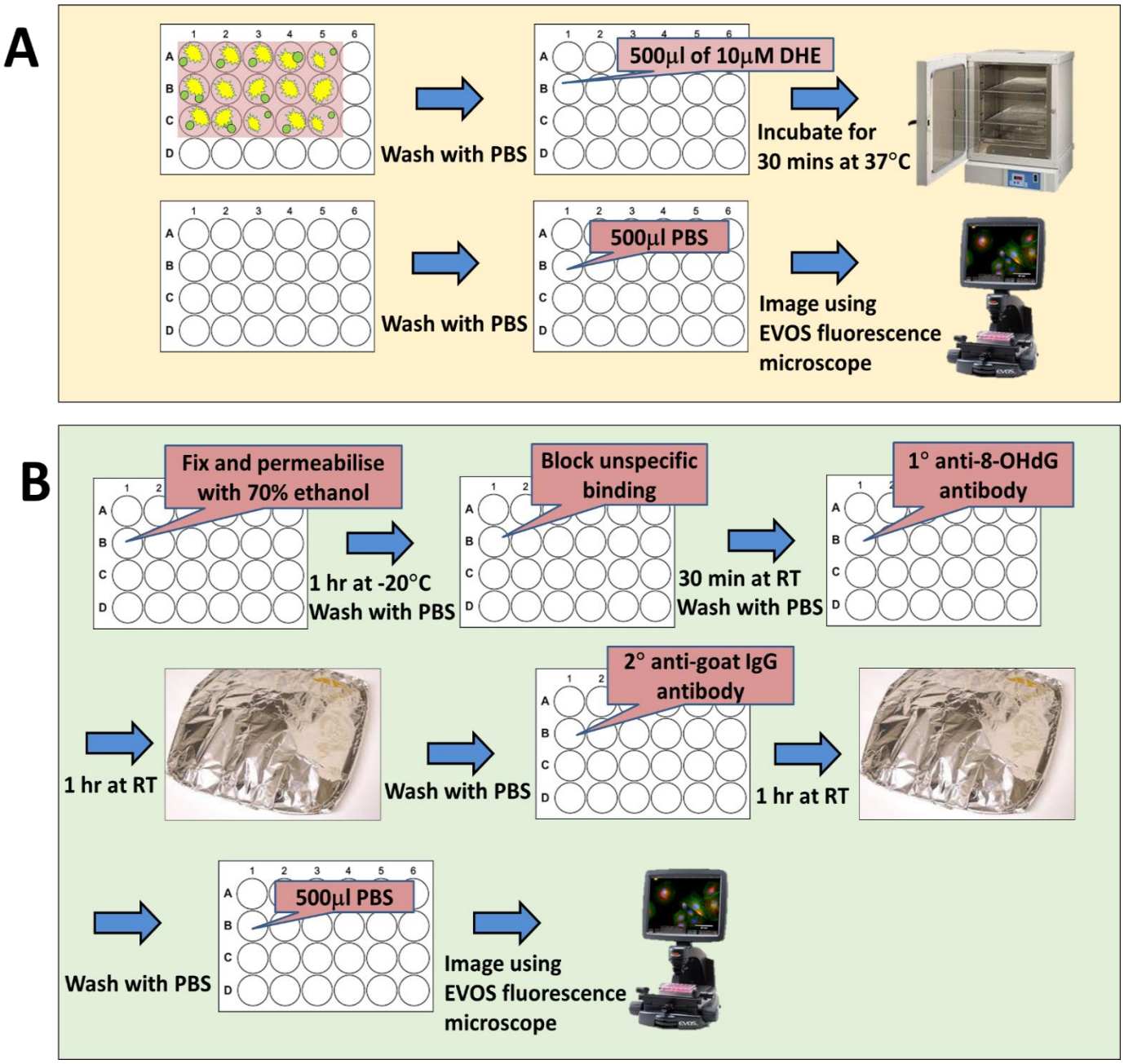


Figure 2.4. Protocols for quantification of ROS (Superoxide) generation using dihydroethidium and VCEC oxidative stress using 8-OHdG labelling. (A) DHE, a cell permeable fluorescent probe, was used to detect intracellular superoxide generation. In the presence of superoxide, it intercalates with nucleic acids and emits a bright fluorescent red (green icons are MSCs and yellow icons are H_2O_2). **(B)** 8-OHdG is a specific marker for oxidative damage of DNA and RNA. A primary anti-8-OHdG antibody and secondary Alexa Fluor 488 donkey anti-goat antibody was used to detect oxidatively damaged VCECs. At the end of the both protocols, images were taken with an EVOS fluorescence microscope with the 20x objective lens. Five images per field were taken for each well.

2.2.5.3. Induction of myocardial IR injury

The anaesthetised mouse was artificially ventilated using a small rodent ventilator (MiniVent®, Biochrom Ltd., Harvard Apparatus) which allowed control of the respiratory rate, pressure and stroke volume of the anaesthetised mouse. Endotracheal intubation was used to connect the ventilator to the mouse. An incision was made along the midline of the neck to expose the trachea. The anterior aspect of a tracheal cartilage was cut to expose the inner side of the trachea. A respiratory tube, which was attached to the ventilator, was passed into the trachea towards the lungs, allowing the ventilator to control lung function. A knot made with a 5-0 suture was used to secure the connecting respiratory tube within the trachea. The ventilator was connected to an oxygen generating machine which delivered a continuous flow of medical grade oxygen at a rate of 130 breaths per minute and a stroke volume of 220µl. Expiratory lung gases during the expiration portion of the respiratory cycle were released through an expiratory tube. The lungs were at atmospheric pressure during these procedures. Peak end expiratory pressure (PEEP) is a pressure applied by the ventilator at the end of each breath to prevent the alveoli from collapsing. A PEEP system was established by placing the end of the respiratory tube 3-5 cm under the surface of water contained in a 15 ml corning tube.

Once artificial ventilation had been achieved, the left carotid artery was then exposed. After the vagus nerve was separated from the artery, a 5-0 suture was placed at the end closest to the head and tied off. The other end of the artery was clamped using an atraumatic mini arterial clamp. A small incision was made in the artery between the clamp and the suture. A cannula, attached to a 1ml syringe filled with PBS, was then passed into the artery and securely tied in place using suture. The arterial clamp was then removed. This intra-arterial

cannula allowed for the injection of fluids, fluorescent dyes/antibodies or stem cells into the mouse as and when required.

An incision was then made in the left thoracic region to expose the pectoral muscles covering the left ribcage and chest wall. The pectoral muscles in this region were removed using a cautery pen in order to gain access to the 3rd and 4th chest ribs. A further incision was made between the 3rd and 4th ribs using castro-viejo scissors to expose the underlying heart – this incision was kept open using a retractor. The surrounding pericardial sac was then removed from the heart. A surgical stereomicroscope was used to identify the LAD coronary artery on the surface of the beating left ventricle and an 8-0 suture was passed gently through the muscle underneath it. The LAD was then temporarily tied against a small piece of 1mm diameter plastic tubing protecting the heart muscle from direct damage from the suture (**Figure 2.6A**). This induced ischaemia to downstream regions of the heart supplied by the LAD artery. The occlusion of the LAD artery was confirmed by the change of colour of the anterior wall of left ventricle below the ligation point to a very pale pink within seconds after ligation. The ischaemic period was allowed to persist for 45 minutes. The thoracic cavity was closed temporarily during the ischaemic process by placing a small piece of wet gauze in the cavity and covering the wound with Saran wrap. After 45 minutes, the ligation was removed to allow reperfusion of blood within the left ventricle for 2-2½ hours. Reperfusion was confirmed by the return of red colour to the anterior wall of the left ventricle after 10 seconds. Thereafter, mice were culled via an appropriate Schedule 1 method. The heart and lungs were harvested for use in experiments detailed later. Sham mice underwent the same surgery as the IR injured mice except the LAD artery was not occluded.

2.2.5.4. Intravital imaging of beating mouse heart *in vivo*

In order to image the sham or IR injured anaesthetised mouse beating heart, an in-house designed and 3D printed stabiliser was attached to the surface of the exposed left ventricle in a region below the LAD ligation point. The 3D printed stabiliser was a ring-shape PLA plastic structure which was required to stabilise a small area of the left ventricle and allow subsequent intravital imaging of the coronary microcirculation on the epicardial side of the muscle. The stabiliser had an internal and external diameter of 2.25mm and 4mm respectively. Motion was sufficiently reduced in the x-y plane such that high-quality imaging of the epicardial coronary microvasculature could be obtained. Importantly, the rest of heart continued to beat normally. The stabiliser was a modified version of one previously described by Lee and colleagues (Lee et al., 2012).

As soon as the LAD artery was un-ligated and reperfusion initiated, a micromanipulator, on to which the arm of the stabiliser was attached, was used to gradually approach the stabiliser towards the left ventricle and attach it using Vetbond®, highly effective biological glue (**Figures 2.6B-C**). It was not possible to attach the stabiliser whilst the LAD artery ligation was still in place; hence why this procedure was performed after the ligation was removed. The central area was kept moist by application of 0.9% w/v saline with the surrounding area covered with saran wrap to prevent loss of moisture. As it took ~20-30 minutes before the beating heart was ready for imaging, the first recording lasting 2 minutes took place from a pre-selected field of view (413µm x 308µm) at 30 minutes post-reperfusion. This also allowed for consistency with regards acquisition of the first intravital recording between experiments. 2-minute videos were subsequently taken every 15 minutes from the same area for 2-2½ hours. This was accomplished using

a Nipkow spinning disk confocal head (Yokogawa CSU, Japan) connected to an upright BX61WI Olympus® microscope with an Evolve EMCCD camera (Photometrics, USA) and a x20 objective lens (Olympus, Japan). The spinning disc head attachment contained 10,000 pinholes in the first spinning disk and with a second disk with also 10,000 of microlens to focus the excitation laser light into each corresponding pinhole. Two disks spun to rapidly scan the field of view, which allowed the rapid moving cells within microcirculation to be captured at the high frame rate (Kavanagh et al., 2019). All data was captured, stored and analysed using Slidebook 6 software (Intelligent Imaging Innovations, USA). Once the intravital experiment was complete, tissue harvesting was conducted of organs of interest (heart and lungs) to be utilised in experiments detailed later.

2.2.5.5. Imaging and quantification of hBM-MSC trafficking to the IR injured beating heart *in vivo*

To intravitally track the homing of hBM-MSCs to the beating heart, $5x10^5$ CFSE-labelled 2D or 3D cultured hBM-MSCs Y201 or hBM-MSCs Y202 in 200µl PBS were slowly infused via the carotid cannula into the systemic circulation at 30 minutes post-reperfusion. The first intravital recording was taken at the same time point as cell infusion. 2-minute long videos were captured every 15 minutes for 2-2½ hours from the same pre-selected region of interest below the LAD ligation point using Slidebook 6.0 capturing software. This also allowed for consistency between experiments.

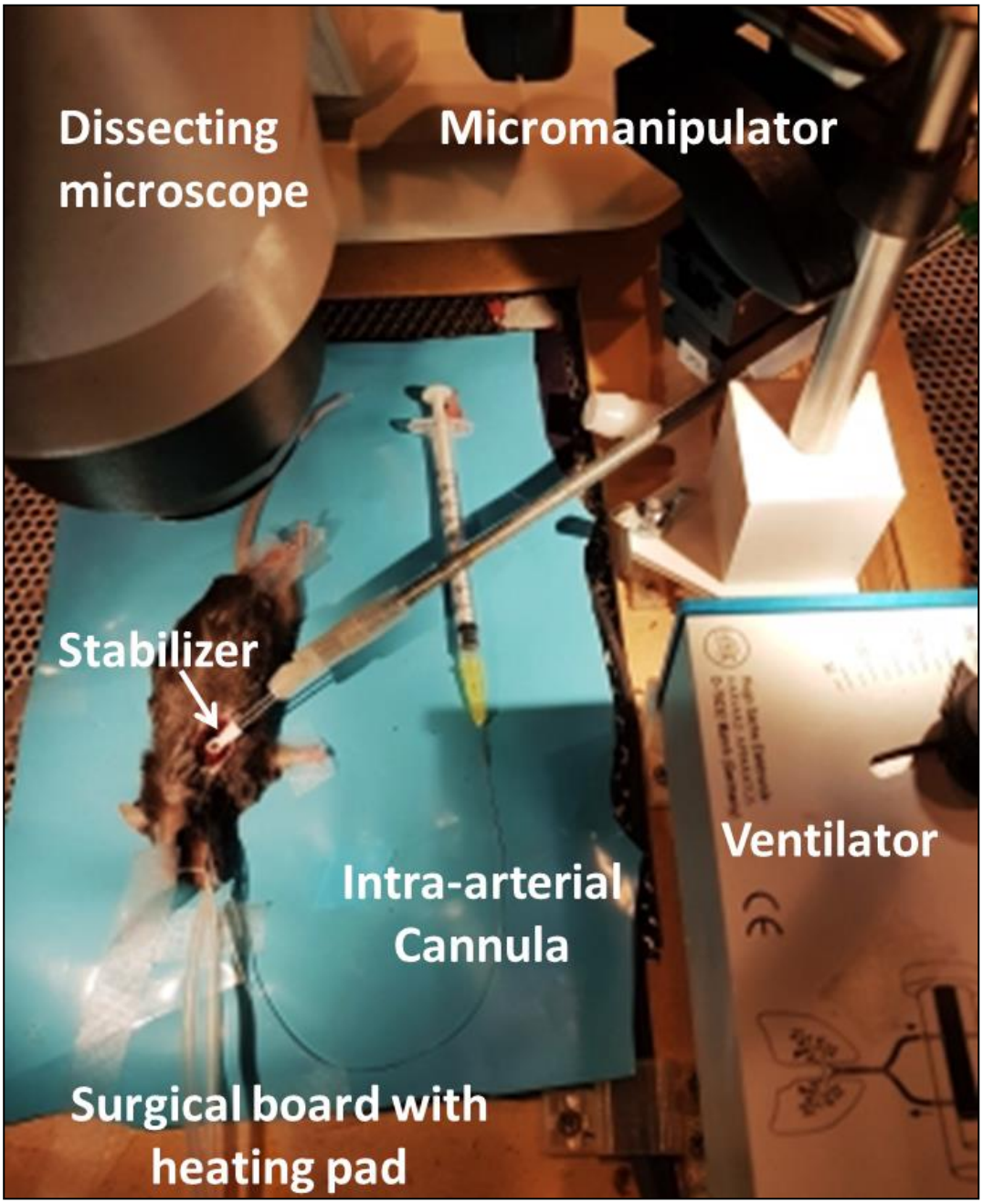


Figure 2.5. Surgical preparation of the anaesthetised male C57Bl/6 mouse for intravital imaging of the exposed beating heart in vivo. The anaesthetised mouse was placed on a heating pad on an in-house designed surgical board. The mouse was artificially ventilated by placing a cannula into the trachea which was attached to a MiniVent ventilator. Oxygen was provided using an oxygen generator machine. A fluid for hydration and infusion of stem cells was given via a cannula placed in the carotid artery. For thoracotomy, the mouse was placed on its right and the hair over the left side of the chest was removed. An incision was made between the 3rd and 4th ribs to expose the heart, specifically the beating left ventricle. For intravital imaging, an in-house designed 3D printed stabilizer was gradually placed onto the left ventricle with a help of a micromanipulator and attached to it using Vetbond®.

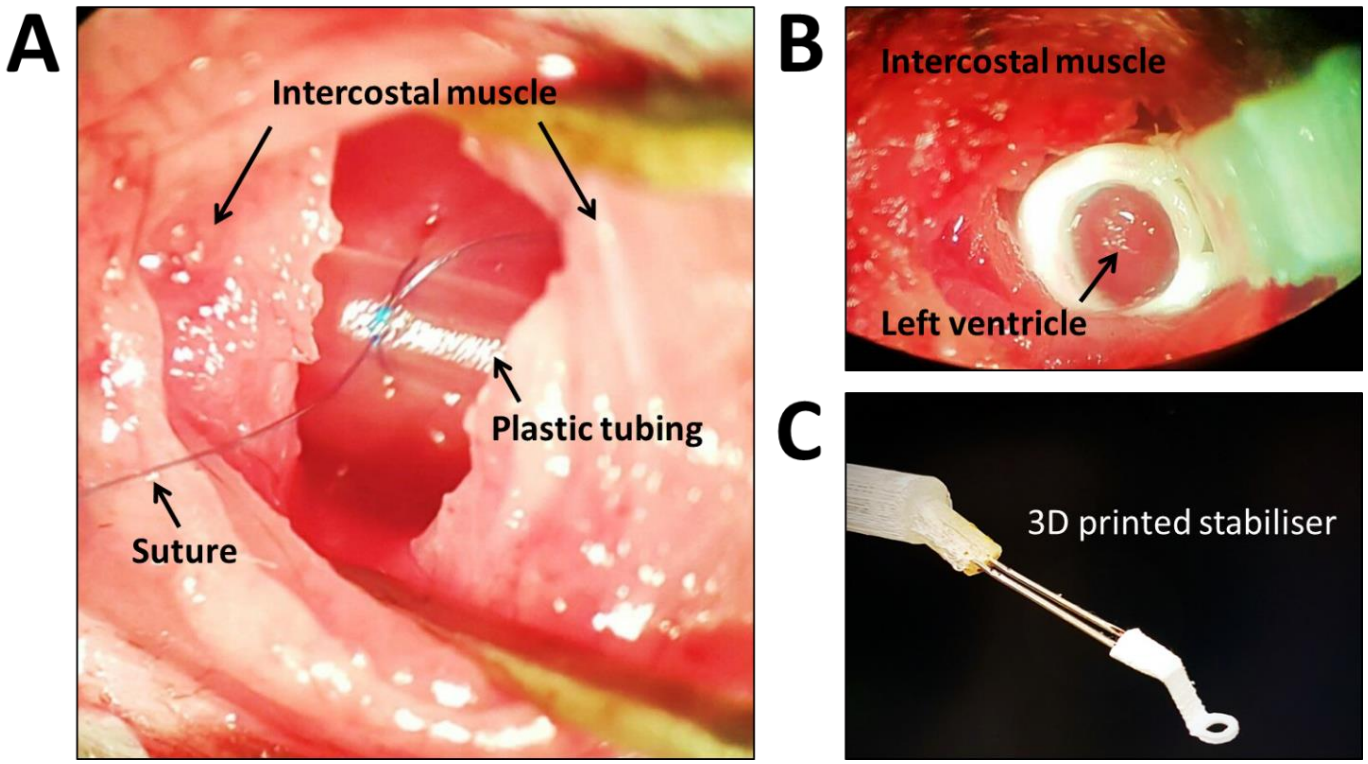


Figure 2.6. Preparation of the anaesthetised C57Bl/6 mouse beating heart for novel intravital imaging *in vivo.* (A) The left anterior descending (LAD) coronary artery was identified on the surface of the left ventricle and temporarily ligated for 45 minutes using the 8-0 suture passed using an attached needle underneath it. It was tied off against a 1 mm plastic tube to avoid damaging and tearing the muscle. Occlusion of the LAD and thus induction of myocardial ischaemia was confirmed by a change of colour of the anterior wall of the left ventricle below the ligation point from red to pale pink. **(B-C)** The arm of a micromanipulator was attached to an in-house designed 3D printed stabiliser and used to help place it gently onto the surface of beating heart. It was placed firmly on the heart using Vetbond®glue and subsequently provided sufficient stability of left ventricle to allow it to intravitally image whilst the heart continued to beat normally. Only a small region of the left ventricle is visible in Image B with rest hidden from view under the intercostal muscles.

After the intravital experiment was finished, mice were culled using a Schedule 1 method and the heart and lungs removed for use in experiments mentioned later. All recorded videos were stored using Slidebook software and analysed later.

Videos were subsequently analysed of-line using Slidebook 6.0 analysis software. Free flowing MSCs were those cells that simply passed through the coronary microcirculation without becoming adherent in a 1 minute duration. These cells were counted twice manually for each video taken every 15 minutes at the same pre-selected region of interest (413µm x 308µm) below the LAD ligation point for the entire experiment to ensure accuracy. Adherent MSCs were classified as those cells that remained stationary in the field of view for $\geq$ 30 seconds during the 2-minute recording time. The number of free-flowing and adherent MSCs was obtained for each 15 minute time point throughout reperfusion.

2.2.5.6. Imaging and quantification of neutrophils and platelets in the IR injured beating heart *in vivo* after hBM-MSC therapy

This study was conducted to investigate the potential anti-inflammatory and anti-thrombotic effects of 2D or 3D cultured hBM-MSCs Y201 and hBM-MSCs Y202 following myocardial IR injury. The number of neutrophils and platelets infiltrating the coronary microcirculation were chosen as parameters to assess as we have previously shown these to be detrimental to the integrity of the microvasculature in the IR injured beating heart (Kavanagh et al., 2019). To quantify the number of thromboinflammatory cells intravitally, these circulating blood cells were fluorescently labelled using antibodies against their specific cell surface markers.

Endogenous neutrophils were fluorescently labelled with a PE-conjugated rat anti-mouse Gr-1 (Ly6G) antibody (0.2mg/ml; 20µl). Endogenous platelets were labelled with an APC-conjugated rat anti-mouse CD41 antibody (0.2mg/ml; 20µl) (Wang et al., 2017, Da et al., 2018). To prepare the final concentration (0.4µg/ml) of antibody solution, 20µl of the specific antibody was mixed with 80µl PBS for 5 minutes. These antibody solutions were prepared fresh minutes prior to their use and introduced intra-arterially 5 minutes before the LAD artery ligation was removed. Thereafter, the stabiliser was attached to the left ventricle as described in **Section 2.2.5.4**. In these experiments, $5x10^5$ cells of unlabelled 2D or 3D cultured hBM-MSCs Y201 or hBM-MSCs Y202 in 200µl PBS were slowly infused intra-arterially at 30 minutes post-reperfusion as described in **Section 2.2.5.5**. Again, 2-minute long videos were recorded every 15 minutes throughout reperfusion and analysed offline using Slidebook 6.0 analysis software.

Free flowing neutrophils were those cells that simply passed through the coronary microcirculation without becoming adherent in 1 minute duration. These cells were counted twice manually for each video taken every 15 minutes to ensure accuracy. Adherent neutrophils were classified as those cells that remained stationary in the field of view for $\geq$ 30 seconds during the 2-minute recording time.

ImageJ (NIH; USA) software was used to quantify the myocardial presence of platelet aggregates or thrombi (**Figure 2.7**). Briefly, selected images at 30, 60 and 90 seconds of the 2 minute recorded videos were uploaded and the background fluorescence or the low-intensity colour was subtracted using the threshold modifier function. This then allowed the area containing just labelled platelets and platelet aggregates to be highlighted or have a mask placed around it. The mean fluorescence intensity of this adjusted intensity colour was

then multiplied with threshold area size (all of the highlighted platelets in the image) as shown in the equation below to obtain a value for the mean integrated fluorescence Intensity, The mean integrated fluorescence intensity was compared between the different experimental groups.

$$\textit{Area of Fluorescence Intensity} \times \textit{Mean Fluorescence Intensity} = \textit{Mean Integrated Fluorescence Intensity}$$

2.2.5.7. Imaging functional capillary density in the IR injured beating heart *in vivo*

In some experiments, the microcirculation was interrogated using FITC-conjugated bovine serum albumin (FITC-BSA). When introduced systemically, it is retained within the vasculature, thereby facilitating easy visualisation of the vasculature and confirming the presence of blood flow (Kalia et al., 2002). 100µl of FITC-BSA was injected into the mouse intra-arterially at the end of certain intravital experiments to qualitatively ascertain any changes in functional capillary density (FCD). The capillaries containing FITC-BSA were characterised a functional capillaries. The FCD were quantified using ImageJ and presented as perfused vascular area (pixel).

2.2.5.8. Dual therapy with hBM-MSC administration and heparin

These experiments were performed to determine whether administration of heparin could enhance the vasculoprotective effects of hBM-MSCs through more effective inhibition of neutrophil and platelet recruitment following myocardial IR injury. Mice were surgically

prepared, as mentioned in **Sections 2.2.5.3** and **2.2.5.4**. After 30 minutes of reperfusion, 400 IU of an unfractionated heparin sodium salt was slowly infused intra-arterially either on its own or alongside infusion of hBM-MSCs. Thereafter, neutrophil and platelet recruitment following myocardial IR injury was imaged intravitally as mentioned in **Section 2.2.5.6**. The timeline for all intravital experiments in which (i) MSC trafficking (ii) MSC vasculoprotective effects and (iii) MSC + Heparin vasculoprotective effects were imaged is shown in **Figure 2.8.**

2.2.6. Multiphoton microscopy studies to image vasculoprotective effects of hBM-MSCs in deeper layers of the IR injured heart muscle – *ex vivo* studies

2.2.6.1. Preparing the excised hearts for multiphoton imaging

Intravital imaging is restricted to imaging the surface of the beating heart *in vivo* and even with the spinning Nipkow confocal attachment only has a penetration depth of approximately 50-60µm, hence only the most superficial epicardial side of the heart was imaged. The development of multiphoton laser-scanning microscopy (MPLSM) offers a potential solution to this problem. It can penetrate directly into tissues at sufficient depths to image tissues in situ without significant phototoxicity. MPLSM provides better image quality and overcomes the single-photon microscope limitation, such as less penetration into the tissue than 50 µm (Wu et al., 2017).

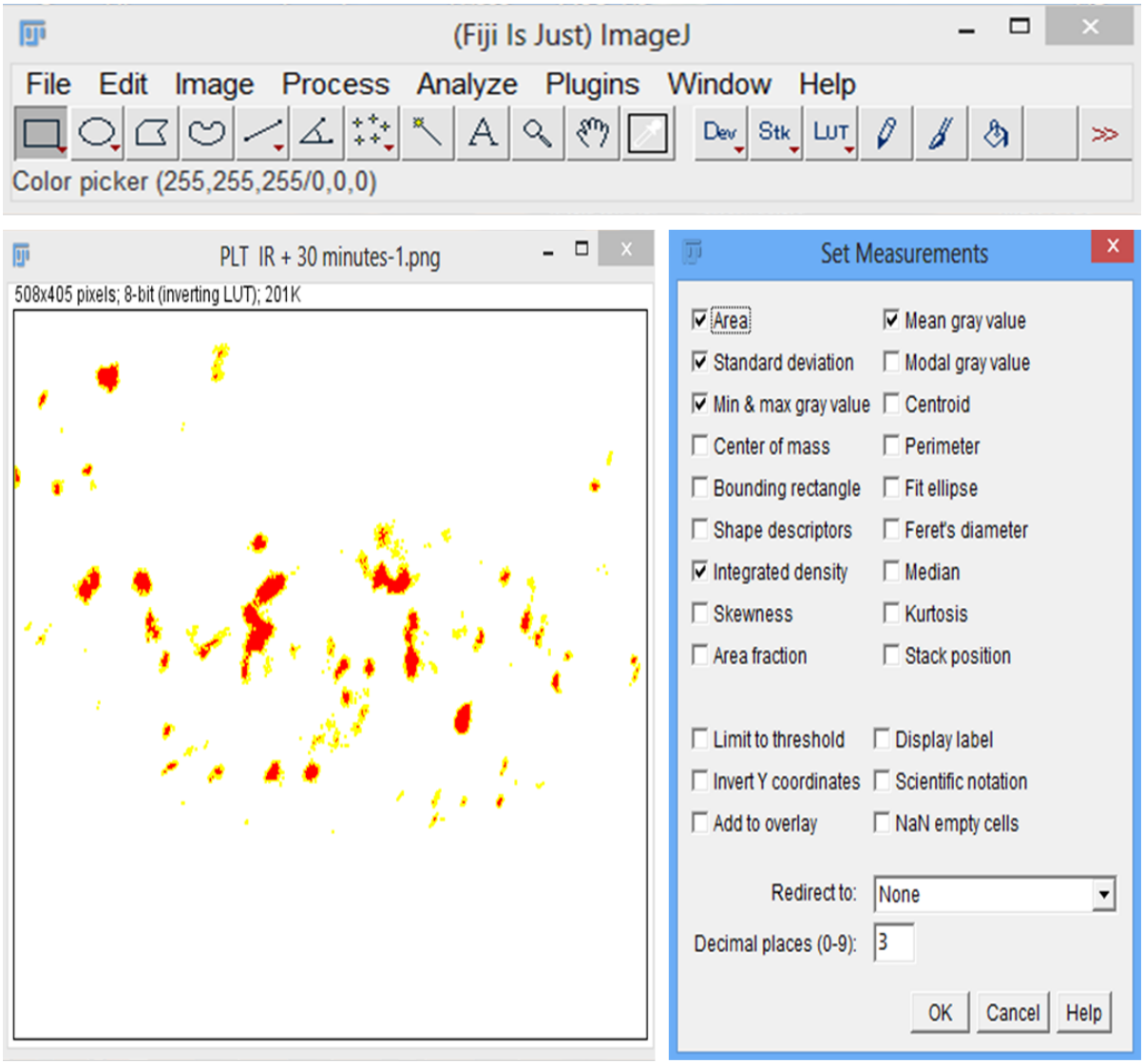


Figure 2.7. Analysis of platelet aggregation within the beating heart coronary microcirculation using Image J software. A selected image from the intravital 2 minute recorded video was uploaded in ImageJ software. The background fluorescence or the low-intensity colour was subtracted using the threshold modifier function. This essentially allowed the area containing just labelled platelets and platelet aggregates to be highlighted or have a mask placed around it (red). The mean fluorescence intensity of this adjusted intensity colour was then multiplied with the threshold area size (all of the highlighted red areas) to obtain a value for the mean integrated fluorescence Intensity. The mean integrated fluorescence intensity was compared between the different experimental groups.

To determine whether any potential surface inhibition of thromboinflammatory events in the presence of hBM-MSCs alone or hBM-MSCs + heparin was also taking place within the deeper myocardium, multiphoton *ex vivo* experiments were also conducted. At the end of some intravital experiments in which neutrophils and platelets were imaged, the hearts were harvested and kept in PBS on ice to prevent the organs from drying out and preserve their freshness. The auricle of the heart was removed manually using a scalpel, and the rest of the heart was placed in a petri-dish ready for vibratome sectioning.

The heart was attached to the specimen holder with the left ventricle side facing up using Liquid-Skin® glue (Chemence Medical Inc, UK). The specimen holder was then attached to a 7000smz Vibrating Blade Tissue Slicer (Campden Instruments Limited, UK). Prior to sectioning, all cutting parameters were set on the vibratome and included a frequency of 60Hz, amplitude of 1.5mm and a tissue thickness of 250µm. Once the tissue was mounted to the specimen holder, the single-edge razor blade was checked to confirm that the sharpened surface was facing upward. The left ventricle was then cut continuously until its whole thickness was sectioned and the heart chamber was reached. Approximately 4 to 5 slices of 250µm thickness each were obtained from the left ventricle (**Figure 2.9**). Forceps were used to lift tissue slices into a PBS chamber. Slices were then placed on the snow-coated slide, covered with a cover glass and could be kept in PBS and stored at 5°C for 3 days.

2.2.6.2. Imaging and quantification of neutrophils and platelets in IR injured hearts after hBM-MSC ± heparin therapy using multiphoton microscope *ex vivo*

Multiphoton microscopy was performed using a FVMPE-RS multiphoton laser scanning microscope (Olympus, UK). Images were obtained using a water-immersion x25 objective lens (XLSLPLN25XSVMP2, Olympus, UK). This system has 4 channels, which can accurately be adjusted to detect emission signals within the range from 400-1600 nm. Two channels were used in this study. These 2 channels were similarly adjusted for the system parameters, including amplifier offset, detector gain and amplifier gain. The excitation wavelength used to capture images of PE-labelled endogenous neutrophils and APC-labelled endogenous platelets was 1040nm and 1200nm respectively. The emission filter sets utilised for detection through the non-descanned detector were the: **(1)** infrared cut filter (BA750), **(2)** SDM570 dichroic mirror (DM) for channel (CH) 1 and the 575/645nm barrier filter (BF) for CH1 **(3)** SDM570 DM for CH3 and 600/670 BF for CH3, **(4)** FV30-FGR filter cube for CH1 detector **(5)** FV30-F475R filter cube for CH3 detector. The coupling mirror for the infrared laser used in these experiments was LCDM690-1050. The speed for image scanning was 4 microsecond per pixel. The resolution of the acquired images was 1024x1024 pixels. Z-stack images were assembled for each 250µm thick sections from the surface (1µm per z-step) at 3 different locations for each section. Overall, 4 slices of the left ventricle were imaged per mouse.

2.2.6.3. Reconstruction, image display and rendering of image stacks from multiphoton experiments

Multiphoton z-stacks were taken from 4 layers, namely the (i) outer epicardial to mid-myocardial (ii) outer mid-myocardial to mid-myocardial (iii) inner mid-myocardial to mid-myocardial and from (iv) inner mid-myocardial to inner endocardial avoiding the last section which had 'missing' myocardium due sectioning through the actual ventricle chamber. Images from each layer were then rendered to form 3D stack images (Figure 2.10). The image Z-stacks were processed and displayed using ImageJ. Rendering of the 3D stack was conducted using the ClearVolume (Github, US) plug-in for ImageJ. The presence of neutrophils and platelets was analysed as the sum of the fluorescence intensity per pixel in each image.

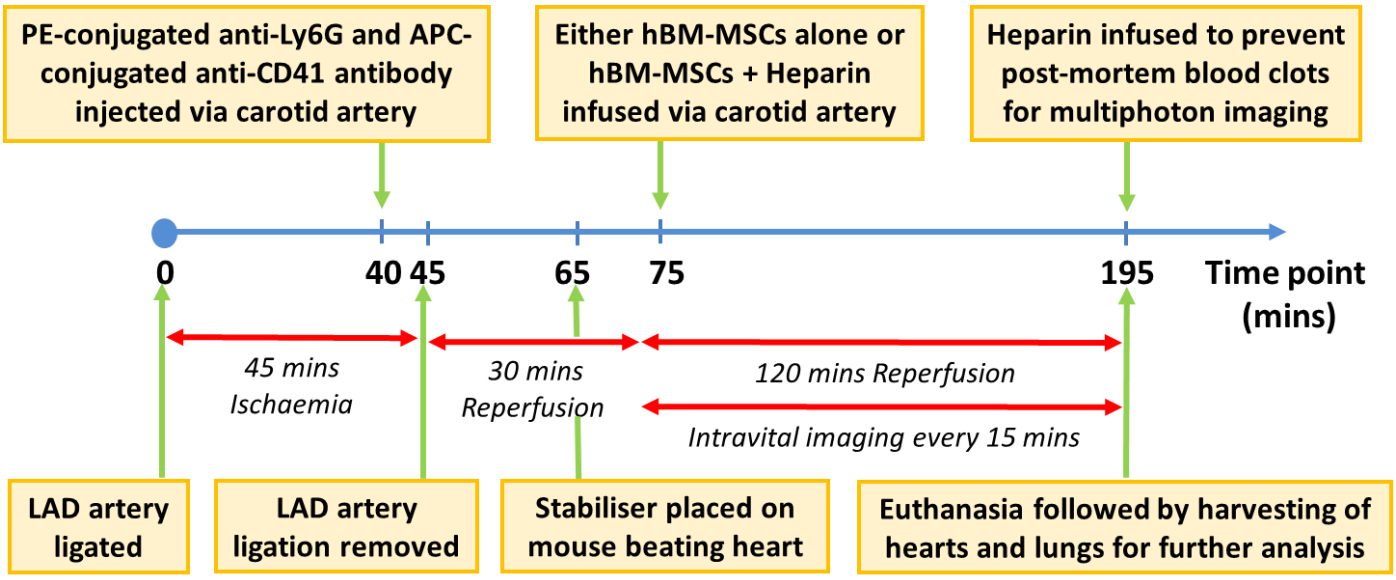


Figure 2.8. Timeline for intravital experiments of the beating mouse heart to image hBM-MSC trafficking and the vasculoprotective effects of delivering them alone or as a dual therapy with heparin. Once mice were adequately anaesthetised, the LAD coronary artery was temporarily suture ligated to induce myocardial ischaemia for 45 minutes after which it was un-ligated and reperfusion initiated. The heart was then prepared for intravital imaging – it took approximately 20-25 minutes to attach the stabiliser to the left ventricle. It was not possible to attach the stabiliser whilst the LAD artery ligation was still in place; hence why this procedure was performed after the ligation was removed. Therefore, the heart was intravitally imaged for the first time at 30 minutes post-reperfusion to ensure consistency between experimental groups. Intravital recordings were taken every 15 minutes for the next 2 hour post-reperfusion. HBM-MSCs were injected via the carotid artery either alone or as a dual therapy with heparin at 30 minutes post-reperfusion at the same time at the first intravital recording. In experiments in which neutrophils and platelets were being imaged, a PE-conjugated anti-Ly6G antibody and an APC-conjugated anti-CD41 was injected via the carotid artery 5 minutes before the LAD was un-ligated. In experiments in which the excised heart was to be subsequently further imaged for deep tissue analysis using multiphoton microscopy, (non-therapeutic) heparin was injected via the carotid artery just prior to culling.

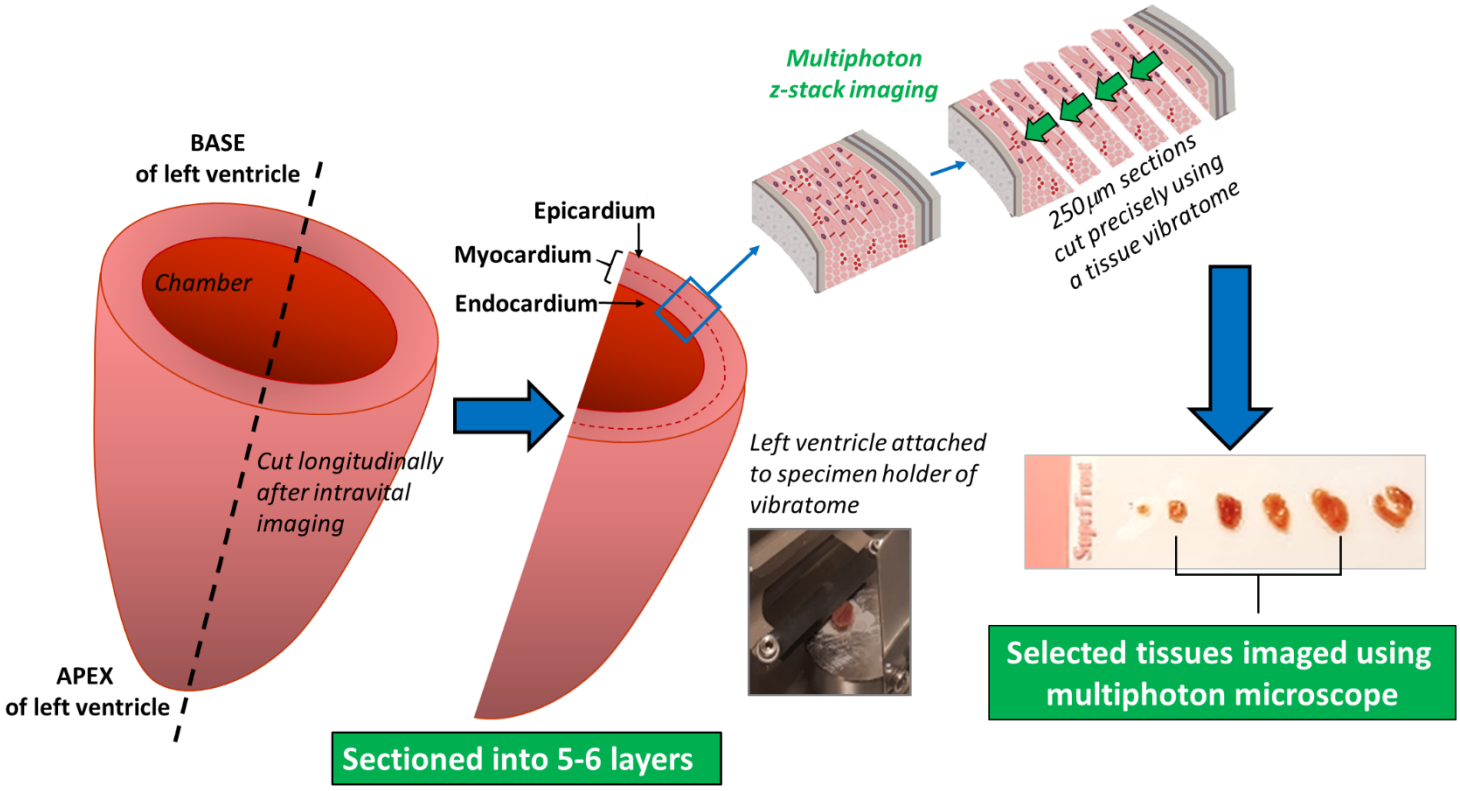


Figure 2.9. Preparing the murine left ventricle for multiphoton imaging following myocardial ischaemia-reperfusion injury *ex vivo.* To ascertain whether any vasculoprotective events imaged using intravital microscopy were also occurring in the deeper layers of the myocardium, multiphoton microscopy was used. The heart was cut in half longitudinally from the base to apex to expose the inner endocardial layer lining the left ventricle chamber. It was then placed on a specimen holder and attached to a tissue vibratome to precisely section the left ventricle wall into 5-6 sections from the epicardial to endocardial side with 250μm thickness sections cut. Multiphoton z-stacks were taken from 4 layers, namely the (i) outer epicardial to mid-myocardial (ii) outer mid-myocardial to mid-myocardial (iii) inner mid-myocardial to mid-myocardial and from (iv) inner mid-myocardial to inner endocardial avoiding the last section which had 'missing' myocardium due to sectioning through the actual ventricle chamber. Images from each layer were then rendered to form 3D stack images.

2.2.7. Flow cytometry experiments to analyse hBM-MSC recruitment, coronary endothelial and cardiomyocyte oxidative damage and endothelial adhesion molecule expression in whole excised digested hearts *ex vivo*

2.2.7.1. Digestion of whole hearts and lungs

Heart and lungs were removed from culled mice at the end of some intravital experiments. They were then digested into single-cell suspensions for flow cytometry analysis of hBM-MSC presence, endothelial and cardiomyocyte oxidative stress and endothelial ICAM-1/VCAM-1 expression. Firstly, mice were surgically prepared and underwent either sham surgery or myocardial IR injury as described in **Sections 2.2.5.2, 2.2.5.3,** and **2.2.5.4**. Some mice received 2D and 3D cultured hBM-MSCs Y201 and hBM-MSCs Y202 as described in **Section 2.2.5.5**. The organs of interest were excised and stored in cold PBS to prevent the organ from drying out and preserve the freshness of organs. The heart and lungs were then finely minced into tiny pieces using a sharp scalpel in a petri-dish. Finely chopped tissues were placed in a 15ml corning tube and mixed with 2ml of 0.1% v/v Collagenase type I solution to start enzymatic digestion. These processes were performed in a cell culture hood. The tube was incubated at 37˚C for 1 hour on the rotator mixer. After incubation, the solution was filtered through a 70µm cell strainer and added to 20ml of warm cell culture medium. The cell suspension was centrifuged at 700 g for 10 minutes and washed with PBS. The cell pellet was collected fixed and permeabilised using 100% v/v ethanol at least 1 hour before labelling cells for oxidative stress or surface adhesion molecules.

2.2.7.2. Quantification of hBM-MSC recruitment in excised whole hearts and lungs of mice following myocardial IR injury

The aim of these experiments was to determine whether the culturing method influenced the homing and myocardial retention of different sub-populations of hBM-MSCs to the IR injured and the lungs. The protocol was used as previously described (Kavanagh et al., 2019). 2D and 3D cultured hBM-MSCs Y201 and hBM-MSCs Y202 were labelled with CFSE as mentioned in **Section 2.2.1.7**. Once tissues were collagenase digested into single-cell suspensions, cell sorting using flow cytometry was conducted immediately after identifying the CFSE-labelled MSC population. Samples were analysed using FACSCalibur flow cytometry. The analysis was conducted on 25,000 events. Summit 4.3 software (Beckman Coulter, US) was used to visualise the data. A gating strategy was conducted to investigate and to quantify the cell population of interest. The data were presented as percentage of total MSCs infused in mice. The percentage of infused hBM- MSCs presence in organ was determined by calculating those found in each organ (heart or lung) compared to the total number of infused hBM-MSCs.

2.2.7.3. Determination of coronary endothelial cell and cardiomyocyte oxidative damage in excised whole hearts and lungs of mice following myocardial IR injury

The aim of these experiments was to assess whether 2D or 3D cultured hBM-MSCs Y201 and hBM-MSCs Y202 were able to reduce oxidative damage of coronary endothelial cells following myocardial IR injury. Furthermore, to determine the sensitivity of these vascular cells to oxidative stress, comparisons were made with cardiomyocytes. The

protocol was used as previously described (Kavanagh et al., 2019). The digested hearts single cell population was labelled with a PE-conjugated anti-CD31 antibody to detect the endothelial cells, with cardiomyocytes detected using an anti-cardiac troponin-T (cTnT) antibody. The oxidative damage of each cell type was detected using an anti-8-OHdG antibody. Permeabilised and fixed single digested heart cell suspensions were centrifuged for 10 minutes at 700 g at 25°C. Cell pellets were collected and washed once in PBS and centrifuged again. To block non-specific binding of the antibody, cells were re-suspended in FACS buffer for 30 minutes. After that, cells were centrifuged to discard the supernatant. Cell pellets were re-suspended with the specific antibody solution: Alexa Fluor 488-conjugated IgG at a ratio of 1:500, PE-conjugated anti-CD31 at a ratio of 1:50, PE-conjugated IgG2a at a ratio of 1:50, PE-conjugated REA control antibody at a ratio of 1:10, PE-conjugated anti-cTnT at a ratio of 1:10 and Alexa Flour 488-conjugated anti-8-OHdG at a ratio of 1:500. Cell suspensions were kept in the Eppendorf tubes covered with aluminium foil and agitated gently on ice for 1 hour. Tubes were again centrifuged and cells re-suspended in 300µl of PBS ready for analysis using flow cytometry. Samples were analysed using FACSCalibur flow cytometry. The analysis was conducted on 25,000 events. Summit 4.3 software (Beckman Coulter, US) was used to visualise the data. The gating strategy is provided (**Figure 4.8**) to investigate and to quantify the cell population of interest. Brifely, cells were gated using SSC vs FS. Individual populations were then gated on before identifying and eliminating cells that have joined together using pulse width vs FS. Live cells (PI-) were gated and shown by FS and SSC. These viable cells were then gated on FL-1 + or FL-2 + events to evaluate the presence of molecules assessed in this study, CD31-PE or cTnT PE and A8-OHdG AF488.

2.2.7.4. Determination of endothelial cell adhesion molecules expression in excised whole hearts and lungs of mice following myocardial IR injury

The aim of these experiments was to assess whether 2D or 3D cultured hBM-MSCs Y201 and hBM-MSCs Y202 were able to reduce the expression level of adhesion molecules expression on the surface of coronary endothelial cells following myocardial IR injury. The protocol was used as previously described (Kavanagh et al., 2019). Digested heart coronary endothelial cells were labelled with a PE-conjugated anti-CD31 at 1:50, PE-conjugated IgG2a control at 1:50, FITC-conjugated anti-ICAM-1 at 1:50, FITC-conjugated IgG2a control at 1:50, PECy7-conjugated anti-VCAM-1 at 1:50, PECy7-conjugated IgG2b control at 1:50. Samples were analysed using FACSCalibur flow cytometry. The analysis was conducted on 25,000 events. Summit 4.3 software (Beckman Coulter, US) was used to visualise the data. A gating strategy was conducted to investigate and to quantify the cell population of interest.

2.2.8. Quantification of systemic inflammatory cytokines in the serum of myocardial IR injured mice after hBM-MSC therapy using multiplex immunoassays

To investigate the ability of 2D or 3D cultured hBM-MSCs Y201 and hBM-MSCs Y202 to reduce serum levels of inflammatory cytokines, a Luminex® multiplex immunoassay was used. Mouse blood was collected after the end of intravital experiments. Briefly, prior to sacrifice, a laparotomy was performed and the intestines were moved to one side to gain easier access to inferior vena cava. A 1ml syringe with a 25G needle was used to withdraw blood from the vena cava. Between 500-1000µl was obtained per mouse and transferred to

an eppendorf tube. To obtain serum, the blood was centrifuged at 1200g for 5 minutes at room temperature. Serum samples were kept at -80°C until used.

Measurement of circulating cytokines was conducted using Bio-Plex pro mouse cytokine 23-Plex assay plate (Bio-Rad Laboratories; USA) and analysed using a Luminex 200 plate reader (Bio-Rad Laboratories; USA). Samples were loaded in triplicate and the protocol supplied by the manufacturer for mouse cytokine assay preparation and analysis was followed for accurate measurements. Briefly, the assay buffer, wash buffer and sample diluent were brought to room temperature whilst frozen serum samples were thawed. Serum samples were diluted 1:4 with the sample diluent. One part of 10x wash buffer was diluted with 9 parts of dH_2O to prepare the 1X wash buffer. The standard was reconstituted and then vortexed for 5 seconds and incubated on ice for 30 minutes. The blank and standard were prepared by four fold dilution as recommended by the manufacturer. The 10x and 20x couple bead were mixed by vortex and protected from the light. To run the assay, the diluted beads were added to the assay plate, washed 2x with 100µl of Bio-Plex wash buffer and then samples, standards and blanks were added to each well. The plate was covered with sealing tape and incubated on a shaker at 850 ± 50 rpm at room temperature. Detection antibodies were diluted 1-fold before the incubation finished. The plate was washed 3 times, and 25 µl of the detection antibodies were added to each well. Plates were again placed on the shaker at 850 ± 50 rpm at room temperature. After washing 3 times, 50µl of 1x SA-PE was added to each well. The serum samples were loaded on the plate in triplicate and the plate was read using the Bio-Plex MAGPIX® multiplex reader (Bio-Rad Laboratories; USA). The data were analysed by Bio-Plex Manager MP Software and Bioplex Manager (Bio-Rad Laboratories; USA) using a standard curve given by the manufacturer.

2.2.9. Quantification of infarct size in IR injured hearts after hBM-MSC ± heparin therapy using the Triphenyl Tetrazolium Chloride (TTC) staining assay

This study aimed to investigate the ability of 2D or 3D cultured hBM-MSCs Y201 and hBM-MSCs Y202 to reduce the infarct size following IR injury. The principle of the assay used is based on the ability of viable mitochondrial dehydrogenases to react with the tetrazolium salts to produce a formazan pigment. Dead tissue would be lacking in these enzymes whereas healthy tissue would not. The assay is most reliable at discriminating dead and viable tissue with durations of reperfusion greater than 3 hours. Hearts were collected from mice that underwent: (i) IR injury alone; (ii) IR injury + 3D cultured hBM-MSCs Y201; or (ii) IR injury + heparin (iv) IR injury + heparin + 3D cultured hBM-MSCs Y201 therapy. IR was induced as described earlier in **Section 2.2.5.3** but with 4 hours of reperfusion to allow the formation of infarct area. After 4 hours of reperfusion, the LAD was re-ligated and 800µl of 0.5% w/v Evans blue solution was infused via the carotid artery. Evans Blue is an azo dye that binds tightly to plasma albumin after systemic injections and distributes itself within perfused tissue staining it dark blue (Yao et al., 2018). It allows clear separation of the regions of the heart affected by IR injury known as the 'area at risk' (AAR) as it stains the perfused myocardium and leaves the infarct side unstained.

The protocol of TTC assay was used as described by Lui and colleagues (Lui et al., 2019). After injection of Evans Blue, the mice were culled using a Schedule 1 method and the hearts were harvested and wrapped in Saran wrap and left at -20 °C for 1-2 hours to allow the tissues to firm so that subsequent sectioning was made easier. 20ml of 1% w/v TTC solution was prepared by mixing 2,2,5- TTC with phosphate buffer containing 23% w/v sodium phosphate monobasic (0.1M) and 77% w/v sodium phosphate dibasic (0.1M). The TTC

solution was adjusted to pH 7.4 and heated in a 37°C water bath before use. Hearts were removed from the freezer, cut transversely into 2mm thickness using a sharp blade and slices incubated in the 1% w/v TTC solution for 20 minutes at 37°C on an orbital shaker. Heart slices were then fixed in 10% v/v formalin for 20 minutes at room temperature. The formalin fixing step helped to enhance the contrast between the living and infarcted tissue as formalin lightened the tissue and turned blood brown which made the infarct area easier to differentiate. After fixation, slices were washed once in PBS, lightly dried with tissue paper and placed on a glass slide for imaging (**Figure 2.10**). A Zeiss stereomicroscope was used for imaging. A 500-gram weight was placed on top of the glass slice outside of the imaging field to guarantee a consistent thickness of the heart slices for all experimental groups.

Analyses of the captured images were performed using ImageJ. In IR injured hearts, dual labelling with Evans blue and TTC identified 3 separated regions. The perfused myocardium unaffected by IR injury was stained blue. The rest of the area that was not stained blue was the AAR (Kakimoto et al., 2013). Within this region, the red area defined the area that was not affected by IR injury and had viable myocardium. However, the white area in the AAR defined the infarcted or necrotic tissue. To quantitate the infarct size, ImageJ was used to measure the area of each of these 3 regions. Overall infarction was presented as the infarcted white region as a percentage of the AAR.

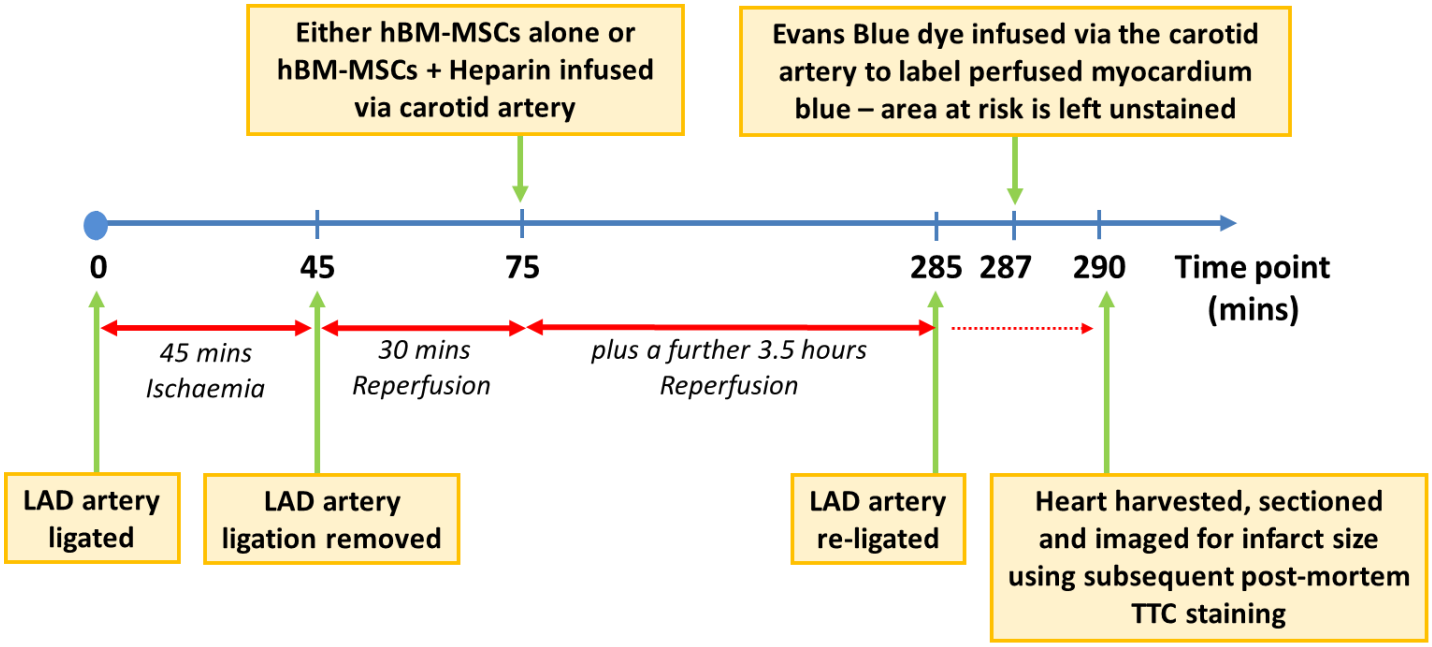


Figure 2.10. Timeline for infarct size experiments to assess whether 3D cultured hBM-MSCs Y201 ± heparin are effective at reducing myocardial infarction following IR injury. Once mice were adequately anaesthetised, the LAD coronary artery was temporarily suture ligated in induce myocardial ischaemia for 45 minutes after which are un-ligated and reperfusion initiated. 3D cultured hBM-MSCs Y201 were injected via the carotid artery either alone or as a dual therapy with heparin at 30 minutes post-reperfusion. Reperfusion was continuing un-interrupted for another 3½ hours. Immediately thereafter, the LAD was again sutured and Evans blue was injected via the carotid artery to identify the perfused regions of the heart. Mice were then culled, the heart harvested, sectioned and stained with Triphenyl Tetrazolium Chloride (TTC) to identify the areas at risk and the infarcted tissue.

2.3 Statistical analysis

To perform the statistical analysis of the data, Graphpad version 6.0 was utilised. Statistical comparison was performed by first testing normality using Kolmogorov–Smirnov test. A student t-test test was used to determine significant differences between experimental groups of interest. To compare differences between 3 or more groups, a one-way ANOVA followed by a Sidak's posthoc test for multiple comparisons was performed. Survival curves were analysed using Mantel-Cox tests. Data were expressed as mean ± standard error of the mean (SEM). A value of $P \leq 0.05$ was considered as statistically significant.

CHAPTER 3

Developing Strategies to Improve Mesenchymal Stem Adhesion to the Ischaemia-Reperfusion Injured Heart – in vitro Studies

3.0 Developing strategies to improve MSC adhesion to the IR injured heart – *in vitro* studies

3.1 Introduction and Hypothesis

3.1.1. Introduction

MSCs may have significant therapeutic potential for the treatment of ischaemic heart disease. However, clinical observations have not matched the initial excitement that surrounded their experimental success (Levy et al., 2020). This may be due to poor homing of systemically delivered exogenous MSCs to the injured heart due to their large size and thus entrapment in tissues such as the pulmonary capillaries (Ullah et al., 2019). Developing strategies that can improve MSC adhesive interactions with myocardial microvessels and concomitantly decrease non-specific recruitment is therefore critical. Alternatively, poor success may be attributable to not yet clearly identifying which MSC population is most likely to yield greater homing and/or therapeutic benefits in the heart. The overall aim of this thesis is to develop a method to monitor the homing of MSCs to the beating heart at a cellular level *in vivo* using intravital microscopy. This would allow us to identify an MSC population that is most adhesive and which may therefore have a more therapeutic effective due to their increased local presence in the injured heart. However, before these studies can be performed, *in vitro* investigations need to be conducted to guide on which MSCs will have the most potential to make firm adhesive interactions with

coronary endothelium *in vivo.* These *in vitro* studies also support the 3Rs principle of reducing animal studies where possible.

One strategy to improve both the adhesive and the therapeutic potential of MSCs is to culture those using 3D rather than using conventional 2D methods (Petrenko et al., 2017). Therefore, this chapter will develop a protocol to culture MSCs in 3D using a relatively simple scaffold-free, hanging drop method. The adhesion of 2D and 3D cultured MSCs will then be tested using frozen heart adhesion assays, static EC adhesion assays and static immobilised protein adhesion assays. Flow cytometric analysis and fluorescent confocal microscopy will also be used to assess surface adhesion molecule and chemokine receptor expression which could provide a mechanistic understanding of any potential variations in adhesion. Importantly, this chapter will test the adhesive capabilities of different MSC populations and sub-populations, namely those derived from the BM and from Wharton's jelly, a gelatinous substance found within the umbilical cord. MSC adhesion will be compared to HSCs which have also been considered for myocardial therapeutic purposes. These *in vitro* studies will help inform which MSCs may confer the most adhesive and therapeutic capacity to the IR injured heart *in vivo.*

3.1.2. Hypothesis

1. HSCs and MSCs cultured using the 3D hanging drop method will form spheroids and present with a different morphology to cells grown using conventional 2D methods.

2. Adhesion of HSCs and MSCs cultured using the 3D hanging drop method to various substrates *in vitro* will be increased when compared to those cells grown using conventional 2D culture.

3. Increase in adhesion is linked to increased surface expression levels of adhesion molecules and/or chemokine receptors on 3D cultured HSCs and MSCs when compared to cells grown in 2D culture.

3.1.3. Specific aims

1. The general morphology of HSCs and three different populations of MSCs cultured using the 3D hanging drop method will be compared microscopically to cells grown using conventional 2D culture. The three different populations of MSCs tested will be human WJ-MSCs and two immortalised human BM-derived MSC sub-populations, namely hBM-MSCs Y201 and hBM-MSCs Y202 cells. The ability of these cells to form spheroids after 1-2 days in culture will be assessed.

2. The adhesive ability of HSCs and three different populations of MSCs cultured using the 3D hanging drop method to snap-frozen murine cardiac tissue sections will be compared to cells grown using conventional 2D culture. Adhesion to both sham

control and IR injured myocardial tissue will be assessed. A modified Stamper-Woodruff *in vitro* adhesion assay will be used.

3. The adhesive ability of HSCs and three different populations of MSCs cultured using the 3D hanging drop method to cardiovascular ECs and immobilized EC adhesion proteins, namely ICAM-1 and VCAM-1, will be compared to cells grown using conventional 2D culture. Adhesion to both vehicle control and TNFα stimulated ECs will be assessed. A modified i*n vitro* static adhesion assay will be used.

4. The ability of three different populations of MSCs cultured using the 3D hanging drop method to modify their surface expression of CXCR4 (chemokine SDF-1α/CXCL12 receptor) and adhesion molecules CD44, ICAM-1 (CD54), VCAM-1 (CD106) and the integrin β7 sub-unit will be investigated and compared to cells grown using conventional 2D culture. Changes in the pattern of expression of these molecules will be investigated either using flow cytometry or confocally.

3.2 Methods

The methods used in this chapter are described in detail in **Chapter 2.** Briefly, to investigate the morphology of different stem cells grown under different culture techniques, HSCs, WJ-MSCs, BM-MSCs Y201 and BM-MSCs Y202 were cultured using either conventional 2D or 3D hanging drop method described in **Section 2.2.1.6.** After 48 hours, stem cells were examined under an inverted light microscope and spheroid formation and general morphology was assessed.

Modified Stamper-Woodruff frozen tissue adhesion assay was performed to investigate the adhesion of these different types of stem cell. Briefly, $1x10^5$ of CFSE labelled HSCs, WJ MSCs, hBM-MSCs Y201 or hBM-MSCs Y202 were incubated on sham or IR injured mouse frozen heart tissue sections at room temperature for 1 hour. The adhesive property of HSCs and MSCs to VCECs was examined using a modified static EC adhesion assay. VCECs were grown on 24 well plates and stimulated with TNF-α or PBS. Thereafter, cell suspensions of HSCs or MSCs, either from 2D or 3D culture methods, were incubated with ECs for 20 minutes at 37°C. A similar static adhesion assay was used to monitor adhesion to immobilised proteins. 96-well plates were coated with 10 µg/ml of rmICAM-1 or 10 µg/ml of rmVCAM-1 protein for 1 hour at room temperature. Fifty thousand HSCs or MSCs, from 2D or 3D culture, were added to each well and incubated for 20 minutes at 37°C.

For flow cytometry experiments, 2D and 3D cultured MSCs were incubated with fluorescently conjugated antibody against CXCR4, CD44, ICAM-1 (CD54), and VCAM-1 (CD106). Moreover, the pattern of expression of β7, CD44 and ICAM-1 on individual 2D and 3D MSCs was also investigated using a Zeiss 780 Zen laser scanning confocal microscope with 40x magnification water immersion lens.

3.3 Results

3.3.1. 3D cultured MSCs were smaller than 2D cultured cells and formed spheroids – HSC failed to form spheroids

WJ-MSCs and hBM-MSCs in 2D culture and those in 3D spheres were firstly dissociated using the Accutase® enzyme to create a single cell suspension. The viability of cells was

confirmed using Trypan blue staining technique. The general morphological appearance of 2D and 3D cultured HSCs, WJ-MSCs, hBM-MSCs Y201 and hBM-MSCs Y202 was observed at 1 and 2 days of culture using an inverted light microscope. 2D and 3D cultured HSCs appeared similar in size to all MSC populations with non-adherent, round, freely floating cells observed in suspension. Although some loose aggregation was observed in 3D, this did not result in spheroid formation as shown in **Figure 3.1A**. As expected, as shown in **Figure 3.1B-D**, 2D cultured WJ-MSCs, hBM-MSCs Y201, and hBM-MSCs Y202 were adherent, elongated and fibroblastic in appearance. However, 3D cultured WJ-MSCs, hBM-MSCs Y201, and hBM-MSCs Y202 formed a network and clumped together after 2 days of incubation and formed a spheroid of more compact, rounded cells.

Figure 3.2 shows the average size of HSCs, WJ-MSCs, and hBM-MSCs. The average size of 2D and 3D cultured HSCs was 12.2µm (range: 9.7-16µm) and 11.7µm (range: 7.9-15.8 µm) respectively. Although 3D cultured HSCs were slightly smaller, this did not attain statistical significance. The average size of 2D and 3D cultured cells WJ-MSCs was 28.3µm (range: 13.4-42µm) and 15.4µm (range: 11.4-28.44 µm) respectively. For hBM-MSCs Y201, the average size of 2D and 3D cultured cells was 40.4µm (range: 28.3-45.5µm) and 24.2µm (range: 19-33.2µm) respectively**.** The average size of 2D and 3D cultured hBM-MSCs Y202 was 42.5µm (range: 29.4-49.5µm) and 26.1µm (range: 14.8-38.7µm) respectively**.** Hence, 3D cultured WJ-MSCs and both hBM-MSCs were significantly smaller than those grown in 2D culture following their removal from culture flasks. The cell size distribution histograms are shown in **Figure 3.2C**.

3.3.2. 3D culture increased HSC and MSC adhesion to injured mouse heart sections

Both 2D and 3D cultured HSCs demonstrated a significantly increased adhesion to IR injured cardiac tissue when compared to their respective 2D and 3D cultured HSC adhesion to sham tissue. Importantly, as shown in **Figure 3.3A** and **E**, adhesion of 3D cultured HSCs on IR injured tissue was also significantly higher than that of 2D cultured cells on IR injured tissue**.**

Although both 2D and 3D cultured WJ-MSCs demonstrated an increased adhesion to IR injured cardiac tissue when compared to their respective 2D and 3D cultured WJ-MSC adhesion to sham tissue, this did not attain statistical significance. However, as shown in **Figure 3.3B**, adhesion of 3D cultured WJ-MSCs on IR injured tissue was significantly higher than that of 2D cultured cells on IR injured tissue. Neither 2D nor 3D cultured hBM-MSCs Y201 demonstrated an increased adhesion to IR injured cardiac tissue when compared to their respective 2D and 3D cultured cell adhesion to sham tissue. However, as shown in **Figure 3.3C**, adhesion of 3D cultured hBM-MSCs Y201 to both sham and IR injured tissue was significantly higher than that of 2D cultured cells on IR injured tissue. Similarly, neither 2D nor 3D cultured hBM-MSCs Y202 demonstrated increased adhesion to IR injured cardiac tissue when compared to their respective 2D and 3D cultured cell adhesion to sham tissue.

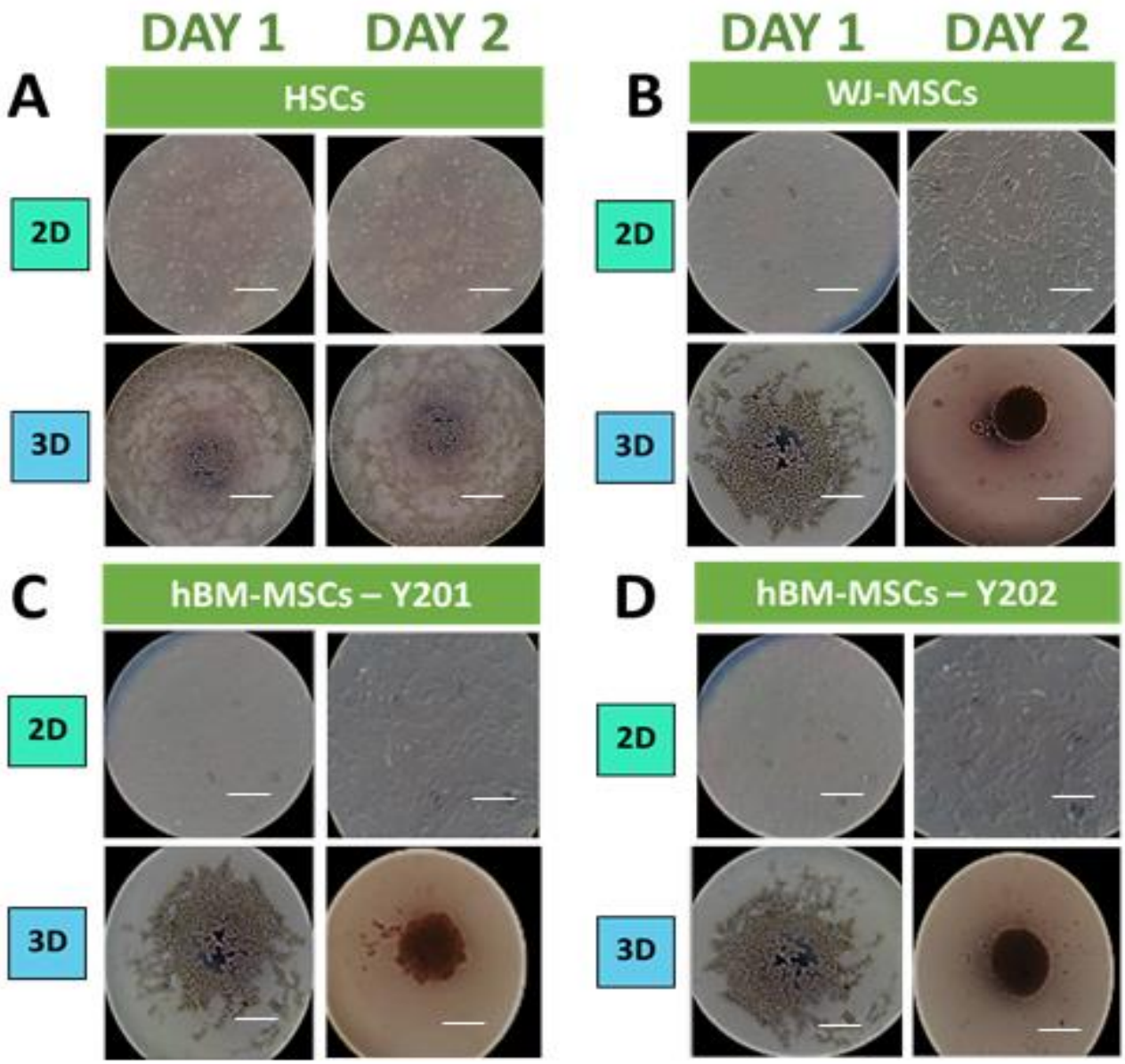


Figure 3.1. Morphology of HSCs and different populations of MSCs cultured using conventional 2D or 3D hanging drop methods. Morphology of 2D and 3D cultured HSCs and MSCs were observed on day 1 and day 2 of the incubation period. Cells were investigated under an inverted light microscope. **(A)** Loose aggregation was observed for 3D cultured HSCs which did not result in spheroid formation. **(B-D)** WJ-MSC, hBM-MSCs Y201 and hBM-MSCs Y202 formed spheres at day 2 using the 3D hanging drop culture technique. Images were captured with a 4x objective. Scale = 400 µm

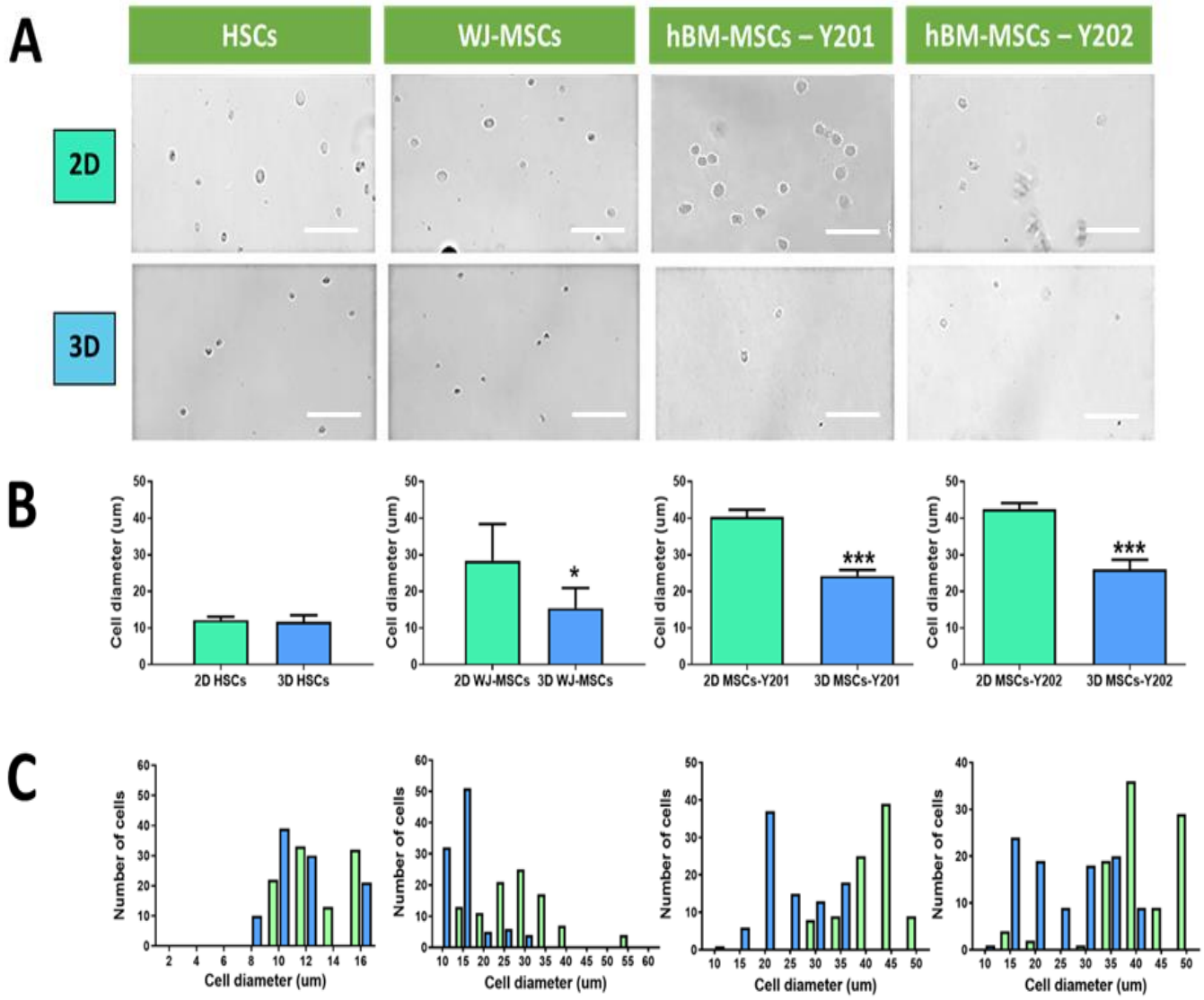


Figure 3.2. Size distribution of HSCs and different populations of MSCs cultured using conventional 2D or 3D hanging drop methods. **(A)** Representative images of conventional 2D cultured and 3D hanging drop technique cultured cells as observed under a light microscope. **(B)** No difference in overall cell size was observed for HSCs cultured using 2D or 3D methods. However, all populations of 3D cultured MSCs were significantly smaller than those grown in 2D culture following their removal from the culture flasks. **(C)** Cell size distribution of 2D and 3D cultured HSCs and MSCs. Data expressed as mean ± SEM. *p<0.05; ***p<0.001 when compared using a Student's t-test; n=50 cells for each group (independent experiments using 2 different donors for each cell type). Images were captured with a 20x objective. Scale bar = 200 µm.

However, as shown in **Figure 3.3D**, adhesion of 3D cultured hBM-MSCs Y202 to IR injured tissue was significantly higher than that of 2D cultured cells on IR injured tissue. Therefore, 3D culture of all SC types led to significantly increased adhesion to IR injured frozen heart section when compared to 2D cultured cell adhesion on IR injured tissue following their removal from culture flasks. Interestingly, HSCs demonstrated the highest level of adhesion (150+ cells) adhesion followed by WJ-MSCs – the least adhesion was noted with both sub-populations of hBM-MSCs.

3.3.3. 3D culture only increased hBM-MSCs Y201 adhesion to TNFα stimulated vena cava ECs

Interestingly, as shown in **Figure 3.4A-D**, neither 2D or 3D cultured HSCs, WJ-MSCs, hBM-MSCs Y201 or hBM-MSCs Y202 demonstrated increased adhesion to TNFα stimulated VCECs when compared to their respective 2D and 3D cultured cell adhesion to PBS stimulated VCECs. In fact, there was a general trend for adhesion to decrease on TNFα stimulated VCECs for all stem cells types. Therefore, adhesion of stem cells did not rely on endothelial activation status. Interestingly, as shown in **Figure 3.4C** and **3.4E**, only 3D cultured hBM-MSCs Y201 demonstrated increased adhesion to PBS and TNFα treated endothelium when compared to 2D cultured hBM-MSCs Y201, although this was only significant for adhesion on TNFα stimulated VCECs.

3.3.4. 3D culture only increased MSC adhesion to ICAM-1 and VCAM-1

As shown in **Figure 3.5A**, 3D culture did not modify the adhesion to HSCs or hBM-MSCs Y201 to ICAM-1. However, 3D cultured WJ-MSCs and hBM-MSCs Y202 demonstrated significantly increased adhesion to immobilised ICAM-1 protein when compared to the adhesion of 2D cultured cells. Although adhesion of both 2D and 3D cultured HSCs to VCAM-1 was higher than that observed on ICAM-1, 3D culture did not increase adhesion to VCAM-1 compared to adhesion of 2D cultured HSCs. However, as shown in **Figure 3.5B**, all populations of 3D cultured MSCs demonstrated significantly increased adhesion to immobilised VCAM-1 protein when compared to the adhesion of 2D cultured cells. Indeed, hBM-MSCs were more adhesive on VCAM-1 than ICAM-1. Notably, **Figure 3.5C** shows that WJ-MSCs derived from conventional 2D culture exhibited a larger cell size and expanded when adherent on ICAM-1 protein**.**

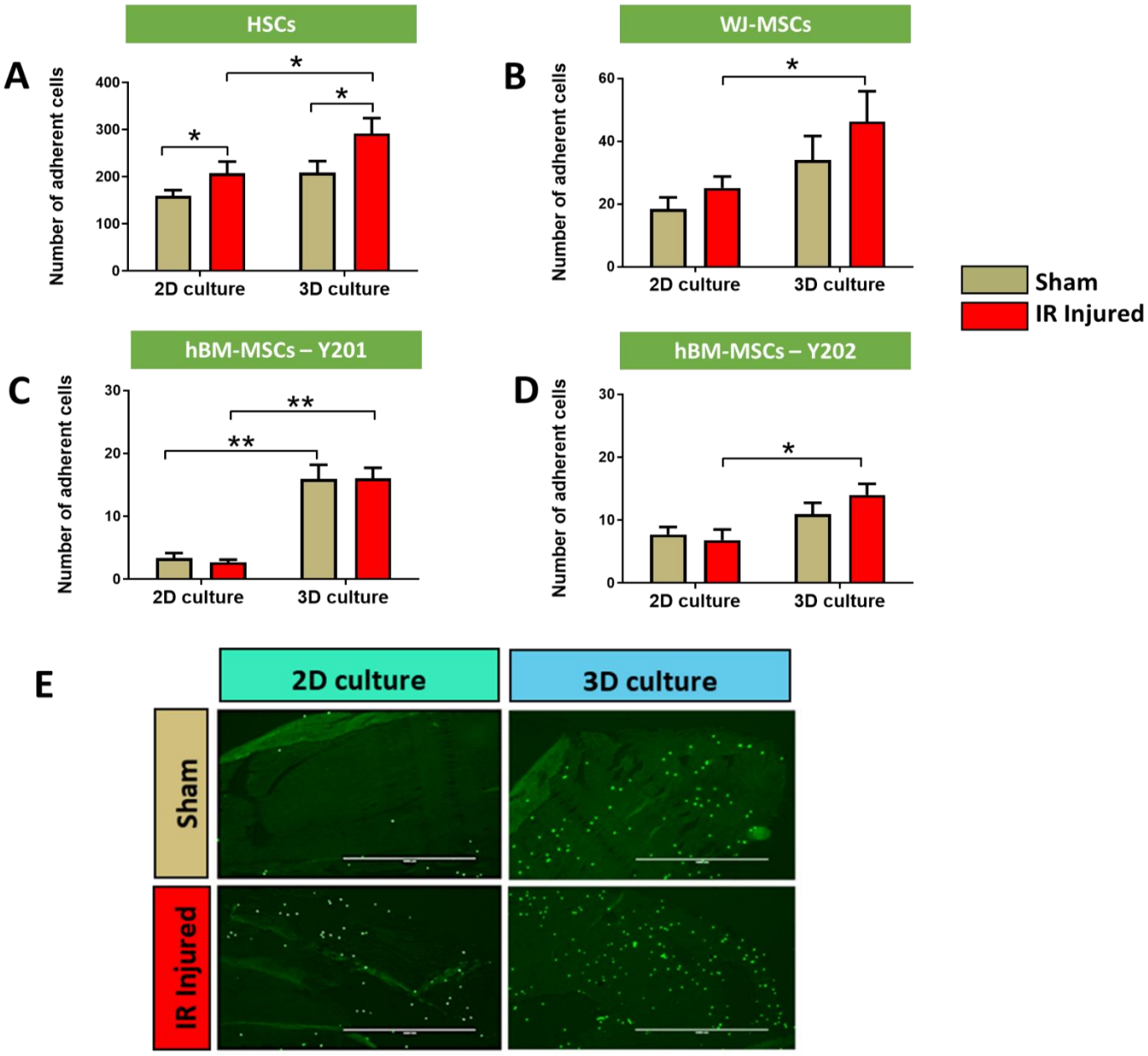


Figure 3.3. Adhesion capacity of HSC and different populations of MSC cultured using conventional 2D or 3D hanging drop methods to sham and IR injured frozen heart sections and assessed using the modified Stamper-Woodruff (S-W) adhesion assay. (A) Both 2D ($p<0.05$) and 3D ($p<0.05$) cultured HSCs demonstrated significantly increased adhesion to injured cardiac tissue when compared to their respective 2D and 3D cultured HSC adhesion to sham tissue. Importantly, adhesion of 3D cultured HSCs on injured tissue was also significantly ($p<0.05$) greater than adhesion of 2D cultured cells on injured tissue. **(B)** Adhesion of 3D cultured WJ-MSCs on injured tissue was only significantly ($p<0.05$) higher than adhesion of 2D cultured cells on injured tissue. **(C)** Adhesion of 3D cultured hBM-MSCs Y201 on both sham ($p<0.01$) and injured ($p<0.01$) tissue was significantly higher than 2D cultured cells. **(D)** Adhesion of 3D cultured hBM-MSCs Y202 on injured tissue was significantly ($p<0.05$) higher than 2D cultured cells on injured tissue. **(E)** Representative S-W images showing increased adhesion of 3D cultured HSCs to both sham and IR injured heart sections. Mean number of adherent cells from 5 randomly selected fields were assessed microscopically. In A, ANOVA showed a significant effect of both culture conditions and treatment; $p<0.05$. In B-D, ANOVA showed a significant effect of culture conditions; $p<0.05$. Data expressed as the mean ± SEM *$p<0.05$; **$p<0.01$ by Sidak's multiple comparison test. n = 5 independent experiments using four different donors for each cell type. Scale = 1000µm.

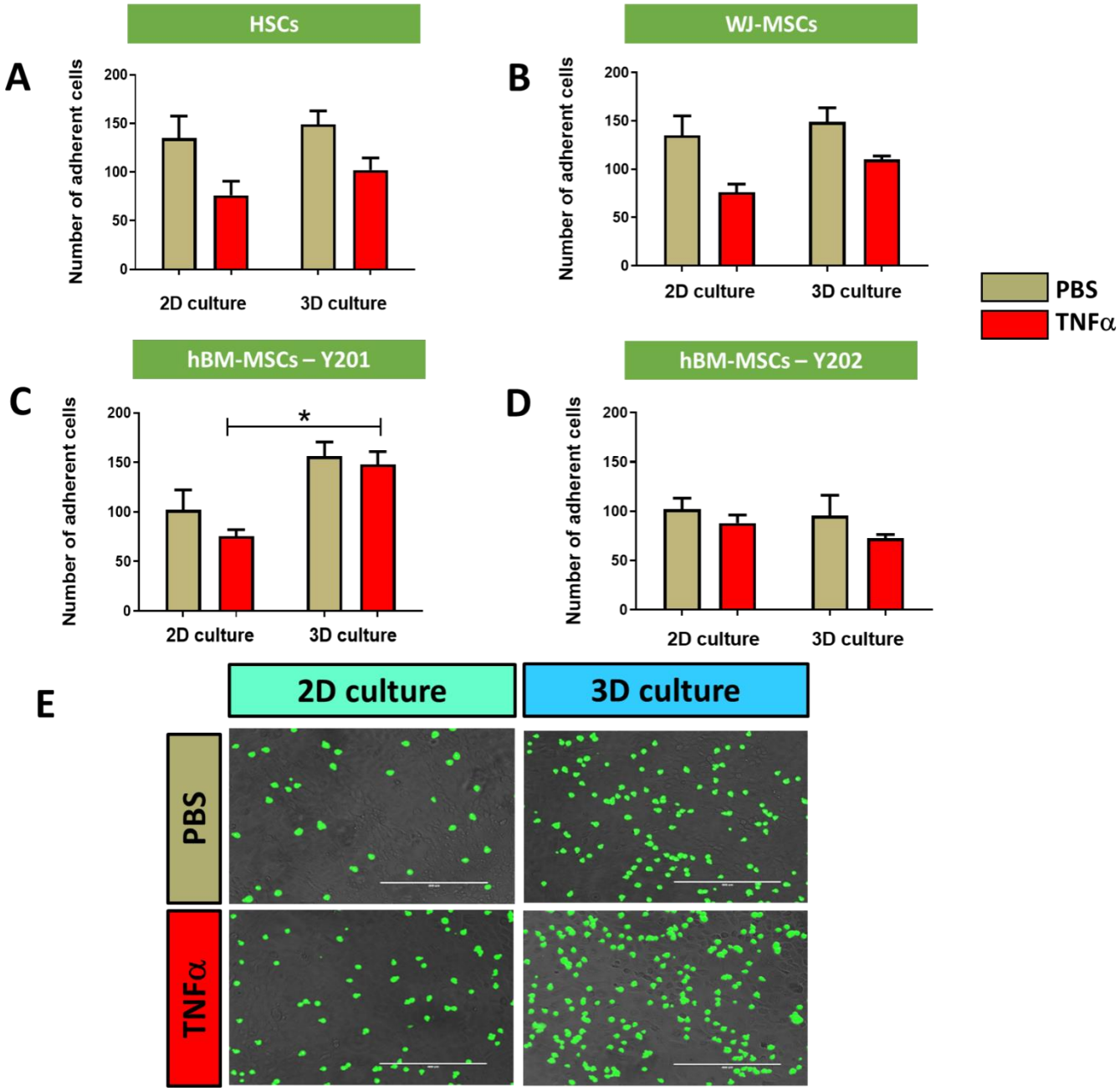


Figure 3.4. Adhesion capacity of HSC and different populations of MSC cultured using conventional 2D or 3D hanging drop methods to vena cava endothelial cells (VCECs) and assessed using static adhesion assays. **(A-B)** Neither 2D or 3D cultured HSCs or WJ-MSCs demonstrated increased adhesion to TNFα stimulated VCECs when compared to their respective 2D and 3D cultured cell adhesion to vehicle control (PBS) treated VCECs. Adhesion of 3D cultured HSCs or WJ-MSCs on TNFα stimulated VCECs was also not higher than that of 2D cultured cells on TNFα stimulated VCECs. **(C)** 3D cultured hBM-MSCs Y201 demonstrated significantly ($p<0.05$) increased adhesion to TNFα treated VCECS when compared to 2D cultured hBM-MSCs Y201 **(D)** 3D cultured hBM-MSCs Y202 did not adhere more to either PBS or TNFα treated VCECs cells when compared to those grown in 2D culture. **(E)** Representative static EC adhesion assay images showing increased adhesion of 3D cultured hBM-MSCs Y201 to both PBS and TNF-α stimulated VCECs. Mean number of adherent cells from 5 randomly selected fields were assessed microscopically. In C, ANOVA showed a significant effect of culture conditions; $p<0.05$. Data expressed as the mean ± SEM *$p<0.05$; by Sidak's multiple comparison test. n=5 independent experiments using four different donors for each cell type. Scale = 400µm.

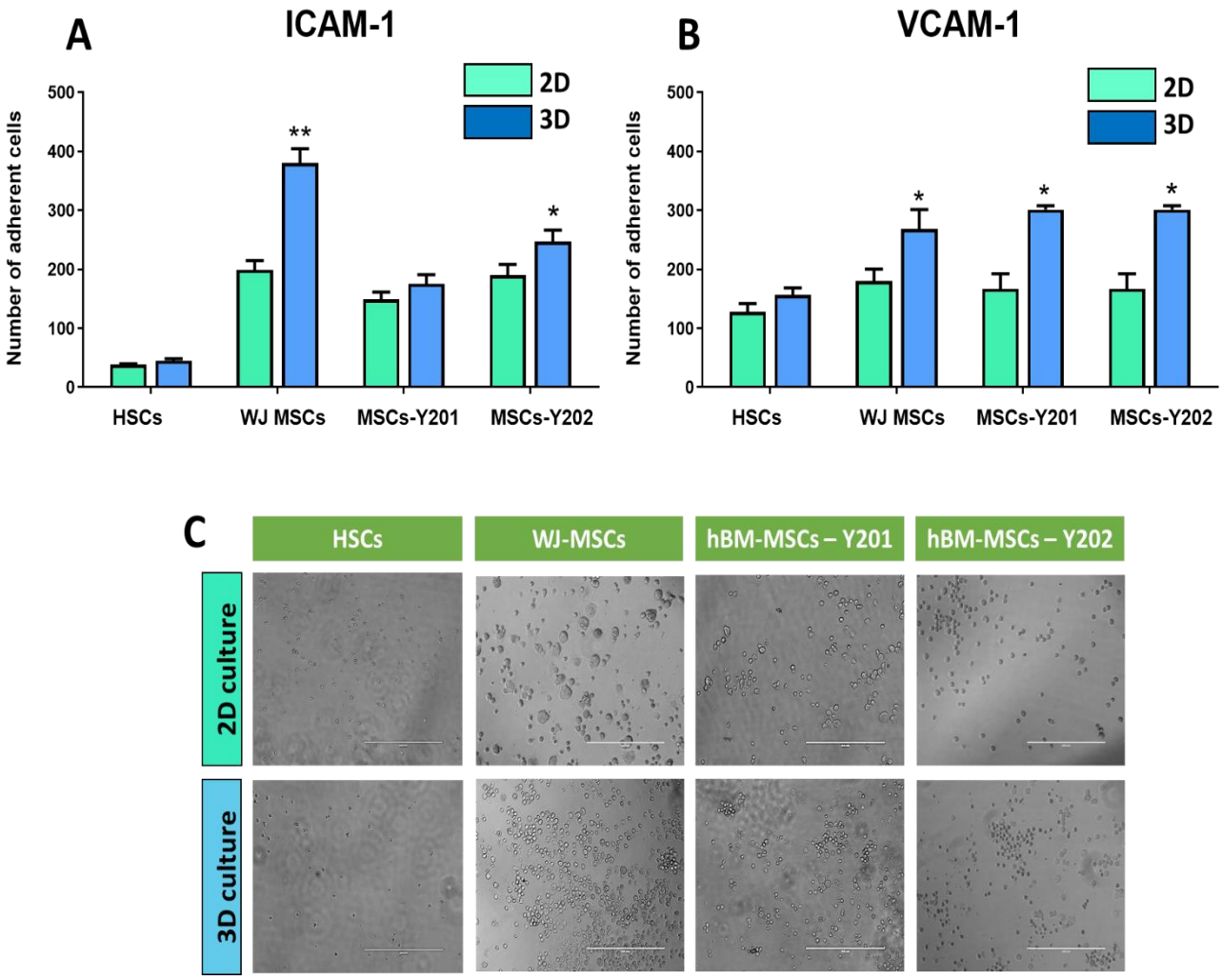


Figure 3.5. Adhesion capacity of HSC and different populations of MSC cultured using conventional 2D or 3D hanging drop methods to immobilised substrate proteins ICAM-1 and VCAM-1 and assessed using static adhesion assays. (A) Only 3D cultured WJ-MSCs ($p<0.05$) and hBM-MSCs Y202 ($p<0.05$) demonstrated significantly increased adhesion to immobilised ICAM-1 protein when compared to those cells grown in 2D culture. **(B)** Only 3D cultured WJ-MSCs ($p<0.05$), hBM-MSCs Y201 ($p<0.05$) and hBM-MSCs Y202 ($p<0.05$) also demonstrated significantly increased adhesion to immobilised VCAM-1 protein when compared to those cells grown in 2D culture. **(C)** Representative static ICAM-1 protein adhesion assay images of 2D and 3D cultured HSCs and MSCs. Mean of adherent cells from 3 randomly selected fields per well were assessed microscopically were assessed microscopically. In A and B, ANOVA showed a significant effect of culture conditions; $p<0.01$. Data were expressed as mean ± SEM.*$p<0.05$; **$p<0.01$ when tested using a Sidak's multiple comparison test. n =3 independent experiments using three different donors for each cell type. Scale bar = 400 µm.

3.3.5. 3D culture increased surface expression of various cells molecules on MSCs – notable increases in CXCR4 on hBM-MSCs Y201

Flow cytometry was used to investigate the surface expression of the SDF-1 receptor CXCR4 and surface adhesion molecules CD44, CD54 (ICAM-1) and CD106 (VCAM-1) on individual 2D and 3D cultured WJ-MSCs, hBM-MSCs Y201 and hBM-MSCs Y202 at 2 days of cultivation. **Figure 3.6A** show that 2D cultured WJ-MSCs did express CXCR4, CD44 and CD54, but did not express CD106. As shown in **Figure 3.6E-F**, although CXCR4 seemed to be downregulated on 3D culture, the CD44 and CD 54 significantly increases with 3D culture. **Figure 3.6B** shows that 2D cultured hBM-MSCs-Y201 did not express CXCR4 and only low levels of CD106. However, expression of CXCR4 was remarkably increased with 3D culture. 2D cultured hBM-MSCs-Y201 also expressed both CD44 and CD54, but 3D culture significantly increased expression of both as shown in **Figure 3.6E-F**. As shown in **Figure 3.6C** and **E**, 2D cultured hBM-MSCs Y202 expressed low levels of CXCR4 and no CD106 which did not increase with 3D culture. 2D cultured hBM-MSCs-Y202 also expressed both CD44 and CD54. Although the expression of both was with increased with 3D culture, this was more remarkable for CD44.

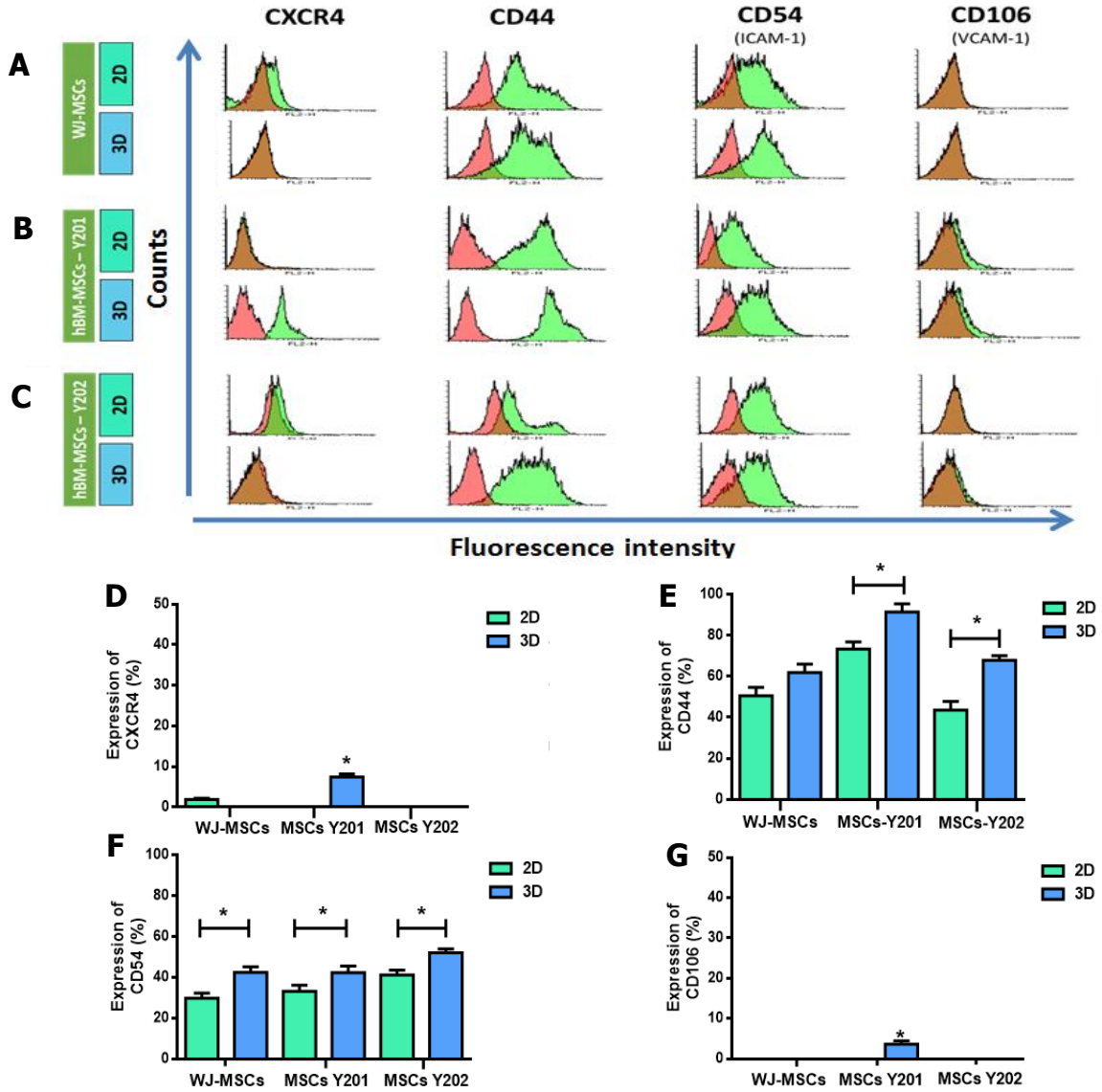


Figure 3.6. Cell surface expression of the SDF-1 receptor and CD44/ICAM-1/VCAM-1 adhesion molecules on different populations of MSC cultured using conventional 2D or 3D hanging drop methods as assessed by flow cytometry at 2 days of cultivation. Cells were dissociated by Accutase® and labelled with FITC conjugated monoclonal antibodies and analysed by flow cytometry. The green filled histograms represent cells from 2D and 3D cultured MSCs. The red filled histogram represents the isotype controls. **(A)** 2D cultured WJ-MSCs did not express CXCR4 or CD106 and expression levels did not change with 3D culture. 2D cultured WJ-MSCs did express both CD44 and CD54 which was increased with 3D culture. **(B)** 2D cultured hBM-MSCs-Y201 did not express CXCR4 or CD106 (low levels) but expression of CXCR4 was remarkably increased with 3D culture. 2D cultured hBM-MSCs-Y201 also expressed both CD44 and CD54. 3D culture slightly decreased CD44 expression but slightly increased CD54 expression. **(C)** 2D cultured hBM-MSCs Y202 also did not express CXCR4 or CD106 and expression levels did not increase with 3D culture. 2D cultured hBM-MSCs-Y202 also expressed both CD44 and CD54. Although the expression of both was with increased with 3D culture, this was more remarkable for CD44. **(D)** Only 3D cultured hBM-MSCs Y201 expressed CXCR4. **(E-F)** 3D cultured MSCs express significantly expressed CD44 and CD54 more than those obtained from 2D culture. **(G)** Only 3D cultured hBM-MSCs Y201 expressed CXCR4. Samples were analyzed using FACSCalibur flow cytometry. The analysis was conducted on 10,000 events. Flowing software 2.5.1(University of Turku, Finland) was used to analyse the data. In D-G, ANOVA showed a significant effect of culture conditions; $p<0.05$. Data expressed as the means ± SEM. Data were representative of 3 independent experiments. *$p<0.05$ when tested using a Sidak's multiple comparison test.

3.3.6. 3D cultured MSCs exhibited more uniform adhesion molecule distribution on their cell surface

Figure 3.7A-B show that only hBM-MSCs Y201 cells, both 2D and 3D cultured, expressed the integrin β7 subunit adhesion molecule. However, this was not observed so much on their cell surface but appeared to be somewhat internalized. hBM-MSCs Y202 dissociated from 3D spheroids expressed CD54 more evenly over their cell surface, whereas on 2D cultured cells CD54 tended to be concentrated on one side of the cell surface as shown in **Figures 3.7C-D**. hBM-MSCs Y202 dissociated from 3D spheroid also expressed CD44 more evenly over their surface as shown in **Figure 3.7E-F**, whereas on 2D cultured cells this adhesion molecule also tended to be concentrated on one side of the cell surface. For WJ-MSCs, **Figure 3.7G** and **H** show that cells dissociated from spheroid expressed CD44 more evenly over their surface, whereas in 2D cultured cells, CD54 was also concentrated on one side of the cell surface.

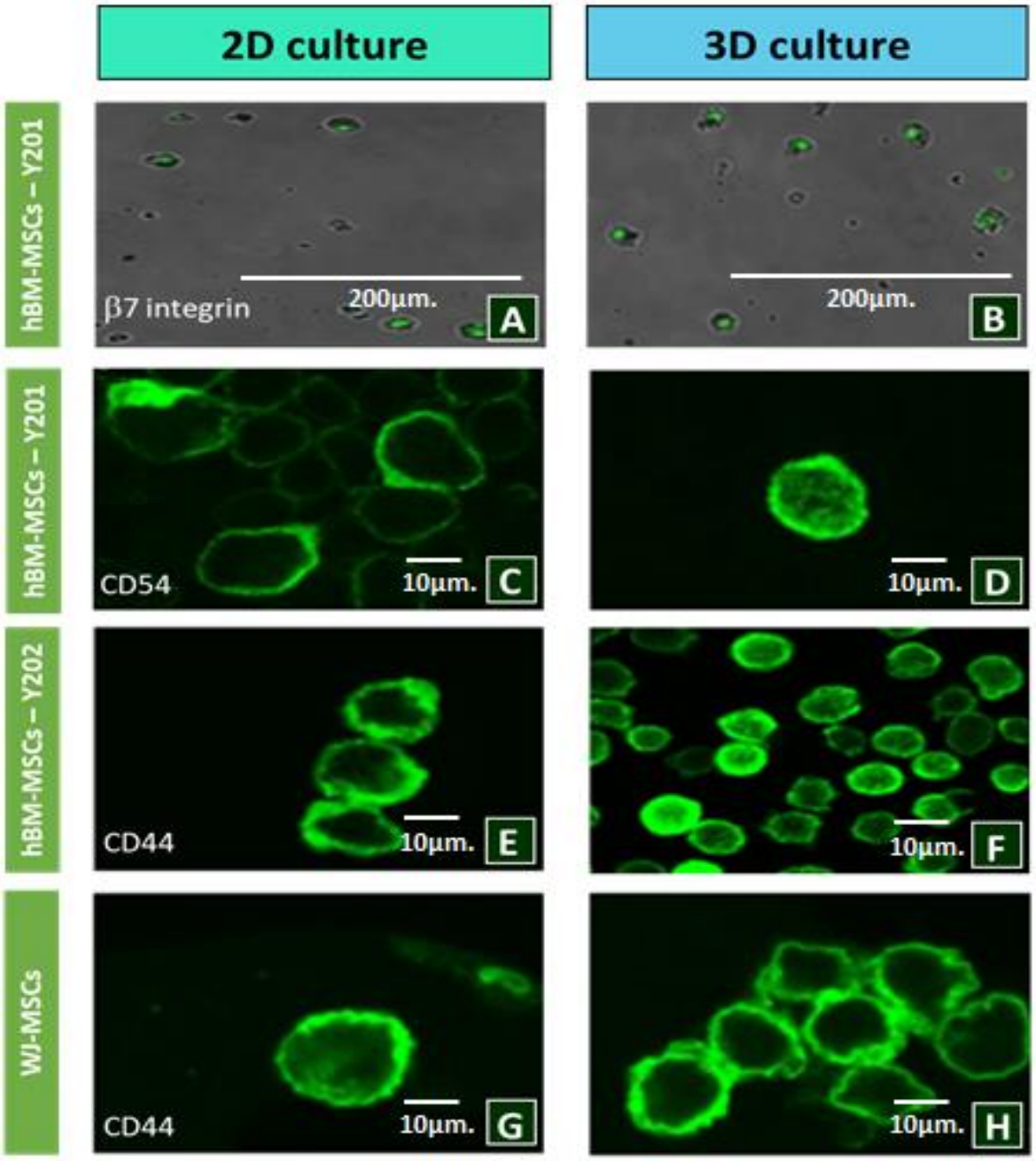


Figure 3.7. Cell expression of the integrin β7 subunit, CD54/ICAM-1 and CD44 on different populations of MSCs cultured using conventional 2D or hanging drop 3D methods and assessed confocally at 2 days of cultivation. (A-B) The expression of the integrin β7 subunit in hBM-MSCs Y201 grown in 2D and 3D culture was noted to be more intracellular. **(C-D)** CD54 expression on 2D cultured hBM-MSCs Y201 tended to be on the edges. However, hBM-MSCs Y201 dissociated from 3D spheroids expressed the adhesion molecule CD54 more evenly over their surface. **(E-F)** CD44 expression on 2D cultured hBM-MSCs Y202 was also localized to one side of the cell. Again, CD44 expression on 3D cultured hBM-MSCs Y202 was more evenly distributed on the cell surface. **(G-H)** CD44 expression of 2D cultured WJ-MSC was again uneven and located more so on one side. CD44 expression on 3D cultured WJ-MSCs was also evenly distributed on the cell surface. Distribution of adhesion molecules was investigated using confocal microscopy at 20X magnification. Images were captured and analysed using ImageJ software.

3.4 Discussion

Myocardial IR injury, which occurs after reperfusion of an occluded coronary artery in MI patients, still has no ideal treatment. Recent studies have suggested that it occurs as a result of specific damage to the coronary microcirculation (Bolognese *et al.,* 2004; Camici & Crea 2007; McAlindon *et al.,* 2018). Increasing clinical recognition that the coronary microcirculation is a primary target of injury has meant identifying effective strategies to improve perturbations within it has gained recent attention (Pries & Reglin. 2016; Lüscher 2017; Sambuceti et al., 2000; Crea et al., 2014). Studies have shown that MSCs release various therapeutic factors that could potentially induce vasculoprotective effects and thereby reduce the damaging effects of inflammation. However, clinical success remains hampered by poor retention (and survival) of MSCs in ischaemic hearts. This may be partially due to MSC size, their adhesive capacity or vasculoprotective potential. Collectively, these various problems may significantly impact the homing capacity and/or the therapeutic effectiveness of MSCs. Therefore, developing strategies to improve myocardial retention of MSCs, and also identification of the most effective MSC type, may improve clinical outcomes of cellular therapy for CVD.

In this chapter we aimed to identify whether 3D culture of MSCs resulted in smaller cells which could potentially home better to the heart *in vivo* by avoiding pulmonary entrapment. We show that MSCs cultured using a simple scaffold-free hanging drop method clumped together, formed compact spheroids and were considerably smaller than those cultured in conventional 2D method. Interestingly, HSCs did not form spheroids nor did different culture methods alter their already smaller size. Furthermore, we show 3D

culture could potentially improve myocardial retention *in vivo* as MSCs cultured using the hanging drop method was more adherent on a variety of different substrates. All populations of 3D cultured MSCs were more adhesive to IR injured frozen heart tissue and immobilised VCAM-1 than those grown in 2D. Surprisingly, only 3D cultured hBM-MSCs Y201 adhered more to TNF-α stimulated ECs *in vitro*. Although a difference in the adhesion of MSC with different tissue origins was not entirely unexpected, it was interesting that sub-populations from the BM also showed differential adhesive capacity, with 3D cultured hBM-MSCs Y201 showing more favourable results *in vitro*. We further demonstrated that mechanistically this could be explained by 3D culture modifying surface receptor and adhesion molecule expression. Indeed, 3D cultured WJ-MSCs, hBM-MSCs Y201 and hBM-MSCs Y202 expressed more CD44 and/or CD54 than 2D cultured cells, with hBM-MSCs Y201 showing remarkable up-regulation of the SDF-1α receptor CXCR4 after 3D culture. Also, 3D cultured MSCs had more uniform adhesion molecule distribution over their cell surface which was in contrast to 2D cultured MSCs where uneven distribution, located on one side of the cell surface, was noted.

3.4.1. 3D cultured MSCs formed spheroids and were smaller in size

MSCs are often grown in easy and relatively inexpensive 2D cultures in which they adhere to plastic surfaces, spread, become flat and greatly increase their size (Sethe *et al.,* 2006, Ksiazek 2009, (Cesarz and Tamama, 2016). When such cells are systemically infused for therapeutic purposes, their large size reduces their ability to circulate in the peripheral blood and reach the injured heart. Indeed, less than 5% of injected MSCs have been noted

to reach the target injured heart with more than 75% of MSCs becoming entrapped with pulmonary capillaries following intravenous administration (Assis et al., 2010, Barbash et al., 2003).

We showed that all MSCs tested in this study were able to form 3D spheres using gravity-induced aggregation in the hanging drop method. In this method there is no cell contact with a solid surface. However, cell-cell contact and aggregation into a single compact sphere in the apex of the liquid droplet is maximised. Previous studies have also shown that MSCs are inclined to self-accumulation and are able to form 3D aggregates when cultured on non-adhesive surfaces *in vitro*, a process that physiologically resembles their aggregation ability *in vivo* (Wang *et al.,* 2009, Baraniak and McDevitt, 2012, Deynoux *et al.,* 2020*)*. Indeed, Sart and colleagues described the self-assembly of MSCs into tightly packed clusters akin to creating an '*in vivo*-like' microenvironment which better preserved their phenotype and innate properties (Sart *et al.,* 2014). In the current study, individual cells, once dissociated from spheroids, were spherical and not elongated or fibroblast-like. Importantly, they were 50-60% smaller in diameter than MSCs grown using conventional 2D culture. This is consistent with recently published studies in which diameter decreases of up to 70% were observed with 3D culture (Dozza et al., 2017, Bartosh et al., 2010, Zhou et al., 2017).

Recent elegant studies have described the mechanisms by which MSCs organize into 3D aggregates (Cecarz and Tamama, 2016). MSCs express a number of surface cell adhesion molecules, namely integrins and cadherins, the expression of which varies depending on the culture method used. Zhou and colleagues cultured human placental MSCs using conventional 2D and 3D hanging drop methods and found a remarkable decline in the

integrin expression but an increase in cadherin levels when cells were immunostained and imaged confocally (Zhou *et al.,* 2017). Other studies have shown that the initial aggregation occurs as a result of homophilic cadherin-cadherin interactions between MSCs expressing high levels of surface cadherin (**Figure 3.8**). These MSCs are located in the centre or interior of the aggregate and are usually more rounded in appearance with low intracellular tension. Cadherin interactions are also involved in increasing the compactness of the aggregate (Egger et al., 2018). This would explain the smaller diameter of the 3D cultured MSCs. MSCs with higher levels of integrins and lower cadherin levels tend to move to the edge of the aggregate and are morphologically flatter or spindle-shaped as they are capable of spreading (Zhou et al., 2017). They can also use their surface integrins to interact with any surrounding extracellular matrix proteins if present in the 3D culture method. Consequently, they have higher levels of intracellular tension (Egger et al., 2018). The small range of cell diameters of cells derived from spheroid could be explained by whether the MSCs were originally located in the interior of the aggregate or dissociated from the outside. Nevertheless, even the larger of the 3D cultured MSCs were still smaller than the majority of MSCs that had been cultured in 2D. Interestingly, BM-MSCs express more N-cadherin and cadherin-11, whilst umbilical cord-MSCs express more E-cadherin (Sart *et al*., 2014). Whether this impacts on their ability to aggregate and subsequently compact with greater or lesser efficacy is not known.

The smaller size of 3D cultured MSCs can also be explained by the fact that these cells have been shown to have significantly reduced cytoplasmic actin levels. This meant cell stiffness or tension was reduced and these cells could readily self-aggregate in 3D culture conditions (Zhou *et al.,* 2017). Indeed, human placental MSCs cultured in 2D presented with multi-

directional branched F-actin stress bundles at the edge of the cell. Moreover, 2D MSCs had an expanded network of β-actin and α-tubulin, which formed the cytoskeleton filaments, leading to the flat and bigger architecture of 2D cultured MSCs (Sart et al., 2004). However, when these MSCs were cultured using a hanging drop method, they developed a more relaxed cytoskeleton tension with decreased β-actin and thin cortical filaments. This potentially allowed the cells to readily aggregate and compact in culture, subsequently resulting in the smaller morphology (Zhou *et al.,* 2017). Collectively, such studies suggest that the change in the actin cytoskeleton is critically responsible for the altered morphology and size of 3D cultured MSCs.

Interestingly, F-actin polymerization can inhibit the shedding of microparticles from the surface of a cell. Therefore, any disruption of a cells cortical actin network results in microparticles being generated more readily. Hence, it is also possible that the decrease in MSC size after 3D culture was linked to increased secretion of extracellular vesicles due to a decrease in F-actin polymerisation (Cesarz and Tamama, 2016). Indeed, Mo and colleagues showed higher levels of vesicles on the MSC surface and in the culture medium of MSCs when cultured using a hanging drop 3D culture condition, which was associated with lower levels of F-actin (Mo *et al.,* 2018). It would have been interesting to have imaged, using scanning electron microscopy, the surface of the WJ-MSCs and BM-MSCs in the current study to see if they had increased vesicle presence on their surface or in the culture media.

It is not clear why HSCs were unable to aggregate to form spheroids in the hanging drop method after 2 days. One reason for this phenomenon might be that HSCs are normally non-adherent cells in culture and easily proliferate in suspension. Although 3D culture has

been used widely for MSCs, few studies have tested the spheroid forming efficacy and benefits of HSCs. Schmal and colleagues used the hanging drop method and found that haematopoietic stem / progenitor cells (HSPCs), when co-cultured with MSCs, did not readily interact or adhere to aggregating MSCs (Schmal et al., 2016). Indeed, it took a week before this happened. HSPC adhesion strength in this model was also weak as they easily dissociated from the spheroid forming MSCs without the need to add digesting enzymes. They concluded that 2D culture was more appropriate for HSCs.

3.4.2. 3D cultured stem cells were more adherent *in vitro*

Increased cell adhesion to inflamed tissue was not unexpected as it is well recognised that expression of EC counterligands are up-regulated during inflammation and injury and become exposed when frozen tissue sections happen to cut through the vasculature (Yemm et al., 2013). The inflammation induced by IR injury is indicated by the remarkable production of pro-inflammatory agents, chemokines, and cytokines (Kany et al., 2019). These activate the endothelium resulting in them expressing higher levels of cellular adhesion molecules such as E-selectin, ICAM-1 and VCAM-1 (Ren et al., 2010). These can interact with integrins on the surface of circulating cells such as leukocytes to mediate their firm adhesion and subsequent tissue extravasation and invasion (Kvietys and Granger, 2012).

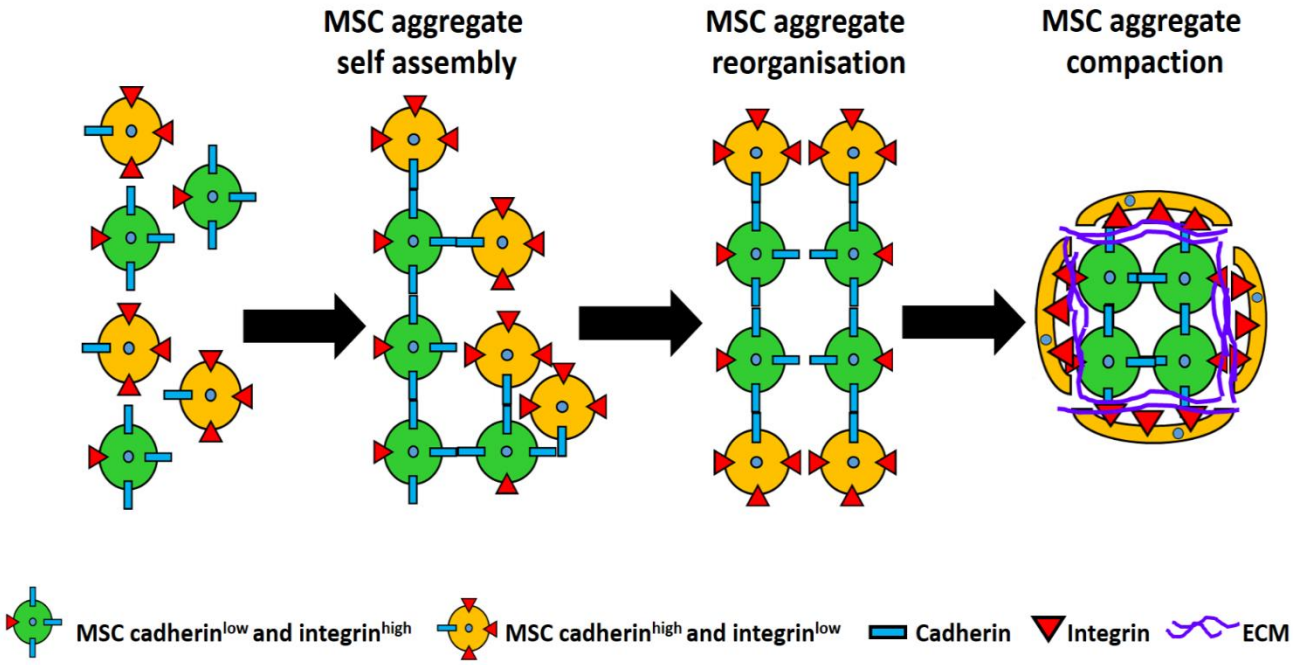


Figure 3.8. Proposed mechanism for mesenchymal stem cell (MSC) aggregation. A three-step mechanism has been proposed involving (i) cell-cell contact (ii) cadherin accumulation and (iii) aggregate compaction. MSCs are a heterogeneous population of cells expressing various levels of integrins and cadherins on their surface. When cultured in 3D conditions, Cadherin^{high} MSCs will start to aggregate using cadherin–cadherin interactions. Increased aggregate compactness is also mediated through cadherins. Hence those MSCs expressing high levels of cadherins will be found in the centre of the aggregate. Cadherin^{low} but integrin^{high} MSCs tend to sort out at the edge of the aggregates. These integrin^{high} MSCs are flatter as they are capable of spreading and as such tend to display a more spindle-shape morphology. They could use their surface integrins to interact with any surrounding extracellular matrix proteins if present. Adapted from Sart *et al.,* 2014.

MSCs also express a broad spectrum of integrins on their surface and use a similar adhesion cascade when being recruited by the microvasculature of injured tissue (Ren et al., 2010). Indeed, they express LFA1 (CD11a/CD18; $\alpha_L\beta_2$), which interacts with endothelial ICAM-1, and VLA4 (CD49d/CD29; $\alpha_4\beta_1$), which interacts with endothelial VCAM-1, to mediate firm cell adhesion (Van Linthout et al., 2011). MSCs also express CD44 and P-selectin which can play important roles in mediating MSC rolling, adhesion to ECs and their subsequent transendothelial migration (Nitzsche et al., 2017).

Importantly, in addition to the expected increased adhesion on IR injured tissue, we further noted that 3D culture significantly enhanced the adhesion of all types of stem cells to both sham and IR injured tissue when compared to adhesion of 2D cells on the appropriate tissue. The percentage increase was most striking for BM-MSCs Y201 cells. Indeed our novel data demonstrated that on average, 2-3 2D cultured hBM-MSCs Y201 were adherent on the heart section per field of view, but this increased to 16-17 when cells were 3D cultured. Although 3D cultured WJ-MSCs were generally the most adherent MSC population, they were also relatively adherent on sham tissues as well. The mechanisms by which this increase may have been mediated are described later (**Sections 3.4.3 and 3.4.4**). Briefly, this is likely linked to the substantial change in the pattern of gene expression of MSCs following 3D culture that has been previously described (Honczarenko et al., 2006, Sackstein et al., 2008, Suila et al., 2014). Indeed, Potapova and colleagues found 1,731 genes were overexpressed in human MSCs cultured as 3D aggregates in hanging drops when compared to monolayer cultured cells (Potapova *et al.,* 2009). Ultimately, this leads to the differential expression of surface adhesion molecules which modify their endothelial interactions.

MSCs obtained from different sources show a difference in both their functionality and phenotype (James et al., 2015). The two different hBM-MSCs used in this study have been extensively characterised by Professor Genever's group who generated these cells and shown to be distinctly different in terms of their differentiation and immunomodulatory and capacity (James et al., 2015; Kay et al., 2018). The characteristics of these two BM-MSC sub-types are summarised in **Table 3.1**. Importantly, they showed that hBM-MSCs Y201 exhibited a significantly higher expression set of genes which were related to vascular interactions and in playing a role in processes such as blood vessel remodelling, blood vessel morphogenesis, development and patterning of vessels. In contrast, hBM-MSCs Y202 rarely associated with CD31+ vascular cells in the BM when imaged using immunohistological staining and did not co-localise with perivascular stroma. This may explain why 3D cultured hBM-MSCs Y201 were able to adhere more readily to ECs than 3D cultured hBM-MSCs Y202.

Interestingly, general adhesion of MSCs to ECs was not dependent upon whether the ECs had been TNFα activated or not. This observation was similar to a previous study by Kavanagh and colleagues (Kavanagh et al., 2013) and previous reports from the Kalia lab which showed that WJ-MSCs adhesive capacity did not correlate with the level of VCAM-1 expression or oxidative damage of ECs. This suggested that the MSC adhesive potential to endothelium did not necessarily depend on vascular injury or cytokine stimulation but could be modified by the culture conditions.

HSCs, WJ-MSCs, hBM-MSCs Y201 and hBM-MSCs Y202 were able to adhere to ICAM-1 and VCAM-1 protein substrates. Both MSCs and HSCs have the same repertoire of receptor and cell surface adhesion molecules as leukocytes which can bind to endothelial counter ligands such as ICAM-1 and VCAM-1 (Sohni and Verfaillie, 2013). Our finding is consistent with previous reports (Huygen et al., 2002, Kavanagh et al., 2013, Kavanagh et al., 2015, Segers et al., 2006). MSCs have been reported to express the $\alpha_4\beta_1$-integrin (VLA-4), which is the primary ligand of endothelial VCAM-1 (Segers *et al.,* 2006). This would explain their ability to interact with VCAM-1 protein. The reason for differences between WJ-MSCs and BM-MSCs adhesion to ICAM-1 could be due to the dissimilarity of the primitive microenvironment from where these cells were obtained (Ullah *et al.*, 2019). Recent work by Petrenko and colleagues demonstrated that WJ-MSCs significantly expressed higher COX2 and ICAM-1 compared to BM-MSCs and adipocyte-derived MSCs cells whereas BM-MSCs expressed higher VCAM-1 than other types of cells (Petrenko *et al.,* 2020). How this would modify their adhesion to immobilised VCAM-1 and ICAM-1 is not clear. Alternatively, differential adhesion could be explained by passage number and cell age (Valcarcel et al., 2008). Indeed, freshly-obtained MSCs show higher homing ability than sub-cultured MSCs which may explain why primary WJ-MSCs, used at passage 5-7, showed the highest adhesion capability to ICAM-1 and VCAM-1, whereas immortalised hBM-MSCs, many passages down the line, showed less capacity.

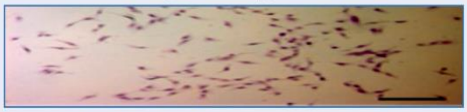
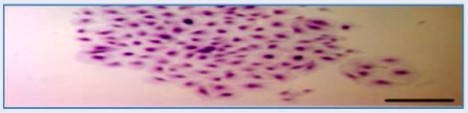
	hBM-MSC Y201	hBM-MSC Y202
Phenotype in culture	Elongated and fibroblastoid *typical of MSCs*	Flattened and spread
Colonies in culture	Dispersed colonies with low cell-cell contact, typical of a migratory phenotype 	High density, compact colonies 
Cell size	Smaller *Perimeter: 190±34µm / Cell area: 857±214µm²*	Larger *Perimeter: 317±107µm / Cell area: 1,649±614µm²*
Tri-lineage (OAC) differentiation potential	Tri-potent	Severely impaired or non-differentiating
CD317 expression	CD317 negative	CD317 positive – 9% of BM-MSCs
Similarity to primary parent BM-MSCs	Similar	Least similar
Expression of genes consistent with vascular interactions	Peri-vascular interactions in BM *genes related to vascular growth, vessel remodelling, development, artery angiogenesis…*	Do not interact with vasculature *higher IL-7⁺ secreting ability*
Immunomodulatory potential	More effective at suppressing T cell proliferation ; increased polarisation of T cells to more anti-inflammatory Th2 cell types compared to Y202	Less effective at suppressing T cell proliferation ; increased polarisation of T cells to more pro-inflammatory Th1 cell types compared to Y201

Table 3.1. Multiparameter analysis of human bone marrow stromal cells identifies distinct subtypes. A heterogeneous population of human BM-derived MSCs (also called marrow stromal cells) were isolated and used to generate 4 phenotypically different immortalised clones by the Genever research group (James et al., 2015). Two of these clones, namely Y201 and Y202, were used in the current study and expressed typical MSC surface markers and were also negative for vascular markers. However, there were a number of differences between these two sub-populations. Y201 were a highly differentiating, $CD317^{neg}$ MSC subset, with expression of genes consistent with perivascular interactions in the BM. Y202 were a sub-population that included non-differentiating, $CD317^{pos}$ BM resident MSCs, which did not express genes associated with vascular interactions. The same group later demonstrated that Y202 cells were less effective at supressing CD4+ T cell proliferation and polarised more of these lymphocytes after 5 days co-culture into a sub-population of T helper cells with a more pro-inflammatory profile when compared to Y201 cells (Kay et al., 2018). The blue components of the table summarise the information and data provided by James and colleagues in 2015. The green component of the table summarises the data provided by Kay and colleagues from the same Genever group in 2018.

3.4.3. 3D culture increased expression primarily of CXCR4 on hBM-MSCs Y201

Conventional 2D culture conditions are known to affect the adhesive potential and morphology of stem cells by decreasing MSC surface adhesion molecules or receptors that respond to chemotactic signals (Ryu et al., 2019). Again, this may explain the limited clinical success of these cells for CVDs. Our result show that the most remarkable observation was that 3D culture improved the expression of CXCR4 on hBM-MSCs Y201, which did not express or had lost expression of this receptor when cultured in 2D monolayers. This observation was consistent with recent studies (Potapova et al., 2008, Wang et al., 2019). Indeed, Potapova and colleagues not only showed that 3D culture increased CXCR4 expression on human MSCs, but that when 3D cultured MSCs were then grown in 2D monolayers, CXCR4 levels reversed back to the levels more characteristic of a monolayer (Potapova et al., 2008). They also similarly demonstrated an increased adhesion to HUVECs. Notable differences to the current work were that they activated ECs in the presence of hypoxia and performed the adhesion assay in the presence of SDF-1α. Increased adhesion of MSCs to VCECs *in vitro* in the current study in the absence of SDF-1 can still be mechanistically explained by the increased surface expression of CXCR4. ECs stimulated *in vitro* with inflammatory factors such as TNF-α can secrete a multitude of chemokines, including IL-8, RANTES and possibly SDF-1α (Potapova et al., 2008). Although CXCR4/SDF-1α signalling primarily induces directional chemotaxis or migration of cells, it is also able to enhance integrin activity, thereby increasing cell adhesion (Peled et al., 2000; Cheng et al., 2012). This would explain the increased adhesion of 3D cultured MSCs expressing more CXCR4 to VCECs *in vitro*. This is however; highly speculative as some studies have shown that TNFα activation of ECs tends to not affect, or actually decreases,

SDF-1α release or gene expression (Salvucci et al., 2004). It is not clear how the increased expression of CXCR4 could mechanistically explain the increased adhesion observed to 'non-living' frozen hearts in the Stamper-Woodruff assays or to immobilised ICAM-1/VCAM-1 in the absence of SDF-1α. Regardless, increased CXCR4 expression would be useful in an *in vivo* setting where SDF-1α would be released from injured tissue such as the heart and could therefore lead to increase integrin mediated retention.

Increased adhesion to the various substrates could also be explained by the fact that 3D culture is known to increase the expression of critical surface integrins. Indeed, expression of ICAM-1 binding LFA-1 was noted to have increased 3-fold in CT26 cancer cells derived from spheroids (Valcarcel et al., 2008). Additionally, expression of VCAM-1 binding VLA-4 significantly increased after 3D culture on CD34+ HSCs. In contrast, Bartosh and colleagues used flow cytometry to demonstrate a decreased surface expression of the VLA-4 integrin sub-unit α4 (CD49d) when MSCs were cultured using a hanging drop method (Bartosh et al., 2010). In the current study, expression levels of these important integrins involved in mediating firm adhesion of circulating cells with ECs were not investigated but would be worthwhile.

Changes in the expression of non-integrin adhesion molecules such as CD44 may also explain the results presented. There are several well-known ligands of CD44 including HA, osteopontin, collagens and matrix metalloproteinases (Viola et al., 2015). HA is a glycosaminoglycan that is expressed within the luminal glycocalyx covering ECs and is considered the major ligand for CD44. The CD44-HA interactions have been shown to be fundamental for leukocyte-EC binding and their subsequent extravasation from blood into inflamed tissue sites (Viola et al., 2015). Importantly, HA synthesis has been found to be

inducible in ECs cultures, and its synthesis is triggered by pro-inflammatory mediators such as TNF-α, IL-1β and lipopolysaccharide (Viola et al., 2015). Therefore, the increased adhesion of 3D cultured hBM-MSCs Y201 and hBM-MSCs Y202 to IR injured heart sections and of hBM-MSCs Y201 to TNFα stimulated VCECs could be linked mechanistically to the somewhat increased expression of CD44 on these MSCs after 3D culture.

3.4.4. 3D cultured hBM-MSCs Y201 increased ICAM-1 expression which was more evenly distributed on its surface

ICAM-1 and VCAM-1 are traditionally considered EC counterligands for LFA-1 and VLA-4 integrins found on the surface of circulating neutrophils and lymphocytes (Burne et al., 2001). Indeed, interactions of ICAM-1 or VCAM-1 with leukocyte integrins mediate their recruitment during inflammatory and immune processes. However, increasing evidence has demonstrated that these same adhesion molecules are also expressed constitutively at low levels on the surface of MSCs and can even serve as markers of MSCs (Ren et al., 2010, Nitzsche et al., 2017). Although their exact function on MSCs remains unclear, increasing evidence has indicated that they can mediate close adhesive interactions of MSCs with immune T-cells (Hu et al., 2019). Indeed, Ren and colleagues demonstrated that increasing ICAM-1 and VCAM-1 expression on MSCs, increased their adhesive interactions with lymphocytes and this was subsequently linked to greater immunosuppressive activity (Ren et al., 2010). Interestingly, MSCs overexpressing ICAM-1 have been found to be more positive for adhesion molecules including the integrin CD29 (β_1) subunit and CD44, are better at tri-lineage differentiation and have superior immunosuppressive activity (Tang et

al., 2018). Hence, it is likely that the increased ICAM-1/CD54 demonstrated flow cytometrically on the surface of 3D cultured hBM-MSCs Y201 would explain their increased adhesion to the various substrates tested in this chapter. It will be interesting to see if hBM-MSCs Y201, with increased CXCR4 and ICAM-1 expression, are better at homing, adhering and being immunomodulatory in the injured heart *in vivo.*

Confocal microscopy showed that cells dissociated from spheroids expressed surface adhesion molecules more evenly over the surface, whereas in 2D cultured cells the adhesion molecules tended to be concentrated or clustered on one side of the cell surface. This site correlated with where they were attached to the bottom of the plastic flask. It has previously been shown that tumour cells grown in 2D tissue culture form monolayers which result in fewer cell-cell contact points, and the clustering of integrins such as β1 at sites of focal adhesion contacts between the cells and the culture surface (Howe et al., 2012). In contrast, the 3D spheroid hanging drop culturing method allowed cells to attach or aggregate together and form spheres rather than sticking to the surface of culture dishes (Ryu et al;, 2019). Therefore, cell-cell contacts are increased and integrins are not clustered at sites of focal contacts, but become more dispersed across the cell membrane at multiple points (Cesarz and Tamama, 2016). Distribution of adhesion molecules over a greater surface area has a significant impact on their ability to successfully form firm adhesive interactions with counter-ligands on inflamed endothelium (Ren et al., 2010). The distribution of surface adhesion molecules is also critical to how well leukocytes can migrate to injured sites (Hocde et al., 2009). It remains to be seen whether this more uniform distribution of adhesion molecules on 3D cultured MSCs impacts their ability to home and become retained within the injured heart *in vivo.*

3.5 Conclusion

This chapter aimed to investigate the characteristics and adhesive capacity of MSCs isolated from different sources, namely the BM and umbilical cord Wharton's jelly, and determine which population or sub-population could mediate adhesive interactions with coronary microvessels in later *in vivo* studies. Two of the MSC populations tested were derived from the same BMS site and generated using a process of cell cloning and telomerase-based immortalisation (James et al., 2015). CD317 was identified as a novel biomarker that allowed isolation of these two sub-sets and was found to be expressed on only 9% of BM MSCs (James et al., 2015; Kay et al, 2018). The immunomodulatory ability of these two populations differed with hBM-MSCs Y202 not able to supress CD4+ T cell proliferation as effectively as hBM-MSCs Y201. Furthermore, they encouraged T cell polarisation into a more pro-inflammatory Th1 subset when compared to hBM-MSCs Y201, which polarised T cells into the more anti-inflammatory Th2 subset (Kay et al., 2018; **Table 3.1**). This clearly suggested single cells were unlikely to possess all properties commonly ascribed to MSCs and that specific functional attributes, such as differentiation or immunomodulatory competency, were found within distinct sub-populations. Our own results supported this conclusion as the adhesive ability of these two subsets to various substrates was also different. This inter- and intra-tissue MSC heterogeneity may be associated with varying homing potential and therapeutic efficacy in the injured heart, which may explain the poor clinical success to date. However, this has not been extensively studied in any injured organ, and data from comparative *in vivo* studies, particularly of intra-tissue MSC sub-populations, are limited.

In this chapter, we also developed a strategy to improve MSC adhesion capacity using a 3D spheroid culture method. Although 3D culture considerably reduced the size of all MSC populations, there were some additional effects that seemed to be observed primarily on hBM-MSCs Y201. Indeed, 3D culture improved: (i) the adhesion of hBM-MSCs Y201 to frozen heart sections more so than other stem cells; (ii) the adhesion of only hBM-MSCs Y201 to inflamed ECs; (iii) the adhesion of hBM-MSCs Y201 to VCAM-1, albeit to a similar degree as other cells; (iv) expression of CXCR4 remarkably only on hBM-MSCs Y201 and to a lesser degree CD54/ICAM-1 and also (v) distributed adhesion molecules more evenly on their surface. Collectively, our data combined with that of previously published work on these specific MSC sub-populations, suggests that hBM-MSCs Y201 may yield more therapeutic benefit in the injured heart *in vivo*.

CHAPTER 4

Developing Strategies to Improve Mesenchymal Stem Adhesion to the Ischaemia-Reperfusion Injured Heart – *in vivo* Studies

4.0 Developing strategies to improve MSC adhesion to the IR injured heart – *in vitro* studies

4.1 Introduction and Hypothesis

4.1.1. Introduction

Myocardial IR injury is indicated by insufficient blood supply to the heart, primarily due to a blockage in one or more of the epicardial coronary arteries, followed by the restoration of flow using pharmacological and surgical interventions. However, reperfusion has adverse consequences leading to greater muscle infarction than ischaemia alone (Kalogeris et al., 2012). Indeed reperfusion mediates a complex sterile inflammatory response in which innate and adaptive inflammatory processes are stimulated by components released by injured or dead cells. Recruitment of thromboinflammatory cells and production of multiple cytokines are triggered which ultimately results in significant perturbations and damage to the coronary microcirculation (Kvietys and Granger, 2012). Hence the coronary microcirculation is both a 'culprit' and a 'victim' of myocardial IR injury (Hausenloy et al., 2019). These multiple vascular events have been characterised in detail *in vivo* using novel intravital imaging of the IR injured beating mouse heart by the Kalia Group (Kavanagh et al., 2019).

Preventing microcirculatory disturbances is essential if the myocardium is to survive. One such option is to utilise stem cells as a form of cell therapy. MSCs provide an interesting therapeutic alternative for treatment of MI, however, clinical success has been poor. This

may be partly explained by their poor recruitment from the peripheral blood, following their exogenous infusion, and subsequent adhesion to the microvessels of the injured heart. Therefore, the degree to which MSCs cells can be recruited to the IR injured heart is an important consideration to make especially as we have shown in the previous chapter that different types of MSCs appear to have differing adhesion capabilities. Indeed, in the previous chapter we also showed that 3D culture of the hBM-MSCs Y201 sub-population, using a hanging drop method, not only reduced their size considerably, modified surface adhesion molecule and chemokine receptor expression, but more importantly improved their adhesion to frozen IR injured heart sections *in vitro* more so than other MSC types. These structural and functional changes may yield more therapeutic benefit in the injured heart *in vivo*. However, to date no studies have previously compared the adhesive capabilities of different MSC types to the IR injured heart *in vivo.* Therefore, in the current chapter, we aimed to intravitally test the ability of this particular bone marrow MSC sub-population to home to and subsequently become adherent in the IR injured beating heart *in vivo*. Whether 3D culture also improved these events *in vivo* will be tested by comparing to the dynamics of cells cultured using conventional 2D methods. Events such as the trafficking / homing of circulating cells, be they stem cells or blood cells, and changes in blood flow and myocardial perfusion are a range of dynamic events that cannot be captured with conventional immunohistochemical analysis, which simply provides a 'static' snapshot in time. Dynamic data of this nature can only be acquired through intravital imaging and not histologically. Although the presence of circulating cells within coronary microvessels can be imaged in tissue sections using immunostaining, these images do not inform us whether cells are genuinely adhere in the heart or simply caught in time passing through it. We also obtain no indication of whether exogenously injected potentially

therapeutic cells cause blockage of blood flow in the blood vessels in which they are captured – if this is significant, it may cause more damage than good and impact on their therapeutic effectiveness.

Poor clinical success using MSCs has also been partly attributed to their exact therapeutic mechanistic properties and mode of action remaining poorly understood due to a lack of robust pre-clinical / basic experimental studies (Levy et al., 2020). It is, therefore, important to understand how MSCs exert benefit, if at all, in order to ascertain how to improve their therapeutic effectiveness in translational and clinical studies. Since microvascular perturbations are an important contributor to IR injury in any organ, this chapter will also focus on identifying whether 2D or 3D cultured hBM-MSCs Y201 could potentially exert myocardial protection through modifying thromboinflammatory events *in vivo* and subsequently improving myocardial perfusion. Immunohistochemical analysis can, at most, provide information on neutrophil and platelet infiltration. However, it cannot indicate whether the heart has adequate blood perfusion, alterations in functional capillary density, whether the velocity of circulating cells has been reduced to a level that is conducive to being pro-adhesive, whether coronary microvessels are viable and not 'leaky' etc (Kavanagh et al., 2019). Therefore, in this chapter we will apply our novel intravital microscopy method to the stabilised beating mouse heart to answer some of these pertinent questions.

4.1.2. Hypothesis

1. 3D cultured MSCs, specifically the hBM-MSCs Y201 sub-population, will have a greater ability to home to, and become adherent within, the IR injured beating heart *in vivo* when compared to those MSCs cultured using conventional 2D culture.

2. 3D cultured hBM-MSCs Y201 will reduce infarct size in the IR injured heart by inhibiting any thromboinflammatory events, protect the structural integrity of the microvessels and increase regional blood flow perfusion through the heart.

4.1.3. Specific aims

1. Intravital studies will be performed on a stabilised small region of the sham or IR injured beating mouse heart left ventricle in order to image the coronary microcirculation *in vivo*. This model will be used to assess the number of free flowing 2D and 3D cultured hBM-MSCs Y201 trafficking through the sham and IR injured heart and also quantitate their subsequent firm adhesion to coronary microvessels. Results will be compared to 2D and 3D cultured hBM-MSCs Y202.
2. MSC recruitment data generated intravitally by imaging a small region of the heart surface will be confirmed by analysing more regions of the heart surface *ex vivo* using EVOS fluorescent microscopy. Additionally, flow cytometry will be performed on digested hearts to quantitate 2D and 3D cultured hBM-MSCs Y201 presence throughout the sham and IR injured whole heart. Results will be compared to 2D and 3D cultured hBM-MSCs Y202.
3. Intravital studies will be performed to determine whether 2D and/or 3D cultured hBM-MSCs Y201 can modify thromboinflammatory responses mediated in the IR injured heart *in vivo*. Specifically, the recruitment of endogenous neutrophils and platelets will be quantitated in IR injured hearts in mice receiving either no cellular therapy or 2D and 3D cultured hBM-MSCs Y201. Changes in functional capillary

density will also be assessed. Results will be compared to 2D and 3D cultured hBM-MSCs Y202.

4. Intravital studies will be performed to determine whether cellular therapy combined with the infusion of the anti-coagulant heparin can enhance the retention and/or potential vasculoprotective effects of MSC therapy in the IR injured heart *in vivo*.

5. Multiphoton microscopy will be used to ascertain whether any modification of neutrophil and/or platelet presence by MSCs was also occurring in the deeper layers of the myocardium.

4.2 Methods

The methods used in the chapter have been described in detail in **Chapter 2**. Briefly, anaesthetised mice underwent temporary ligation of the LAD artery for 45 minutes after which it was removed to initiate reperfusion for 2-2.5 hours. Anaesthetised sham mice underwent the same surgical procedure without the ligation of LAD. To determine the recruitment of 2D or 3D cultured hBM-MSCs Y201 or hBM-MSCs Y202 to the beating heart, they were firstly fluorescently labelled by incubating with 5µM of CFSE stain for 20 minutes before injection (**Section 2.2.6**). $5x10^5$ cells were then administered via the cannulated carotid artery at approximately 20 minutes post-reperfusion with the first intravital recording taking place at 30 minutes post-reperfusion. The analysis of intravital images was carried out using Slidebook 6.0 capturing software (3i Inc; USA).

The homing of exogenously administered MSCs to the heart was analysed by manually counting the number of free flowing MSCs trafficking through the coronary microcirculation within a small region of the stabilised beating heart during a 2 minute

period of recording. Similarly, adherents MSCs were quantitated as those present in the field of view microvasculature during 2 minutes of recording time. Adherent MSCs were considered to be those cells that remained stationary within the microvessel for ≥ 30 seconds, whereas other cells were recognised as free-flowing. A similar protocol was used to quantitate endogenous adherent neutrophils labelled using a PE-conjugated rat anti-mouse Gr-1 (Ly6G) antibody. Endogenous platelets were labelled with an APC-conjugated rat anti-mouse CD41 antibody and ImageJ was used to quantitate their presence by calculating the mean integrated fluorescence density. Perfused vasculature was identified intravitally by injecting FITC-BSA at the end of imaging.

At the end of intravital experiments, the heart and lungs were collected from culled mice to determine the presence of CFSE-labelled MSCs *ex vivo* using fluorescent EVOS and deep tissue multiphoton microscopy. For some experiments, the hearts and lungs were collagenase digested to a single cell suspension and analysed flow cytometrically for fluorescent MSC presence. Dual Evan's blue and TTC staining was used to identify infarcted muscle which measured by calculating the infarct region as a percentage of the area at risk (AAR). GraphPad 6.0 software was used to perform statistical analysis with data presented as the mean ± SEM.

4.3 Results

4.3.1. Increased 3D cultured MSC adhesion within injured coronary microcirculation

HPC-7s have been routinely used by the Kalia lab to investigate HSC homing to various organs *in vivo* and to track them intravitally. Intravital studies monitoring HSC trafficking has been limited due to difficulties in isolating sufficient numbers for *in vivo* experimentation. As a result, many HSC trafficking studies have relied heavily on HSC lines. In the current project, HPC-7s were only used for *in vitro* studies. In Chapter 3, we noted that MSCs were generally more adhesive to IR injured frozen heart sections *in vitro*. Whether this was also true in the presence of flow *in vivo* was investigated intravitally in the IR injured beating heart and compared to mice undergoing sham surgery.

In initial experiments, exogenous hBM-MSCs at a concentration of $1x10^6$ cells/mouse were injected via the carotid artery as a single bolus dose at 30 minutes post-reperfusion. However, as shown in **Figure 4.1A**, the survival rate after cell transplantation was very low with the majority of mice unable to survive beyond 2 hours of cell administration. The large aggregates of CFSE-labelled hBM-MSCs were found in pulmonary blood vessels of the dead mice as shown in **Figure 4.1B**. We concluded that the mice died from MSCs pulmonary embolism. Therefore, the concentration of cells was adjusted to $5x10^5$ cells/mouse, injected at 30 minutes post-reperfusion, which greatly improved the survival rate. Therefore, this concentration was used for all subsequent intravital experiments.

Adhesion of 2D cultured hBM-MSCs Y201 was low in sham hearts. Immediately after infusion, between 0-3 cells were identified adherent within the imaged field of view (413µm x 308µm). This number did not change much over the two hours of intravital imaging. However, as shown in **Figure 4.2A**, adhesion of 3D cultured hBM-MSCs Y201 in the IR injured heart was significantly higher at all-time points than those observed in sham mice. Although ~4-5 cells were adherent at the time of infusion, this gradually increased to 6-8 cells with time. For 3D cultured hBM-MSCs 201, again adherent MSCs in sham hearts remained low with ~3-7 cells/field imaged. However, an almost 3-fold significant increase in adherent cells was noted in IR injured hearts with ~8-17 adherent cells observed. **Figure 4.2B** shows that sharp rise was noted after 15 minutes of infusion. Adhesion of 3D cultured hBM-MSCs 201 was higher in both sham and injured hearts compared to 2D cultured cells.

As shown in **Figure 4.2C**, adhesion of 2D cultured hBM-MSCs Y202 was also low in sham hearts with ~0-4 cells/field adherent which did not change over the period of imaging. However, injury again significantly increased MSC adhesion at all-time points 4-10 adherent cells/field observed. Again, 3D cultured MSCs Y202 showed a low retention in sham hearts but this significantly increased at all-time points in injured hearts with 6-14 adherent cells observed as shown in **Figure 4.2D**. Adhesion of 3D cultured hBM-MSCs 201 was higher in both sham and injured hearts compared to 2D cultured cells. In conclusion, both MSC sub-populations appeared to be more adhesive to the coronary microcirculation of IR injured hearts with 3D cultured cells the most adhesive.

4.3.2. 3D culture technique increases free flowing and adherent hBM-MSCs Y201 in the healthy sham heart

IVM was used to investigate whether culturing technique impacted on MSC homing capacity to the sham heart. Immediately after infusion, ~3-6 free-flowing 2D cultured hBM-MSCs Y201 were observed trafficking through the heart in the imaged field of view. This was significantly increased with 3D cultured hBM-MSCs Y201 at the time of infusion with ~9-12 cell observed trafficking through the heart. As shown in **Figure 4.3A**, free flowing MSC number was greatly reduced after the initial point of cell infusion for both 2D (0-5 cells/field of view) and 3D (0-5 cells/field of view) cultured hBM-MSCs Y201. No significant differences in free flowing cells were observed at these later time points. Number of adherent 3D cultured hBM-MSCs Y201 (~5 cells/field of view) was significantly greater than 2D cultured hBM-MSCs Y201 (~2 cells/field of view) at all time points (**Figure 4.3B**). Interestingly, as shown in **Figure 4.3C**, IVM was able to detect the smaller size of 3D cultured hBM-MSCs Y201 *in vivo* when compared to those grown in 2D culture**.**

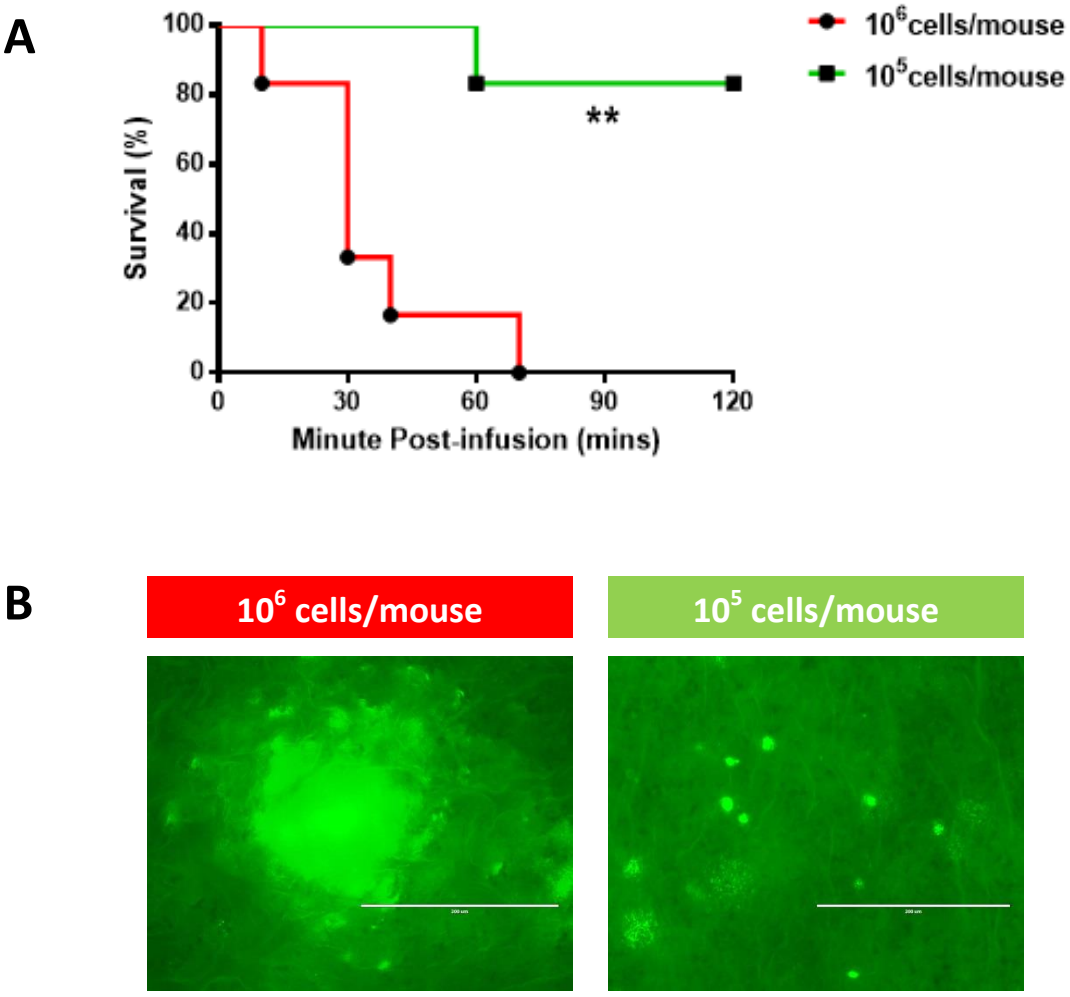


Figure 4.1. Survival rate of hBM-MSCs transplanted mice following myocardial IR injury. At the end of intravital experimentation, animals were culled and the lungs were removed and imaged on their surface using an EVOS fluorescent microscope. **(A)** The survival rate of mice received exogenous hBM-MSCs at the concentration of 10^5 cells/mouse was significantly higher when compared to mice received hBM-MSCs at the concentration of 10^6 cells/mouse. **(B)** Representative images taken from the surface lungs are shown. Interestingly, large clumps or aggregates of 2D cultured hBM-MSCs Y202 were present in pulmonary blood vessels in mouse received hBM-MSCs at the concentration of 10^6 cells/mouse, whilst smaller aggregates or individual 2D cultured hBM-MSCs Y201 were observed in mouse transplanted with hBM-MSCs at the concentration of 10^5 cells/mouse. Data were analyzed by Mantel Cox tests. N=5, **p<0.01. Images were captured with a 20x objective. Scale bar = 200µm.

Similar significant results were obtained for free-flowing hBM-MSCs Y202 in sham hearts. Interestingly, the number of both 2D and 3D cultured free flowing hBM-MSCs Y202 was greater than those observed for hBM-MSCs Y201, with ~11 and 21 hBM-MSCs Y202 observed at the time of cell infusion respectively. Again, as shown in **Figure 4.4A**, no significant difference in free flowing MSCs was observed after the time of infusion. Although adhesion of 3D cultured hBM-MSCs Y202 was increased when compared to 2D cultured cells (**Figure 4.4B**), this did not reach statistical significance.

4.3.3. Increased myocardial recruitment of 3D cultured hBM-MSC confirmed *ex vivo* using EVOS microscopy with significant entrapment within lungs of all MSCs

To confirm the data obtained from intravital imaging of the beating heart, the recruitment ability of MSCs was also imaged and qualitatively assessed in the same healthy sham heart *ex vivo* using EVOS fluorescence microscopy. At the end of intravital experimentation (2½ hours post-reperfusion / 2 hrs post-MSC infusion), animals were culled and the heart and lungs removed and imaged on their surface using an EVOS fluorescent microscope. Images were taken from a number of regions on the surface of the left ventricle of the heart and from the left and right lung lobes. Generally, in the heart, as shown in **Figure 4.5A**, it appeared as if more 3D cultured hBM-MSCs Y201 were identified attached to blood vessels compared to 2D cultured cells. Interestingly, as shown in **Figure 4.5C** and **D**, 3D cultured significantly increased hBM-MSCs Y201 recruitment in the heart and significantly decreased hBM-MSCs Y201 in the lung.

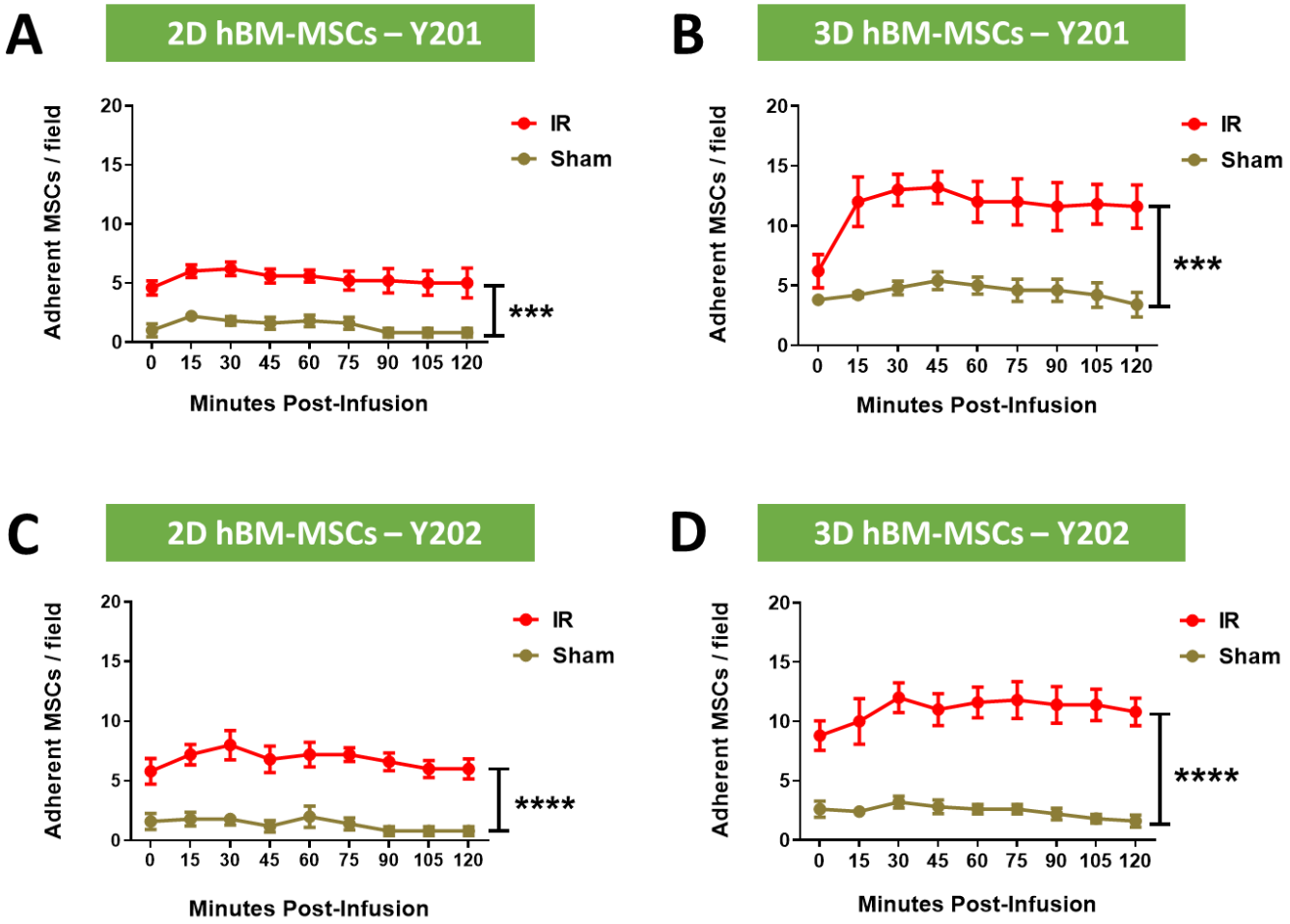


Figure 4.2. Intravital microscopy demonstrated an increased adhesion of both CFSE-labelled MSC sub-populations within the IR Injured heart with 3D cultured cells most adhesive. **(A)** 2D hBM-MSCs Y201 were significantly more adherent within IR injured hearts when compared to sham hearts at all time points. **(B)** Similar results were observed with 3D hBM-MSCs Y201. Furthermore, adhesion of 3D cultured hBM-MSCs Y201 was higher in both sham and injured hearts when compared to 2D cultured hearts. **(C)** 2D hBM-MSCs Y202 were also significantly more adherent within IR injured hearts when compared to sham hearts at all time points. **(D)** Similar results were observed with 3D hBM-MSCs Y201. Again, 3D cultured hBM-MSCs Y201 adhesion was higher in both sham and injured hearts compared to 2D cultured hearts. The first intravital videos of the beating heart were captured immediately after infusion of a single dose of $5x10^5$ MSCs/ml via the intra-carotid artery. In IR injured hearts, this was at 30 minutes post-reperfusion. Hence the above 0 time point is the equivalent of 30 minutes post-reperfusion. Results presented as mean ± SEM. Statistical analysis performed using Student's t-test. ***p<0.001, ****p<0.0001; N=5 mice per group.

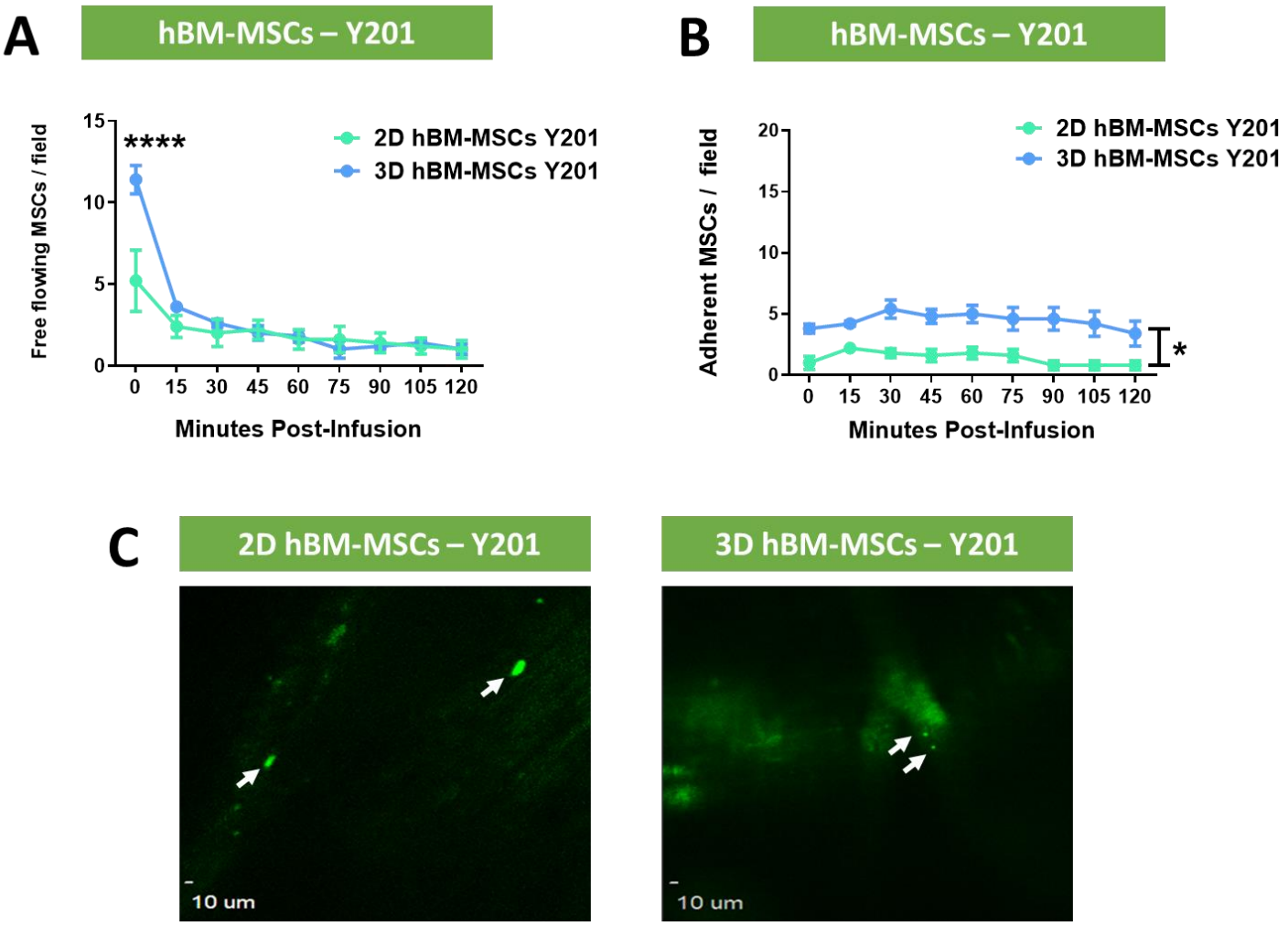


Figure 4.3. Intravital microscopy demonstrated that 3D culture improved numbers of hBM-MSCs Y201 trafficking through the healthy sham beating heart after systemic infusion and their adhesion within the coronary microcirculation *in vivo*. **(A)** 3D culture significantly increased numbers of hBM-MSCs Y201 observed freely flowing in the healthy heart immediately after their systemic infusion. Free flowing MSC number was greatly reduced after the initial point of cell infusion for both 2D and 3D cultured hBM-MSCs Y201 with no significant differences observed. **(B)** 3D culture significantly increased the adhesion of hBM-MSCs Y201 at all time points within the healthy sham heart when compared to 2D cultured cells, with more than a doubling of the number of cells seen**. (C)** Representative intravital images of CFSE-labelled 2D and 3D culture hBM-MSCs Y201 (arrows) trafficking or adherent within myocardial microvessels. Interestingly, most cells derived from 3D culture appeared smaller when injected *in vivo*. The first intravital videos of the beating heart were captured immediately after infusion of a single dose of $5x10^5$ MSCs/ml via the intra-carotid artery. Results presented as mean ± SEM. Statistical analysis performed using Student's t-test. N = 5 mice per group. *p<0.05; ****p<0.0001. Scale bar = 10µm.

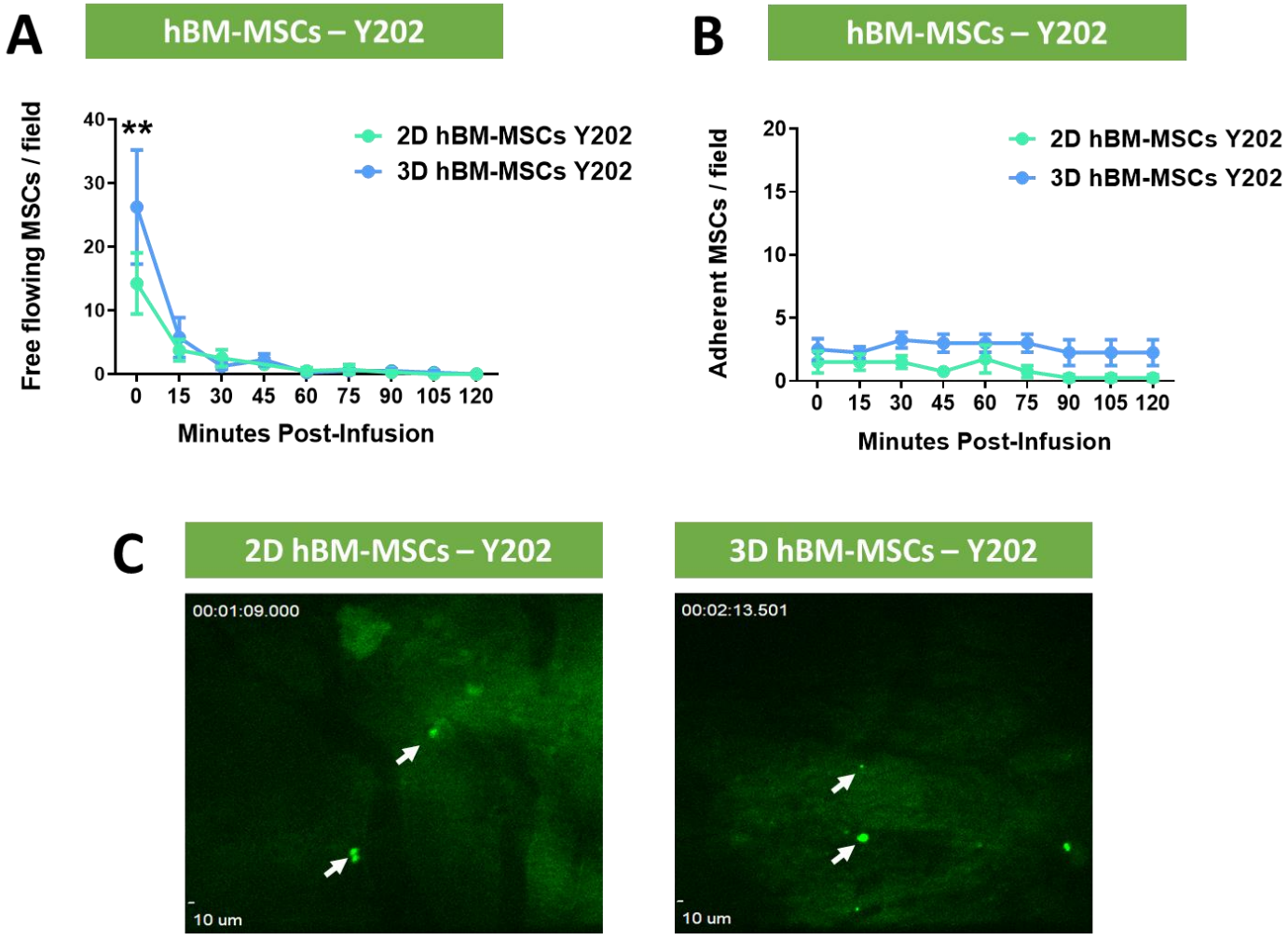


Figure 4.4. Intravital microscopy demonstrated that 3D culture improved numbers of hBM-MSCs Y202 trafficking through the healthy sham beating heart after systemic infusion and their adhesion within the coronary microcirculation *in vivo*. **(A)** 3D culture significantly increased numbers of hBM-MSCs Y202 observed freely flowing in the healthy heart immediately after their systemic infusion. Free flowing MSC number was greatly reduced after the initial point of cell infusion for both 2D and 3D cultured hBM-MSCs Y202 with no significant differences observed. **(B)** Although 3D culture increased the adhesion of hBM-MSCs Y202 within the healthy sham heart when compared to 2D cultured cells, this did not attain statistical significance. **(C)** Representative intravital images of CFSE-labelled 2D and 3D culture hBM-MSCs Y202 (arrows) trafficking or adherent within myocardial microvessels. Interestingly, most cells derived from 3D culture appeared smaller when injected *in vivo*. The first intravital videos of the beating heart were captured immediately after infusion of a single dose of $5x10^5$ MSCs/ml via the intra-carotid artery. Results presented as mean ± SEM. Statistical analysis using Student's t-test. N = 5 mice per group. **p<0.01. Scale bar = 10µm.

Within the lungs, the numbers of 2D and 3D cultured hBM-MSCs Y201 appeared to be relatively similar. Interestingly, as shown in **Figure 4.5B**, large clumps or aggregates of 2D cultured hBM-MSCs Y201 presented in the blood vessels of lung, whilst smaller aggregates or individual 3D cultured hBM-MSCs Y201 were observed. Furthermore, the size of individual 3D cultured hBM-MSCs Y201 detected in the lungs appeared to be smaller than 2D cultured hBM-MSCs Y201. Similar *ex vivo* observations were made in the hearts and lungs of healthy sham mice receiving infusions of 2D or 3D cultured hBM-MSCs Y202 as shown in **Figures 4.6A-B**. However, 3D cultured did not increased hBM-MSCs Y202 recruitment in the heart and decreased hBM-MSCs Y202 in the lung. Overall, the intravital data demonstrating increased cardiac retention of 3D cultured BM-MSCs was confirmed in *ex vivo* using EVOS microscopy that sampled a greater area of the heart than that just imaged within the centre of the stabiliser *in vivo.*

4.3.4. 3D culture increases both free flowing and adherent hBM-MSCs Y201, but only adhesion of hBM-MSCs Y202, to the IR injured heart

We next investigated whether culture method impacted MSC homing capacity to IR injured heart. Immediately after infusion, ~7 cells free-flowing 2D cultured hBM-MSCs Y201 were observed trafficking through the heart in the imaged field of view. Although this increased with 3D culture at the time of infusion, this did not reach statistical significance. As shown in **Figure 4.7A**, Free flowing MSC number was greatly reduced thereafter for both 2D and 3D cultured hBM-MSCs Y201 with no significant differences in free flowing cells was observed at these later time points.

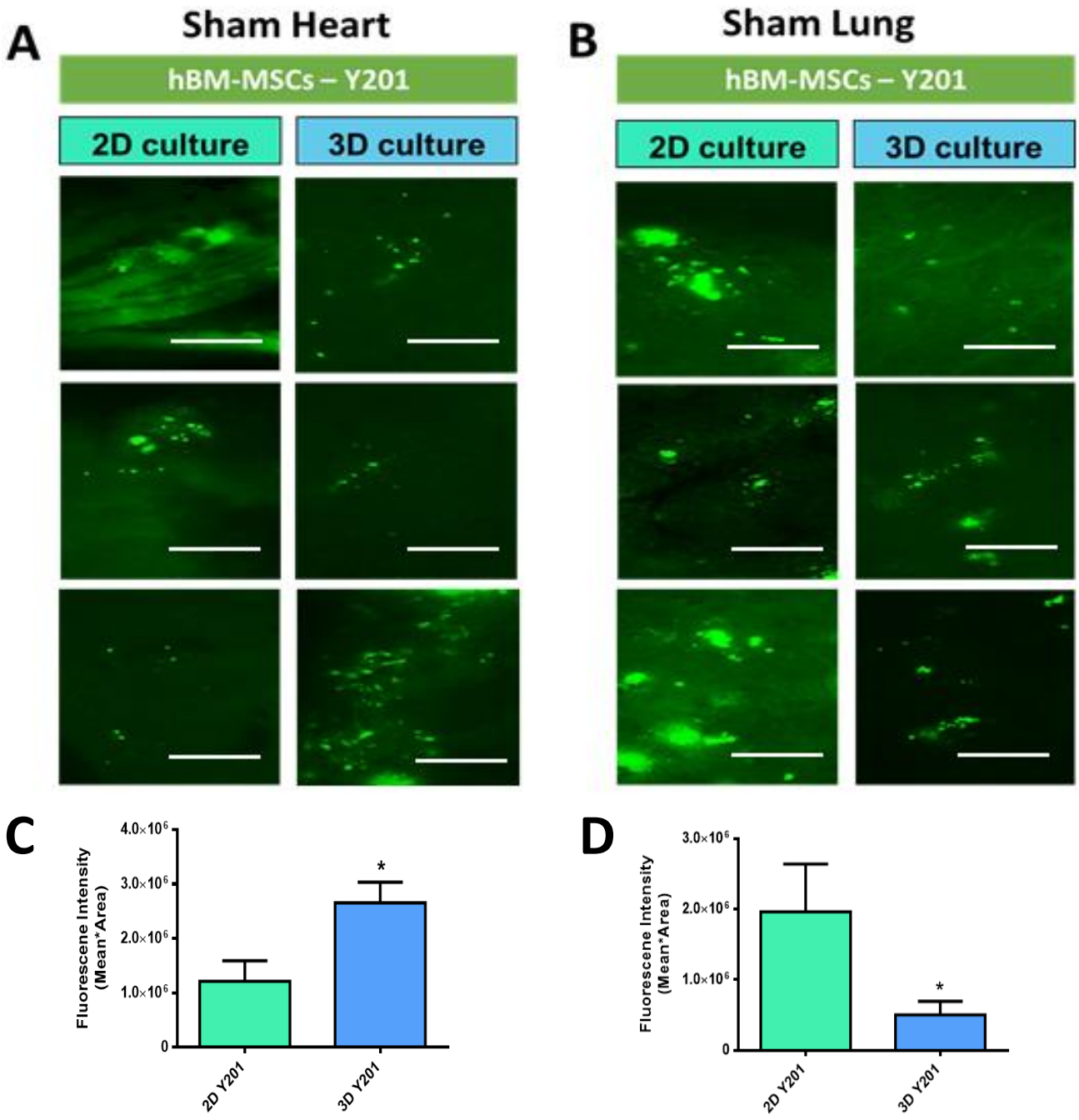


Figure 4.5. Increased myocardial recruitment of 3D cultured hBM-MSCs Y201 in healthy sham hearts confirmed *ex vivo* with significant entrapment within lungs of all MSCs. At the end of intravital experimentation (2½ hours post-reperfusion / 2 hrs post-MSC infusion), animals were culled and the heart and lungs removed and imaged on their surface using an EVOS fluorescent microscope. Representative images taken from 3 regions on the surface of the left ventricle of the heart and lungs are shown. **(A)** Generally, in the heart more CFSE-labelled 3D cultured hBM-MSCs Y201 were identified within the vasculature compared to 2D cultured cells. **(B)** Within the lungs, 2D and 3D cultured hBM-MSCs Y201 number appeared to be relatively similar. Interestingly, large clumps or aggregates of 2D cultured hBM-MSCs Y201 were present in pulmonary blood vessels, whilst smaller aggregates or individual 3D cultured hBM-MSCs Y201 were observed. Furthermore, the size of individual 3D cultured hBM-MSCs Y201 detected in the lungs appeared to be smaller than 2D cultured hBM-MSCs Y201. **(C)** 3D cultured significantly increased hBM-MSCs Y201 in the heart. **(D)** 3D cultured significantly decreased hBM-MSCs Y201 in the lung. Results presented as mean ± SEM. Statistical analysis using Student's t-test. n = 3 independent experiments using at least two different donors for each cell type.*$p<0.05$. Images were captured with a 20x objective. Scale bar = 200µm.

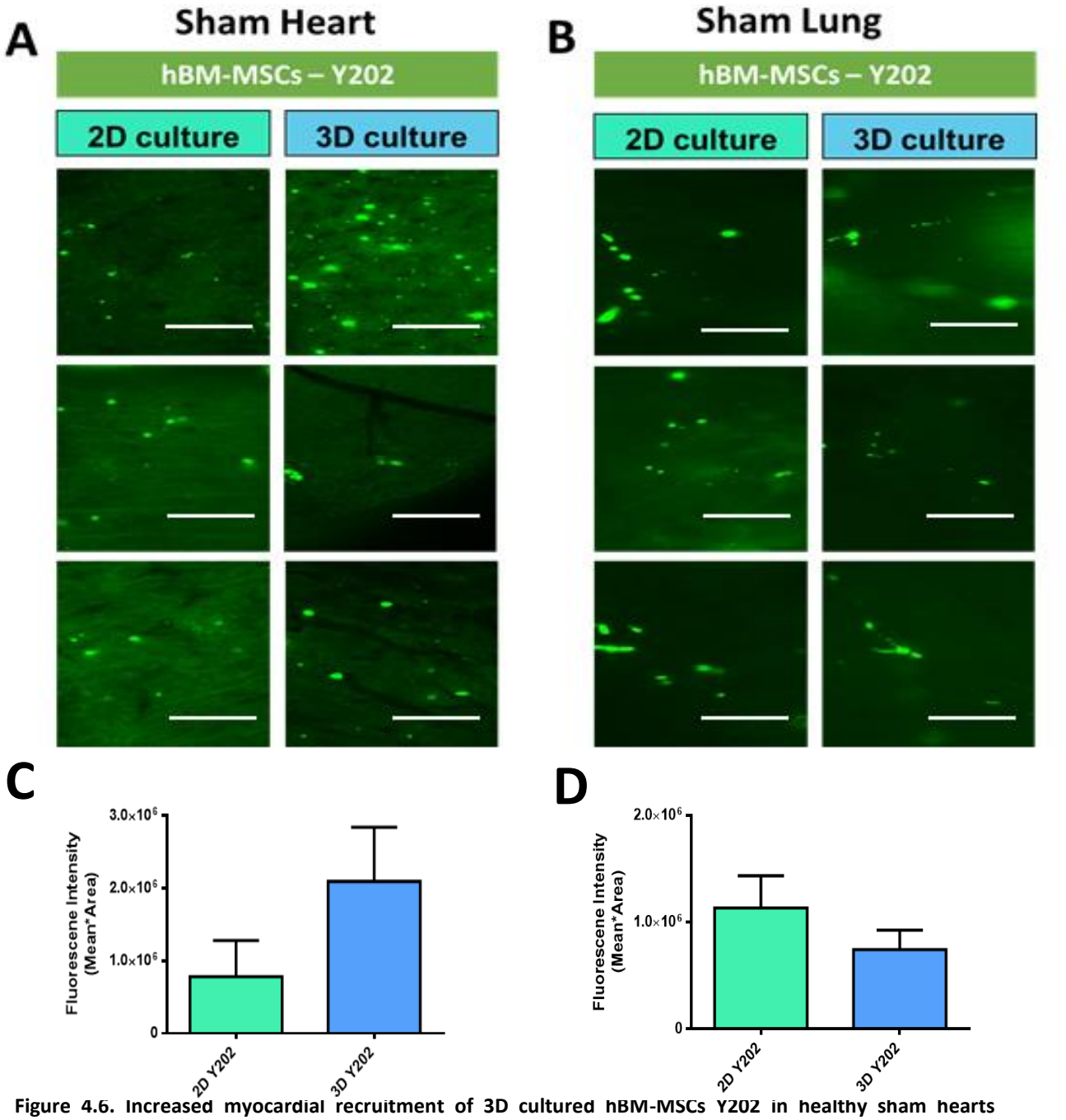


Figure 4.6. Increased myocardial recruitment of 3D cultured hBM-MSCs Y202 in healthy sham hearts confirmed *ex vivo* with significant entrapment within lungs of all MSCs. At the end of intravital experimentation (2½ hours post-reperfusion / 2 hrs post-MSC infusion), animals were culled and the heart and lungs removed and imaged on their surface using an EVOS fluorescent microscope. Representative images taken from 3 regions on the surface of the left ventricle of the heart and lungs are shown. **(A)** Generally, in the heart more CFSE-labelled 3D cultured hBM-MSCs Y202 were identified within the vasculature compared to 2D cultured cells. **(B)** Within the lungs, 2D and 3D cultured hBM-MSCs Y201 number appeared to be relatively similar. Interestingly, large clumps or aggregates of 2D cultured hBM-MSCs Y201 were present in pulmonary blood vessels, whilst smaller aggregates or individual 3D cultured hBM-MSCs Y201 were observed. Furthermore, the size of individual 3D cultured hBM-MSCs Y202 detected in the lungs appeared to be smaller than 2D cultured hBM-MSCs Y202. **(C)** 3D cultured increased hBM-MSCs Y202 in the heart. **(D)** 3D cultured slightly significantly decreased hBM-MSCs Y202 in the lung. Results presented as mean ± SEM. Statistical analysis using Student's t-test. n = 3 independent experiments using at least two different donors for each cell type.Images were captured with a 20x objective. Scale bar = 200µm.

Number of adherent 3D cultured hBM-MSCs Y201 (~12 cells/field of view) was significantly greater than 2D cultured cells (~7 cells/field of view) at all time points in the IR injured heart. As shown in **Figure 4.7B**, the number of 3D cultured hBM-MSCs Y201 increased progressively until a plateau was reached 30 minutes post-infusion. **Figure 4.7C** shows that IVM was again able to detect more 3D cultured hBM-MSCs Y201 *in vivo* in the injured heart that were of a smaller size when compared to those grown in 2D culture. 3D culture technique did not improve the free flow hBM-MSCs Y202 in injured heart when compared to cells cultured in 2D. However, as shown in **Figure 4.8A**, the trend for increased homing immediately upon infusion with a decrease thereafter was still observed. However, as shown in **Figure 4.8B**, adhesion of 3D cultured hBM-MSCs Y202 (~13 cells/field of view) within the injured heart was significantly higher adhesion of 2D cultured cells (~6 cells/field of view) but only at the end of imaging at 105 and 120 minutes after cell administration. Again 3D cultured hBM-MSCs Y202 were of a smaller size when compared to those grown in 2D culture as shown in **Figure 4.8C**. Interestingly, no significant differences in the adhesive ability between the two sub-populations to either sham or IR injured hearts were noted.

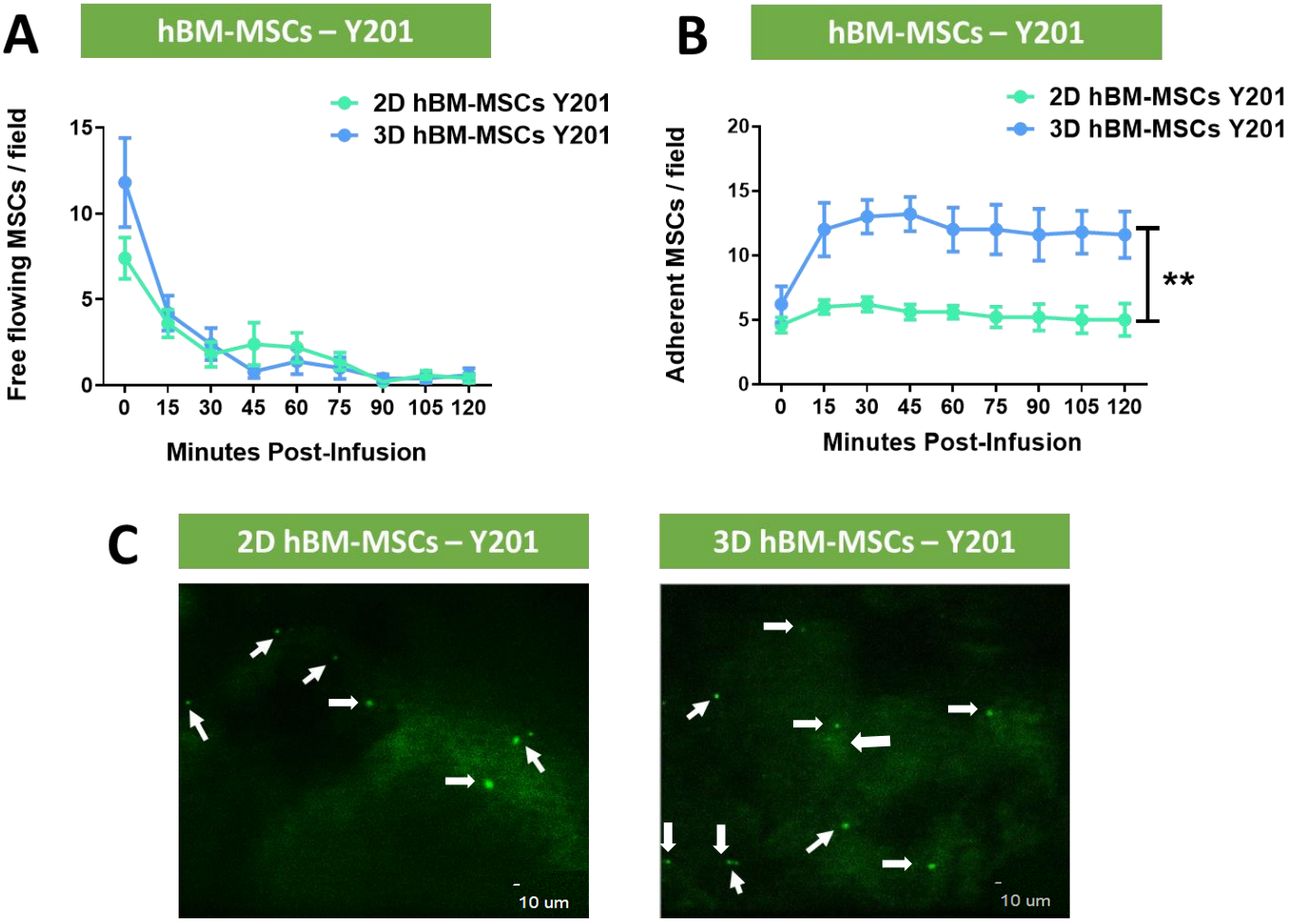


Figure 4.7. Intravital microscopy demonstrated that 3D culture improved numbers of hBM-MSCs Y201 trafficking through the IR injured beating heart after systemic infusion and their adhesion within the coronary microcirculation *in vivo*. **(A)** 3D increased numbers of hBM-MSCs Y201 observed freely flowing in the injured heart immediately after their systemic infusion although this did not attain statistical significance. Free flowing MSC number was greatly reduced after the initial point of cell infusion for both 2D and 3D cultured hBM-MSCs Y201 with no significant differences observed. **(B)** 3D culture significantly increased the adhesion of hBM-MSCs Y201 at all time points within the injured heart when compared to 2D cultured cells, with more than a doubling of the number of cells seen**. (C)** Representative intravital images of CFSE-labelled 2D and 3D culture hBM-MSCs Y201 (arrows) trafficking or adherent within myocardial microvessels. Interestingly, most cells derived from 3D culture appeared smaller when injected *in vivo*. The first intravital videos of the beating heart were captured immediately after infusion of a single dose of $5x10^5$ MSCs/ml via the intra-carotid artery. These were injected at 30 minutes post-reperfusion. Hence the above 0 time point is the equivalent of 30 minutes post-reperfusion. Results presented as mean ± SEM. Statistical analysis performed using Student's t-test. N = 5 per group. **p<0.01. Scale bar = 10µm.

4.3.5. Increased myocardial recruitment of 3D cultured hBM-MSCs Y201 Confirmed *ex vivo* using flow cytometry, but the same effect is not seen with hBM-MSCs Y202

Intravital studies of the beating heart were restricted to imaging just one superficial epicardial region of the left ventricle within the centre of the stabiliser. To confirm whether 3D culture actually improved the homing and subsequent recruitment of hBM-MSCs to the whole heart, flow cytometry studies was also performed. To detect the presence of CFSE-labelled infused MSCs in heart and lung, the organs were removed at the end of intravital imaging and digested with 0.1% v/v collagenase for 1 hour at 37˚C and analysed flow cytometrically. **Figure 4.11A** shows that the number of 3D cultured hBM-MSCs Y201 identified in the digested IR injured heart was significantly higher than hBM-MSCs Y201 retrieved from 2D culture. However, the same culture technique did not significantly affect the presence of hBM-MSCs Y202 in the IR injured heart (**Figures 4.11A**). As expected, overall there was a much higher presence of both MSC sub-populations with the lungs compared to the heart, but culturing technique did not affect their presence (**Figures 4.11B**). Overall, flow cytometric analysis showed that hBM-MSCs Y201 obtained from 3D spheroids had a greater homing and retention capacity within the IR injured hearts than hBM-MSCs Y201 grown in 2D culture.

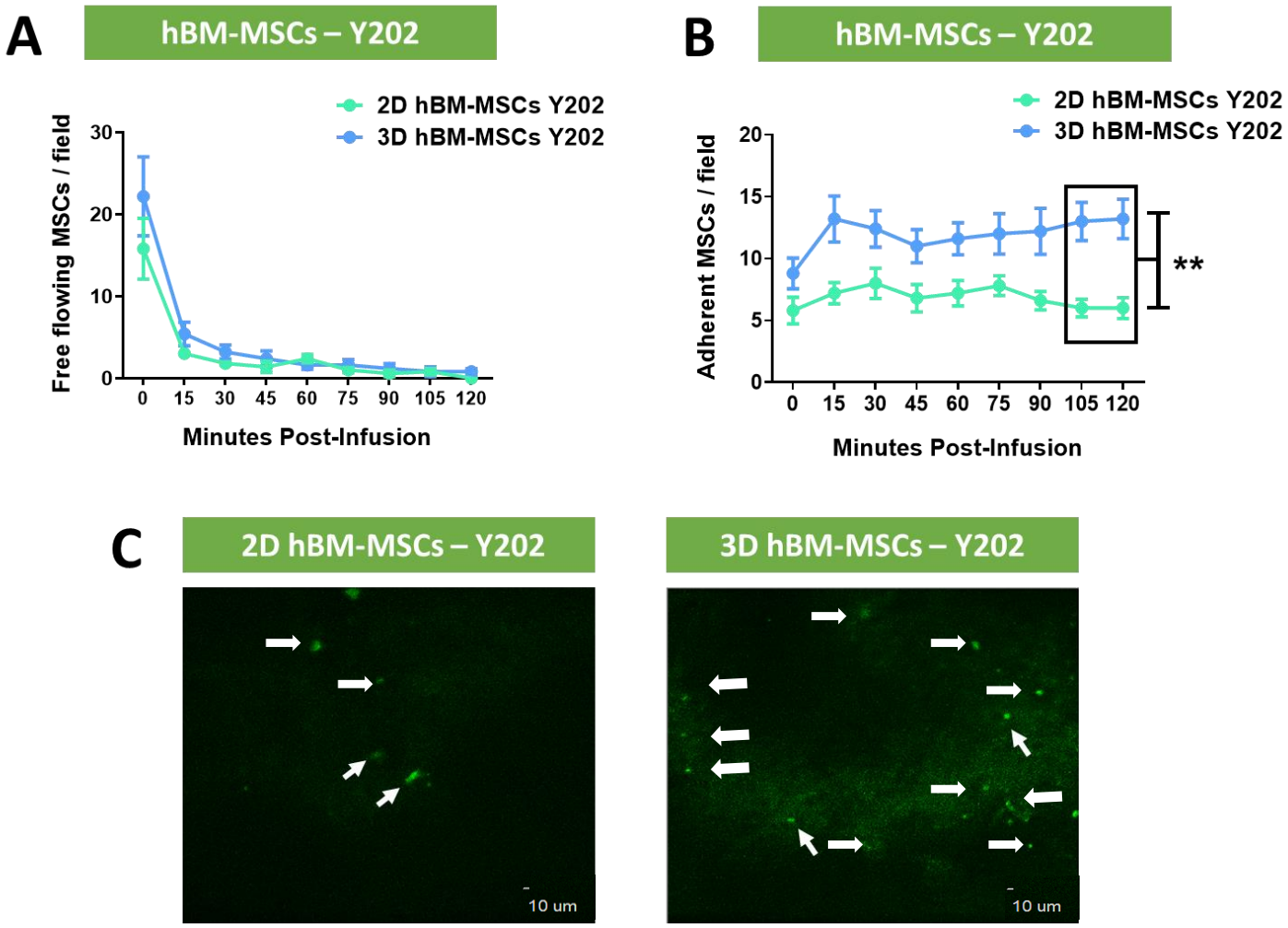


Figure 4.8. Intravital microscopy demonstrated that 3D culture does not increase numbers of hBM-MSCs Y202 trafficking through the IR injured beating heart after systemic infusion but does increase their adhesion within the coronary microcirculation *in vivo*. **(A)** No difference in the trafficking of 2D or 3D cultured hBM-MSCs Y202 in the injured heart immediately after their systemic infusion was observed. Free flowing MSC number was greatly reduced after the initial point of cell infusion for both 2D and 3D cultured hBM-MSCs Y202, but again no significant differences were observed. **(B)** 3D culture increased the adhesion of hBM-MSCs Y202 within the injured heart when compared to 2D cultured cells, but this was only significant at 105 AND 120 minutes post-infusion of cells. **(C)** Representative intravital images of CFSE-labelled 2D and 3D culture hBM-MSCs Y202 (arrows) trafficking or adherent within myocardial microvessels. Interestingly, most cells derived from 3D culture appeared smaller when injected *in vivo*. The first intravital videos of the beating heart were captured immediately after infusion of a single dose of $5x10^5$ MSCs/ml via the intra-carotid artery. These were injected at 30 minutes post-reperfusion. Hence the above 0 time point is the equivalent of 30 minutes post-reperfusion. Results presented as mean ± SEM. Statistical analysis performed using Student's t-test. N = 5 mice per group. **p<0.01. Scale bar = 10µm.

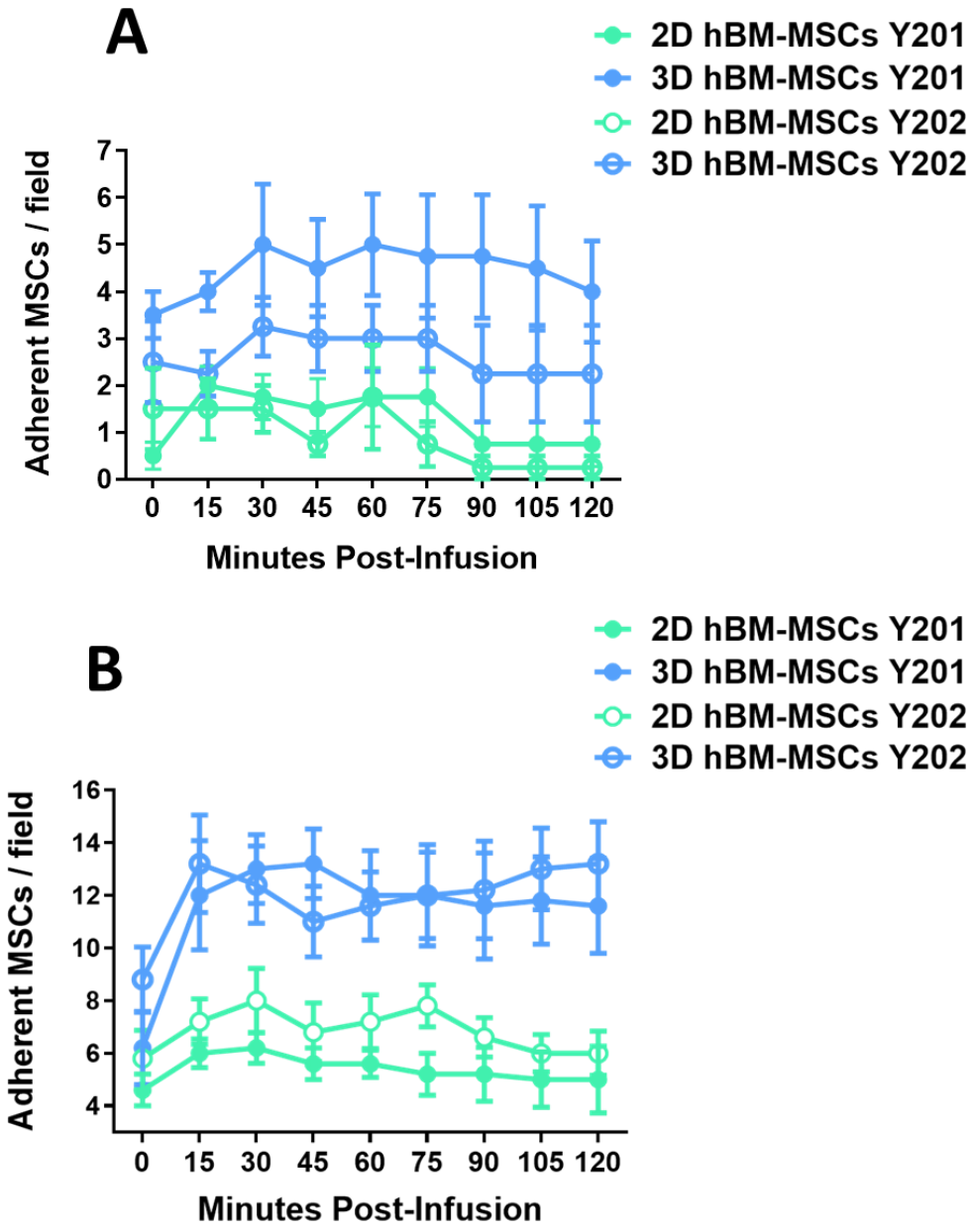


Figure 4.9. Intravital microscopy demonstrated that 3D culture increases adhesion of both hBM-MSCs Y201 and hBM-MSCs Y202 to a similar level within the sham and IR injured coronary microcirculation *in vivo.* **(A)** Although 3D culture increased adhesion of both MSC sub-populations in healthy sham hearts, there was no significant difference between the adhesive capabilities of the two different MSC types. However, 3D cultured hBM-MSCs Y201 demonstrated the greatest adhesion. **(B)** 3D culture also increased the adhesion of both MSC sub-populations to the IR injured heart. However, again no significant differences were observed between the two different MSC types. The first intravital videos of the beating heart were captured immediately after infusion of a single dose of $5x10^5$ MSCs/mice via the intra-carotid artery. These were injected at 30 minutes post-reperfusion. Hence the above 0 time point is the equivalent of 30 minutes post-reperfusion. Results presented as mean ± SEM. ANOVA showed no effect of culture conditions on MSC recruitment ; p=0.12. N = 5 mice per group.

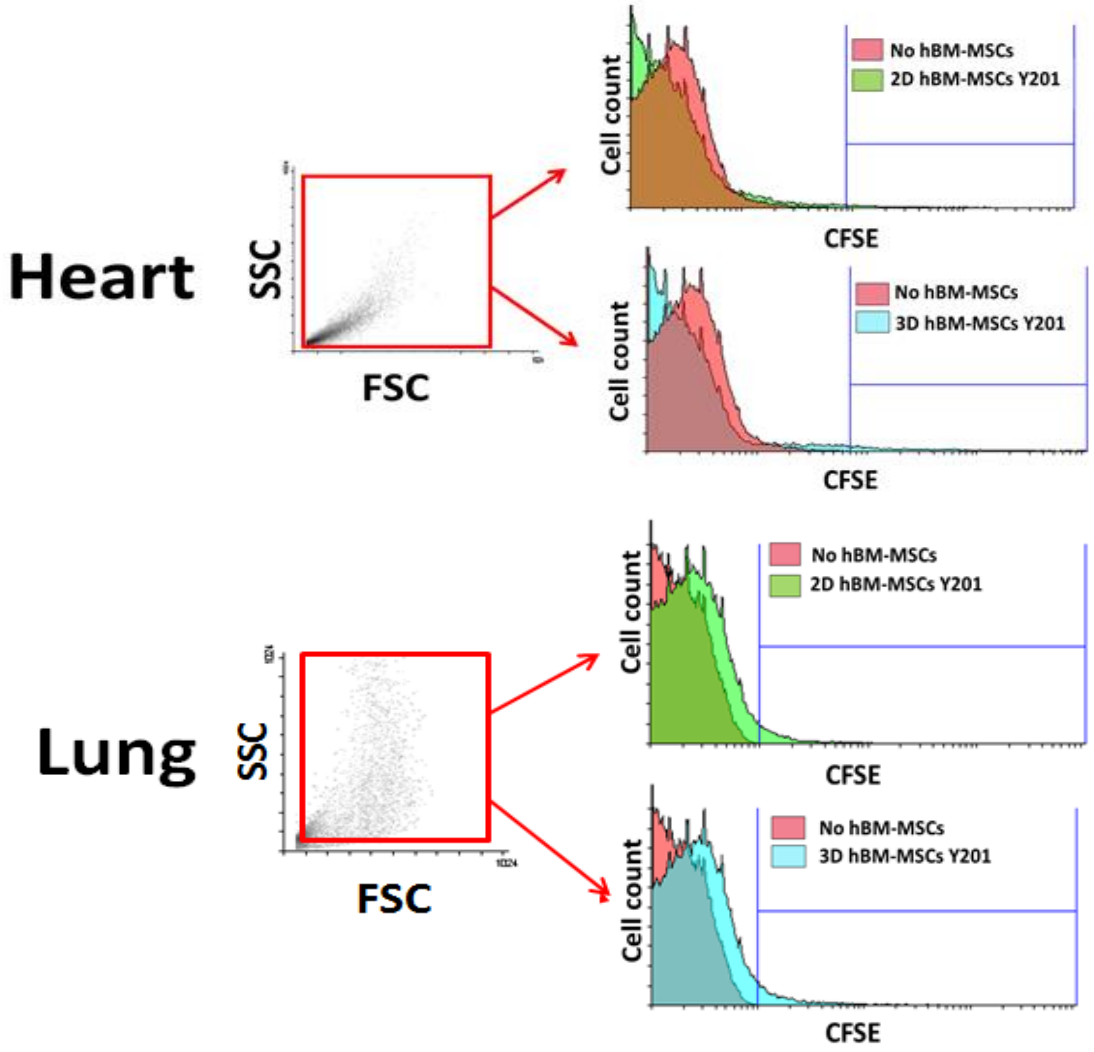


Figure 4.10. The presence of 3D cultured hBM-MSCs Y201 in the heart and lungs of mice undergoing myocardial IR injury was also determined *ex vivo* using flow cytometry. A gating strategy was conducted to investigate and to quantify the cell population of interest. Cells were gated by side scatter vs front scatter. Representative histograms showing the gating technique utilised to isolate CFSE-labelled BM-MSCs Y201 from collagenase digested heart and lung tissue. Samples were analyzed using FACSCalibur flow cytometry. The analysis was conducted on 25,000 events. Summit 4.3 software (Beckman Coulter, US) was used to visualise the data.

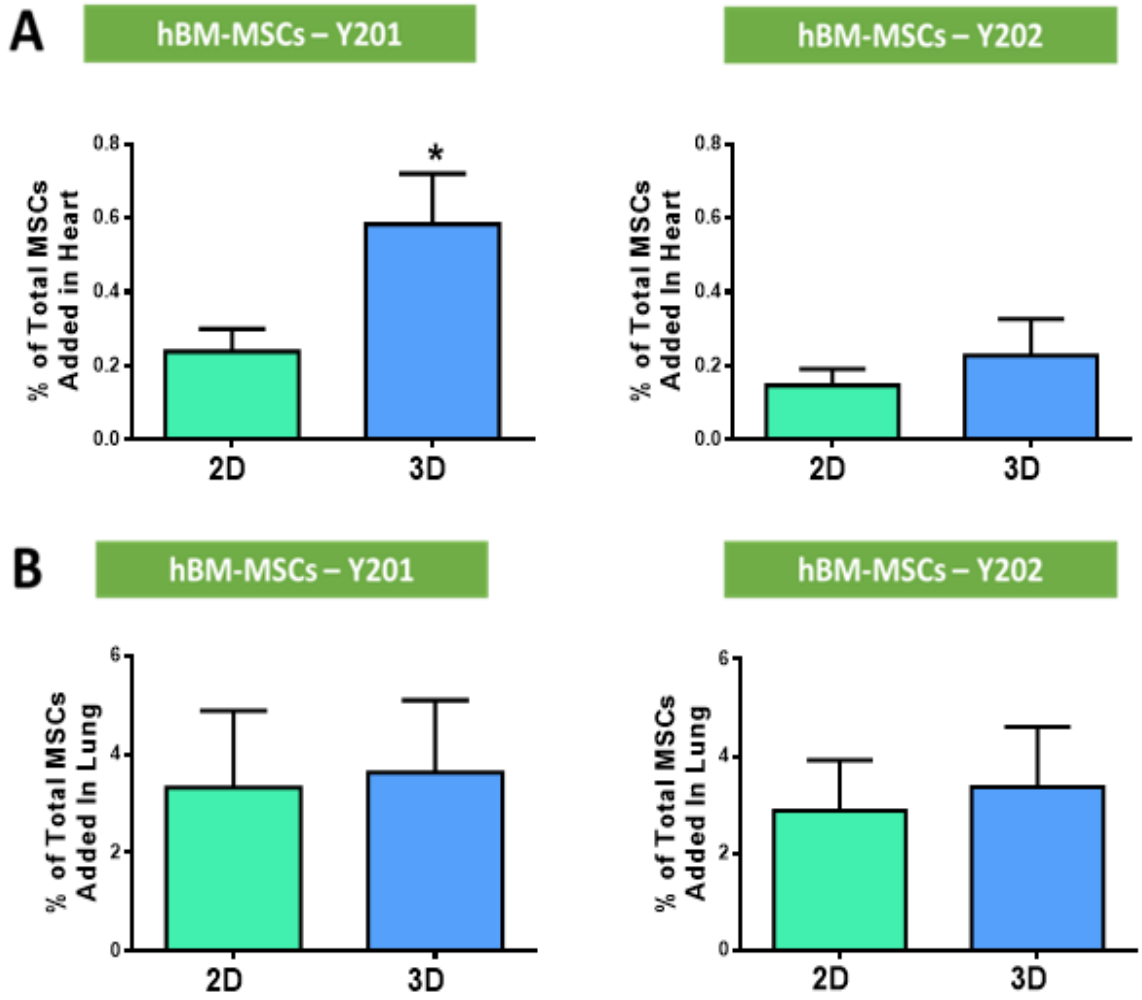


Figure 4.11. Increased myocardial recruitment of 3D cultured hBM-MSCs Y201 confirmed *ex vivo* using flow cytometry, but the same effect is not seen with hBM-MSCs Y202. (A) The presence of 3D cultured hBM-MSCs Y201 in the digested IR injured heart was significantly higher than cells obtained from 2D culture. However, culture method did not improve the presence of hBM-MSCs Y202 in the injured heart. **(B)** A much greater presence of both sub-populations of hBM-MSCs was detected in the lungs compared to the heart. Culture technique had no effect on cell present in the lung. Samples were analyzed using FACSCalibur flow cytometry. The analysis was conducted on 25,000 events. Flowing software 2.5.1 (University of Turku, Finland) was used to analyse the data. Data presented as the mean ± SEM. *$p<0.05$, when using a Student's t-test. N=3 mice per group.

4.3.6. Only 3D cultured hBM-MSCs Y201 reduce neutrophil recruitment within the IR injured coronary microcirculation *in vivo*

Our group have previously reported that myocardial IR injury induces a striking increase in endogenous inflammatory neutrophil recruitment to the beating heart *in vivo* (Kavanagh et al., 2019). The current study aimed to investigate whether MSCs could therapeutically benefit the IR injured heart by conferring a vasculoprotective effect. Moreover, we wanted to determine whether different culture techniques and sub-populations of MSCs had any differential effects at the level of the coronary microcirculation *in vivo*. Following myocardial IR injury, adherent neutrophils were detected within the coronary microcirculation, confirming previous investigation by the Kalia group (**Figure 4.12A**). Most of these were adherent within coronary capillaries.

Figure 4.13A and 4.14A show that hBM-MSCs Y201 or hBM-MSCs Y202 derived from different culture techniques were infused at 30 minutes after reperfusion. Both 2D hBM-MSCs Y201 (~123 cells/field of view) and 2D hBM-MSCs Y202 (~120 cells/field of view) slightly reduced neutrophil recruitment but this did not attain statistical significance. However, as show in **Figure 4.13A**, 3D cultured hBM-MSCs Y201 induced a significant decrease at all points from 75 minutes post-reperfusion onwards i.e. 45 minutes after cell transplantation. Indeed, the number of adherent neutrophils decreased to ~108 cells/field of view in the hearts of mice receiving 3D cultured hBM-MSCs Y201 cell therapy mice compared to approximately 130- 140 cells/field of view in the hearts of non-treated injured mice. However, as shown in **Figure 4.1A**, this anti-inflammatory benefit was not observed with 3D cultured hBM-MSCs Y202.

4.3.7. hBM-MSCs Y201 and hBM-MSCs Y202 marginally reduce platelet presence within the IR injured coronary microcirculation *in vivo*

Our group have previously reported that accumulation of platelet microthrombi within the coronary capillaries can lead to multiple occlusive events within the coronary microcirculation *in vivo* following IR injury (Kavanagh et al., 2019). Therefore, the current study also investigated potential anti-platelet effects of MSCs in the same injury model. Platelet aggregation was quantitated as their integrated fluorescence density. **Figure 4.12** shows that pure platelet aggregates were present in the coronary microvessels when intravitally imaged at the first time point at 30 minutes post-reperfusion. They were observed primarily within coronary capillaries as spherical / circular aggregates or extending the length of capillaries**.** Sometimes, neutrophils were seen to be attached to platelet aggregates, forming bigger mixed microthrombi. As shown in **Figure 4.13B** and **4.14B,** although systemic infusion of either 2D or 3D cultured hBM-MSCs Y201 or hBM-MSCs Y202 marginally reduced their presence, this did not attain statistical significance.

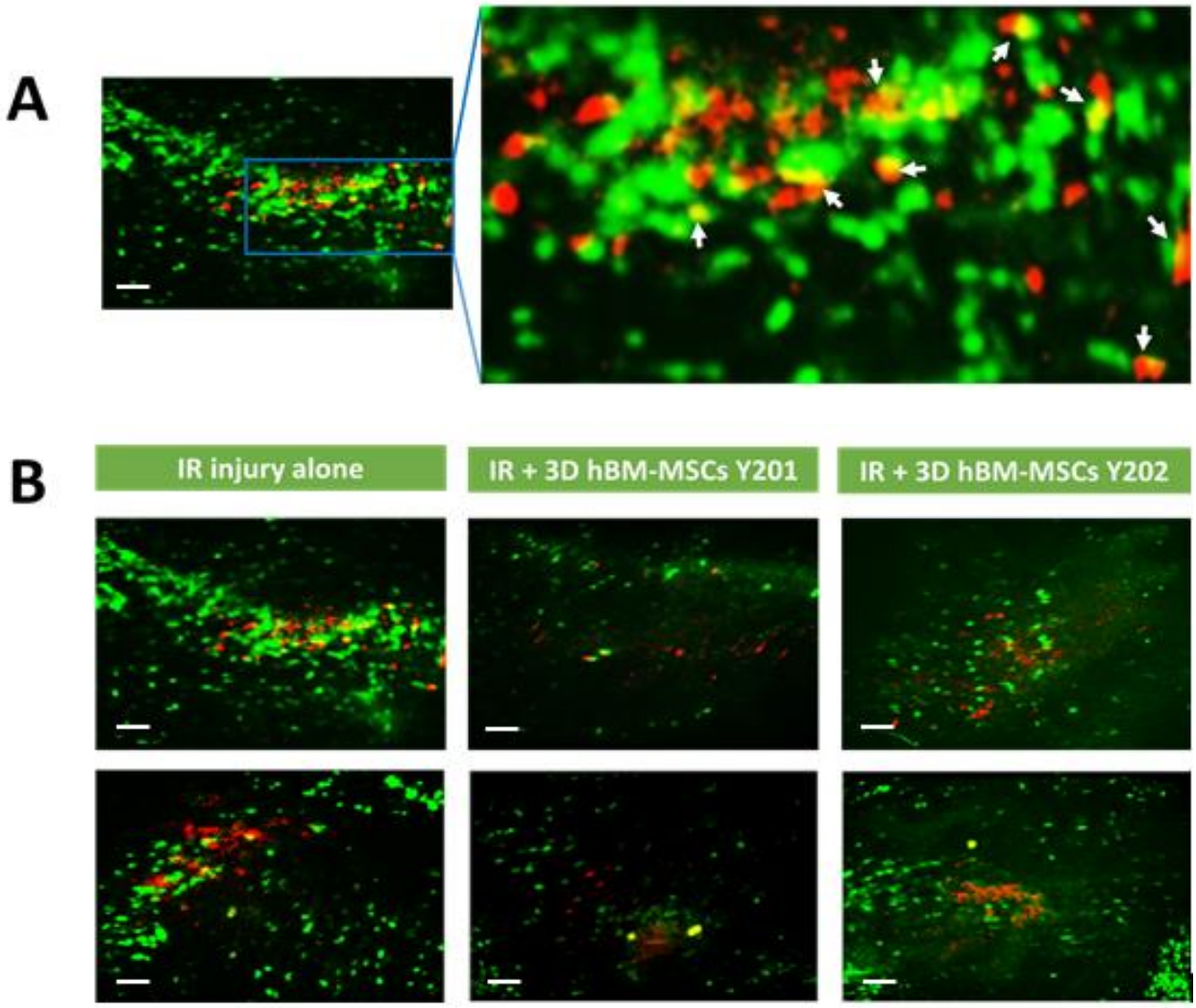


Figure 4.12. Intravital microscopy demonstrated a high burden of adherent neutrophils and platelet microthrombi in the IR injured heart. (A) Representative intravital images taken from the left ventricle of the beating mouse heart showing an extensive number of neutrophils (green) were identified in the IR injured coronary microvasculature *in vivo,* but mostly as individual neutrophils. Platelets (red) were seen forming either pure platelet-platelet or mixed platelet-neutrophil aggregates (white: arrows). **(B)** These inflammatory effects were most effectively decreased in mice receiving 3D cultured hBM-MSCs Y201. Endogenous neutrophils labelled using a PE-conjugated rat anti-mouse Gr-1 (Ly6G) antibody and endogenous platelets labelled with an APC-conjugated rat anti-mouse CD41 antibody. Scale bar = 100 µm.

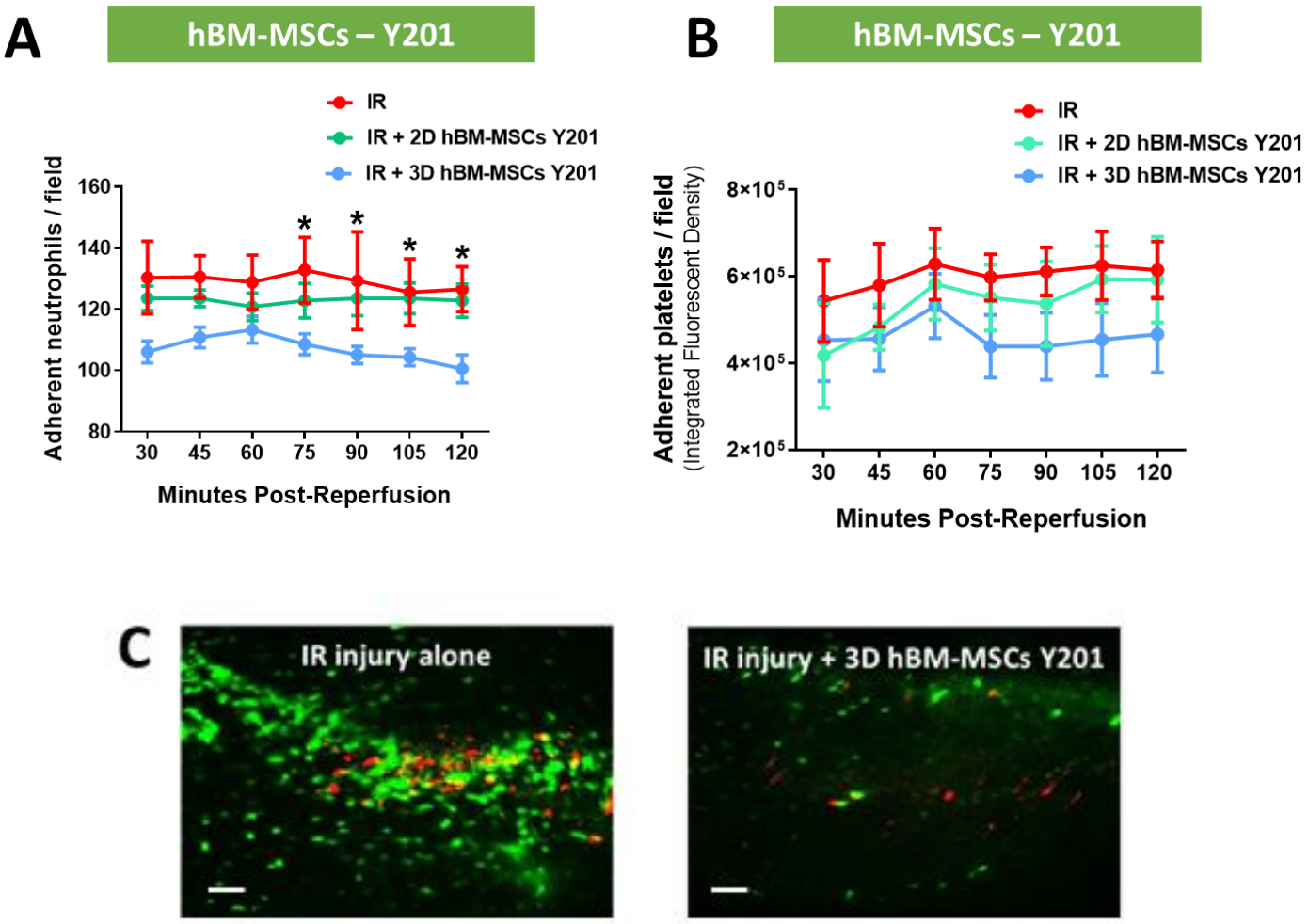


Figure 4.13. Intravital microscopy demonstrated that 3D culture of hBM-MSCs Y201 decreased endogenous neutrophil adhesion in the IR injured beating heart *in vivo*. **(A)** There was a high volume of adherent neutrophils in the IR injured coronary microcirculation, which did not change with the duration of reperfusion. hBM-MSCs Y201 were infused at 30 minutes after reperfusion. 3D cultured hBM-MSCs Y201 induced a significant decrease in neutrophils adhesion at all points from 75 minutes post-reperfusion onwards i.e. 45 minutes after cell transplantation. **(B)** Platelet aggregation was quantitated as integrated fluorescence density and was observed at all time point post-reperfusion. Although 2D and 3D cultured hBM-MSCs Y201 marginally reduced their presence, this did not attain statistical significance. **(C)** Representative intravital images demonstrating a high burden of neutrophil adhesion (green) and platelet recruitment (red) within the IR injured heart which decreased with 3D cultured hBM-MSCs Y201 – the second image is taken at 120 minutes post-reperfusion. The first intravital videos of the beating heart were captured immediately after infusion of a single dose of $5x10^5$ MSCs/ml via the intra-carotid artery. These were injected at 30 minutes post-reperfusion. Hence the above 0 time point is the equivalent of 30 minutes post-reperfusion. Endogenous neutrophils labelled using a PE-conjugated rat anti-mouse Gr-1 (Ly6G) antibody and endogenous platelets labelled with an APC-conjugated rat anti-mouse CD41 antibody. ANOVA showed a significant effect of 3D cultured hBM-MSCs Y201 on decreasing neutrophil recruitment, but not platelet in IR injured mice; $p<0.05$.Statistical analysis was performed using two-way ANOVA with Sidak's multiple comparison test. *$p<0.05$. N=5 mice per group. Scale bar = 100 µm.

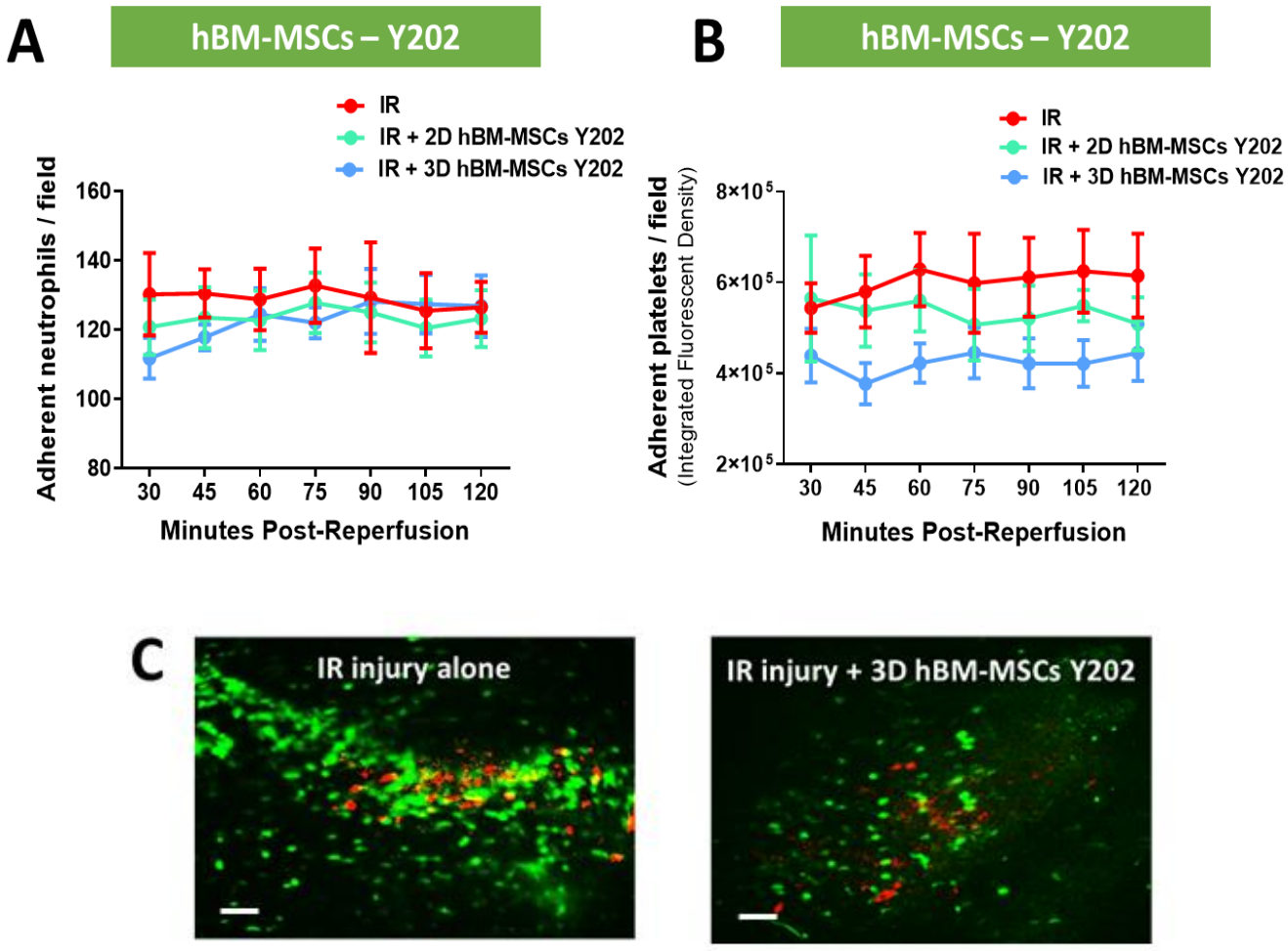


Figure 4.14. Intravital microscopy demonstrated that 3D culture of hBM-MSCs Y201 decreased endogenous neutrophil adhesion in the IR injured beating heart *in vivo.* (A) There was a high volume of adherent neutrophils in the IR injured coronary microcirculation, which did not change with the duration of reperfusion. hBM-MSCs Y202 were infused at 30 minutes after reperfusion. Neither 2D nor 3D cultured hBM-MSCs Y202 decreased neutrophils in the IR injured heart. **(B)** Platelet aggregation was quantitated as integrated fluorescence density and was observed at all time point post-reperfusion. Although 2D and 3D cultured hBM-MSCs Y202 marginally reduced their presence, this did not attain statistical significance. **(C)** Representative intravital images demonstrating a high burden of neutrophil adhesion (green) and platelet recruitment (red) within the IR injured heart which was not decreased with hBM-MSCs Y202. The first intravital videos of the beating heart were captured immediately after infusion of a single dose of $5x10^5$ MSCs/ml via the intra-carotid artery. These were injected at 30 minutes post-reperfusion. Hence the above 0 time point is the equivalent of 30 minutes post-reperfusion. Endogenous neutrophils labelled using a PE-conjugated rat anti-mouse Gr-1 (Ly6G) antibody and endogenous platelets labelled with an APC-conjugated rat anti-mouse CD41 antibody. ANOVA showed no effect of both 2D and 3D cultured hBM-MSCs Y202 on decreasing neutrophil and platelet recruitment in IR injured mice; p=0.18. Statistical analysis was performed using two-way ANOVA with Sidak's multiple comparison test. Results presented as mean ± SEM. N=5 mice per group. Scale bar = 100 µm.

4.3.8. Heparin slightly increases the presence of adherent 3D cultured hBM-MSCs Y201 following myocardial IR injury

Our group has previously demonstrated that platelet microthrombi are amongst the main contributors of occlusive events within the coronary capillaries (Kavanagh et al., 2019). In the current study we showed that although hBM-MSC therapy could reduce neutrophil adhesion, it was not efficient at reducing the quantity of platelet aggregation following myocardial IR injury. We therefore further examined whether co-transplantation with the anti-coagulant heparin enhanced the homing of hBM-MSC and/or their thromboinflammatory properties. Unfractionated soluble heparin was infused at 30 minutes post-reperfusion intra-arterially via the carotid artery followed by immediate infusion of MSCs. Since only 3D cultured hBM-MSCs Y201 were capable of decreasing neutrophil adhesion, we only selected this sub-population for heparin co-administration studies. As shown in **Figure 4.15A**, Immediately after their infusion, the number of freely flowing 3D cultured hBM-MSCs Y201 was observed to be significantly higher than observed with heparin administration in IR injured hearts when compared using Student t-test. Indeed, ~25 cells/field of view were observed compared to ~12 cells/field with no heparin. However, the number of free-flowing MSCs decreased in both groups with time. The adhesion of 3D cultured hBM-MSCs Y201 was slightly increased in the presence of heparin at all time points as shown in **Figure 4.15B**, but this increase was not statistically significant.

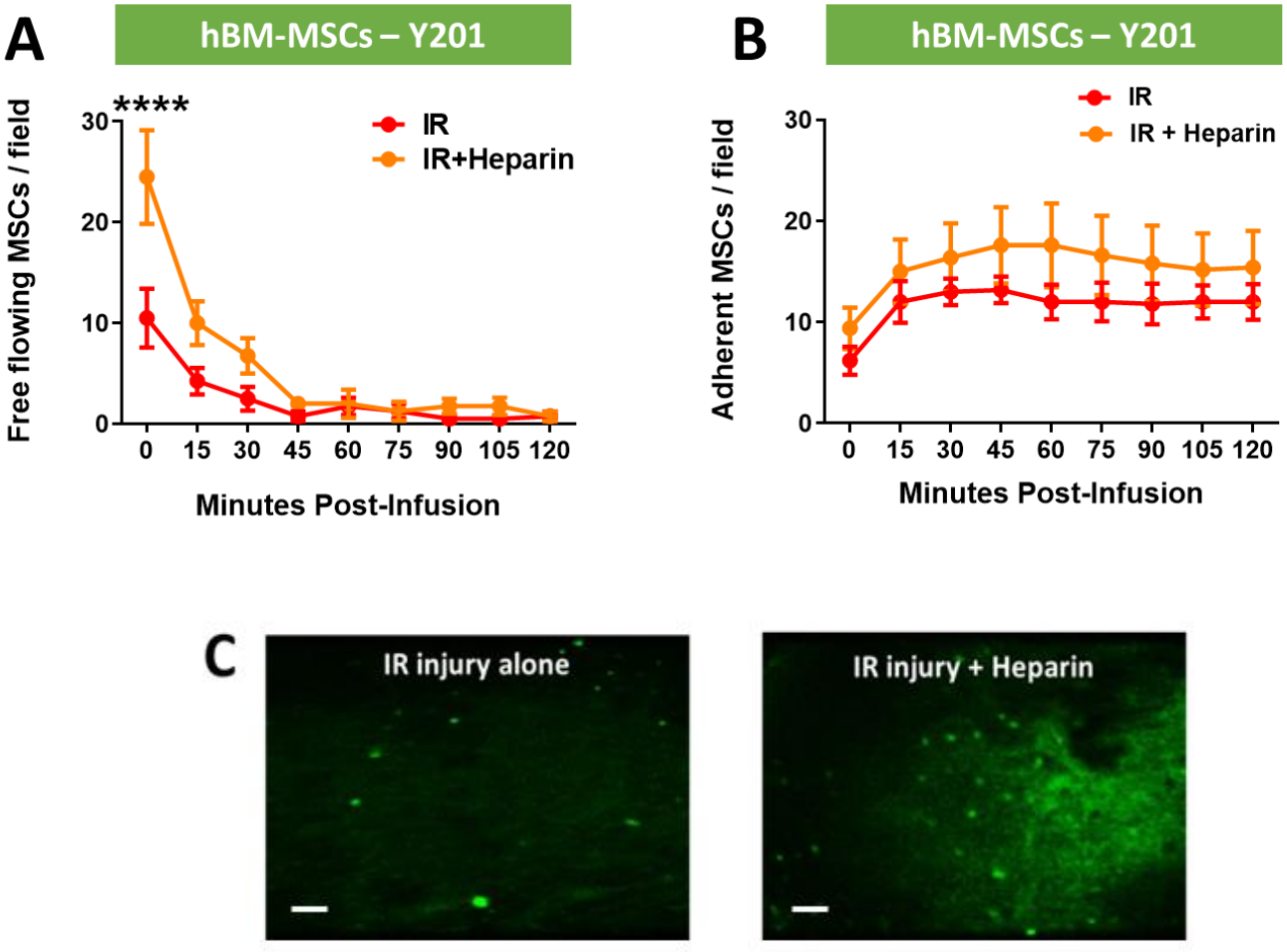


Figure 4.15. Intravital microscopy demonstrated that heparin infusion 30 minutes post-reperfusion did not increase adhesion of 3D cultured hBM-MSCs Y201 within the IR injured beating heart *in vivo*. **(A)** Heparin significantly increased the number of 3D cultured HBM-MSCs Y201 observed freely flowing in the injured heart immediately after their systemic infusion. Free flowing MSC number was greatly reduced after the initial point of cell infusion in mice both receiving heparin and in those who did not at all other time point with no significant differences observed. **(B)** Heparin infusion did not modify the adhesion of hBM-MSCs Y201 within the injured heart. **(C)** Representative intravital images of CFSE-labelled 3D cultured hBM-MSCs Y201 trafficking or adherent within myocardial microvessels. The first intravital videos of the beating heart were captured immediately after infusion of a single dose of $5x10^5$ MSCs/ml via the intra-carotid artery. These were injected at 30 minutes post-reperfusion (alongside heparin). Hence the above 0 time point is the equivalent of 30 minutes post-reperfusion. Results presented as mean ± SEM. Statistical analysis performed using Student's t-test. N = 5 mice per group. ****p<0.0001. Scale bar = 100 µm.

4.3.9. Dual therapy with heparin induces an earlier onset of 3D hBM-MSCs Y201 mediated anti-inflammatory effects following myocardial IR injury

We further determined intravitally whether co-transplantation of MSCs with heparin could improve the thromboinflammatory property of 3D cultured hBM-MSCs Y201. Firstly, the effects of heparin alone on neutrophil activity were intravitally assessed in the IR injured heart. No effect on the trafficking of neutrophils in the IR injured heart was observed. Indeed a decreased passage of neutrophils through the coronary microcirculation was observed with time post-reperfusion in IR injured hearts with and without heparin (**Figure 4.16A**). However, as shown in **Figure 4.16B**, systemic administration of unfractionated heparin increased the number of adherent neutrophils (from ~130 cells/field of view to 170 cells/field of view) by 2 hours post-reperfusion although this did not reach statistical significance at any time point. Not only did this demonstrate that heparin itself was not anti-inflammatory, surprisingly it showed that it was gradually quite pro-inflammatory**.**

Despite these observations, we still investigated whether co-administration of heparin with 3D cultured hBM-MSCs Y201 enhanced their earlier described thromboinflammatory properties. Surprisingly, as shown in **Figure 4.17A**, 3D cultured hBM-MSCs Y201 co-administration with heparin significantly decreased neutrophil recruitment at all time points within IR injured hearts when compared to IR injured mice not receiving any treatment. Indeed, neutrophil adhesion in injured hearts receiving 3D cultured hBM-MSCs Y201 plus heparin was ~100 cells/field of view compared to ~130 cells/field of view in injured but untreated mice**.** This significant anti-neutrophil effect was observed at all time points, unlike with 3D cultured hBM-MSCs Y201 which demonstrated a beneficial effect only after 75 minutes of myocardial reperfusion. This interesting data suggests co-

transplantation of cellular therapy with heparin induced an earlier onset of MSC mediated anti-inflammatory effects in the IR injured heart *in vivo.* As shown in **Figure 4.17B**, Systemic infusion of either heparin with 3D cultured hBM-MSCs Y201 marginally reduced the anti-platelet effects mediated by 3D cultured hBM-MSCs Y201 alone but this was not statistically significant.

4.3.10. Multiphoton microscopy visualised neutrophil adhesion and platelet aggregation within deeper layers of the myocardium in IR injured hearts

Intravital microscopy imaged coronary neutrophil and platelet recruitment *in vivo* on the superficial epicardial side of the left ventricle with a depth of approximately 50-60μm. To ascertain whether these events were also occurring in the deeper layers of the myocardium, multiphoton microscopy was used. In initial studies, the heart was removed after intravital imaging and cut in half longitudinally from the base to apex to expose the inner endocardial layer lining the left ventricle chamber. The left ventricle wall was then crudely sectioned sagitally into two sections and imaged using the multiphoton (**Figure 4.18A**). However, we found that the quality of the images became progressively poorer as z-stacks were taken from the outer epicardial to mid-myocardial section and the mid-myocardial to inner endocardial section. Therefore, we modified the method by using a tissue vibratome to precisely section sagitally the left ventricle wall into 5-6 sections with a thickness of 250μm. Multiphoton z-stacks were then taken from 4 of these sections, namely the: (i) outer epicardial to outer mid-myocardial; (ii) outer mid-myocardial to mid-myocardial; (iii) mid-myocardial to inner mid-myocardial and from; (iv) inner mid-

myocardial to inner endocardial (**Figure 4.18B)**. Individual Z-stack images from each section were then rendered to form a single 3D stack image. All neutrophils and platelets in each section were analysed and a mean single mean fluorescence intensity value was obtained.

Generally, we noted that many neutrophils were present in all 4 layers as oval cells or with a more elongated appearance. A significant presence of platelet aggregates was also observed in all layers of the heart muscle wall. However, we suspected that this very high platelet presence was not indicative of genuine actively induced thrombotic events due to IR injury but was highly likely due to post-mortem 'congealing' of blood. To overcome this problem, 50 IU of the anti-coagulant heparin was infused intra-arterially immediately before culling to prevent platelet 'coagulation' immediately after death (not to be confused with earlier experiments in which heparin was injected as a therapy 5 mins pre-reperfusion as a therapy). This would not have disrupted or 'dissolved' any existing platelet aggregates that would have genuinely formed as a result of IR injury as heparin is not a thrombolytic but prevents existing microthrombi from getting bigger or new ones forming post-mortem. However, in such pre-cull heparin treated mice, neutrophils and platelet aggregates could still be seen in IR injured hearts, but importantly, in all 4 sections at different depths of the ventricular wall. **Figure 4.19** shows that larger vessels were easily identified when they were clearly demarcated by platelet-rich thrombi or neutrophils. As shown in **Figure 4.20**, similarly to the intravital studies, platelet-neutrophil mixed aggregates were also common.

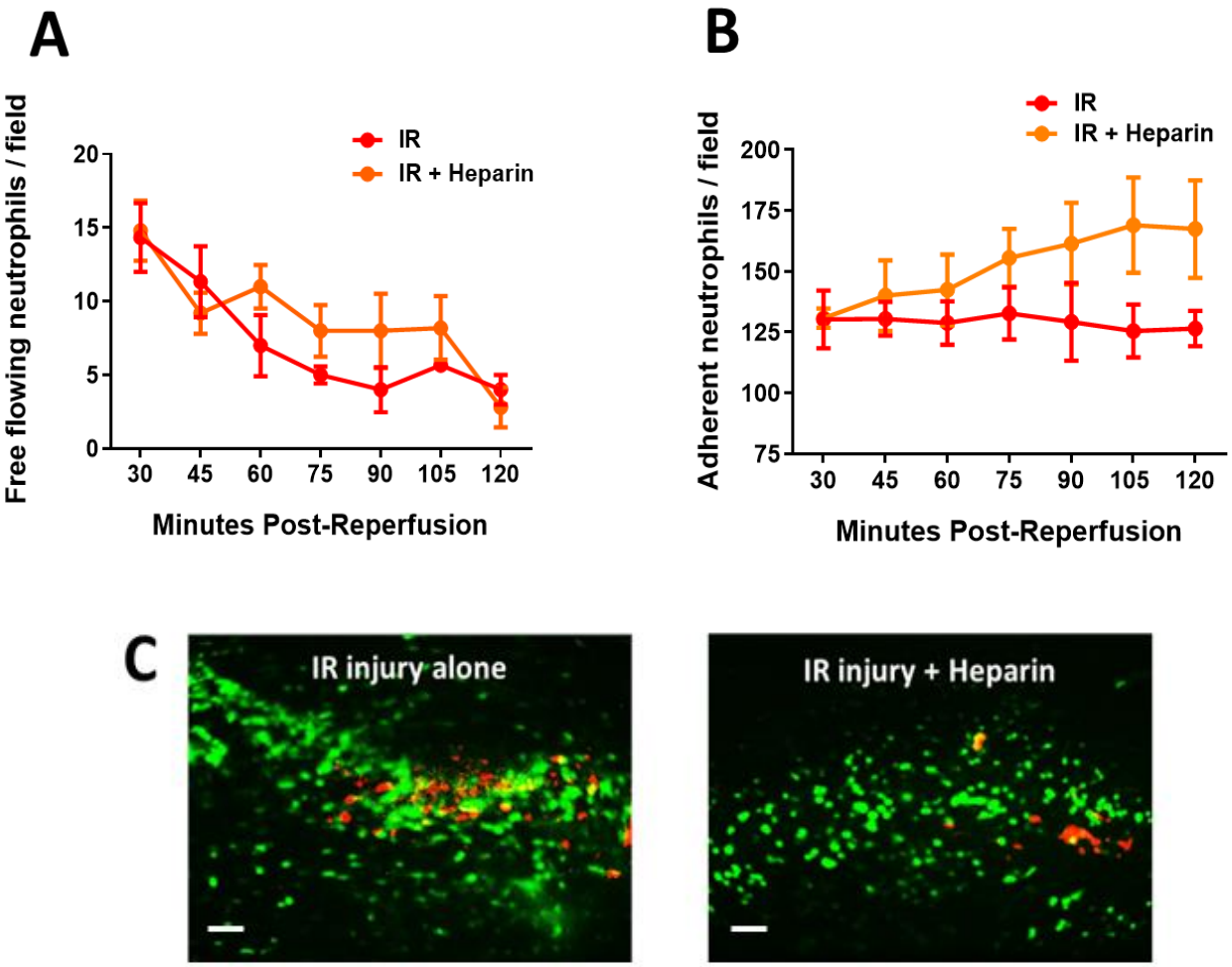


Figure 4.16. Intravital microscopy demonstrated that heparin infusion 30 minutes post-reperfusion marginally increased neutrophil recruitment within the IR injured beating heart *in vivo*. **(A)** No effects on the trafficking of neutrophils in the IR injured heart were observed. Indeed a decreased passage of neutrophils through the coronary microcirculation was observed with time post-reperfusion in IR injured hearts with and without heparin. **(B)** Systemic administration of unfractionated heparin increased the number of adherent neutrophils over time although this did not reach statistical significance at any time point. Indeed, ~130 cells/field of view were observed in IR injured hearts which increased to ~170 cells/field of view in IR injured hearts receiving heparin by 2 hours post-reperfusion. **(C)** Representative intravital images of CFSE-labelled 3D cultured hBM-MSCs Y201 trafficking or adherent within myocardial microvessels. The first intravital videos of the beating heart were captured immediately at 30 minutes post-reperfusion. Endogenous neutrophils labelled using a PE-conjugated rat anti-mouse Gr-1 (Ly6G) antibody and endogenous platelets labelled with an APC-conjugated rat anti-mouse CD41 antibody. Statistical analysis was performed using two-way ANOVA with Sidak's multiple comparison test. Results presented as mean ± SEM. N=5 mice per group. Scale bar = 100 µm.

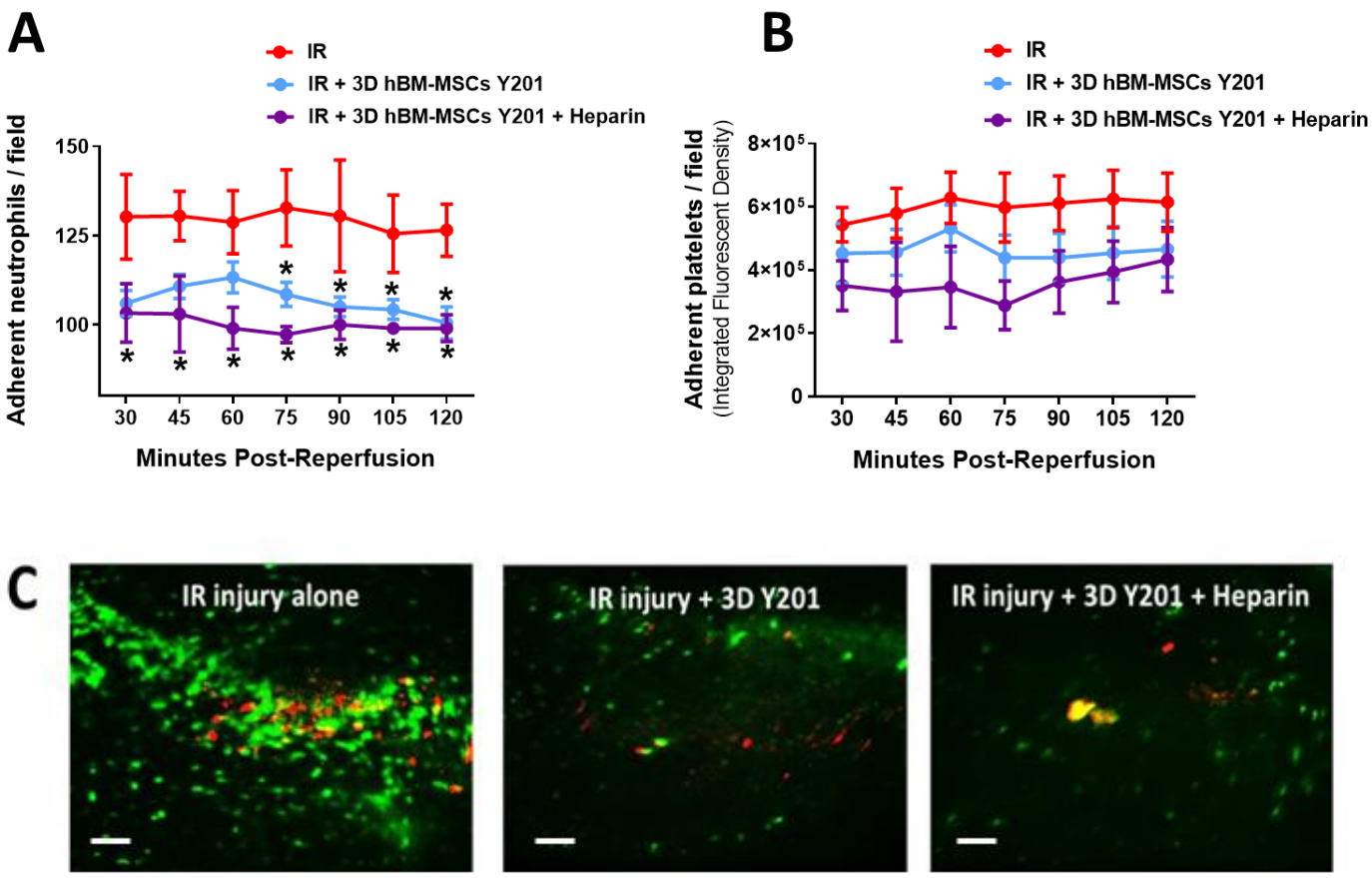


Figure 4.17. Intravital microscopy demonstrated that dual therapy with heparin induced an earlier onset of 3D hBM-MSCs Y201 mediated anti-inflammatory effects following myocardial IR injury. (A) 3D cultured hBM-MSCs Y201 co-administration with heparin significantly decreased neutrophil recruitment at all time points within IR injured hearts when compared to IR injured mice not receiving any treatment. Indeed, neutrophil adhesion in injured hearts receiving 3D cultured hBM-MSCs Y201 plus heparin was ~100 cells/field of view compared to ~130 cells/field of view in injured but untreated mice. This significant anti-neutrophil effect was observed at all time points, unlike with 3D cultured hBM-MSCs Y201 which demonstrated a beneficial effect only after 75 minutes of myocardial reperfusion. **(b)** Infusion of heparin did not significantly reduce the quantity of platelet microthrombi in IR injured hearts, although lower aggregation was noted in mice receiving both heparin + 3D hBM-MSCs Y201. **(C)** Representative intravital images of CFSE-labelled 3D cultured hBM-MSCs Y201 trafficking or adherent within myocardial microvessels. The first intravital videos of the beating heart were captured immediately at 30 minutes post-reperfusion. Endogenous neutrophils labelled using a PE-conjugated rat anti-mouse Gr-1 (Ly6G) antibody and endogenous platelets labelled with an APC-conjugated rat anti-mouse CD41 antibody. Statistical analysis was performed using two-way ANOVA with Sidak's multiple comparison test. Results presented as mean ± SEM. *$p<0.05$ N=4 mice per group. Scale bar = 100 µm.

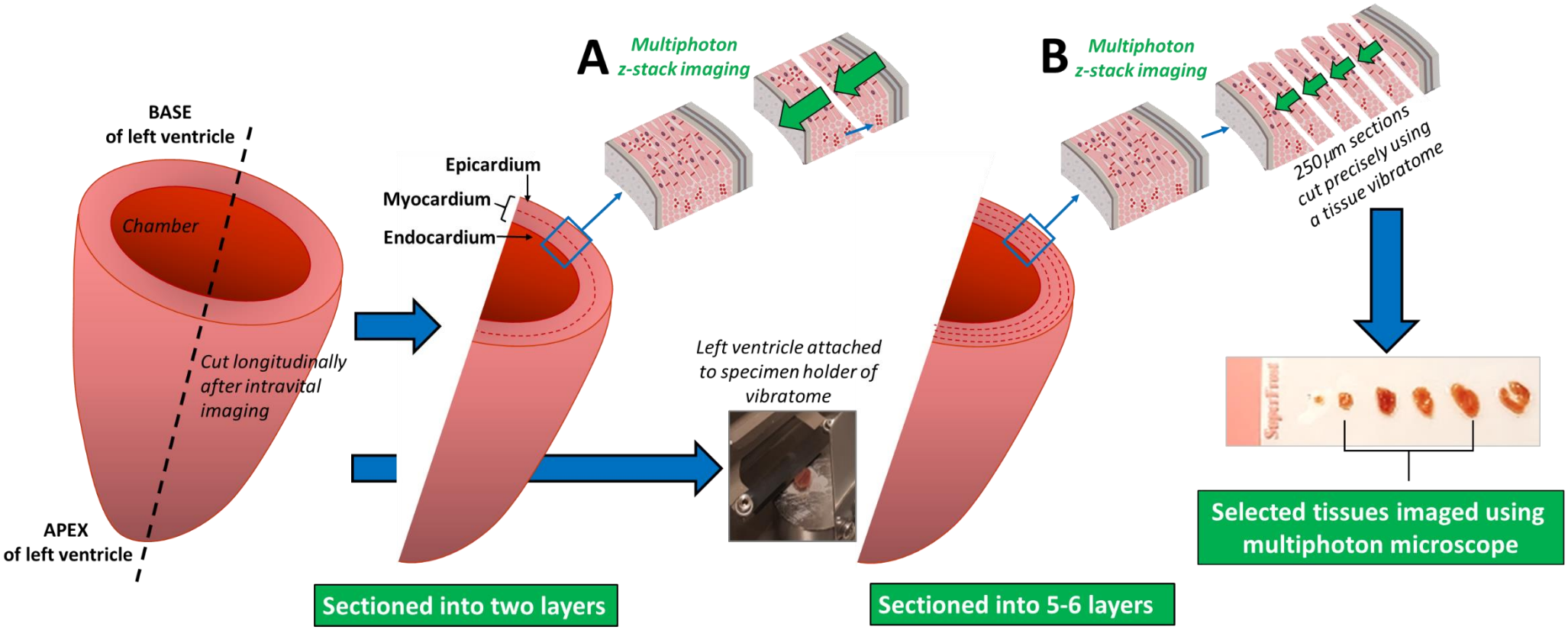


Figure 4.18. Preparing the murine left ventricle for multiphoton imaging following myocardial ischaemia-reperfusion injury *ex vivo.* To ascertain whether events imaged using intravital microscopy were also occurring in the deeper layers of the myocardium, multiphoton microscopy was used. The heart was cut in half longitudinally from the base to apex to expose the inner endocardial layer lining the left ventricle chamber. **(A)** In initial studies, the left ventricle wall was then crudely sectioned sagitally into two layers and imaged using the multiphoton. However, we found that the quality of the images became progressively poorer as z-stacks were taken from the outer epicardial to mid-myocardial and from the mid-myocardial to inner endocardial layers. **(B)** The procedure was then modified by using a tissue vibratome to more precisely section the left ventricle wall into 5-6 sections from epicardial to endocardial side as 250μm thickness in order to provide better quality of the images. Multiphoton z-stacks were taken from 4 layers, namely the (i) outer epicardial to mid-myocardial (ii) outer mid-myocardial to mid-myocardial (iii) inner mid-myocardial to mid-myocardial and from (iv) inner mid-myocardial to inner endocardial avoiding the last section which had 'missing' myocardium due sectioning through the actual ventricle chamber . Images from each layer were then rendered to form 3D stack images.

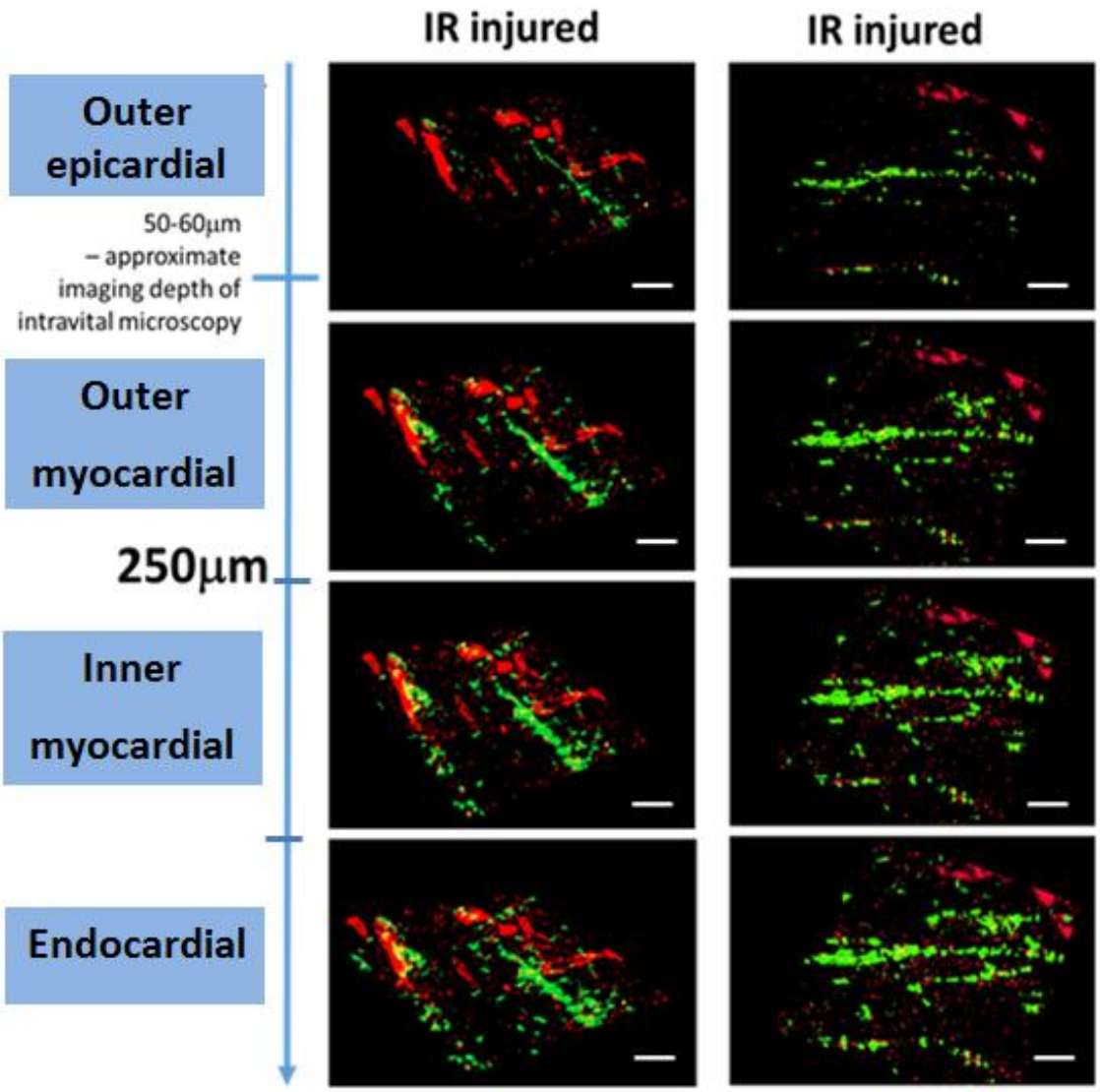


Figure 4.19. Multiphoton *ex vivo* imaging revealed the accumulation of platelet and neutrophil within the coronary microcirculation even within the deeper layers of the left ventricular muscle wall. The IR injured left ventricle was removed at the end of intravital experimentation, with 50 IU heparin infused immediately before culling. It was then vibratome cut into sections of 250µm thickness. Representative 250µm sections from two different mice undergoing myocardial IR injury are shown above. These 4 z-stack images are from an epicardial to mid-myocardial section and show thromboinflammatory presence at all depths of this section. Intravital imaging of the beating heart would not have been able to image beyond 50-60µm. Each image shows all of the present cells for that z-stack and above imaged z-stacks with the final image showing all of the cells within the 250µm muscle thickness. Individual neutrophils (green) mostly had a mostly oval or elongated appearance and appeared larger in bigger blood vessels. Platelet aggregates (red) of varying size were also observed at all depths. Larger blood vessels were easy to identify as they were often demarcated by the neutrophils and/or platelets lining them. Endogenous neutrophils labelled using a PE-conjugated rat anti-mouse Gr-1 (Ly6G) antibody and endogenous platelets labelled with an APC-conjugated rat anti-mouse CD41 antibody. The image was taken using an Olympus multiphoton microscope and a 25X objective lens. Scale bar = 100µm.

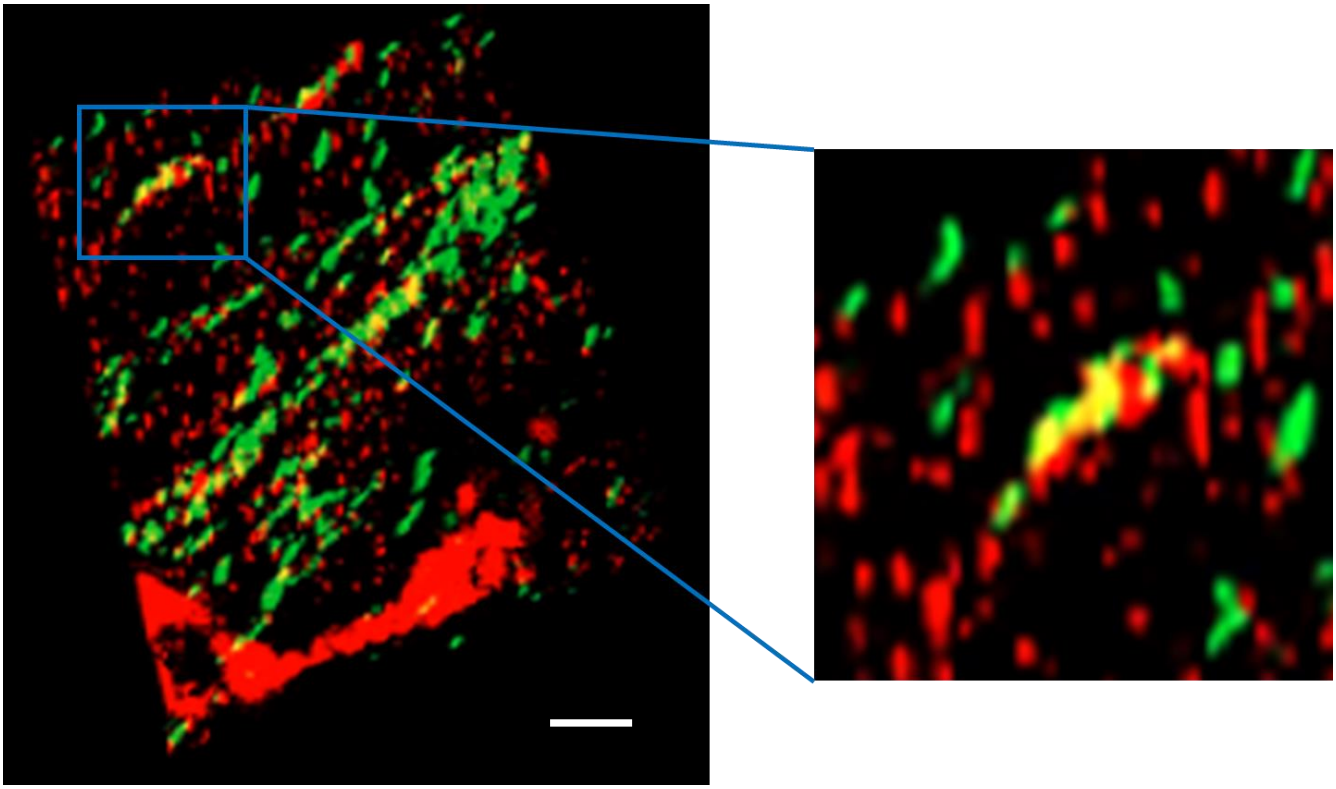


Figure 4.20. Multiphoton *ex* vivo imaging revealed the accumulation of mixed platelet-neutrophil aggregates within the coronary microcirculation even within the deeper layers of the left ventricular muscle wall. The IR injured left ventricle was removed at the end of intravital experimentation, with 50 IU heparin infused immediately before culling. It was then vibratome cut into sections of 250µm thickness. A representative 250µm section from a mouse undergoing myocardial IR injury is shown above, with all of the neutrophils (green) and platelets (red) within the entire 250µm section shown. Mixed aggregates composed of both cell types appeared yellow. Endogenous neutrophils labelled using a PE-conjugated rat anti-mouse Gr-1 (Ly6G) antibody and endogenous platelets labelled with an APC-conjugated rat anti-mouse CD41 antibody. The image was taken using an Olympus multiphoton microscope and a 25X objective lens. Scale bar = 100µm.

4.3.11. Multiphoton microscopy demonstrated that co-administration of heparin with 3D cultured hBM-MSCs Y201 was vasculoprotective even within the deep layers of the heart

Neutrophils were identified in all 4 sections of the IR injured heart ventricle, although their presence was highest in the outermost epicardial-to-mid-myocardial layer of the heart. Interestingly, in this epicardial layer, IR injured mice receiving heparin as a therapy 5 mins prior to reperfusion showed a significantly higher number of neutrophils when compared to those receiving no treatment. However, this was significantly decreased when compared to mice receiving heparin + 3D cultured 3D hBM-MSCs Y201. In the next 2nd (outer myocardial layer in **Figure 4.21**), 3rd (inner myocardial layer in **Figure 4.21**) and 4th endocardial layer in **Figure 4.21**) sections, neutrophil adhesion was similar in all three groups but there was a trend for adhesion to decrease to the lowest value in the IR injured group receiving heparin + 3D cultured 3D hBM-MSCs Y201. This decrease was statistically significant in the 3rd section (**Figure 4.21**). The neutrophil data for all 4 sections was then combined to provide data for the entire imaged thickness of the left ventricle. Again, a rise in neutrophil adhesion as a result of heparin was observed which was significantly decreased when compared to mice receiving heparin + 3D cultured 3D hBM-MSCs Y201. Importantly, this dual therapy group had significantly less neutrophils that IR injured mice receiving no therapy (**Figure 4.22A)**. Platelets were also present in all 4 sections with the least identified in the inner section closest to the endocardium. There was a general trend for their presence to decrease in IR injured hearts treated with heparin alone but this did not attain statistical significance when compared to mice receiving no therapy. Platelet presence was lowest in all 4 sections in IR injured mice treated with heparin + 3D cultured

3D hBM-MSCs Y201 which was statistically significant in section 1, section 2 and section 4 when compared to mice receiving no treatment (**Figure 4.21**). As shown in **Figure 4.22B**, platelet data for all 4 sections was also combined to provide data for the entire imaged thickness of the left ventricle and showed a significant decrease in mice receiving heparin alone but was the lowest in mice receiving dual therapy when compared to non-treated IR injured mice.

4.3.12. Myocardial IR injury reduces functional capillary density which is restored by pre-treatment with 3D hBM-MSCs Y201

One of the main advantages of intravital imaging is the ability to assess dynamic processes such as tissue perfusion or blood flow which is not possible with traditional static histological studies. To qualitate this, FITC-BSA was infused via the carotid artery after 2 hours of reperfusion. FITC-BSA circulates through blood vessels allowing areas of perfusion to be identified. An extensive network of FITC-BSA perfused capillaries was observed in sham mice, paralleling the arrangement of muscle fibers, with cross connections along their length. Focusing up and down on the field of view showed no areas devoid of perfused capillaries. **Figure 4.23** shows well perfused medium-sized vessels were also visible in some fields of view. However, in hearts undergoing IR injury, multiple areas were detected in which FITC-BSA did not perfuse, resulting in patchy areas devoid of any microvasculature. This indicated that the functional capillary density (FCD) was reduced in these hearts. Indeed, in some fields of view, up to half the imaged area appeared non-perfused. Interestingly, medium sized vessels were still readily visible and well perfused in

injured hearts. In IR injured mice receiving 3D cultured hBM-MSCs Y201, but not those receiving 2D cultured hBM-MSCs Y202, capillaries were better perfused with less discontinuous FITC-BSA filled blood vessels. The difference in microvascular perfusion was significant between the sham and IR injured mice and IR injured vs IR injured + 3D cultured hBM-MSCs mice.

4.3.13. 3D cultured hBM-MSCs Y201 therapy decreases infarct size following myocardial IR injury which is further decreased when combined with heparin

Dual Evans blue and TTC staining was used to determine the area and size of infarction of the heart after myocardial IR injury in mice receiving no therapy, heparin alone, 3D hBM-MSCs Y201 alone or heparin + 3D hBM-MSCs Y201. **Figure 4.24** shows the results from TTC assay. The infarct size was large in the hearts of mice undergoing myocardial IR injury at 49.59% ± 5.85 (as a % of the area at risk). Although heparin alone led to a decrease in the infarct size to 41.48% ± 4.69, this was not statistically significant when compared to IR injured mice receiving no treatment using two-way ANOVA with Sidak's multiple comparison test. However, 3D cultured hBM-MSCs Y201 treatment significantly reduced the size of the infarct to 27.25% ± 2.14 when compared to IR injured hearts receiving no treatment. Interestingly, co-administration of both heparin with 3D cultured hBM-MSCs Y201 therapy significantly reduced the infarct size further to 23.69% ± 3.95 when compared to mice receiving no treatment and also when compared to mice receiving heparin alone. However, there was no significant difference in the infarcted area between IR injured mice treated with MSCs and those receiving heparin and MSCs.

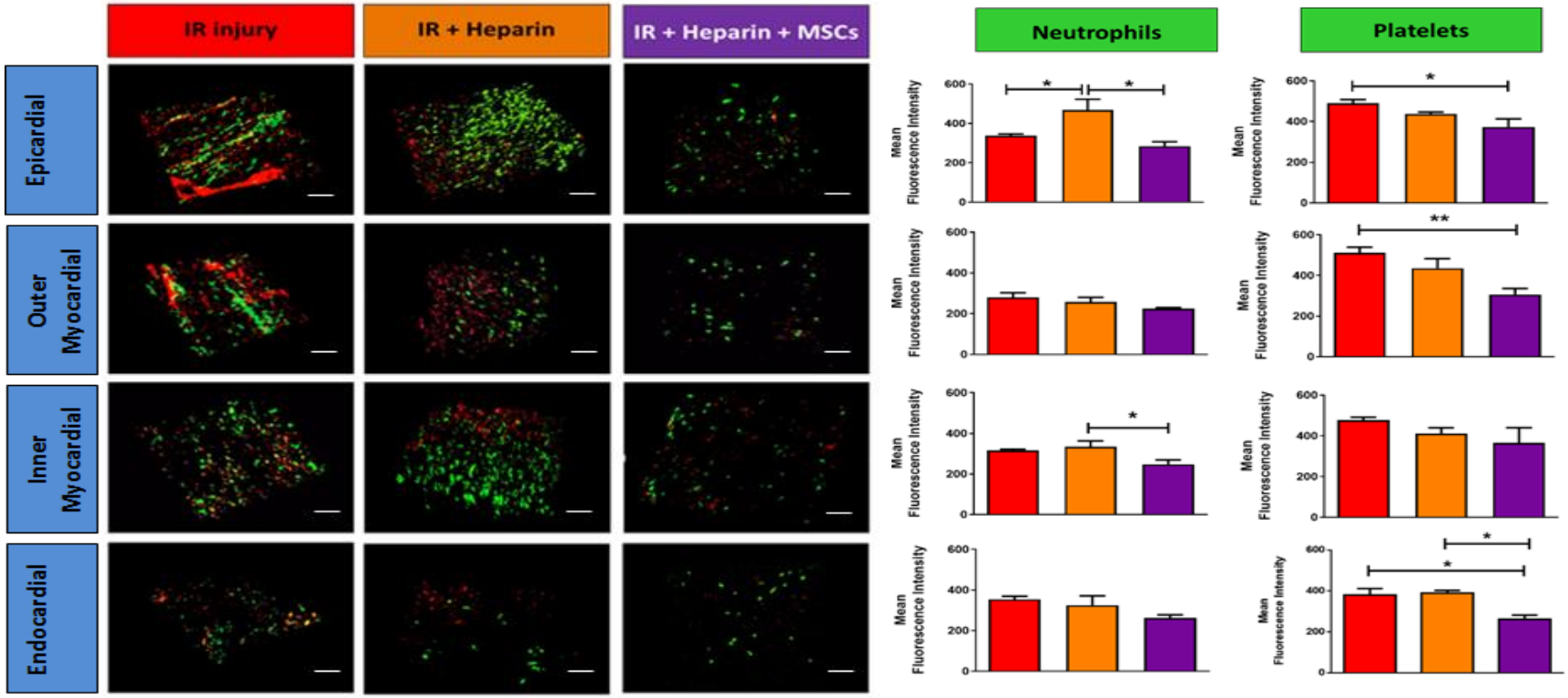


Figure 4.21. Multiphoton microscopy demonstrated that co-administration of heparin with 3D cultured hBM-MSCs Y201 was vasculoprotective from the epicardial to endocardial layer of left ventricle following myocardial IR injury. Representative multiphoton images demonstrated the accumulation of neutrophil (green) and platelet aggregation (red) within the microcirculation in each layer of the heart. Neutrophils were identified in all 4 sections of the IR injured heart ventricle, although their presence was highest in the outermost epicardial-to-inner myocardial layer of the heart. Heparin pre-treatment at 5 mins prior to reperfusion increased their presence in this outermost section. However, in all layers, there was a general trend for neutrophil presence to decrease in IR injured hearts receiving dual therapy treatment with heparin + 3D cultured 3D hBM-MSCs Y201. Platelets were also present in all 4 sections with the least identified in the inner section closest to the endocardium. There was a general trend for their presence to decrease in IR injured hearts treated with heparin alone. Platelet presence was the lowest in all 4 sections in IR injured mice treated with heparin + 3D cultured 3D hBM-MSCs Y201. Endogenous neutrophils labelled using a PE-conjugated rat anti-mouse Gr-1 (Ly6G) antibody and endogenous platelets labelled with an APC-conjugated rat anti-mouse CD41 antibody. ANOVA showed a significant effect of Heparin + 3D cultured hBM-MSCs Y201 on decreasing platelet recruitment in epicardial, outer myocardial and endocardial layer of IR injured heart; $p<0.05$. ANOVA showed a significant effect of Heparin + 3D cultured hBM-MSCs Y201 on decreasing neutrophil recruitment in epicardial and inner myocardial layer of IR injured heart; $p<0.05$. Statistical analysis was performed using two-way ANOVA with Sidak's multiple comparison test. Results presented as mean ± SEM. *$p<0.05$, **$p<0.01$; N=3 hearts per group. Scale bar = 100µm.

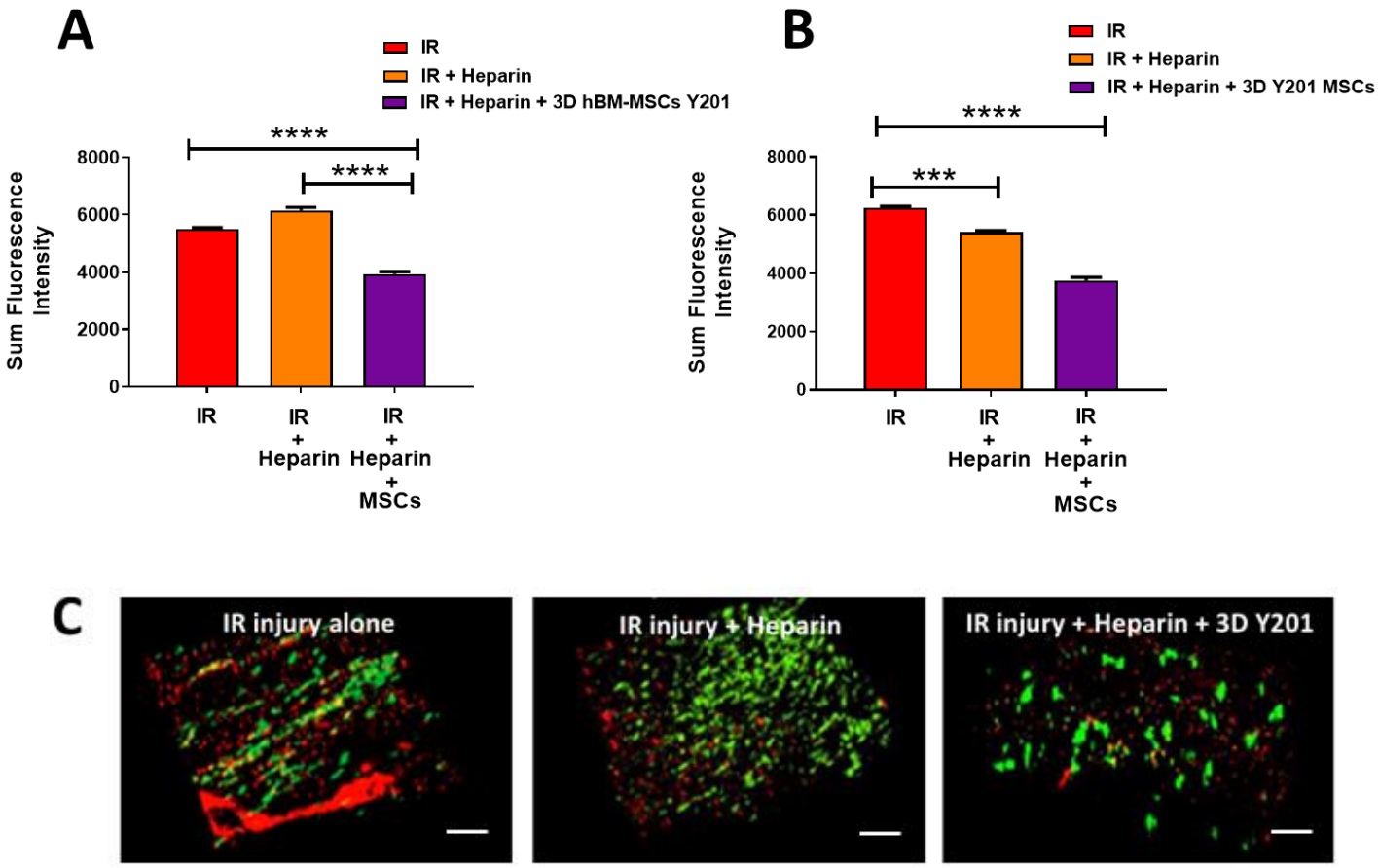


Figure 4.22. Multiphoton microscopy demonstrated that co-administration of heparin with 3D cultured hBM-MSCs Y201 was vasculoprotective even within the deep layers of the heart following myocardial IR injury. **(A)** The neutrophil data shown in figure 4.20 for all 4 sections was combined to provide data for the entire imaged thickness of the left ventricle. A rise in neutrophil adhesion as a result of heparin was observed which decreased when compared to mice receiving heparin + 3D cultured 3D hBM-MSCs Y201. Importantly, the dual therapy group had significantly less neutrophils that IR injured mice receiving no therapy. **(B)** Platelet data for all 4 sections was also combined to provide data for the entire imaged thickness of the left ventricle and showed a decrease in mice receiving heparin alone but was lowest in mice receiving dual therapy when compared to non-treated IR injured mice. **(C)** Representative multiphoton images demonstrated the accumulation of neutrophil (green) and platelet aggregation (red) within the microcirculation in each layer of the heart. Endogenous neutrophils labelled using a PE-conjugated rat anti-mouse Gr-1 (Ly6G) antibody and endogenous platelets labelled with an APC-conjugated rat anti-mouse CD41 antibody. ANOVA showed a significant effect of Heparin + 3D cultured hBM-MSCs Y201 on decreasing platelet and neutrophil recruitment in IR injured heart; $p<0.001$. Statistical analysis was performed using two-way ANOVA with Sidak's multiple comparison test. Results presented as mean ± SEM. ***$p<0.001$, ****$p<0.0001$; N=3 hearts per group. Scale bar = 100µm.

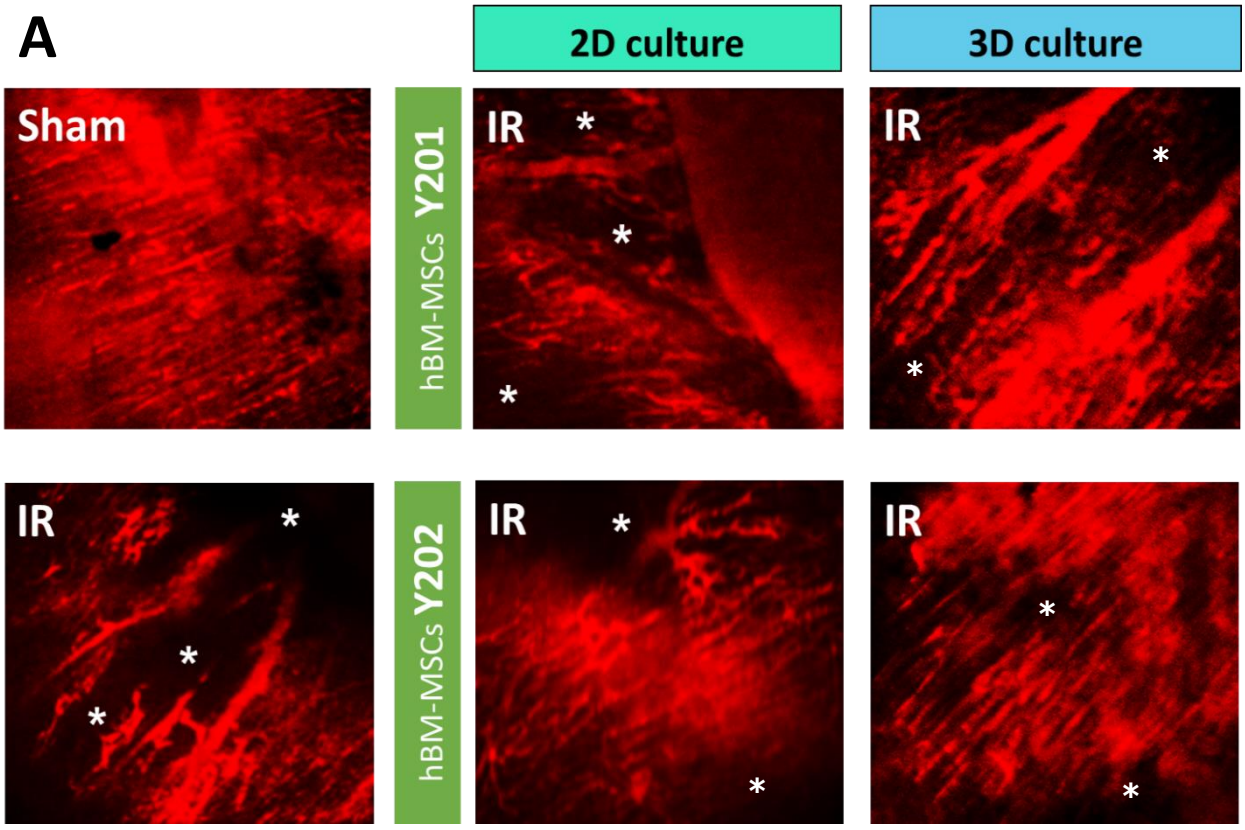


Figure 4.23. Intravital microscopy demonstrated that 3D cultured hBM-MSCs Y201 was able to improve functional capillary density following myocardial IR injury. FITC-BSA was injected after 2 hours of reperfusion. (A) Representative intravital images showed a dense network of perfused coronary capillaries in sham mice. Most capillaries parallel the arrangement of the muscle fibers with cross connections that run obliquely to fibers along their length. Well perfused medium-sized vessels were also being seen in some fields of view (not in the sham image above). However, IR injury was associated with multiple areas in which FITC-BSA did not perfuse, resulting in patchy areas devoid of any vasculature (*). In some fields of view, at least half the imaged area could appear non-perfused. Interestingly, medium sized vessels remained perfused and thus readily visible. Similar disruption was noted in mice receiving 2D cultured hBM-MSCs Y202 whereas in the hearts of those receiving 3D cultured hBM-MSCs Y201, perfusion was restored. **(B)** The difference in microvascular perfusion was significant between the sham and IR injured mice ($p<0.05$) and IR injured vs IR injured + 3D cultured hBM-MSCs mice ($p<0.05$). Statistical analysis was performed using a one-way ANOVA with Sidak's multiple comparison tests. N = 3 mice per group.

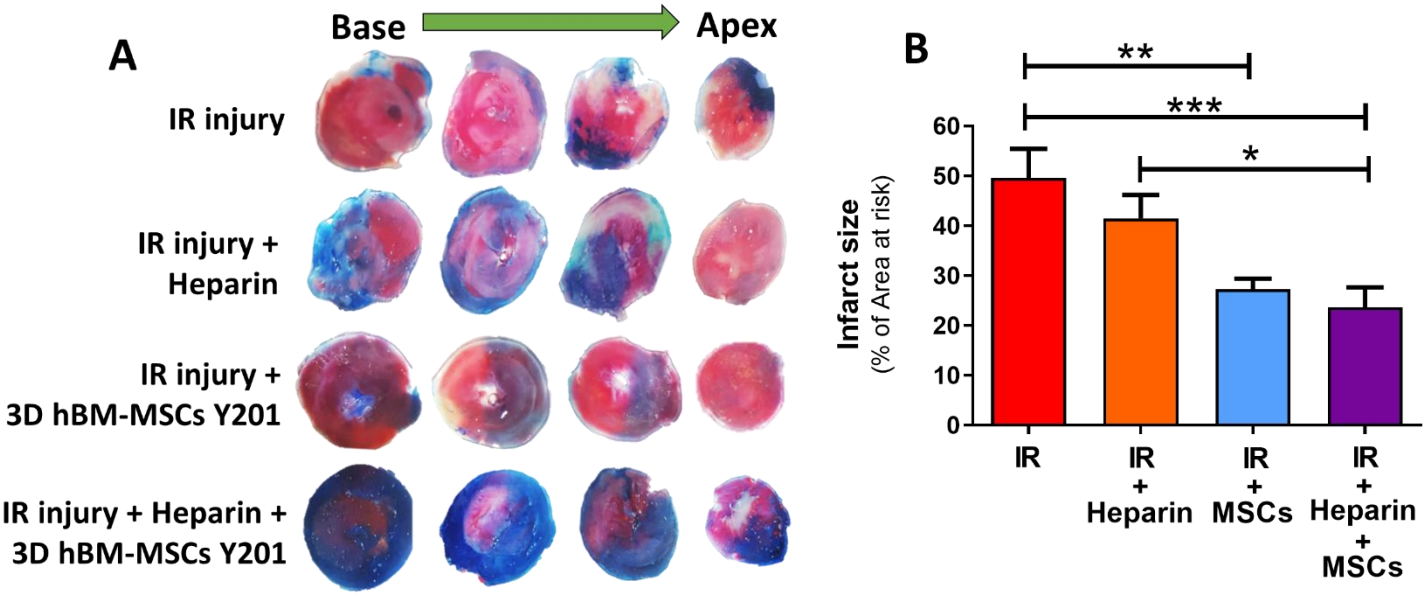


Figure 4.24. 3D cultured hBM-MSCs Y201 therapy decreases infarct size following myocardial IR injury which is further decreased when combined with heparin. (A) Dual Evans blue and TTC staining showing the non-ischaemic area (blue), area of the viable tissue at risk (red) and infarct area (white) after myocardial IR injury in mice receiving no therapy, heparin alone, 3D hBM-MSCs Y201 alone or heparin + 3D hBM-MSCs Y201. **(B)** IR injured hearts of mice not receiving any treatment showed the largest necrotic area presented as a % of the area at risk (AAR). The AAR represents the entire myocardial perfusion bed distal to an occluded artery. Although heparin alone led to a decrease in the infarct size, this was not statistically significant when compared to IR injured mice receiving no treatment. However, 3D cultured hBM-MSCs Y201 treatment significantly reduced the size of infarction when compared to IR injured hearts receiving no treatment. Interestingly, co-administration of both heparin with 3D hBM-MSCs Y201 therapy significantly reduced the infarct size further which was significantly different when compared to mice receiving no treatment and also when compared to mice receiving heparin alone. However, there was no significant difference in the infarcted area between IR injured mice treated with MSCs and those receiving heparin and MSCs. Statistical analysis was performed using two-way ANOVA with Sidak's multiple comparison test. Results presented as mean ± SEM. *p<0.05; **p<0.01; ****p<0.0001. N = 12 per group.

4.4 Discussion

Reperfusion injury post-PCI remains one of the top 10 unmet clinical needs in cardiology (Fuster, 2014). In the past decade, the use of stem cells and precursor cells has been suggested as therapeutic agents for the treatment of ischaemic heart conditions and interest in their clinical use has been rising. In particular, adult MSCs have been extensively studied and have, in a number of pre-clinical experimental studies, exhibited potential to repair and regenerate various damaged tissues and organs including the heart (Karantalis and Hare, 2015). Mechanistically, studies have demonstrated that MSCs reduce inflammation by releasing a whole host of therapeutic factors. Nevertheless, clinical success rate remains low and this may be linked to their poor trafficking and homing to the injured heart after systemic administration. Indeed, more than 80% of exogenously infused MSCs become entrapped in the lung with only 0.1-3 % detected in the target organ (Deak et al., 2010).

This may be linked to the fact that they are normally expanded using conventional 2D culture, which we and others have shown leads to a large fibroblastic cell phenotype. However, no studies have actually imaged the ability of MSCs to home to and become retained within the coronary microcirculation at a cellular level *in vivo.* Moreover, the mechanism(s) governing their therapeutic action of MSCs remains unclear. There is now an increased clinical recognition of the importance of the coronary microcirculation in MI patients (Pries et al., 2017). However, whether MSCs can protect these delicate structures following myocardial IR injury has not been investigated *in vivo.* This chapter applied powerful intravital imaging to the murine beating heart to answer fundamental questions

about the real-time kinetics of MSC homing to the IR injured heart and also detail their potential *in vivo* vasculoprotective effects.

In the *in vitro* studies outlined in Chapter 3 we identified 3D cultured hBM-MSCs Y201 and 3D cultured hBM-MSCs Y202 as likely candidates to test *in vivo* because they showed greater adhesion to frozen heart sections, inflamed ECs, VCAM-1 protein. However, only 3D cultured hBM-MSCs Y201 expressed CXCR4 remarkably on their surface. We therefore focused on investigating the recruitment of these BM-derived MSC sub-populations and comparing their myocardial homing and benefits with 2D cultured cells. Furthermore, to determine whether recruitment was similar for all BM-derived MSCs, comparisons were made with 2D and 3D cultured hBM-MSCs Y202. We are the first group to intravitally image, at a cellular level and in real-time, the kinetics of MSC recruitment to the beating mouse heart after myocardial IR injury. We firstly showed that both hBM-MSC sub-populations were more adhesive to an injured coronary microcirculation than the healthy heart. Furthermore, 3D culture improved their adhesion but most significantly within injured rather than sham hearts. Interestingly no significant difference between the adhesive capabilities of the two cell types was noted to either healthy sham or injured hearts. In an attempt to enhance local MSC recruitment and adhesion, combination therapy with heparin was investigated. However, this had no modifying effect on MSC adhesion. Interestingly, the 'first pass' of MSCs through the heart immediately after their infusion was also significantly increased in both healthy and injured hearts with 3D culture for both MSC types, but only at this time point.

More importantly, we demonstrated that 3D cultured hBM-MSCs Y201 were able to decrease neutrophil recruitment within the inflamed coronary microcirculation almost

immediately. However, this only became statistically significant 45 minutes after their infusion at which point an approximate 25-30% decrease in neutrophil presence was noted. This anti-inflammatory benefit was not observed with 3D cultured hBM-MSCs Y202. Additional vasculoprotective effects of 3D cultured hBM-MSCs Y201 was their ability to improve the density of perfused capillaries in the heart. No anti-thrombotic effects were demonstrated with any form of cellular therapy given alone. Despite this, 3D cultured hBM-MSCs Y201 therapy did significantly decrease the size of infarction. Interestingly, although dual therapy with heparin did not improve local MSC presence in the heart, it did accelerate the anti-neutrophil ability of MSCs, decreased platelet presence in the heart and reduced final infarct size more so than MSCs alone. Overall, our novel studies suggested that 3D culture of the hBM-MSCs Y201 sub-population was superior in their ability to reduce inflammation, improve flow and decrease infarct size after myocardial IR injury, with heparin co-administration providing further benefit of reducing inflammation at the level of the coronary microvasculature.

4.4.1. IR injured coronary vasculature targeted by systemically delivered MSCs

We are the first group to directly demonstrate *in vivo* at a cellular level that all MSC sub-types were able to home better and become firmly adherent within the IR injured beating coronary microvasculature compared to healthy sham hearts. This clearly indicated that circulating MSCs were responsive to microvascular and/or myocardial injury. The ability for MSCs to circulate to the injured heart has been previously demonstrated (Saito et al., 2002). Indeed Saito and colleagues isolated BM-MSCs, labelled them with a LacZ reporter

gene, and injected them into donor mice one week before the heart was injured using permanent LAD ligation (Saito et al., 2002). They showed histologically that only the IR injured hearts, but not the sham hearts, contained MSCs. Interestingly, they also showed that 1 day after LAD ligation, most MSCs were within blood vessels surrounding the infarct, but not within it because the artery that supplied the infarcted area had been permanently occluded (Saito et al., 2002). However, 2 weeks later, MSCs were seen in the infarcted myocardium, suggesting they had migrated to the injured site. They concluded that their findings were due to signals being released from the damaged myocardium which initiated MSC recruitment from the BM and their migration to the injured heart (Saito et al., 2002).

Specific retention within injured sites has also been demonstrated for other organs. For example, MSC recruitment was also increased within the mouse abdomen after irradiation-induced damage (Mouiseddine et al., 2007). Previous reports have also used whole animal IVIS (*in vivo* imaging system) to demonstrate MSCs at the site of puncture wounds and tumour injured organs days after their infusion (Kidd et al., 2009). However, IVIS does not have the cellular resolution of intravital imaging and requires labelled cells to be clustered at a high density before they can be imaged. Collectively these studies, with our own, demonstrate MSC recruitment tropism is more specific to injured organs. It is worth noting that this differs to our own previously published work on MSC recruitment to the IR injured gut, where we found no differences in the adhesion within the mucosal villous capillaries between sham and injured gut (Kavanagh et al., 2015). Furthermore, it was not possible to improve MSC adhesion with the villous capillaries even with a variety of pre-treatment strategies. Nevertheless, we believe injury is a good cue for MSC homing which was not

effective in the gut simply due to the very small size and narrow angle of submucosal arterioles in the gut, which limited the recruitment of large MSCs (Kavanagh et al., 2015).

Previous studies have agreed that the efficacy of MSCs in cell therapy depends on their homing ability and engraftment into the injury site (Lin et al., 2017). The mechanisms governing their recruitment are complex but appear to involve similar processes to those identified for inflammatory cells (Fue et al., 2019). After IR injury, necrotic cells release a number of cell components and mediators, called damage-associated molecular patterns (DAMP), into the bloodstream thereby inducing an inflammatory response. DAMPs bind toll-like receptors (TLRs) on immune cells to activate them, leading to influx of neutrophils followed by monocyte and lymphocytes (Van den Akker et al., 2013). Surprisingly, DAMPs not only activate TLR on immune cells but also on MSCs. hBM-MSCs present various TLRs such as TLR7, TLR 9 and TLR10. The response of TLR activation on MSCs influences their homing capacity and possibly their paracrine activity too (van den Akker et al., 2013). hBM-MSC migration can also be enhanced by TLR ligand activated by LPS as demonstrated in transwell migration assays (Tomchuck et al., 2008). Moreover, the release of pro-inflammatory mediators from damaged cells, such as IFN-γ, TNF-α and IL-1, have been shown to induce the expression of selectins on ECs leading to the initiation of MSC migratory processes to injured sites (Linfert et al., 2009). IR injury also oxidatively damages the endothelium which, when activated in this way, increases their permeability and up-regulation of various adhesion molecules, such as ICAM-1 and VCAM-1 (Linfert et al., 2009). MSCs express various adhesion molecules, such as L-selectin, P-selectin, CD44, CD49d and chemokine receptors such as CXCR4, which enable them to become activated and subsequently adhere to ECs (Rowart et al., 2015).

These same mechanisms could therefore explain the increased retention of 3D cultured hBM-MSCs Y201 in our IR injured beating heart model. Indeed in Chapter 3 we showed that 3D culture increased the expression of critical chemokine receptors and adhesion molecules which are likely involved in mediating the identified increased adhesive capacity of 3D cultured MSCs in the injured heart *in vivo*. Once recruited BM-MSCs can undergo diapedesis through blood vessel walls to enter the surrounding parenchyma (Fu et al., 2019). However, in the intravitally imaged beating heart the resolution was not sufficient to determine whether any of the adherent cells had actually transmigrated into the myocardium during the 2-2½ hour imaging duration.

4.4.2. 3D culture enhances myocardial hBM-MSCs Y201 recruitment *in vivo*

We are the first to provide exciting data that 3D culture improved retention within both the healthy sham and injured coronary microcirculation. Not only this, but the numbers of 3D cultured hBM-MSCs Y201 and hBM-MSCs Y202 freely circulating through the beating heart was also significantly higher at the time of infusion, which may have increased the likelihood of subsequent firm adhesive interactions taking place. In Chapter 3 we showed that the size of MSCs released from hanging drop spheres was significantly smaller than those obtained from conventional 2D culture. Such smaller cells may have escaped entrapment within the pulmonary vasculature and thus led to the maintenance of a circulating pool of MSCs in the peripheral circulation (Guo et al., 2014). Indeed, this was confirmed by Bartosh and colleagues who showed that hanging drop derived MSCs were half the size of monolayer MSCs, which allowed them to pass through the healthy mouse lung microvasculature and distribute more efficiently into other tissues (Bartosh et al.,

2010). This was assessed using real-time PCR of lung tissue collected 15 mins after MSC infusion and showed that the number of trapped cells decreased by 25% with a larger fraction recovered from liver, spleen, kidney and heart (Bartosh et al., 2010). Although actual numbers were not quantitated, we noticed that 2D cultured MSCs tended to appear as large clumps in the lungs after systemic administration whereas 3D cultured MSCs were present more so as individual cells (**Figure 4.4**). Collectively, these data emphasizes that MSC diameter is critical and needs to be evaluated before systemic injection.

Despite this, the numbers of freely flowing 3D cultured hBM-MSCs Y201 and hBM-MSCs Y202 was observed to be higher only at the first time point imaged immediately after their systemic infusion. This is consistent with previous studies within the Kalia group for both MSCs and HSCs imaged intravitally in other IR injured solid organs (Kavanagh et al., 2019c, White et al., 2013). This may be explained by the increased myocardial blood flow or hyperaemic response that takes place post-reperfusion in the same injury model and previously reported by our group (Kavanagh et al., 2019). This was quantitated using laser speckle contrast imaging, which monitored overall perfusion in the whole left ventricle of the IR injured beating mouse heart. Immediately after the LAD artery was un-ligated, an immediate hyperaemic response was noted. This increased delivery of blood to the ischaemic heart may have led to the delivery of more MSCs to the IR injured coronary microcirculation (Kavanagh et al., 2019).

The increased homing and subsequent recruitment of 3D cultured cells may also be linked to the fact that certain critical receptors for MSC migration and homing, such as CXCR4, are lost when MSCs are cultured using conventional 2D methods but recovered with 3D culture (Cheng et al., 2013, Potapova et al., 2008). Indeed, we noticed this to be the case in

Chapter 3 where our flow cytometry studies detailed the expression of surface CXCR4 only on 3D cultured hBM-MSCs Y201, which was otherwise lost on 2D cultured cells. Signaling events mediated after interactions of the potent stem cell chemoattractant SDF-1α, released in abundance from ischaemic tissues, with its CXCR4 receptor, leads to the differential expression of 30 genes in MSCs of which 11 are involved in cellular movement processes (Stich et al., 2009). Hence restoring expression of CXCR4 on 3D cultured hBM-MSCs Y201 may have contributed to their increased homing to the IR injured heart. Notably, we showed that cells derived from spheroids also expressed surface adhesion molecules evenly over their surface, whereas on 2D cultured cells expression was more concentrated or clustered on one side of the cell surface. The dispersion of adhesion molecules over the cell surface has significance on their availability and capacity to form strong bonds with counterligands on the surface of ECs (Ren et al., 2010). Indeed, the effectiveness of leukocyte migration to injured sites is affected by the surface distribution of adhesion molecules (Hocde et al., 2009).

Interestingly, we found that the 3D culture technique increased the retention of hBM-MSCs Y201, but not hBM-MSCs Y202 within the coronary microcirculation of healthy sham hearts. Similar results were showed by Kavanagh and colleagues (Kavanagh et al., 2019). They demonstrated that HSCs were found in the sham heart using the same murine myocardial IR injury model as the current study. It is possible that some degree of injury due to the sham surgical procedure may have taken place as a suture was passed through the left ventricle muscle and placed under the LAD artery but not tied around it. Any resultant low level injury induced by the surgical procedure may have mildly stimulated

coronary ECs to express vascular adhesion molecules priming them for active MSC recruitment.

4.4.3. 3D culture enhances hBM-MSCs Y201 recruitment – supporting evidence

Intravital imaging is limited by the fact that it can only image the surface of the left ventricle with an imaging depth in solid organs of about 50-60μm (Wu et al., 2017). Furthermore, in other solid organs you could easily scan the surface and image from more than one region, however this is technically difficult in our stabilised heart model as there is limited room for imaging inside the inner ring of the stabiliser. Due to these limitations, flow cytometry experiments were carried out to confirm whether 3D culture did indeed increase MSC presence, but had the added benefit of analysing the whole heart. Results confirmed the intravital observations that 3D culture increased MSC myocardial retention with IR injured hearts, but unlike the superficial imaging intravital studies, this was only (remarkably) significant for the hBM-MSCs Y201 sub-population. Earlier described changes in the cell size, chemokine receptor expression and adhesion molecule expression in chapter 3 may explain this. However, it is also possible that the potential location of these MSCs in their native BM origin may also provide an explanation. The Genever group who clonally expanded the tested hBM-MSCs demonstrated that hBM-MSCs Y201 significantly overexpressed vascular support/interaction gene sets, such as those related to blood vessel development and remodeling and artery morphogenesis, and were located in a more perivascular location (James et al., 2015). It is therefore possible that perivascular hBM-MSCs Y201 were thus

more likely to interact with ECs due to these inherent characteristics. However, hBM-MSCs Y202, were reported to rarely associate with $CD31^+$ vascular cells and did not commonly co-localize with endothelial and perivascular stromal cells (James et al., 2015). Collectively, these studies support the theory that different sub-populations of MSCs, despite residing in the same tissue of origin, may play specific roles and exhibit distinct characteristics which could influence their therapeutic capacity (An et al., 2018).

4.4.4. Extensive neutrophil and platelet presence throughout the ventricular wall

We previously demonstrated that IVM is a powerful technique for investigating dynamic events in the beating heart coronary microcirculation following myocardial IR injury. However, the limitation of this technique is that it only allowed data to be acquired from a small region on the epicardial side of the heart and with limited tissue depth imaging (Kavanagh et al., 2019). In order to overcome this limitation, MPLSM was introduced to image the impact of IR injury on thromboinflammatory events *ex vivo* within deeper layers of the left ventricular muscle. MPLSM has been used to determine cardiovascular diseases *in vivo* and *ex vivo* in animal models (Scherschel and Rubart, 2008). MPLSM provides better image quality and overcomes the single-photon microscope limitation, such as photobleaching, photo-toxicity, and less penetration into the tissue than 50 µm. We modified our initial attempts for preparing the isolated heart for multiphoton imaging in order to obtain better quality images. This included using a tissue vibratome to precisely section the heart sagitally into thin 250µm consecutive sections rather than manually cutting thicker sections. As far as we are aware, no previous studies have used a similar

method to image thromboinflammatory events post-IR injury within the left ventricle at various depths, let alone to determine the vasculoprotective benefits of cellular therapy. We confirmed neutrophil and platelet presence in the deeper coronary microvessels with neutrophils identified in the highest concentration in the outermost layer of the heart. The advantage of MPLSM is the capacity to investigate the dynamic of disease in thick tissue up to 1 mm (depending on the tissues' type) (Wu et al., 2017). The use of MPLSM allows the tracking of single-cell and studying of adhesion and migration of leukocyte (Lee et al., 2012). Maffia and colleagues demonstrated that MPLSM provides the functional, structural and subcellular information from the contracting vessels and beating hearts, which allows the investigation of cellular processes, including the leukocytes characteristic and behavior in their natural environment (Maffia et al., 2007). More importantly, MPLSM provides the true 3D tissue structure, which gives more information about cells and organ structure. Therefore, MPLSM grants a useful and insightful data link between the basic research and clinical study since it can be used in both *in vitro* and *in vivo* experiments (Wu et al., 2017). We conclude that MPLSM can overcome the limitation to examine the deep tissue. Therefore, to investigate the inflammation in the thick tissue or organ, using MPLSM should be considered to gain more information to understand the disease's mechanism.

4.4.5. 3D cultured hBM-MSCs Y201 are vasculoprotective in the injured heart

Mo and colleagues also suggested that MSCs are a heterogeneous population comprising of cells with diverse physical characteristics and functional capacity (Mo et al., 2016). This was found to be true in the current chapter when the anti-thromboinflammatory efficacy of two MSC sub-populations derived from the same

origin was investigated. We have previously detailed the main microcirculatory perturbations in the IR injured heart intravitally which include increased neutrophil recruitment and platelet aggregation with ensuing decreases in the density of functional coronary capillaries (Sezer et al., 2018). The current study is the first to show that only 3D cultured hBM-MSCs Y201 were able to confer vasculoprotection, by reducing neutrophil recruitment and improving myocardial perfusion, and also decreased infarct size. An increasing number of studies have shown that various MSCs can secrete anti-inflammatory cytokines which can attenuate neutrophil infiltration, such as IL-2, IL-4, IL-6, CXCL2 and CXCR2 (Joel et al., 2019, Harrell et al., 2019). MSCs can also suppress ROS secreted by neutrophils, which would protect the ECs, with which neutrophils make close adhesive contact, from oxidative injury (Konari et al., 2019). By increasing the presence of MSCs in the heart, it is possible that a high concentration of these beneficial factors were released locally.

Concerns have been raised regarding the compatibility of MSCs with blood with recent studies having shown them to have pro-coagulant or thrombogenic properties after transplantation in patients (Coppin et al., 2019). This appears to be linked to the expression of pro-coagulant factors such as tissue factor on the surface of cultured MSCs or through their direct adhesion to platelets rather than platelet activation *per se*. Local studies demonstrated the ability of human umbilical cord-derived MSCs to bind to platelets *in vitro* in flow assays and circulating platelets in mice due to podoplanin's expression to form clots. Still, interestingly this was not demonstrated for hBM-MSCs (Sheriff et al., 2018). In contrast, Netsch and colleagues recently published that MSCs from different origins (bone marrow, adipose and cord blood) inhibited agonist-induced activation and aggregation of

platelets in platelet-rich plasma and whole blood using a mechanism involving release of adenosine, a known platelet inhibitor (Netsch et al., 2018). An anti-platelet capability of MSCs has also been shown by others (Mendelson et al., 2019). Our intravital imaging showed that both hBM-MSC sub-populations demonstrated a general trend to reduce microthrombi in the injured heart, but this was not statistically significant. However, the mechanism governing the ability of our hBM-MSCs to reduce platelet presence is still not clear. We noted platelet recruitment was initiated very early post-reperfusion – the first intravital images were taken at 30 mins and platelets were already adherent at this time point. hBM-MSCs were also injected at this time point and so it is possible that for a more heightened anti-platelet effect to be elicited, they needed to be infused before platelets formed aggregates. The time point of cellular therapy should therefore be re-considered.

A barrier to realize the therapeutic potential of MSCs is the intrinsic heterogeneity of cells isolated from different and even same sites (James et al., 2015). This was clearly highlighted in the current study whereby the vasculoprotective potential of two different BM-derived MSCs varied. Although the anti-inflammatory properties of MSCs have been receiving increasing interest, a growing body of data suggests that MSCs may also exhibit pro-inflammatory properties in certain instances, perhaps to stimulate pathogen clearance (Jiang and Xu, 2020). The Genever group identified CD317 as a novel biomarker that allowed isolation of two distinct MSC sub-sets (James et al., 2015; Kay et al, 2018). hBM-MSCs Y202 were surface $CD317^{+}$ cells, that made up 9% of the BM MSC population, with hBM-MSCs Y201 being CD318- (Kay et al., 2018; James et al., 2015). CD317 is also known as tetherin (also BST-2 and HM1.24) which is best known for its ability to inhibit the spread of viral infection by 'tethering' viruses to the membrane within infected cells and thereby

inhibiting their release from the infected cell (James et al., 2015). It is a transmembrane protein expressed on the surface of many cells including mature B-cells, macrophages and BM-MSCs. In addition, tetherin activates NF-*κ*B, a transcriptional activator that leads to the rapid expression of pro-inflammatory cytokines. This would contribute to the antiviral defense response of the host (Gustin and Douglas, 2013). Therefore, $CD371^{+}$/$tetherin^{+}$ MSCs could potentially have a role in the clearance of viral infections (Gustin and Douglas 2013; O'Connor 2019). We speculate that in an inflamed organ, recruitment of these specific $CD317^{+}$ MSCs would not be beneficial and may enhance the inflammatory response. Although this was not noted in the heart, this sub-population was certainly not anti-inflammatory unlike $CD317^{-}$ hBM-MSCs Y201. Therefore it is possible that this particular surface marker may molecularly identify an MSC subset with specific vasculoprotective properties in the IR injured heart.

The Genever group also demonstrated that these two cell types' immunomodulatory ability was different, with hBM-MSCs Y202 not able to suppress CD4+ T cell proliferation as effectively as hBM-MSCs Y201 (James et al., 2015). In fact hBM-MSCs Y202 encouraged T cell polarisation into a more pro-inflammatory Th1 subset when compared to hBM-MSCs Y201, which polarised T cells into the more anti-inflammatory Th2 subset (Kay et al., 2018; **Table 3.1**). This clearly suggested single cells were unlikely to possess all properties commonly ascribed to MSCs and that specific functional attributes, such as immunomodulatory competency, was found within distinct sub-populations. Our own results supported this conclusion as the *in vitro* and *in vivo* adhesive ability and *in vivo* vasculoprotective efficacy of these two subsets in the IR injured heart was clearly different.

4.4.6. Combination therapy with heparin?

We have previously demonstrated that one of the key contributors to the decreased density of functional capillaries in the IR injured heart is the occlusion of coronary capillaries by platelet microthrombi rather than by the adherent neutrophils (Kavanagh et al. 2019). It was therefore disappointing that this particular microvascular perturbation was not drastically reduced by our MSC therapy. We, therefore, investigated whether co-transplantation of MSCs with a potent anticoagulant heparin could enhance, not only the homing and retention of MSCs, but also their anti-thromboinflammatory properties. Heparin was chosen as it is a widely used, safe drug which could be used clinically as an adjuvant if it was noted to improve MSC therapy (Ghadrdoost et al., 2018). Indeed, co-administration of heparin has been shown to enhance the migration of MSCs to the colon of colitis mice which was linked to reduced colon inflammation, mortality and body weight loss (Liao et al., 2017). Interestingly, the authors of this work were concerned that MSCs would cause coagulation when systemically infused which was their reasoning for using heparin (Liao et al., 2017). This differed to our own justification which was to test a combination therapy, with heparin and MSCs targeting infiltrating platelets and neutrophils respectively.

Although heparin is known as an anti-coagulant, it has also been shown to possess anti-inflammatory activity due to its ability to bind adhesion molecules involved in leukocyte trafficking and thereby preventing these molecules from binding to their counter-ligands on vascular endothelium (Brown et al., 2012). The current study shows that administration of heparin alone increased neutrophil presence in this layer confirming the *in vivo* data obtained intravitally. We speculate that heparin may have removed the platelet

microthrombi and therefore unblocked occluded capillaries. This increased functional capillary density would have increased neutrophil trafficking through the coronary microcirculation and thus led to the observed gradual increase in neutrophil adhesion. Heparin has been reported to induce the leukocytosis in various species, such as humans, mice, and cow (Bradfield et al., 1974, Sasaki et al., 1967). In humans, leukocytosis occurs around 0.44% of patients receiving heparin (Zhang et al., 2012). Indeed, heparin should be used with consideration with it possible side effect. Despite this pro-inflammatory response, we still tested the vasculoprotective efficacy of a combination therapy of heparin and MSCs noted by others to be therapeutic in the heart. In the current study, it was exciting to note that combination therapy resulted in a significant reduction of neutrophils and a remarkable decrease in platelets throughout the depth of the ventricular wall. The use of a non-anticoagulant fraction of heparin inhibited neutrophil recruitment into the mouse lung and cremaster muscle (visualised intravitally) after stimulation with LPS (Riffo-Vasquez et al., 2016). It is possible that such studies used different doses of heparin which would explain the different outcomes. However, similar results to ours have also been observed by others in different injury models such as peritonitis (Arimateia et al., 2015, Bradfield and Born, 1974, Zhang et al., 2012). The decreased platelet presence was not noted when we investigated the superficial layer of the heart intravitally. Alone, intravital imaging would have led us to believe that this combination therapy was not beneficial for inhibiting platelet events. However, when two different imaging approaches were used, a clear effect on thrombotic cells was also apparent. To our knowledge, we are the first group to demonstrate using multiphoton imaging the vasculoprotective effectiveness of a combination therapy in all layers of the IR injured heart.

Inhibiting thromboinflammation and improving perfusion within the coronary microcirculation is clearly vital but should be associated with improvements in the myocardium's viability. Mice receiving 3D cultured hBM-MSCs Y201 therapy did indeed present with infarcts that were 45% reduced when compared to infarcts in mice receiving no treatment. Many studies showed the therapeutic effects of MSCs in reducing heart infarction (Janssens et al., 2006, Quevedo et al., 2009, Williams et al., 2013). MSCs treatment in swine chronic ischemic cardiomyopathy model reduced the infarct size by 25% with improving LV chamber volumes (Williams et al., 2013). This suggested that infarct size reduction after MSC therapy plays an essential part in the therapeutic effects of ventricular remodelling. The mechanism of myocardial infarct size reduction with MSC treatment is still unclear. Curtis and colleagues showed that inhibition of neutrophil adhesion by anti-inflammatory agent reduced the myocardial infarct size by 51% compared to the control group (Curtis et al., 1993). This may explain why 3D cultured hBM-MSCs Y201 infusion reduced infarction size since they inhibited neutrophil recruitment following myocardial IR injured.

Combining therapy with heparin to inhibit multiple perturbations within the coronary microcirculation resulted in the infarct size being reduced by 52% of the size in untreated mice. Ghadrdoost and colleagues demonstrated that combination therapy of heparin enhanced the beneficial effect of MSCs in the rabbit myocardial infarction model (Ghadrdoost et al., 2018). They found that MSCs + heparin reduced the fibrotic area of the infarcted heart and increased level VEGF and angiogenesis. Indeed, this combination therapy had a faster onset of anti-neutrophil activity and even lowered platelet presence more so than that seen in the hearts of mice receiving MSCs alone. In this scenario, we postulate that

heparin would have targeted the platelets, and MSCs would have prevented any IR-mediated and heparin-mediated neutrophil adhesion.

4.5 Conclusion

In conclusion, this chapter provided valuable data on the real-time kinetics of 2D and 3D cultured MSC, neutrophil and platelet trafficking within the coronary microcirculation of the IR injured beating heart. The migratory and adhesive abilities of MSCs have been routinely assessed using *in vitro* transwell assays. This has been achieved *in vivo* by tracing luciferase labelled cells using a bioimaging system such as IVIS (Cao et al., 2016). However, the cellular resolution of the IVIS is not sufficient to track individual cells. We are the first to not only provide novel insights into the trafficking capabilities of individual 2D and 3D cultured MSC sub-populations, but importantly within the coronary microcirculation *in vivo* in real-time. Our studies highlighted how smaller MSCs could circulate more freely through the coronary capillaries immediately upon infusion which, importantly, improved their local retention. Whether this phenomenon was directly linked to the observed therapeutic efficacy of 3D cultured MSCs is difficult to conclusively state, but nevertheless 3D culture did improve their vasculoprotective capabilities. Moreover, despite improved adhesion of both BM-derived MSCs, their ability to protect the microvessels differed, with hBM-MSCs Y201 more effective. We present novel data that an MSC sub-population which normally resides in a more perivascular location was more vasculoprotective. Mechanisms to explain how vasculoprotection was afforded may be linked to MSC release of beneficial proteins, exosomes and cytokines capable of reducing inflammation within an IR injured milieu (Jaukovic et al., 2020a). Moreover, 3D cultured MSCs have been reported to have better

retention and survival capacity with hypoxic areas which may have led to a better anti-inflammatory capacity (Petrenko et al., 2017).

CHAPTER 5

Mechanisms by which MSCs may confer Vasculoprotection following Myocardial Ischaemia-Reperfusion Injury – *in vitro* and *in vivo* Studies

5.0 Mechanism by which MSC confer vasculoprotection following myocardial IR injury – *in vitro* and *in vivo* studies

5.1 Introduction and Hypotheses

5.1.1. Introduction

Cell-based therapeutic strategies to ameliorate CVD have been of interest for over 2 decades. MSC cellular therapy is considered one of the most promising strategies due to their potent regenerative and immunomodulatory capacity as well as their therapeutic paracrine activity (Ward et al., 2018). However, clinical success has been limited and it is generally agreed that a lack of a thorough understanding of the therapeutic mechanisms they employ to confer benefit is partly to blame. There are still gaps in our understanding of which populations and sub-populations of MSCs confer the best therapeutic capacity in the diseased heart, and whether this mechanistically involves at a cellular level preserving the coronary microcirculation from damage. If vasculoprotection is indeed afforded, then in order to optimize MSC-based therapies, the mechanism by which this occurs needs to be fully understood.

We have previously shown in Chapter 3 and Chapter 4 that 3D culture of the hBM-MSCs Y201 sub-population, that likely resides in a perivascular niche within the BM, demonstrated a greater adhesive capacity to inflamed ECs *in vitro* and expressed remarkably CXCR4 on their surface and, importantly, were better recruited and retained within the IR injured heart *in vivo.* Moreover, hBM-MSCs Y201 demonstrated a superior

ability to protect the coronary microcirculation from thromboinflammatory events following myocardial IR injury *in vivo*. We further found that 3D spheroid culture remarkably enhanced the homing of these MSCs on first pass to the heart, which was probably linked to their smaller diameter, resulting in MSCs being able to better escape entrapment within the pulmonary microvasculature. Additionally, 3D culture enhanced the expression of surface adhesion molecules such as CD44 and CD54 on this cell population, as well as induced higher expression levels CXCR4, the receptor for the important stem cell homing chemokine SDF-1α.

In this chapter, we aimed to investigate the mechanisms by which 3D cultured hBM-MSCs Y201 were actually mediating their vasculoprotective effects. ROS, as well as downstream activated cytokines, have been identified in a number of studies to play key and potent roles in the pathophysiology of myocardial IR injury (Granger and Kvietys, 2015). ROS, which include the free radicals superoxide ($O_2\bullet^-$) and hydroxyl radical (•OH), but also non-radical species such as hydrogen peroxide (H_2O_2), are produced during normal metabolic processes (Cadenas, 2018). When produced at low levels, they are important signalling molecules involved in muscle contraction and immune responses (Schieber et al., 2014). However, ROS generation can go unchecked when natural anti-oxidants, such as superoxide dismutase, catalase and glutathione, become overwhelmed during pathological conditions such as myocardial IR injury, resulting in injurious cellular oxidative stress as the homeostasis of the redox pathway is disturbed by redundant ROS production (Zuo et al., 2015). A vicious cycle also ensues when ROS leads to EC activation and subsequent inflammatory cell recruitment, with these circulating cells further releasing secondary ROS themselves (Cadenas, 2018). ROS induce direct or indirect cell injury by triggering

inflammatory cytokine secretion from damaged cells. This occurs as ROS are capable of triggering the activation of MAPKs in cardiomyocytes and vascular endothelium, which results in the activation of transcription factors such as NFκB (Zhang et al., 2014). NF-κB activation can promote inflammatory gene expression for multiple cytokines including IL-1β, IL-6, IL-10 and TNF-α, and also adhesion factors such as ICAM-1, VCAM-1 and E-selectin (Valen et al., 2001). Hence ROS production following IR injury can lead to the production of a whole host of inflammatory cytokines and up-regulation of endothelial adhesion molecules that can both activate and capture passing thromboinflammatory cells leading to coronary microvascular perturbations and injury (Granger and Kvietys, 2015).

Therefore, in this Chapter we aimed to investigate whether the specific 3D cultured hBM-MSCs Y201 sub-population mediated vasculoprotection by reducing ROS generation from, and oxidative damage to, EC. Additionally, we investigated their ability to modify endothelial ICAM-1 and VCAM-1 expression, which are well recognised markers of inflammatory injury. Since cytokine generation can mediate a plethora of inflammatory disturbances, we also aimed to determine whether their release into host serum could be modified and thus provide an additional mechanism to explain their therapeutic action. The list of cytokines examined included well established potent pro-inflammatory cytokines such as IL-1β, IL-6, IL-8 (KC), TNFα and IFNγ, as well as major anti-inflammatory cytokines including IL-4, IL-10 and IL-13. Of these, pleiotropic IL-10 has been demonstrated to possess potent anti-inflammatory properties as it can inhibit the release of IL-1β, TNF-α and IL-6 and their receptors, and increase anti-cytokine generation (Zhang et al., 2007). For all studies in this Chapter, direct comparison was made with 2D cultured hBM-MSCs Y201 and also with 2D and 3D cultured hBM-MSCs Y202. Collectively this data would provide us with

a mechanistic understanding of the beneficial effect of MSC-based cellular therapy in the setting of myocardial IR injury.

5.1.2. Hypothesis

1. 3D cultured hBM-MSCs Y201 are most effective at inhibiting the generation of ROS from injured cardiovascular ECs *in vitro.*
2. 3D cultured hBM-MSCs Y201 are most effective at inhibiting oxidative damage in injured cardiovascular ECs *in vitro*.
3. 3D cultured hBM-MSCs Y201 are most effective at inhibiting oxidative damage in coronary ECs following myocardial IR injury.
4. 3D cultured hBM-MSCs Y201 are most effective at inhibiting the surface expression of ICAM-1 and VCAM-1 on coronary ECs following myocardial IR injury.
5. 3D cultured hBM-MSCs Y201 are most effective at reducing the serum levels of pro-inflammatory cytokines and increasing levels of anti-inflammatory cytokines following myocardial IR injury.

5.1.3. Specific aims

1. The ability of 3D cultured hBM-MSCs Y201 to inhibit the generation of ROS from injured ECs will be investigated *in vitro* and compared to that of 2D cultured hBM-MSCs Y201. VCECs co-cultured with 2D or 3D cultured hBM-MSCs Y201 will be damaged using hydrogen peroxide (H_2O_2), a free radical known to be generated

during IR injury, and generation of ROS will be assessed by immunostaining for DHE. To determine whether the ROS inhibition of hBM-MSCs Y201 is superior, comparisons will be made with 2D and 3D cultured hBM-MSCs Y202.

2. The ability of 3D cultured hBM-MSCs Y201 to specifically prevent ROS mediated oxidative damage of ECs will be investigated *in vitro* and compared to that of 2D cultured hBM-MSCs Y201. VCECs co-cultured with 2D or 3D cultured hBM-MSCs Y201 will be damaged using H_2O_2 and EC oxidative damage induced specifically by this ROS will be assessed by immunostaining for 8-OHdG. To determine whether the ROS inhibiting of hBM-MSCs Y201 is superior, comparisons will be made with 2D and 3D cultured hBM-MSCs Y202.

3. The ability of 3D cultured hBM-MSCs Y201 to decrease ROS mediated oxidative damage and decrease ICAM-1 / VCAM-1 expression on coronary ECs following IR injury will be determined using flow cytometry and compared to that of 2D cultured hBM-MSCs Y201. Hearts will be removed from mice undergoing IR injury ± hBM-MSCs Y201 and digested to single cells. ROS mediated oxidative injury will again be investigated on $CD31^+$ coronary ECs using an anti-8-OHdG antibody, with adhesion molecules assessed using antibodies against ICAM-1 and VCAM-1. To further assess whether vasculoprotection is the only underlying mechanism of therapeutic action, the expression of 8-OHdG on cardiac troponin positive ($cTnT^+$) cardiomyocytes will also be determined. To determine whether the ROS inhibition of hBM-MSCs Y201 is superior, comparisons will be made with 2D and 3D cultured hBM-MSCs Y202.
4. The ability of 3D cultured hBM-MSCs Y201 to modify the release of anti- and pro-inflammatory cytokines following myocardial IR injury will be assessed by

quantitating serum levels of a number of cytokines using a Luminex assay. Comparisons will be again be made with 2D cultured hBM-MSCs Y201 and also 2D and 3D cultured hBM-MSCs Y202.

5.2 Methods

The methods used in the chapter were previously outlined in **Chapter 2**. Briefly, DHE immunostaining was carried out to investigate the presence of generated $O_2\bullet^-$ in live cells. VCECs were co-cultured with 1ml of $5x10^4$ hBM-MSCs or 1ml vehicle media in 24 well plates for 72 hrs (Kavanagh et al., 2019). 500µl of 10µm of H_2O_2 was added to all wells to induce oxidative damage to the monolayer of VCECs and plates were then incubated at 37°C and 5% CO_2. This was repeated every 24 hrs for 72 hrs. At 72 hrs, $O_2\bullet^-$ generation was visualised using 500µl of 10µm DHE added for 10 mins. To investigate the level of VCECs undergoing oxidative stress, cells were firstly fixed, permeabilised and then immunostained with 300µl of a 1:500 dilution of a primary anti-8-OHdG antibody for 1 hr in the dark at room temperature followed by addition of a secondary antibody. This experiment was repeated in triplicate with five images per well captured using an EVOS fluorescence microscope. Images analysis was conducted using ImageJ software. The area of absent and low-intensity colour was excluded from the analysis using the threshold modifier. The formula used to calculate the fluorescence intensity was the area of intensity multiplied with mean intensity.

To quantitate oxidative damage of primary coronary ECs following myocardial IR injury, mice underwent LAD ligation and 2 hrs reperfusion in the presence or absence of infused hBM-MSCs. At the end of reperfusion, mice were culled and isolated hearts underwent

collagenase digestion. Coronary ECs were labelled with a PE-conjugated anti-CD31 antibody whilst cardiomyocytes were labelled with an anti-cTnT antibody. The oxidative damage of each cell was then detected using an anti-8-OHdG antibody. Samples were analysed using FACSCalibur flow cytometry with a gating strategy conducted to investigate and quantify the cells of interest.

Luminex® multiplex immunoassay was used to investigate the effect of MSCs on the serum levels of 23 different pro- and anti-inflammatory cytokines. To assess the cytokine profile, 500µl of anti-coagulated blood was collected at the end of 2 hrs reperfusion and centrifuged (700 g, 5 min) at room temperature to obtain serum. Serum was then stored at -80°C until ready for use. Circulating cytokine concentrations were identified in serum samples obtained from mice following sham surgery, IR injury, or IR injury + hBM-MSC administration. Samples were loaded in triplicate onto a BIO RAD® Bio-Plex Pro mouse cytokine 23-Plex assay plate and analysed using Bio-Plex MAGPIX® plate reader (Bio-Rad Laboratories; USA). The protocol supplied by the manufacturer was followed for accurate measurements.

5.3 Results

5.3.1. hBM-MSCs did not reduce ROS generation from injured VCECs *in vitro*

When VCEC-MSC co-cultures were imaged using at 72 hrs, interestingly, as shown in **Figure 5.1A**, both 2D cultured hBM-MSCs Y201 and 2D cultured hBM-MSCs Y202 were frequently observed as elongated fibroblast-like cells growing on top of the VCECs with some stem cells appearing to have incorporated within the VCEC monolayer. Furthermore, VCECs co-cultured with 2D hBM-MSCs Y201 and 2D hBM-MSCs Y202 tended to arrange into clusters. However, this was not noticed as extensively with 3D cultured hBM-MSCs Y201 and 3D cultured hBM-MSCs Y202 which did not appear as elongated on the VCECs. The VCECs also appeared as continuous monolayers rather than in clusters. As shown in **Figure 5.1B**, the size of fibroblast-like cells in 2D cultured hBM-MSCs were significantly larger than those grown in 3D culture. As shown in **Figure 5.2A-C**, neither 2D nor 3D cultured hBM-MSCs were able to reduce the *in vitro* production of ROS from H_2O_2 injured VCECs, although a very marginal reduction with 3D cultured hBM-MSCs Y201 was noted.

5.3.2. Only 2D and 3D cultured hBM-MSCs Y201 reduced oxidative damage of H_2O_2 injured VCECs cells *in vitro*

Although MSCs did not reduce ROS presence in H_2O_2 injured VCECs at 72 hours, we still investigated whether endothelial oxidative injury could be prevented by co-culturing VCECs with hBM-MSCs. Oxidative stress was determined by immunostaining with an anti-8-OHdG

antibody (**Figure 5.3A**). 8-OHdG is a marker of oxidative DNA damage, used to confirm the extent of injury produced specifically by ROS.

Interestingly, 2D and 3D cultured hBM-MSCs Y201 were able to significantly decrease the fluorescence intensity of anti-8-OHdG staining when compared to control VCECs cultured in the absence of hBM-MSCs. As shown in **Figure 5.3A** and **B**, the degree to which 2D and 3D cultured hBM-MSCs Y201 reduced VCEC oxidative damage was similar with no significant differences between the two groups. Hence, culture technique did not influence the ability of hBM-MSCs Y201 to protect against oxidative stress induced by H_2O_2**.** The level of oxidative stress detected in VCECs co-cultured with 2D and 3D cultured hBM-MSCs Y202 was similar to the level detected in VCECs without MSCs control group **(Figure 5.3C)**.

5.3.3. Coronary endothelial cells are more susceptible to oxidative stress than cardiomyocytes following myocardial IR injury – All hBM-MSCs reduce endothelial oxidative damage

Flow cytometric analysis was performed on digested whole hearts undergoing sham, IR injury and IR injury + hBM-MSCs procedures. The selective gating strategy utilized to identify primary $CD31^+$ coronary ECs and $cTnT^+$ cardiomyocytes, and their corresponding oxidative damage levels as evidenced by being $8\text{-}OHdG^+$, is provided in **Figure 5.4A**. The percentage of ECs obtained was approximately 9% of the total viable cells analysed from the digested hearts regardless of the experimental group.

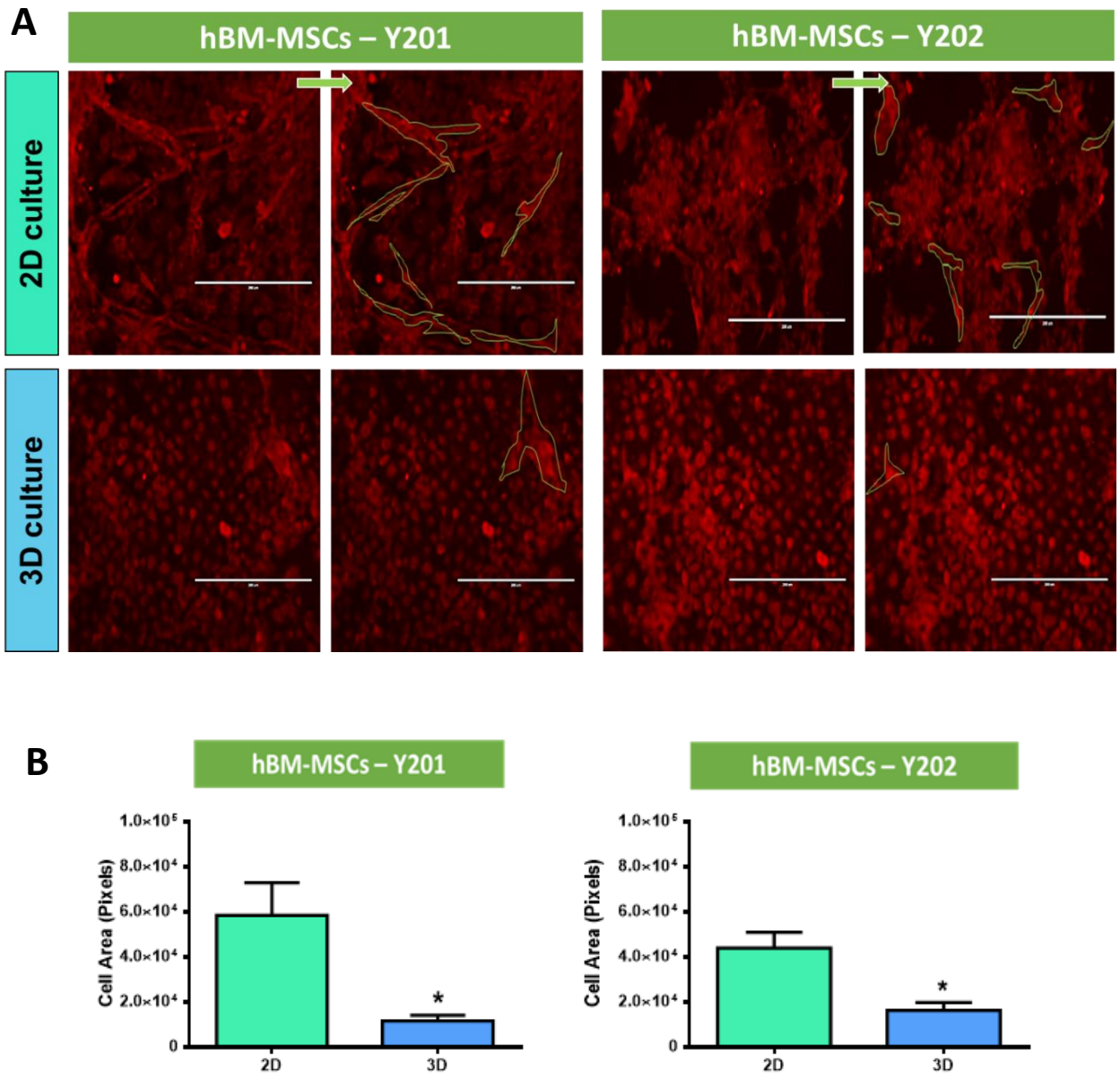


Figure 5.1. Representative images from co-culture assays of murine vena cava endothelial cells (VCECs) with 2D and 3D cultured hBM-MSCs Y201 and hBM-MSCs Y202 taken at 72 hours. (A) Both 2D cultured hBM-MSCs Y201 and 2D cultured hBM-MSCs Y202 were frequently observed as elongated fibroblast-like cells (outlined in green) growing on top of the VCECs (red), with some stem cells appearing to have incorporated within the VCEC monolayer. Furthermore, VCECs co-cultured with 2D hBM-MSCs Y201 and 2D hBM-MSCs Y202 tended to arrange into clusters – note the black areas lacking coverage with the VCEC monolayer. However, this was not noticed as extensively with 3D cultured hBM-MSCs Y201 and 3D cultured hBM-MSCs Y202, which did not appear to spread as extensively on the VCECs. The VCECs also appeared as continuous monolayers rather than in clusters. **(B)** The fibroblast-like cells in 2D cultured hBM-MSCs were significantly larger than those grown in 3D culture. Images were captured using EVOS microscope with a 20x objective. Statistical analysis was performed using Student t-tests. *$p<0.05$. $N\geq4$. Scale bar is 200μm.

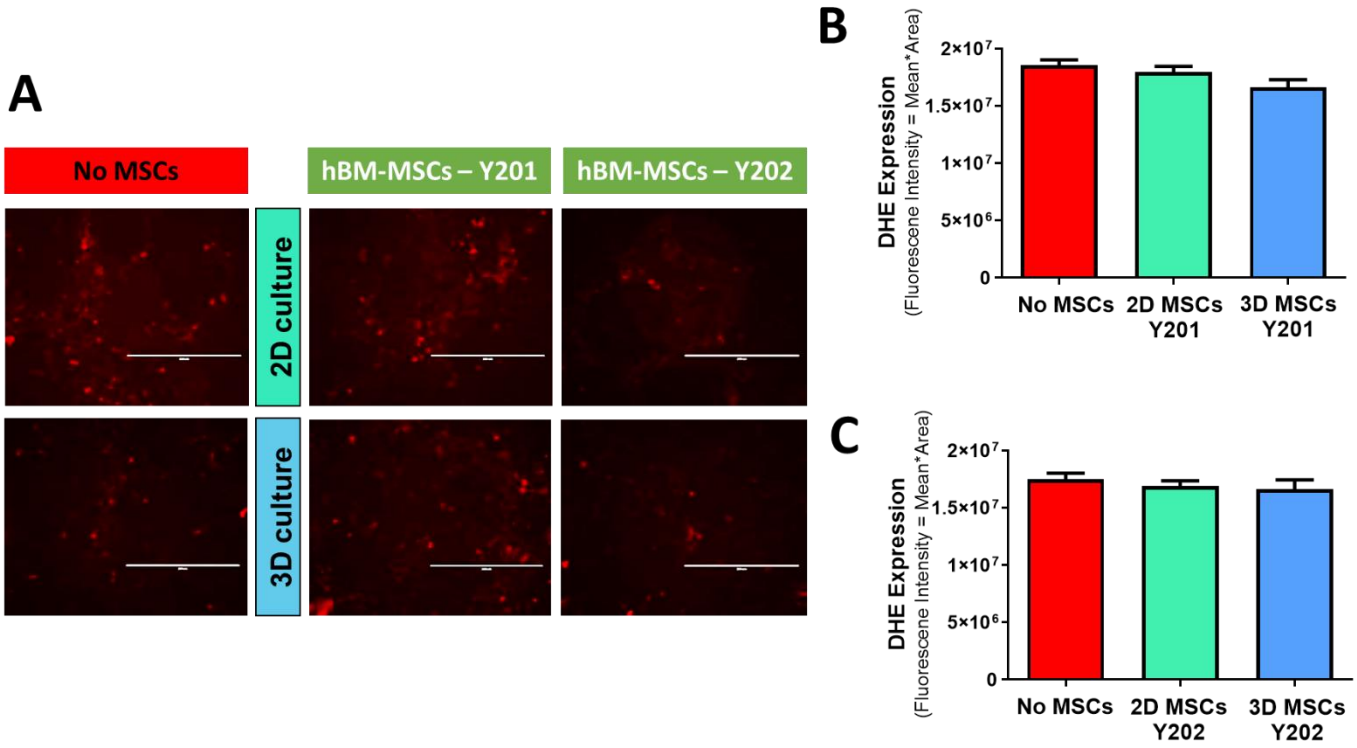


Figure 5.2. Neither 2D or 3D cultured hBM-MSCs Y201 nor did hBM-MSCs Y202 decreased the generation of ROS by H2O2 injure VCECs *in vitro* at 72 hours. (A) Representative images of DHE (red) fluorescence staining of H_2O_2 injured VCECs co-cultured with or without hBM-MSCs. Endothelial-stem cell co-culture assays were performed in 24 wells plates using mouse VCECs. The control group consisted of VCECs cultured in the absence of stem cells. VCECs were damaged using 10µl of H_2O_2 introduced concurrently with MSCs. After 72 hours, DHE staining was used to measure ROS generation. **(B-C)** Neither 2D nor 3D cultured hBM-MSCs Y201 neither (B) nor hBM-MSCs Y202 (C) reduced the level of ROS production although there was a marginal decrease with 3D cultured hBM-MSCs Y201. Statistical analysis was performed using a one-way ANOVA with Sidak's multiple comparison tests. ANOVA showed no effect of treatment on endothelial DHE expression; p=0.12. Data were presented as the mean ± SEM. N ≥4. Scale bar is = 200µm.

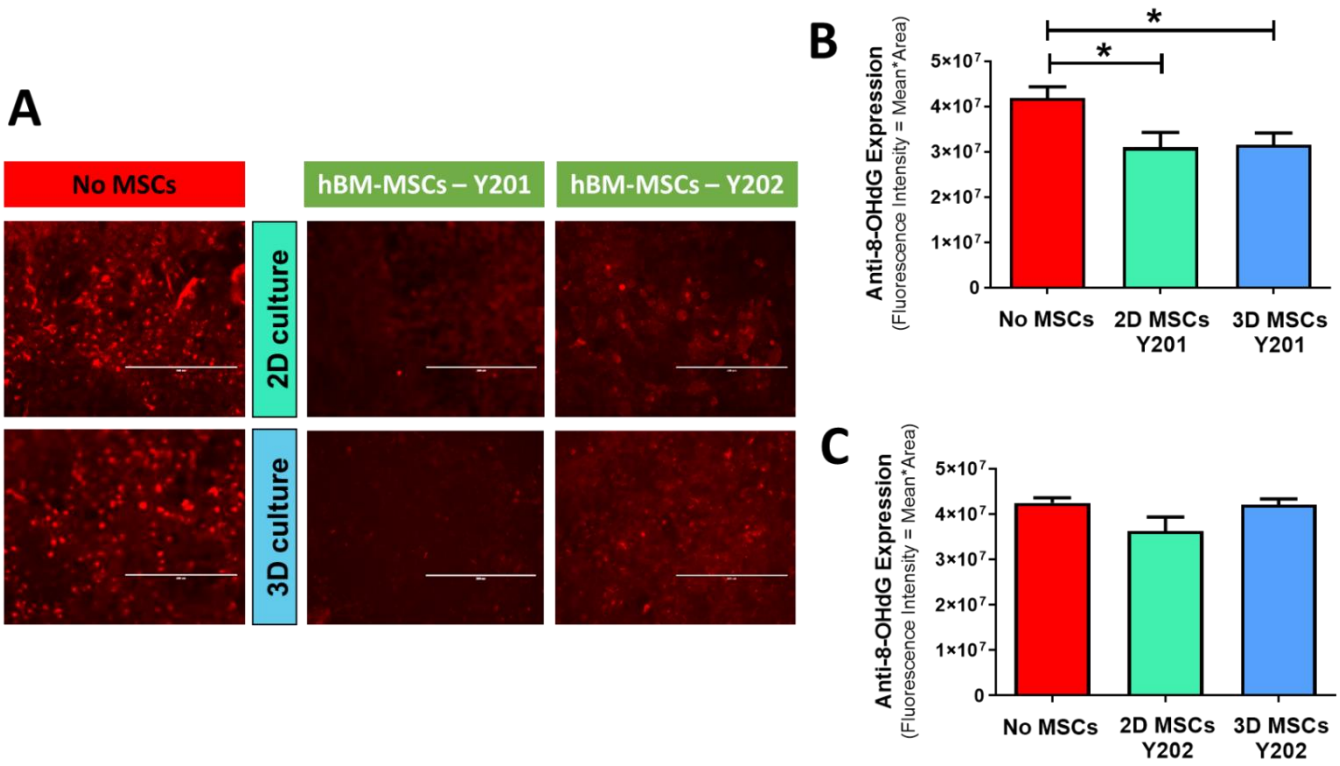


Figure 5.3. Both 2D and 3D cultured hBM-MSCs Y201 significantly decrease oxidative damage of H_2O_2 injured VCECs *in vitro* at 72 hours. (A) Representative images of the oxidative injury marker 8-OHdG (red) in H_2O_2 injured VCECs co-cultured with or without hBM-MSCs. Endothelial-stem cell co-culture assays were performed in 24 wells plates using mouse VCECs. The control group consisted of VCECs cultured in the absence of stem cells. VCECs were damaged using 10µm of H_2O_2 introduced concurrently with MSCs. After 72 hours, immunostaining using an anti-8-OHdG antibody was used to measure ROS specific damage of VCECS. **(B)** Both 2D and 3D cultured hBM-MSCs Y201 significantly reduced oxidative damage to a similar degree as noted by the decreased appearance of red stained cells. The degree to which 2D and 3D cultured hBM-MSCs Y201 reduced VCEC oxidative damage was similar with no significant differences between the two groups. **(C)** No statistically significant decrease was noted between with 2D or 3D cultured hBM-MSCs Y202. Statistical analysis was performed using a one-way ANOVA with Sidak's multiple comparison tests. ANOVA showed a significant effect of treatment on ECs 8-OHdG expression; $P<0.05$. Data were presented as the mean ± SEM. *$p<0.05$ by Sidak's multiple comparison test**.** N ≥4. Scale bar is = 200µm.

The percentage of cardiomyocytes obtained was much higher at around 66% of the total viable cells analysed from the digested hearts regardless of the experimental group (**Figure 5.4B**). These numbers are in agreement with our previously published work (Kavanagh et al., 2019).

As shown in **Figure 5.5.A**, the degree of oxidative injury in coronary ECs was significantly higher in IR injured hearts compared to sham hearts. Indeed, a quarter (25.07% ± 3.88) of the total ECs analysed underwent oxidative damage after IR injury compared to less than two percent (1.12% ± 0.48) in sham hearts. Interestingly, 2D cultured hBM-MSCs Y201 (15.54%± 9.02), 3D cultured hBM-MSCs Y201 (8.63 ± 1.25), 2D cultured hBM-MSCs Y202 (8.80% ± 1.40;) and 3D cultured hBM-MSCs Y202 (12.42% ± 2.08) reduced EC oxidative damage following IR injury. The greatest reduction was noted with 3D cultured hBM-MSCs Y201. However, these reductions were not significantly different when compared to IR injured hearts receiving no cellular therapy**.**

As shown in **Figure 5.5B**, cardiomyocytes also demonstrated a degree of oxidative damage after myocardial IR injury. Indeed, 11.10% ± 2.77 of the total cardiomyocytes analysed were susceptible to oxidative damage following IR injury when compared to cardiomyocytes in sham hearts (3.89% ± 2.63). However, this was not statistically significant. Furthermore, this level of damage was not as remarkable as that observed for ECs (11.10% vs 25.07%) indicating cardiomyocytes were not as susceptible as vascular structures to oxidative injury at 2hrs post-reperfusion. Nevertheless, 2D cultured hBM-MSCs Y201 (7.42% ± 1.64), 3D cultured hBM-MSCs Y201 (6.16% ± 1.65), 2D cultured hBM-MSCs Y202 (3.15%± 0.64) and 3D cultured hBM-MSCs Y202 (4.39% ± 1.46) were able to reduce the oxidative stress in cardiomyocytes. Again, the greatest reduction was noted

with 3D cultured hBM-MSCs Y201. However, these reductions did not attain statistical significance when compared to IR injured hearts receiving no cellular therapy.

5.3.4. ICAM-1 and VCAM-1 expression increases on coronary endothelial cells following myocardial IR injury – all hBM-MSCs reduce endothelial adhesion molecule expression

The degree of endothelial adhesion molecule expression was also determined using flow cytometric analysis on digested whole hearts undergoing sham, IR injury and IR injury + hBM-MSCs procedures. The selective gating strategy utilized to identify $CD31^+$ coronary ECs, and their corresponding ICAM-1 and VCAM-1 expression levels, is provided in **Figures 5.4A and 5.4C.** The level of ICAM-1 expression in coronary ECs significantly increased in IR injured hearts when compared to sham hearts. Indeed 40.91 ± 5.65% of analysed IR injured coronary ECs expressed ICAM-1 compared to only 18.26 ± 0.59% of sham ECs. Interestingly, 2D cultured hBM-MSCs Y201 (27.94 ± 4.23%), 3D cultured hBM-MSCs Y201 (26.74 ± 1.36%), 2D cultured hBM-MSCs Y202 (25.83± 1.95%) and 3D cultured hBM-MSCs Y202 (28.50 ± 3.55%) reduced ICAM-1 expression following IR injury. However, the reduction of ICAM-1 expression was not significant when compared to IR injured hearts receiving no therapy **(Figure 5.6B)**.

The degree of VCAM-1 expression on analysed coronary ECs cells also significantly increased in IR injured hearts when compared to sham hearts as shown in **Figure 5.6D**. Indeed 37.50 ± 6.11% of analysed IR injured coronary ECs expressed VCAM-1 compared to only 12.59 ± 1.89% of sham ECs. 2D cultured hBM-MSCs Y201 (17.70 ± 1.23%), 3D cultured

hBM-MSCs Y201 (15.21 ± 1.56%), 2D cultured hBM-MSCs Y202 (19.01 ± 3.80%) and 3D cultured hBM-MSCs Y202 (22.51 ± 1.70%) were able to significantly reduce VCAM-1 expression following IR injury when compared to IR injured hearts receiving no therapy**.**

Interestingly, as shown in **Figure 5.6E**, there was no significant difference in the basal expression of ICAM-1 and VCAM-1 on coronary ECs neither in sham hearts nor in their inducible expression following IR injury. This was somewhat surprising as inflammatory disorders have been shown to increase VCAM-1 expression more so than ICAM-1.

5.3.5. 3D cultured hBM-MSCs Y201 are most potent at reducing serum levels of multiple circulating pro-inflammatory factors *in vivo*

Furthermore, we evaluated 23 different circulating cytokines in the serum of sham, IR injured and IR injured + hBM-MSCs mice using a multiplex immunoassay. Circulating serum levels of 9 pro-inflammatory cytokines and 1 major anti-inflammatory cytokine, namely IL-10, were significantly elevated in the IR injured group compared to sham (**Table 5.1**). The highest pro-inflammatory cytokine increases, more than 6-fold, were seen for IL-6, IL-12(p40), G-CSF, KC, MCP-1 and MIP-1β cytokines. 2D hBM-MSCs Y201 did not significantly reduce any of the 23 cytokines analysed in the serum when compared to IR injured mice. Interestingly, circulating levels of IL-17 ($p<0.05$) and Eotaxin (CCL11; $p<0.01$) were both significantly increased. However, in mice receiving 3D cultured hBM-MSCs Y201, serum levels were significantly ($p<0.05$) decreased for 9 pro-inflammatory cytokines when compared to IR mice.

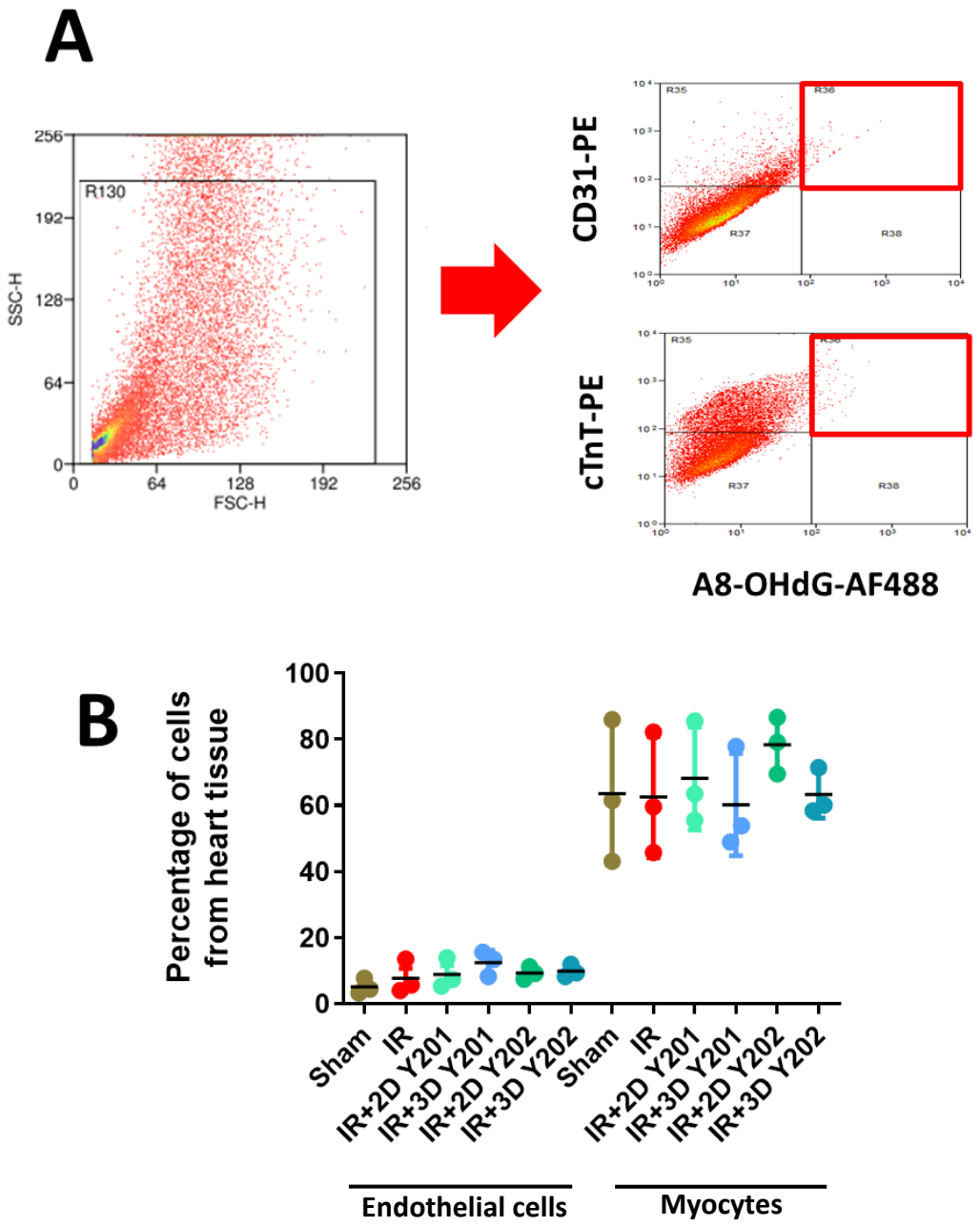


Figure 5.4. Flow cytometric analysis of whole digested hearts in sham, IR injured and IR + hBM-MSCs mice. (A) Representative scatter plot demonstrating the selective gating strategy utilized to identify $CD31^{+}$ coronary ECs and $cTnT^{+}$ cardiomyocytes from digested heart samples. Cells were gated by side scatter vs front scatter. The oxidative damage level was detected by using an anti-8-OHdG antibody (red squares). **(B)** The percentage of ECs and cardiomyocytes obtained from digested whole heart. The analysis was conducted on 20,000 events with samples analyzed using a FACSCalibur flow cytometer. Flow software was used to visualize the data. Data were presented as the mean ± SEM. N = 3 per group.

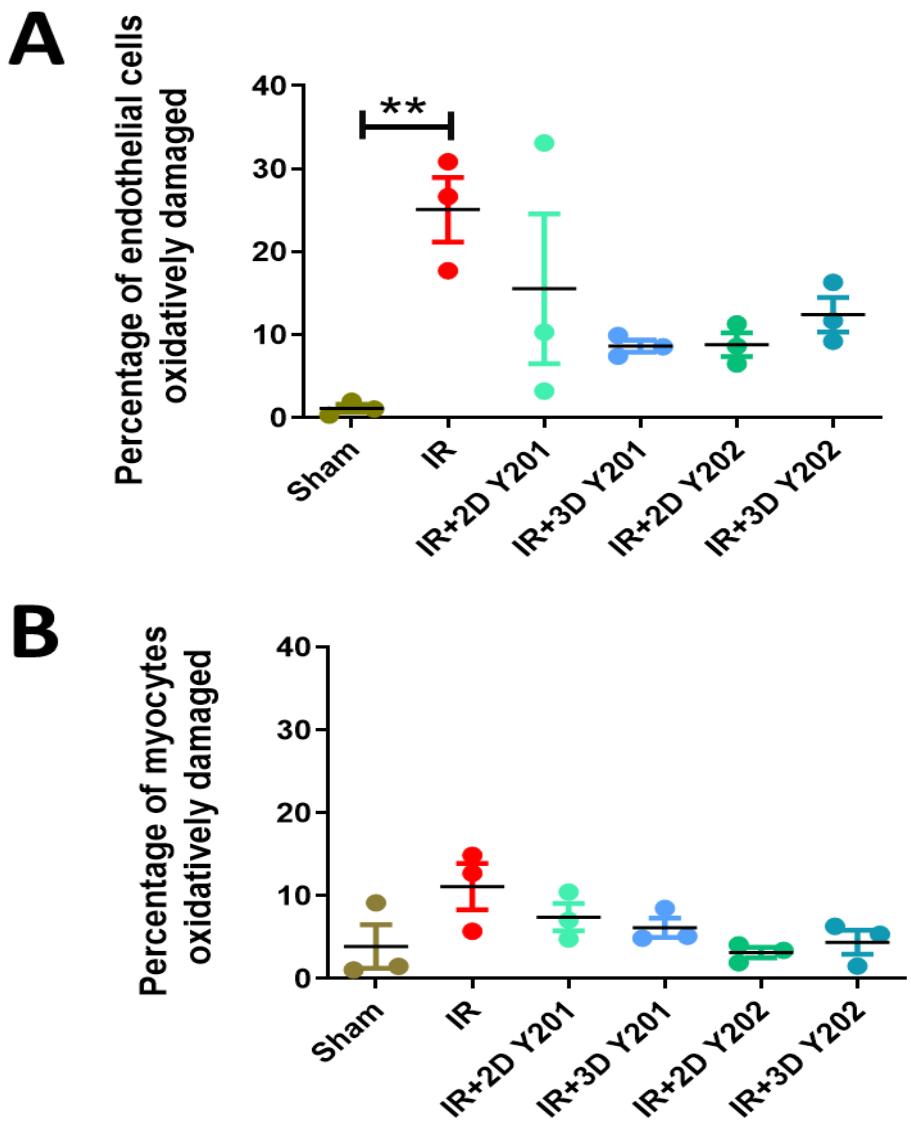


Figure 5.5. Coronary endothelial cells (ECs) are more susceptible to oxidative stress than cardiomyocytes following IR injury, but all populations of 2D and 3D cultured hBM-MSCs are able to protect the ECs (and cardiomyocytes) from oxidative damage. (A) Myocardial IR injury significantly ($p<0.01$) increased oxidative damage in ECs when compared to sham at 2 hrs reperfusion. This increase was reduced by both 2D and 3D cultured hBM-MSC sub-populations. **(B)** Cardiomyocytes also showed a degree of oxidative damage following IR injury but this was not significant nor as extensive as that seen in ECs. Nevertheless, both 2D and 3D cultured hBM-MSC sub-populations were able to decrease this oxidative damage. The analysis was conducted on 20,000 events with samples analyzed using a FACSCalibur flow cytometer. Flow software was used to visualize the data. ANOVA showed a significant effect of treatment on oxidative damaged of ECs; $p<0.01$. Data were presented as the mean ± SEM. N = 3 per group. **$p<0.01$ when compared to sham using one-way ANOVA with Sidak's multiple comparison tests.

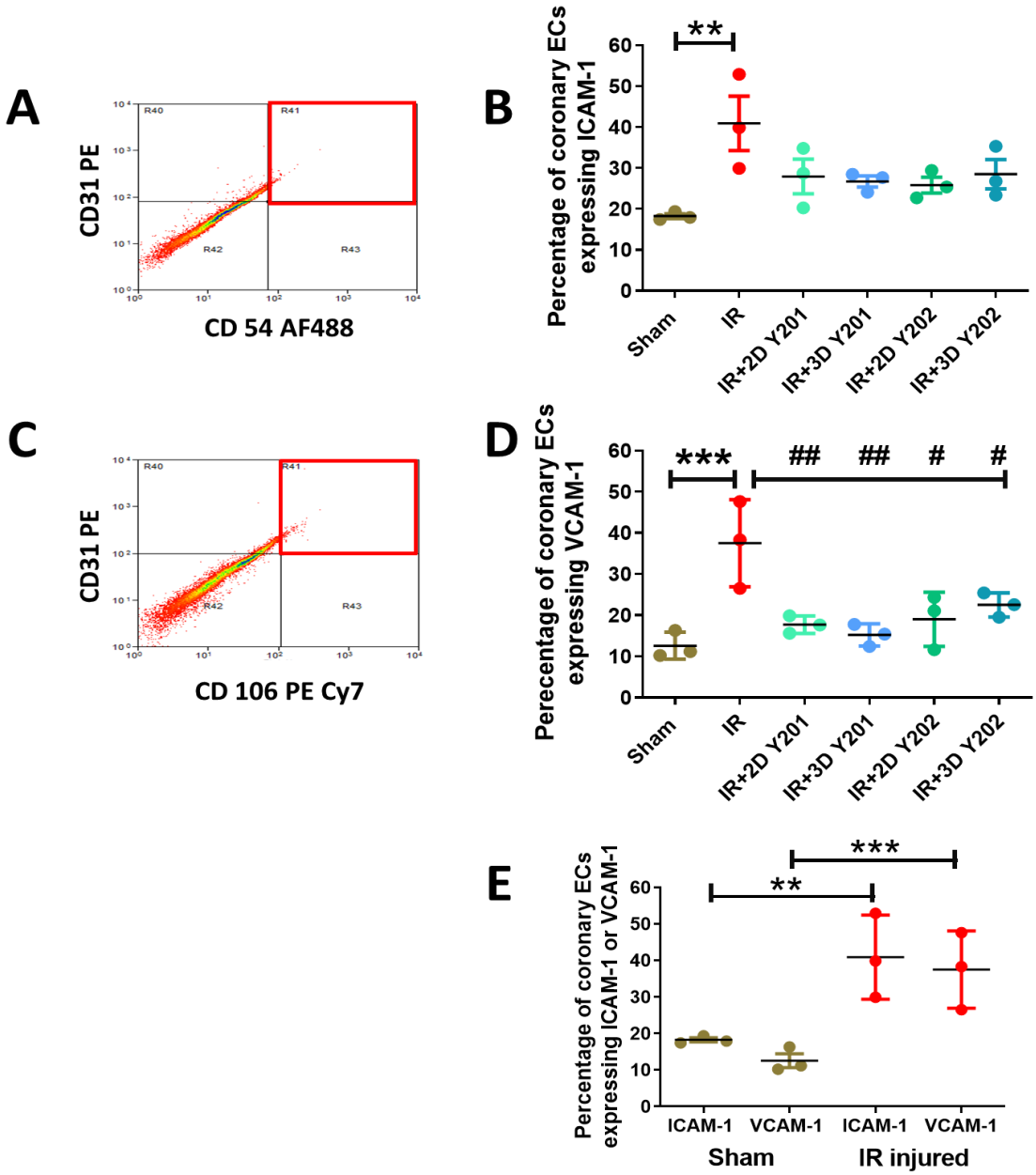


Figure 5.6. ICAM-1 and VCAM-1 expression increases on coronary endothelial cells (ECs) following myocardial IR injury, but all populations of 2D and 3D cultured hBM-MSCs are able to reduce their expression. **(A & C)** Representative scatter plots demonstrating the selective gating strategy utilized to identify $CD31^{+}$ coronary ECs on digested heart cells. Cells were gated by side scatter vs front scatter. The two adhesion molecules were detected by using an anti-CD54/ICAM-1 and an anti-CD106/VCAM-1 antibody (red squares). **(B)** Myocardial IR injury increased endothelial ICAM-1 expression at 2 hrs reperfusion, but all types of hBM-MSCs were able to reduce this to levels similar to that found in sham hearts. However, the reduction of ICAM-1 level was not significantly different when compared to IR injury hearts. **(D)** Myocardial IR injury also increased endothelial VCAM-1 expression which was also reduced with all types of hBM-MSCs. However, this decrease was significant when compared to endothelial VCAM-1 expression on IR injured endothelium. **(E)** There was no difference in the basal ICAM-1 and VCAM-1 expression on coronary ECs neither in sham nor in IR injured heart. The analysis was conducted on 20,000 events with samples analyzed using a FACSCalibur flow cytometer. Flow software was used to visualize the data. Statistical analysis was performed using a one-way ANOVA with Sidak's multiple comparison tests. ANOVA showed a significant effect of treatment on ICAM-1 and VCAM-1 expression of ECs; $p<0.01$. Data were presented as the mean ± SEM. N = 3 per group. **$p<0.01$ and ***$p<0.001$ when compared to sham; #$p<0.05$ and ##$p<0.01$ when compared to IR injured hearts.

These included IL-1α, IL-5, IL-6, IL-12 (p40), G-CSF, CXCL1/KC, CCL2/MCP-1, CCL3/MIP-1α and CCL4/MIP-1β. Furthermore, 2 major anti-inflammatory cytokines, IL-10 and IL-13, were also significantly ($p<0.05$) decreased. Significantly increased levels were also observed for 4 pro-inflammatory cytokines namely IL-2 ($p<0.05$), IL-12(p70; $p<0.01$), IL-17 ($p<0.01$) and IFNγ ($p<0.01$). Interestingly, treatment with 2D cultured hBM-MSCs Y202 also reduced 7 pro-inflammatory cytokine levels in mice serum including IL-1α ($p<0.01$), IL-3 ($p<0.01$), IL-9 ($p<0.05$), IL-12(p40; $p<0.05$), G-CSF ($p<0.05$), CCL4/MIP-1β ($p<0.05$) and TNFα ($p<0.05$). Furthermore, 1 anti-inflammatory cytokine, IL-10, was also significantly ($p<0.05$) decreased. Again, significant increases were observed for IL-2 ($p<0.01$), IL-5 ($p<0.05$), IL-17 ($p<0.05$) and Eotoxin (CCL11; $p<0.01$). Only three pro-inflammatory cytokine levels were significantly ($p<0.05$) reduced in IR injured mice receiving 3D hBM-MSCs Y202 which included IL-1α, IL-12 (p40) and CCL4/MIP-1β with significant increases in 3 pro-inflammatory cytokines including IL-5 ($P<0.01$), IL-17 ($p<0.05$) and Eotaxin ($p<0.01$).

5.3.6. Circulating peripheral blood cell panel following myocardial IR injury

To assess the thromboinflammatory circulating cell profile of peripheral blood, 500µl of anti-coagulated blood was collected from the vena cava of sham, IR injured and IR injured + hBM-MSCs mice and run through a Horiba blood counter machine. Results were obtained immediately. As shown in **Table 5.2**, following myocardial IR injury, there was a tendency for the total number of circulating white blood cells and platelets to decrease when compared to sham numbers. This decrease was most marked for neutrophils. Indeed the concentration of circulating neutrophils in IR injured mice was approximately 10-fold lower

than that observed in sham peripheral blood. Interestingly, all hBM-MSC cellular therapies were able to attenuate this decrease in circulating neutrophil numbers with the most effective response observed for 2D and 3D cultured hBM-MSCs Y202. With regards to circulating platelets, myocardial IR injury also decreased their circulating numbers. This was also reversed by all types of MSC therapies to some extent. Interestingly, an increase in monocyte numbers was noted with cellular therapy, particularly with 3D cultured hBM-MSCs Y201. However, statistical analysis of all the data obtained indicated that these trends were not statistically significant.

5.4 Discussion

Previous chapters have demonstrated that the hBM-MSCs Y201 sub-population, when cultured using a 3D hanging drop method, was the most effective at inhibiting thromboinflammatory events, and increasing the density of perfused capillaries, within the IR injured beating heart microcirculation *in vivo*. Although these results were novel and exciting, to maximise the potential of using these cells in a clinical setting, it was important to understand the mechanisms governing their ability to confer this coronary vasculoprotection. The novel data presented in this chapter indicated that the therapeutic effectiveness of 3D cultured hBM-MSCs Y201 may rise from their ability to reduce oxidative damage in ECs which was demonstrated both in co-culture experiments and also using flow cytometry analysis of IR injured digested hearts.

Cytokines	Sham	IR injury	IR + 2D Y201	IR + 3D Y201	IR + 2D Y202	IR + 3D Y202
Interleukin-1α	14.07 ± 2.90	18.62 ± 3.95	13.22 ± 1.99	7.13 ± 1.87#	8.33 ± 0.79##	10.63 ± 2.04#
Interleukin-1β	37.18 ± 5.06	42.84 ± 4.37	49.79 ± 10.80	33.92 ± 3.40	40.70 ± 2.67	45.73 ± 7.10
Interleukin-2	14.92 ± 3.00	11.65 ± 0.86	17.10 ± 2.76	14.07 ± 1.04#	15.69 ± 0.88##	13.88 ± 1.96
Interleukin-3	17.13 ± 2.45	16.46 ± 1.67	13.68 ± 2.67	20.23 ± 1.91	10.72 ± 1.14##	14.84 ± 2.81
Interleukin-4	15.71 ± 3.34	13.46 ± 2.69	12.02 ± 3.02	17.43 ± 3.38	9.37 ± 2.59	19.54 ± 3.55
Interleukin-5	32.63 ± 11.95	31.56 ± 5.69	58.28 ± 19.28	19.42 ± 1.48#	62.24 ± 12.95#	78.14 ± 14.77##
Interleukin-6	351.11 ± 126.42	1993.53 ± 841.45*	8258.03 ± 3053.95	495.75 ± 95.47#	2169.67 ± 356.71	5555.47 ± 2012.10
Interleukin-9	51.29 ± 7.54	45.76 ± 4.83	39.92 ± 5.87	52.82 ± 4.97	33.22 ± 3.52#	28.76 ± 6.26
Interleukin-10	143.57 ± 9.06	222.70 ± 45.84*	202.09 ± 16.63	132.55 ± 11.73#	126.73 ± 5.33#	154.59 ± 10.41
Interleukin-12(p40)	2253.75 ± 350.50	14588.86 ± 5889.30*	2943.45 ± 246.52	1040.67 ± 54.70#	1930.09 ± 203.49#	2042.37 ± 222.78#
Interleukin-12(p70)	501.84 ± 85.43	555.36 ± 57.31	665.98 ± 90.92	845.47 ± 88.45##	487.45 ± 36.06	735.89 ± 122.67
Interleukin-13	278.182 ± 51.10	337.87 ± 38.67	338.73 ± 76.32	250.53 ± 25.51#	279.56 ± 28.81	326.23 ± 49.17
Interleukin-17	18.70 ± 2.68	14.50 ± 1.22	71.15 ± 21.59*	223.36 ± 24.34##	43.72 ± 11.59#	117.62 ± 45.04#
CCL11 (Eotaxin)	992.67 ± 113.83	1607.58 ± 50.43*	3690.49 ± 345.05**	1811.43 ± 125.62	2354.80 ± 94.37##	2944.77 ± 196.19##
G-CSF	395.23 ± 97.79	2720.72 ± 1272.80*	1345.84 ± 287.82	259.23 ± 42.33#	544.76 ± 79.95#	577.34 ± 57.34
GM-CSF	54.52 ± 7.25	61.95 ± 6.50	65.34 ± 11.55	55.94 ± 5.24	49.87 ± 3.42	61.36 ± 8.84
IFNγ	46.44 ± 7.28	42.25 ± 4.50	44.16 ± 5.34	67.00 ± 6.33##	33.50 ± 3.63	46.14 ± 9.68
CXCL1 / KC	326.15 ± 93.22	1769.48 ± 783.47*	1307.16 ± 285.36	289.87 ± 51.56#	901.31 ± 147.50	1180.94 ± 163.29
CCL2 / MCP-1	638.92 ± 121.67	5016.62 ± 2117.35*	3795.82 ± 1505.67	514.98 ± 63.93#	1481.29 ± 62.80	2191.60 ± 513.48
CCL3 / MIP-1α	21.84 ± 8.95	48.51 ± 21.69	25.12 ± 9.19	7.04 ± 1.09#	35.12 ± 11.01	21.80 ± 5.28
CCL4 / MIP-1β	169.46 ± 56.60	1545.83 ± 736.81*	321.19 ± 132.70	72.36 ± 9.10#	138.52 ± 20.65#	178.29 ± 47.41#
CCL5 / RANTES	108.06 ± 15.03	248.96 ± 79.09*	274.16 ± 16.38	200.72 ± 9.37	233.20 ± 25.34	257.36 ± 9.64
TNFα	191.95 ± 29.16	369.49 ± 95.21*	219.90 ± 32.44	349.34 ± 34.21	168.99 ± 16.04#	245.22 ± 46.77
Total Decreased		0	0	9 pro-inflammatory 2 anti-inflammatory	7 pro-inflammatory 1 anti-inflammatory	3 pro-inflammatory
Total Increased		9 pro-inflammatory 1 anti-inflammatory	2 pro-inflammatory	4 pro-inflammatory	4 pro-inflammatory	3 pro-inflammatory

Table 5.1. 3D cultured hBM-MSCs Y201 is the most effective at reducing serum levels of multiple pro-inflammatory cytokines. Using a Luminex cytokine array kit, 16 of the tested 23 cytokines were increased in the serum following myocardial IR injury – **major anti-inflammatory cytokines boxed in red**. Indeed, 10 out of 23 cytokines were significantly higher in the IR injury group when compared to sham serum (**blue**). Of these, IL-6, IL-12, G-CSF, CCL1/KC, CCL2/MCP-1, and CCL3/MIP-1β showed greater than 6-fold increases. All MSC sub-populations, apart from 2D cultured hBM-MSCs Y201, were able to significantly reduce some cytokines when compared to the IR injured group including, those that were increased as a result of injury and even those that were not significantly increased by IR injury (**green**). However, 3D cultured hBM-MSCs Y201 were the most effective cells as they reduced 11 of the 23 cytokines tested, including 7 of the 10 cytokines significantly increased by IR injury. Interestingly, some cytokines level increased when compared to IR injured levels (**yellow**). ANOVA showed a significant effect of treatment on level of serum cytokines; $p<0.05$. Data presented as the mean ± SEM pg/ml. *$p<0.05$ when compared to sham hearts; #<0.05; #$p<0.01$ when compared to IR injured heart values using Sidak's multiple comparison test. n=3 independent experiments using three different serum donors.

Cell type ($10^3/mm^3$)	Sham	IR injury	IR + 2D Y201	IR + 3D Y201	IR + 2D Y202	IR + 3D Y202
Total WBCs	6.23 ± 1.00	1.30 ± 0.44	5.1 ± 0.57	4.3 ± 0.51	4.93 ± 1.08	2.26 ± 2.27
Neutrophils	2.59 ± 1.06	0.24 ± 0.17	2.40 ± 0.05	2.71 ± 1.06	2.07 ± 0.82	1.02 ± 1.44
Monocytes	0.20 ± 0.12	0.33 ± 0.05	1.13 ± 0.37	1.16 ± 0.79	0.77 ± 0.26	0.39 ± 0.39
Eosinophils	0.02 ± 0.02	0.02 ± 0.02	0.03 ± 0.01	0.04 ± 0.02	0.02 ± 0.01	0.01 ± 0.02
Lymphocytes	1.47 ± 0.62	1.01 ± 0.21	1.54 ± 0.08	2.22 ± 1.36	2.07 ± 0.09	0.80 ± 0.70
Atypical Lymphocytes	0.023 ±0.01	0.02 ± 0.00	0.11 ± 0.02	0.14 ± 0.10	0.11 ± 0.05	0.10 ± 0.14
Basophils	0.02 ± 0.03	0.01 ± 0.01	0.04 ± 0.01	0.05 ± 0.03	0.04 ± 0.04	0.01 ± 0.02
Large Immature Cells	0.04 ± 0.02	0.03 ± 0.02	0.13 ± 0.04	0.23 ± 0.17	0.09 ± 0.07	0.07 ± 0.08
Platelets	593.33 ± 46.40	359.33 ± 87.60	453.50 ± 58.99	492.70 ± 138.42	600.33 ± 24.54	405.66 ± 270.7

Table 5.2. Circulating cell profile in murine blood following myocardial IR injury. Using a Horiba haematology analyser machine, the concentration of different types of white blood cells were quantified in the peripheral blood of sham, IR injured and IR injured + hBM-MSCs mice. Overall, a general decrease in platelets and WBCs, most notably in neutrophils, was observed following myocardial IR injury. This trend was reversed following therapy with all types of hBM-MSCs. A similar decrease for circulating platelet numbers was also noted in IR injury which was again reversed with all types of hBM-MSC therapy. Interestingly, an increase in monocyte numbers was noted with cellular therapy, particularly with 3D cultured hBM-MSCs Y201. However, statistical analysis of the data obtained indicated that these trends were not statistically significant. Statistical analysis was performed using a one-way ANOVA with Sidak's multiple comparison tests. N=3 per group.

Moreover, 3D cultured hBM-MSCs Y201 were able to decrease the expression of endothelial ICAM-1 and VCAM-1 adhesion molecules in IR injured digested hearts. We also demonstrate that additional mechanisms of vasculoprotection may include their ability to most effectively reduce the levels of circulating pro-inflammatory cytokines. Indeed, 3D cultured hBM-MSCs Y201 were the most potent of the tested stem cells to reduce pro-inflammatory cytokines. Collectively, this data highlights the multiple mechanisms utilised by an MSC sub-population obtained from a BM perivascular niche to protect the coronary microcirculation from myocardial IR injury. These novel results may help fill the existing knowledge gap in this area and provide new approaches to enhance the effectiveness of MSC cytotherapy.

5.4.1. hBM-MSCs do not reduce endothelial ROS generation

Oxidative stress, a situation where there is a change from the physiological redox state to one with an increase in ROS, is closely linked to several inflammatory pathologies, including myocardial IR injury (Zhang et al., 2014). Excessive ROS can mediate a number of deleterious effects including inducing cellular lipid peroxidation leading to increased in cell membrane permeability, structurally damage proteins by proteolysis, deactivated enzymes and cause DNA strand breakage (Granger and Kvietys, 2015). Growing recent evidence suggests MSCs may exert antioxidant properties in various experimental models of disease, which may provide an explanation for their cytoprotective and anti-thromboinflammatory benefits (Stavely and Nurgali, 2020). This has been shown to happen indirectly by releasing antioxidants (superoxide dismutase (SOD), catalase, glutathione peroxidase) as

demonstrated by the fact that MSC conditioned media was effective at reducing ROS accumulation and cell death in fibroblast *in vitro* (Motegi et al., 2017, Stavely and Nurgali, 2020). The molecular mechanisms involved include scavenging ROS, enhancing host anti-oxidant defenses and modulating inflammatory responses (Motegi et al., 2017). For example, MSCs have been recently shown to enhance (rather than release themselves) SOD activity, an endogenous antioxidant, from cells exposed to oxidative stimuli *in vitro* and also in murine models of inflamed gut (Jung et al., 2020) and ageing (Calio et al., 2014).

However, in our co-culture studies, we found that none of the tested hBM-MSCs were able to decrease the amount of ROS generated by H_2O_2 damaged VCECs. These finding confirmed our previous data which showed that primary MSCs, isolated from the tibias and femurs of mice, were also unable to modify ROS generation in similarly H_2O_2 damaged VCECs either at 24 or 72 hrs of co-culture (A. Lokman PhD thesis, University of Birmingham; unpublished data). It is possible that the MSCs were themselves damaged after exposure to the H_2O_2 in the culture media. However, they are well known to be able to resist oxidative stress which may explain why despite being exposed to H_2O_2 in the co-culture environment and not modifying ROS generation, they were still able to protect the ECs from damage (discussed later) (Stavely and Nurgali, 2020). It is also possible that the limitations of DHE staining technique could explain the inability to detect any changes in ROS (Griendling et al., 2016). Dihydroethidium/DHE is widely used to detect $O_2\bullet^-$ due to its high sensitivity and ease of use (Griendling et al., 2016). Oxidation of DHE by $O_2\bullet^-$ yields the fluorescent product 2-hydroxyethidium (2OH-E^+). However, other oxidants for example H_2O_2 and •OH can also produce the electron oxidation product ethidium (E^+) with similar fluorescence characteristics to 2OH-E^+. Therefore, superoxide detection by DHE is not specific due to the

overlapping fluorescence of superoxide-specific 2OH-E+ and nonspecific E+. Moreover, DHE can also be oxidized spontaneously by light-induced oxidation and atmospheric oxidation which also produce E+ (Griendling et al., 2016). If this occurred in our experiments, then this could have masked any genuine ability of MSCs to reduce ROS production.

5.4.2. hBM-MSCs Y201 co-culture protects endothelial cells from oxidative damage

Despite not modifying ROS generation, we still investigated whether 3D cultured hBM-MSCs Y201 could prevent ROS mediated oxidative damage of sensitive ECs. Two different approaches were used to experimentally assess this in ECs – firstly using an anti-8-OHDG antibody to measure oxidative damage in ECs in co-culture with MSCs and secondly using the same antibody to measure oxidative stress in IR injured ECs in digested hearts. In co-culture experiments, we showed that both 2D and 3D cultured hBM-MSCs Y201 could lower the oxidative damage of VCECs induced by H_2O_2 at 72 hrs. The mechanism behind this reduction was unlikely to be specifically due to the $O_2\bullet^-$ radical attenuation as no significant reduction was seen in DHE staining. This result is in line with other reports in which MSC anti-oxidant potential was described during inflammation in various models (Sun et al., 2015). In a mouse model of colitis, transplantation of adipose derived MSCs prevented injury mediated decreased in glutathione, an important non-enzymatic antioxidant, and increased the activity of SOD (da Costa Goncalves et al., 2017). Overall, by preventing the impairment of antioxidants in the inflamed colon, MSCs significantly reduced colon damage. Recently, it has been shown that MSCs can also release extracellular vesicles containing active catalase which can break down harmful H_2O_2 into

oxygen and water (de Godoy et al., 2018). Indeed, de Godoy and colleagues used electron microscopy to show extracellular exosomes and microvesicles with diameters ranging from 30-200nm and 400-600nm respectively.

Moreover, several studies report that MSCs can also fight against oxidative stress injury using a novel mechanism involving delivering their own mitochondria through thin membrane channels called "tunneling nanotubes" (TNTs) to the injured cells (Han et al., 2016). This was elegantly demonstrated using confocal imaging of IR injured rat heart ventricular cells (H9c2 line) co-cultured with BM-MSCs in which mitochondria trafficking could be imaged after staining with Mito-Tracker Deep Red (Han et al., 2016). TNTs are long F-actin based plasma membrane protrusions or tubules which connect cells together in order for cell-to-cell communications to take place, but can also be used to transfer mitochondria from donor cells to recipient cells (Vignais et al., 2017). This novel mechanism of 'stem cell-derived mitochondrial transplantation' can maintain ATP production and aerobic respiration within receiver cells, which protects against mitochondrial dysfunction in IR injured or inflamed tissues (Mahrouf-Yorgov et al., 2017).

Importantly, in the current chapter we found that only hBM-MSCs Y201 but not hBM-MSCs Y202 were able to reduce injured VCEC oxidative stress. Heterogeneous populations of MSCs hold disparate functional characteristics (James et al., 2015). Indeed, in Chapter 3 we demonstrated that 3D cultured hBM-MSCs Y201 were more adhesive to unstimulated and stimulated ECs than 2D or 3D cultured hBM-MSCs Y202. It is therefore possible that the beneficial antioxidative effects of hBM-MSCs Y201 were improved by their close cell-to-cell contact with VCECs in co-culture over 72 hrs. This raises the possibility that improving MSC retention within the coronary microvessels of the IR injured heart may subsequently

enhance their therapeutic effect. However, in the co-culture experiments, 2D cultured hBM-MSCs Y201 demonstrated an equally therapeutic benefit against oxidative damage as 3D cultured hBM-MSCs Y201. This may be explained by the fact that in these studies, an equal number of 2D and 3D cultured MSCs were placed directly on the endothelial monolayers and left there for 72 hrs allowing firm interactions with VCECs to take place. Therefore, since there would have been no difference in the quantity of 2D and 3D cultured MSCs interacted with ECs in these co-culture wells, it may explain the lack of antioxidant differences between cells derived from 2 different culture methods.

5.4.3. Coronary endothelium is an early target for oxidative damage but protected by hBM-MSC

The above scenario would differ from that *in vivo* in which we demonstrated a significantly greater presence of adherent 3D cultured hBM-MSCs in the IR injured beating heart *in vivo* compared to 2D cultured hBM-MSCs. Therefore, subsequent experiments were conducted in which IR injured hearts were removed from mice receiving MSC or no cellular therapy and assessed for endothelial oxidative stress using flow cytometry.

We firstly showed that following myocardial IR injury, there was indeed a remarkable increase in oxidative stress demonstrated in approximately 25% of $CD31^+$ coronary ECs. Interestingly, cardiomyocytes also demonstrated a degree of oxidative damage, but were not as susceptible to this as the ECs. Oxidative damage of cardiomyocytes was not in itself surprising as the role of oxidative stress in mediating muscle damage following myocardial IR injury is well reported (Hausenloy and Yellon, 2013). However, the fact that flow

cytometry demonstrated coronary endothelium, rather than cardiomyocytes, as the primary and initial target of oxidative injury was interesting and has been reported by us previously (Kavanagh et al., 2019). Others have also shown this differential susceptibility to injury with endothelial and cardiomyocyte apoptotic death occurring at 5 and 60 minutes respectively in isolated perfused hearts (Scarabelli et al., 2001, Singhal et al., 2010). Collectively these studies highlight the coronary microcirculation as an early and principal therapeutic target to prevent ensuing muscle damage (Leucker et al., 2013). It was therefore exciting to see that all types of hBM-MSCs could reduce the burden and impact of oxidative stress on coronary ECs and reduce the level of oxidative damage by 1/3rd from ~25% to ~9% in the case of 3D cultured hBM-MSCs Y201. Although not statistically significant, this may just be due to the fact these experiments were conducted on hearts derived from 3 mice (note that for 3D cultured hBM-MSCs Y201 the p value was 0.08). The fact that all MSCs could do this in IR injured hearts *in vivo*, but only hBM-MSCs Y201 could in H_2O_2 injured VCECs *in vitro*, was interesting. It is possible that the hBM-MSCs Y202 sub-population were less able to resist chronic exposure to the free radical H_2O_2 *in vitro.* We are not aware of any comparative studies that have examined the anti-oxidant capacity of MSCs from different sources or indeed sub-populations from the same source and so this is worthy of future consideration. Nevertheless, in our hands, an ability to rapidly modify oxidative stress *in vivo* appears to be an innate capability of BM-derived MSCs.

Increasing the local presence of MSCs within injured coronary microvessels may be necessary to realise the maximal anti-oxidant potential of MSCs. Interestingly, the ability of 2D and 3D cultured hBM-MSCs to confer anti-oxidative effects in co-culture experiments even at 72 hrs suggest they can continue to be beneficial long after they are introduced to

a damaged environment in culture. This has important *in vivo* implications as it suggests that if their myocardial presence can be maintained, either through survival or delivery of more MSCs at later time points, they can continue conferring vasculoprotective benefits.

5.4.4. Reducing endothelial ICAM-1 / VCAM-1 – another therapeutic mechanism

In Chapter 4, an increased neutrophil recruitment was observed within coronary capillaries after myocardial IR injury intravitally. It is well established that neutrophil adhesion to activated ECs is facilitated by endothelial expression of ICAM-1 adhesion molecules. An anti-inflammatory capability is an increasingly recognised mechanism underpinning the therapeutic effectiveness of MSCs (Weiss et al., 2019). Indeed, in Chapter 4 we too found that 3D cultured hBM-MSCs Y201 were able to significantly reduce neutrophil recruitment within injured coronary capillaries, with heparin dual therapy leading to a faster onset of therapeutic action. Therefore, we investigated whether hBM-MSCs could also mediate vasculoprotection through an ability to reduce the expression of ICAM-1 and VCAM using flow cytometric analysis of ECs within digested heart samples.

As expected, we firstly demonstrated a significant increase in both ICAM-1 and VCAM-1 expression on $CD31^+$ ECs from IR injured hearts. This result is in line with previously published studies (Burne et al., 2001, Wilhelmi et al., 2005). Increased endothelial ICAM-1 / VCAM-1 expression, as well as E-selectin, has been noted in response to oxidative damage (Boyle et al., 1999). Hence it is likely that our observed increased oxidative damage of coronary ECs may have contributed, in part, to this raised adhesion molecule expression. Interestingly, all MSC groups tested were able to reduce the overexpression of both ICAM-

1 and VCAM-1, with greater and significant responses observed for the latter. Again it seems that an ability to rapidly modify inflammatory markers *in vivo* appears to be an innate capability of BM-derived MSC sub-populations and is supported by other studies. Although there was no significant difference in the *in vivo* antioxidant and anti-ICAM-1 and VCAM-1 adhesion molecules ability of all 4 MSC groups, 3D cultured hBM-MSCs Y201 consistently demonstrated itself to be the most effective. These multiple beneficial effects at a molecular level may explain why this particular MSC group was able to significantly tame neutrophil recruitment within the injured beating heart as shown in Chapter 4.

Similar reductions in endothelial ICAM-1/VCAM-1 have been observed by different groups, albeit using immunostaining and RT-PCR methods. Qui and colleagues showed a reduction of endothelial ICAM-1 expression after human umbilical cord MSC treatment in a renal model of IR injury (Qiu et al., 2014). Rahbarghazi and colleagues more recently stated that there was limited data on the modulatory effects of MSCs on the expression levels of ICAM-1 and VCAM-1 in lung tissues and so investigated this in rat asthmatic models. They also found BM-MSCS decreased expression of both on pulmonary endothelium (Rahbarghazi et al., 2019). In their study, they further tested whether this benefit could be conferred via a paracrine effect by performing parallel experiments using BM-MSC conditioned media. Although conditioned media was effective, the ability to decrease adhesion molecule expression was more evident in the cell-treated group.

5.4.5. 3D cultured hBM-MSCs Y201 are most potent at reducing circulating serum levels of pro-inflammatory factors *in vivo*

Myocardial IR injury induces an intense inflammatory response triggered by the release of various pro-inflammatory cytokines, such as TNF-α, IL-1β and IL-6 (Sharma and Das, 1997). This may be mediated by ROS generation, and in addition to ROS, these cytokines can also activate ECs and circulating leukocytes to express surface integrins and cell adhesion molecules resulting in subsequent recruitment of inflammatory cells to the site of injury. To assess whether the beneficial effects of 3D cultured HBM-MSCS Y201 could also be mediated through reductions in the serum level of established inflammation associated cytokines, a multiplex array consisting of 23 anti- and pro-inflammatory cytokines was used. Firstly we demonstrated that myocardial IR injury, by 2 hours reperfusion, had significantly increased the serum levels of 9 pro-inflammatory cytokines of which IL-6, IL-12, G-CSF, CCL1/KC, CCL2/MCP-1 and CCL3/MIP-1β showed greater than 6-fold increases. The levels of obvious and potent inflammatory candidates were also increased, including IL-1β and TNFα as expected. Interestingly, the level of IL-10, a naturally occurring potent anti-inflammatory cytokine, was also significantly increased. Increased levels of this particular cytokine have been identified in the plasma of MI patients (Malarstig et al., 2008). Furthermore, inducing myocardial IR injury in IL-10 deficient mice was associated with increased ICAM-1 expression, massively enhanced neutrophil infiltration and larger infarcts (Yang et al., 2000). This study by Yang and colleagues was the first to provide direct evidence that endogenous IL-10 was produced in an attempt to protect the heart from IR injury (Yang et al., 2000). Clearly, its ability to be protective is overwhelmed by the multiple pro-inflammatory cytokines that are concomitantly generated.

Interestingly, mice that received 2D cultured hBM-MSCs Y201 did not demonstrate any ability to decrease cytokine serum levels. It was, therefore, quite remarkable that simply culturing these cells in hanging drops improved their ability to decrease cytokine serum levels so much so that 3D cultured hBM-MSCs Y201 were transformed into the most effective sub-population. This was evidenced by 9 pro-inflammatory cytokine serum levels being reduced in IR injured mice compared to 7 and 3 in mice receiving 2D and 3D cultured hBM-MSCs Y202 respectively. This result clearly indicated the ability of 3D culture to improve the immunomodulatory effect of MSCs. Indeed, recent studies reported that MSCs cultured as spheroids demonstrated intense anti-inflammatory effects mediated via the up-regulation of TNFAIP6/TSG6 (Bartosh et al., 2010). Moreover, 3D culture up-regulated PGE2, which could suppress the increases in inflammatory cytokine release (Ylostalo et al., 2012).

Luminex analysis of 23 cytokines highlighted how MSC therapy does not discriminate between the pro and anti-inflammatory cytokines and their ability to increase and decrease them. In fact, the whole process seems to be somewhat random. This is evidenced by the fact that 3D cultured hBM-MSCs Y201 not only decreased the levels of 9 pro-inflammatory cytokines but also 2 anti-inflammatory cytokines, namely IL-10 and IL-13. In addition, it further raised the levels of 4 pro-inflammatory cytokines as well. There was also little overlap with the modification made by 2D and 3D cultured hBM-MSCs Y201. Hence it is difficult to ascertain which modification(s) was critical if at all.

However, an interesting observation was the ability of all the effective sub-populations to decrease levels of IL-1α, IL-12(p40) and CCL4/MIP-1β. Indeed remarkable reductions in these three were also noted with 2D cultured hBM-MSCs Y201, but these did not attain

statistical significance. Not only did MSC therapy reduce these circulating cytokines back down to sham levels, but it also reduced the levels of other proinflammatory cytokines that did not significantly increase during IR injuries, such as IL-1, IL-2 and IL-3. It is well known that IL-1α and IL-6 are cytokines which can exasperate myocardial IR injury (Sharma and Das, 1997). Hence, the reduction of multiple cytokine pathways may explain the anti-inflammatory and associated therapeutic effects of MSCs. Lugrin and colleagues showed that necrotic cardiomyocytes from mice exposed to MI released IL-1α in plasma *in vivo* (Lugrin et al., 2015). Also, IL-1α blocking Ab and IL-1 receptor antagonist reduced post ischemic inflammation and infarct size and suppressed cardiac fibroblast immune activation. They suggested that IL-1α plays important role as a vital danger signal in the infarcted heart (Lugrin et al., 2015). IL-1β has received the most attention in the setting of CVD, especially in light of the ground-breaking recent CANTOS clinical trial which was the first major randomised double-blind trial of canakinumab, a therapeutic monoclonal antibody targeting IL-1β (Ridker et al., 2017). The trial involved 10,061 patients with a previous history of MI receiving the anti-IL-1β antibody subcutaneously every 3 months. The main endpoints, non-fatal MI/stroke or cardiovascular death, were measured ~3½ years later. Patients receiving canakinumab demonstrated modest, yet significant, beneficial effects with regards to these cardiovascular outcomes. This study sparked a renewed interest in the role of inflammation in MI, with experts interpreting the results of the CANTOS trial as evidence that anti-inflammatory drugs, particularly those targeting the IL-1β pathway, could effectively prevent subsequent cardiovascular events. It is possible, therefore, that the universal ability of our tested MSCs to target these potent inflammatory cytokines is a critical therapeutic mechanism.

5.5 Conclusion

It is essential that the mechanisms governing the biological activity of MSC therapies be determined in order for them to reach their full clinical potential and thus enhance their treatment efficacy. Oxidative stress is associated with injury to the microvasculature, which can lead to thromboinflammation following myocardial IR injury (Mussbacher et al., 2019). The oxidatively stressed coronary endothelium can rapidly mediate leukocyte recruitment. Furthermore, its loss or denudation can also expose underlying extracellular matrix / collagen, which lead to platelet activation and aggregation. Therefore, protecting *in vivo* this delicate monolayer of cells lining microvessels is critical to prevent the deleterious thromboinflammatory events we observed in the IR injured beating heart

In this chapter, we provide valuable information that hBM-MSCs potentially utilise multiple protective mechanisms to confer vasculoprotective benefit within the coronary microcirculation following myocardial IR injury. These include significantly reducing (i) the ability of ROS to damage ECs (ii) the expression of critical endothelial adhesion molecules and (iii) serum levels of multiple potent inflammatory cytokines. 3D cultured hBM-MSCs Y201 were most effective at modifying all three of these events thus providing an explanation for the *in vivo* results provided in the previous chapter (**Figure 5.8**).

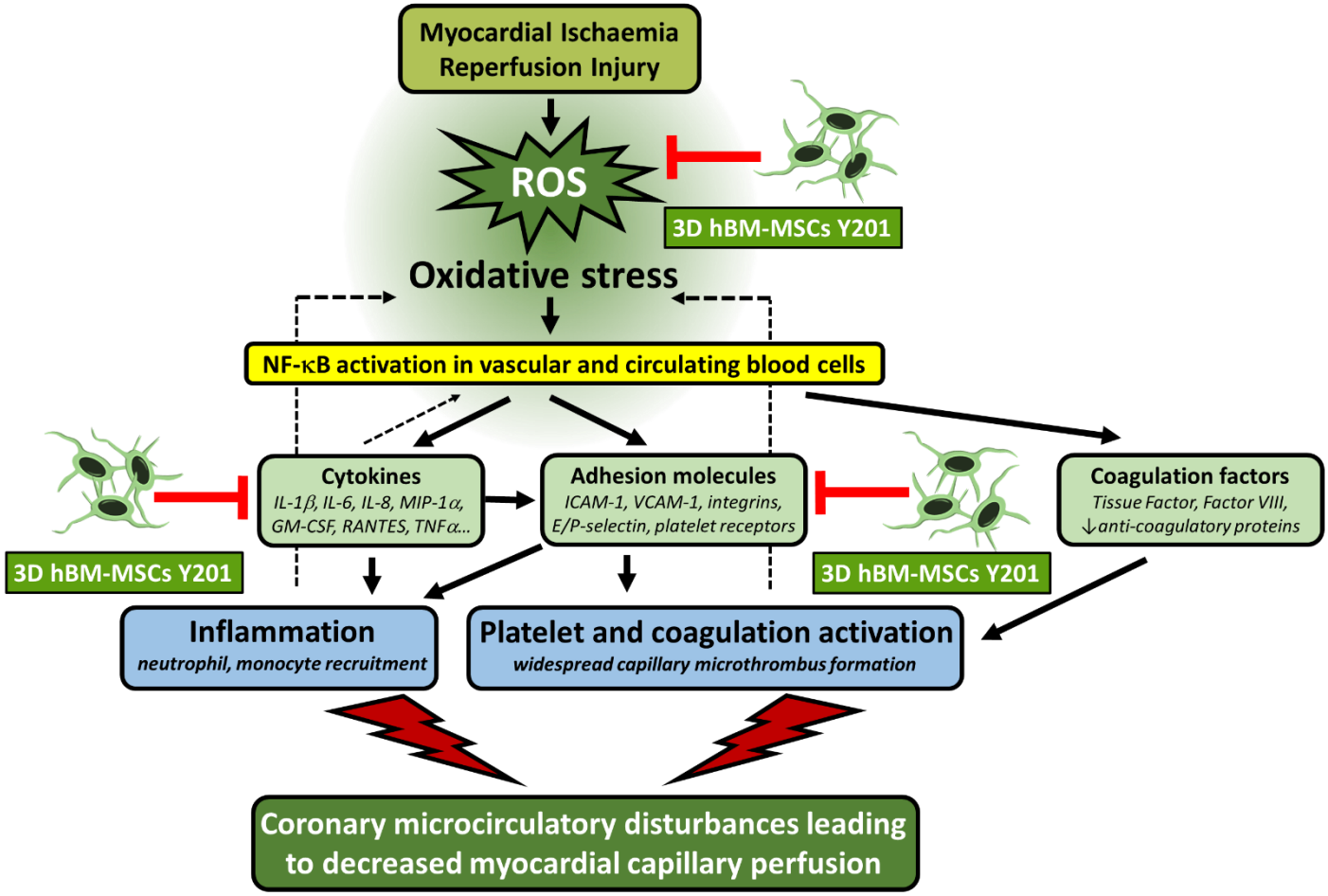


Figure 5.7. Increased vascular and non-vascular production of reactive oxygen species (ROS) within the IR injured heart leads to local tissue oxidative stress and ultimately damage to the vital yet delicate coronary microvessels. When cellular production of ROS increases, such as during myocardial IR injury, it overwhelms the host anti-oxidant capacity, leading to a state of oxidative stress. In addition to causing direct damage to cellular proteins, lipids and nucleic acids, ROS are also key signalling molecules that can mediate a number of additional indirect thromboinflammatory pathophysiological responses. This occurs after ROS activate the cytoplasmic transcription factor nuclear factor-κB (NF-κB) that is of central importance in mediating thromboinflammation. NF-κB is expressed in vascular and circulating cells, including anucleate platelets. Three downstream effects of NF-κB are shown and include: **(i)** expression of pro-inflammatory genes encoding a multitude of pro-inflammatory cytokines and chemokines; **(ii)** endothelial dysfunction leading to their expression of inflammatory adhesion molecules; and **(iii)** the induction of pro-coagulatory mechanisms through up-regulation of tissue factor and factor VIII (as well as decreased anti)coagulatory mechanisms). Collectively, these actions lead to extensive neutrophil recruitment and widespread microthrombus formation and subsequent occlusion within the coronary capillaries as demonstrated in Chapter 4 using intravital imaging of the mouse IR injured beating heart**.** We present novel data that 3D culture and subsequent systemic infusion of a specific exogenous sub-population of bone marrow-derived MSCs, hBM-MSCs Y201, can modify at least three of these processes post-reperfusion injury – coronary endothelial oxidative damage, expression of coronary endothelial ICAM-1/VCAM-1 and serum concentrations of a plethora of pro-inflammatory cytokines. This could mechanistically explain their ability to reduce thromboinflammation and confer vasculoprotection in the coronary microcirculation *in vivo*. (**Figure courtesy of Dr Neena Kalia, University of Birmingham)**

CHAPTER 6

General Discussion

6.0 General Discussion

6.1 Summary of the main findings and general discussion

CVDs are a group of disorders that cause dysfunction to the heart and the blood vessels. Although mortality rates for this condition have gradually declined over the last few decades in western countries, approximately 30% of the world population still dies from CVDs making it the most significant cause of mortality globally (Sun et al., 2016). The biggest contributor to CVD is MI, which induces reversible or irreversible ischaemic damage to the heart depending upon how quickly reperfusion can be instigated. Contemporary treatments to open the occluded epicardial artery or arteries includes pharmacological thrombolytic medications, PPCI or heart surgery (Briffa et al., 2009). Despite the success of these therapeutic strategies, a significant proportion of patients still have a low quality of life and frequently return to the hospital due to non-reversible tissue damage leading to progressive heart failure (Terashvili and Bosnjak, 2019). Growing evidence suggests a critical role for the coronary microcirculation in reperfusion mediated damage and the development of the 'no-reflow' phenomenon. Hence, there is a need to develop treatments to improve the prognosis of patients clinically through preservation of the coronary microcirculation.

In the past 20 years, stem cell-based therapies have been identified as having the most potential for changing the way multiple diseases, including CVDs, are treated (Stavely and Nurgali, 2020). MSCs have been considered a potential treatment to treat a broad range of diseases due to their unique ability to evade the host immune system and the ease of rapidly expanding them in culture. Furthermore, the secretome of MSCs has been

identified to be therapeutic in many disease models both *in vitro* and *in vivo* (Ferreira et al, 2018). The positive outcomes noted after using them in a plethora of experimental studies have driven hundreds of clinical trials (Eleuteri et al., 2019). *ClinicalTrials.gov* is an official database of privately and publicly funded clinical studies conducted around the world. A search of this database using the term 'mesenchymal stem cells' revealed 1,124 clinical studies using MSCs to treat various conditions ranging from diabetic neuropathy, Crohn's, lupus, psoriasis, liver disorders, as well as heart diseases (as of September 2020) (ClinicalTrial.gov 2020). Indeed, 27 studies appear in this search engine in which MSCs have been used, or are still being used in on-going clinical trials, specifically for treating MI patients. MSCs have the ability to improve the cardiac microenvironment and trigger the repair and regeneration of damaged cardiac myocardium and its vasculature in order to recover heart function (ClinicalTrial.gov 2020).

However despite these clinical trials, to date, no suitable stem cell treatment has been successfully adopted to become a stand-alone or adjuvant therapy for effectively treating CVDs (Lee et al., 2016). The obstacles that may explain the failure to incorporate MSCs into current treatment regimens have been many and include the fact that they exhibit poor retention and survival in the ischaemic target organ (Tang et al., 2018). There is also still no consensus on which population of stem cell confers the most therapeutic capacity to treat heart disease. Furthermore, the cellular targets of MSC actions and the mechanisms explaining their therapeutic effects are still not fully understood (Muller et al., 2018). The pleiotropic properties of MSCs, such as their immunomodulatory effects, ability to alleviate inflammation as well as stimulate tissue regeneration, means it is critical to unequivocally

identify the (i) exact molecular and cellular impact of (ii) a defined MSC population on a (iii) specific disease using an appropriate clinically relevant disease model.

This thesis aimed to develop a using 3D hanging culture protocol in order to improve the delivery and subsequent capture of MSCs within the IR injured beating mouse heart. Also, we aimed to determine whether microcirculatory vasculoprotective effects were a possible mechanism of therapeutic action utilised by all or some sub-populations of hBM-MSCs. We used various *in vitro*, *in vivo* and *ex vivo* techniques to determine the adhesion capabilities of MSCs and identify beneficial mechanisms. State-of-the-art IVM was used for the first time to image at a cellular level and in real-time the kinetics of MSC trafficking to the IR injured heart. Furthermore, the consequences of infusing these cells on platelet and neutrophil presence and on the density of perfused capillaries were also assessed in the coronary microcirculation. Flow cytometry of digested heart tissue was used to not only to support the intravital MSC retention data but also detail their specific beneficial events on ECs and cardiomyocytes. Moreover, further mechanisms governing vasculoprotection were determined using a multiplex immunoassay. The major novel findings from this thesis include the following and are summarised in **Figure 6.1**:

- Two sub-populations of hBM-MSCs, Y201 and Y202, originally derived from the same BM site, possessed different adhesive potential both *in vitro* to different substrates and, importantly, *in vivo* within the beating IR injured heart. Moreover, their anti-inflammatory benefits were either present or absent in the injured coronary microcirculation, with the more adhesive hBM-MSCs Y201 sub-population being vasculoprotective.

- hBM-MSCs known to be confined potentially within a more perivascular niche of the BM possessed superior adhesion capacity *to* inflamed ECs *in vitro* and vasculoprotective ability *in vivo*. This clearly demonstrated that in terms of their retention and protective ability, not all BM-derived MSCs were the same.
- More importantly, the superior adhesive and protective ability was only noted when hBM-MSCs Y201 were derived from spheres grown using a 3D hanging drop method. Mechanistically, this was likely due to this culture technique increasing ICAM-1 and CXCR4 expression on the surface of these cells and also distributing adhesion molecules more uniformly on their surface. 3D cultured hBM-MSCs Y201 were also much smaller than those grown in a 2D culture. This likely reduced their pulmonary microvascular entrapment leading to the observed increase in their trafficking through the heart on first pass subsequent. This may have contributed to the increased likelihood of capture and retention in the heart.
- Combination therapy, which involved administering 3D cultured hBM-MSCs Y201 with unfractionated heparin, further reduced the recruitment of neutrophils and platelets within the coronary microcirculation following IR injury with a more rapid onset of therapeutic action noted than just using MSCs. Indeed, when the whole thickness of the left ventricle was imaged using multiphoton microscopy, this dual therapy was noted to be particularly effective at significantly decreasing neutrophil and platelet presence in the IR injured heart. This may have been linked to increased homing of MSCs to the heart on first pass with a trend for their adhesion to increase. We postulate that heparin would have targeted the platelets and the MSCs would have prevented the neutrophil adhesion. To our knowledge, we are the

first group to demonstrate using multiphoton imaging the vasculoprotective effectiveness of a combination therapy in all layers of the IR injured heart.

- The ability of 3D cultured hBM-MSCs Y201 to ameliorate the perturbations within the IR injured microvasculature may have been accomplished by reducing coronary EC oxidative stress and/or by reducing the levels of plasma pro-inflammatory cytokines including IL-1α, IL-5, IL-6, IL-10, IL-12 (p40), IL-13, G-CSF, IFN-γ, KC, MCP-1, MIP-1a and MIP-1b.
- Critically, all of these beneficial actions resulted in an increase in the density of perfused coronary capillaries and a concomitant decrease in infarct size in mice receiving cellular 3D cultured hBM-MSCs Y201 therapy.

To our knowledge, we are the first group to directly image in real-time the kinetics of MSC recruitment and their impact on microvascular events at a cellular level in a mouse beating and injured heart model. Just as understanding the pharmacokinetics of drugs is important in drug development, we believe that increasing our understanding of the *in vivo* kinetics of MSCs are also important and will allow us to determine and enhance their therapeutic potential. There is significant scope, therefore, for using our novel beating heart imaging method to further increase our understanding of the microvascular events modified by cellular therapy and develop strategies to improve their vasculoprotective efficacy. In the current study we clearly show that hBM-MSCs are rapidly responsive to coronary reperfusion injury immediately after their infusion. Although others have shown that MSCs can respond to signals released following tissue damage we are the first to show how rapid this response is and the extent of their local capture at a cellular level *in vivo* (Rennert et al., 2012, Fong et al., 2011, Lin et al., 2017). Interestingly, in comparison to the intravital data on neutrophil recruitment within the IR injured heart, the recruitment of MSCs was

much lower. Indeed, 100-150 neutrophils were adherent within an imaged field of view whereas less than 20-30 MSCs were captured. This may simply be due to the fact that only 500,000 exogenous MSCs were actually infused and most of these MSCs became entrapped elsewhere after the first pass.

However, despite this comparatively limited MSC presence, we are also the first to show that these cells have a remarkable ability to reduce thromboinflammatory events in the heart. We are the first to directly demonstrate that MSCs can rapidly affect the adhesion of neutrophils and platelets in a diseased organ *in vivo* in the presence of pathological flow. However, this was very much dependent on the culture method and the MSC sub-population used. 3D culture promoted the expression of adhesion molecules and restored expression of the SDF-1α receptor CXCR4. This chemokine receptor and surface adhesion molecules may have facilitated their migration and homing to the damaged organ by interacting with the triggering signals emitted from the injured ECs (Hmadcha et al., 2020). We also demonstrated that MSCs obtained from 3D culture expressed adhesion molecules more uniformly on their cell surface. Collectively, these 3D culture induced changes may have promoted MSC homing and adhesion by increasing the chances of the likelihood of firm interactions taking place with activated ECs. Indeed, it has previously been reported that the distribution of adhesion molecules on the cell surface affected the potency of neutrophil binding to activated ECs (Hocde et al., 2009). The presence of 3D cultured hBM-MSCs Y201 and 3D cultured hBM-MSCs Y202 was not significantly different in the IR injured heart, yet only one cell type was beneficial. This suggests that local presence may not have been an important pre-requisite for MSCs to be more therapeutically effective and that the actual cell type used is more critical.

Heterogeneity of the composition of MSC cultures hinders their use in regenerative medicine and this may be a key factor associated with their poor clinical success. In the case of the reperfusion injured heart, we believe there is a critical need for future studies to identify a sub-population that has superior vasculoprotective and anti-inflammatory effects. Once identified, such MSCs can be manufactured on a large scale to accelerate the effective translation of MSC therapeutics for treatment of CVD in clinical practice. $CD317^{pos}$ MSCs make up about 9% of the BM MSC population (James et al., 2015; Kay et al., 2018). However, we found that this sub-population i.e. the hBM-MSCs Y202, were not able to protect the coronary microvessels from an IR inflammatory insult despite being recruited to the heart in similar numbers to hBM-MSCs Y201. Current MSC based therapies do not account for the MSCs that are $CD317^{pos}$. It is therefore possible that infusing a heterogeneous MSC population that includes a fraction of non-migratory, non-differentiating, proliferative and potentially pro-inflammatory cells could contribute to the poor outcome of MSCs in clinical interventions for MI. In addition to the work by the Genever group, our novel data also strengthens the case for negative selection of MSCs using the biomarker CD317 for thromboinflammatory disorders of the heart and using a more purified population (Kay et al., 2018).

CD317 is not the only surface marker than can potentially select for a more potent immunomodulatory MSC sub-population (O'Connor, 2019). Surface markers that select for colony-forming MSCs, such as CD271 and STRO-1, have been used to enrich MSCs with increased immunosuppressive capacity (Kuci et al., 2010; Nasef et al., 2009). In addition to these biomarkers, other antigens have been identified that detect cell-to-cell variation in the immunoregulatory activity of MSCs (Yang et al., 2013; Ortiz et al., 2007). Of these, the

expression of VCAM-1 (CD106) on MSCs has been extensively studied (Yang et al., 2013; Ren et al., 2010). MSC-induced suppression of T-cell proliferation is achieved after T-cell adhesion to MSCs, which can be reversed with a VCAM-1 function blocking antibody (Ren et al., 2010). Furthermore, when MSCs derived from human placental chorionic villi were divided into VCAM-1^- and VCAM-1^+ subsets, the latter was far more effective in suppressing the secretion of inflammatory cytokines by activated peripheral blood mononuclear cells and stimulating the formation of anti-inflammatory regulatory T cells (Yang et al., 2013). Collectively, all of these studies, including our own, strongly point towards developing and testing the vasculoprotective efficacy of MSCs purified for a specific marker.

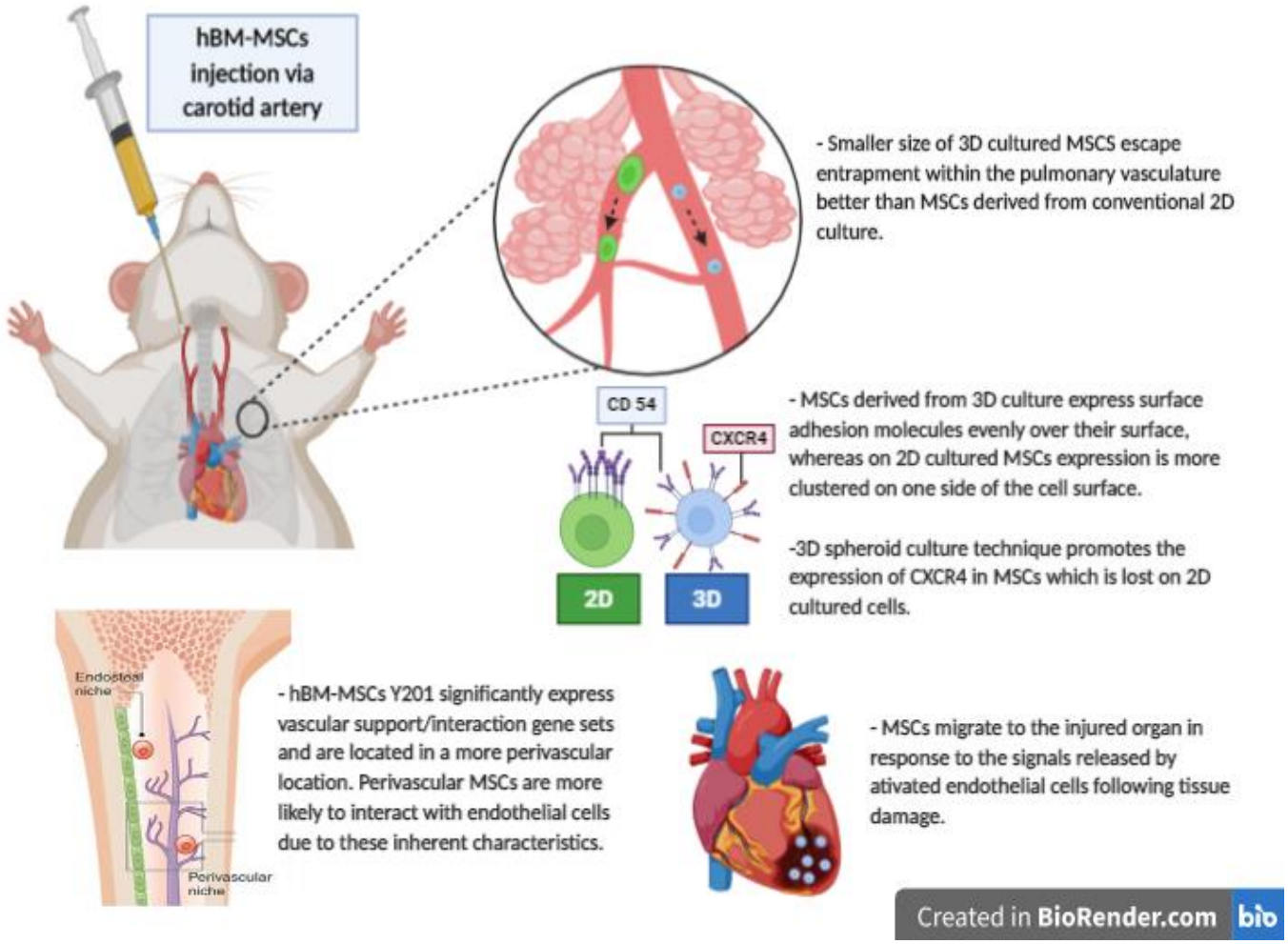


Figure 6.1. Proposed mechanism explaining how 3D culture may enhance the homing and recruitment of hBM-MSCs Y201 within coronary microvessels following myocardial IR injury. The size of MSCs released from hanging drop generated spheres is significantly smaller than those obtained from conventional 2D culture. Such smaller cells may have escaped entrapment within the pulmonary capillaries which would have maintained a circulating pool of MSCs in the peripheral circulation. MSCs obtained from spheroids also expressed surface adhesion molecules evenly over their surface, whereas on 2D cultured cells expression was more concentrated or clustered on one side of the cell surface. The dispersion of adhesion molecules over the cell surface has significance on their availability and capacity to form strong bonds with counter ligands on the surface of endothelial cells. The increased homing and subsequent recruitment of 3D cultured cells may also be linked to the fact that as CXCR4, lost when MSCs are cultured using conventional 2D methods, is recovered with 3D culture. The Genever group, who clonally expanded the tested hBM-MSCs, demonstrated that hBM-MSCs Y201 significantly overexpressed vascular support/interaction gene sets, such as those related to blood vessel development and remodelling and artery morphogenesis, and were located in a more perivascular location. It is, therefore, possible that perivascular hBM-MSCs Y201 were more likely to interact with endothelial cells due to these inherent characteristics.

6.2 Future work

Although a positive therapeutic effect was noted regarding preventing neutrophil recruitment, the 3D cultured MSCs when administered alone at 30 minutes post-reperfusion did not significantly reduce platelet aggregation. Therefore, future studies would need to consider optimising the time point at which MSCs are injected and/or the dose in order to determine whether the beneficial effect of MSC therapy can be maximised. It could be that what we have shown is the limit of MSC effectiveness and cannot be improved upon, but this has to be proven. Testing the efficacy of MSCs delivered either before reperfusion is initiated or within minutes of reperfusion would be worthwhile. Such studies will also allow us to determine whether the microvascular damage mediated by ischaemic injury alone is sufficient to recruit MSCs or whether the additional damage that occurs as a result of reperfusion is needed to capture circulating MSCs. Many previous studies have focused on the innate immune response in myocardial IR injury. However, the adaptive immune response is also involved. $CD4^+$ T lymphocytes have been reported to be sequestrated in the perfused myocardium and can also contribute to the development of IR damage (Boag et al., 2017). To determine whether 3D cultured hBM-MSCs Y201 can also modify cells of the heart's adaptive immune system needs to be determined.

We successfully demonstrated that co-administration of unfractionated heparin improved the vasculoprotective capacity of 3D hBM-MSCs Y201 throughout the myocardial wall. Combination of MSCs with other pharmacological drugs, contemporary anti-platelet drugs already used in clinics, or other types of stem cells may further improve their

vasculoprotective effects at the level of the coronary microcirculation and so this is also worth investigating.

6.3 Concluding remarks

The clinical focus for heart attack patients is to open occluded epicardial arteries to improve outcome. However, further improvements to patient outcome will depend on addressing problems in the microcirculation that arise during reperfusion. Therefore, developing strategies directed at restoring microvascular function appear to be of paramount importance. MSC cytotherapy is a promising strategy to treat myocardial IR injury, particularly the damage incurred by the coronary microcirculation. However, clinical success has been limited. When transplanting exogenous MSCs for therapeutic purposes, a major goal is to achieve maximum retention in the injury site. Recent studies have attempted to genetically manipulate SCs in order to enhance their recruitment, for example, by transfecting integrins or chemokine receptors on their surface or injecting chemokines into the heart to attract circulating MSCs. However, we find 3D culture of MSCs, which is a non-invasive and non-genetically engineered approach, may have greater clinical applicability. 3D culture also improves the vasculoprotective ability of MSCs in a manner that is probably not linked to increased local presence in the IR injured heart. Indeed, unlike pharmacological drugs, the 3D cultured MSCs appeared to combine a number of protective mechanisms to resolve the thromboinflammatory damage such as inhibiting ROS endothelial damage, reducing inflammatory adhesion molecule expression and modifying the inflammatory cytokine profile in plasma. It is anticipated that this culturing strategy will promote more efficient SCs delivery to the injured coronary

microcirculation and subsequently improve thromboinflammatory scores when tested clinically. When combined with the use of a specific $CD317^{pos}$, purified BM sub-population of MSCs, this could be a powerful new cellular treatment for improving the structure and function of the perturbed coronary microvessels post-reperfusion. The possibility of an anti-platelet effect when MSCs are used as a combination therapy with something like heparin is exciting, and may open up the use of MSCs for many CVDs in which the major pathology is associated with platelet adhesion or thrombosis. To summarise, this thesis provides essential data that culturing a specific sub-population of BM-derived MSCs does indeed improve and accelerate their vasculoprotective potential within the injured beating coronary microcirculation.

CHAPTER 7

REFERENCES

7.0 References

ABRAM, C. L. & LOWELL, C. A. 2009. The ins and outs of leukocyte integrin signaling. *Annu Rev Immunol,* 27**,** 339-62.

AGUIRRE, A. D., VINEGONI, C., SEBAS, M. & WEISSLEDER, R. 2014. Intravital imaging of cardiac function at the single-cell level. *Proceedings of the National Academy of Sciences,* 111**,** 11257-11262.

ALLAN-RAHILL, N. H., LAMONT, M. R. E., CHILIAN, W. M., NISHIMURA, N. & SMALL, D. M. 2020. Intravital Microscopy of the Beating Murine Heart to Understand Cardiac Leukocyte Dynamics. *Front Immunol,* 11**,** 92.

ALLEN, D. G. & XIAO, X. H. 2000. Activity of the Na+/H+ exchanger contributes to cardiac damage following ischaemia and reperfusion. *Clin Exp Pharmacol Physiol,* 27**,** 727-33.

AN, Z., SABALIC, M., BLOOMQUIST, R. F., FOWLER, T. E., STREELMAN, T. & SHARPE, P. T. 2018. A quiescent cell population replenishes mesenchymal stem cells to drive accelerated growth in mouse incisors. *Nat Commun,* 9**,** 378.

ANDRIENKO, T., PASDOIS, P., ROSSBACH, A. & HALESTRAP, A. P. 2016. Real-Time Fluorescence Measurements of ROS and [Ca2+] in Ischemic / Reperfused Rat Hearts: Detectable Increases Occur only after Mitochondrial Pore Opening and Are Attenuated by Ischemic Preconditioning. *PLoS One,* 11**,** e0167300.

ANDRIENKO, T. N., PASDOIS, P., PEREIRA, G. C., OVENS, M. J. & HALESTRAP, A. P. 2017. The role of succinate and ROS in reperfusion injury - A critical appraisal. *J Mol Cell Cardiol,* 110**,** 1-14.

ARAI, M., LEFER, D. J., SO, T., DIPAULA, A., AVERSANO, T. & BECKER, L. C. 1996. An anti-CD18 antibody limits infarct size and preserves left ventricular function in dogs with ischemia and 48-hour reperfusion. *J Am Coll Cardiol,* 27**,** 1278-85.

ARIMATEIA, D. S., DA SILVA BRITO, A., DE AZEVEDO, F. M., DE ANDRADE, G. P. & CHAVANTE, S. F. 2015. Heparin fails to inhibit the leukocyte recruitment for an extended time following inflammatory stimulus. *Pharm Biol,* 53**,** 72-7.

AUFFRET, V., LAURIN, C., LEURENT, G., DIDIER, R., FILIPPI, E., HACOT, J. P., ZABALAWI, A., ROUAULT, G., SAOULI, D., DRUELLES, P., COUDERT, I., BOULANGER, B., BOT, E., TREUIL, J., BEDOSSA, M., BOULMIER, D., LOIRAT, A., SHAROBEEM, S., GUELLEC, M. L., GILARD, M. & BRETON, H. L. 2020. Pharmacoinvasive Strategy Versus Primary Percutaneous Coronary Intervention for ST-Segment Elevation Myocardial Infarction in Patients >/=70 Years of Age. *Am J Cardiol,* 125**,** 1-10.

AVERY, M. B., BELANGER, B. L., BROMLEY, A., SEN, A. & MITHA, A. P. 2019. Mesenchymal Stem Cells Exhibit Both a Proinflammatory and Anti-Inflammatory Effect on Saccular Aneurysm Formation in a Rabbit Model. *Stem Cells Int,* 2019**,** 3618217.

BARANIAK, P. R. & MCDEVITT, T. C. 2012. Scaffold-free culture of mesenchymal stem cell spheroids in suspension preserves multilineage potential. *Cell Tissue Res,* 347**,** 701-11.

BARBASH, I. M., CHOURAQUI, P., BARON, J., FEINBERG, M. S., ETZION, S., TESSONE, A., MILLER, L., GUETTA, E., ZIPORI, D., KEDES, L. H., KLONER, R. A. & LEOR, J. 2003. Systemic delivery of bone marrow-derived mesenchymal stem cells to the infarcted myocardium: feasibility, cell migration, and body distribution. *Circulation,* 108**,** 863-8.

BARRABES, J.A., INSERTE, J., MIRABET, M., QUIROGA, A. 2010. Antagonism of P2Y12 or GPIIb/IIIa receptors reduces platelet-mediated myocardial injury after ischaemia and reperfusion in isolated rat hearts. *Thromb Haemost*, 104(1), 128-135.

BARTOSH, T. J., YLOSTALO, J. H., MOHAMMADIPOOR, A., BAZHANOV, N., COBLE, K., CLAYPOOL, K., LEE, R. H., CHOI, H. & PROKOP, D. J. 2010. Aggregation of human mesenchymal stromal cells (MSCs) into 3D spheroids enhances their antiinflammatory properties. *Proc Natl Acad Sci U S A,* 107**,** 13724-9.

BARTOSH, T. J. & YLOSTALO, J. H. 2014. Preparation of anti-inflammatory mesenchymal stem/precursor cells (MSCs) through sphere formation using hanging-drop culture technique. *Curr Protoc Stem Cell Biol,* 28**,** Unit 2B 6.

BECKER, B. F., FISCHER, J., HARTMANN, H., CHEN, C. C., SOMMERHOFF, C. P., TSCHOEP, J., CONZEN, P. C. & ANNECKE, T. 2011. Inosine, not adenosine, initiates endothelial glycocalyx degradation in cardiac ischemia and hypoxia. *Nucleosides Nucleotides Nucleic Acids,* 30**,** 1161-7.

BENSIDHOUM, M., CHAPEL, A., FRANCOIS, S., DEMARQUAY, C., MAZURIER, C., FOUILLARD, L., BOUCHET, S., BERTHO, J. M., GOURMELON, P., AIGUEPERSE, J., CHARBORD, P., GORIN, N. C., THIERRY, D. & LOPEZ, M. 2004. Homing of in vitro expanded Stro-1- or Stro-1+ human mesenchymal stem cells into the NOD/SCID mouse and their role in supporting human CD34 cell engraftment. *Blood,* 103**,** 3313-9.

BERNARDI, P. & DI LISA, F. 2015. The mitochondrial permeability transition pore: molecular nature and role as a target in cardioprotection. *J Mol Cell Cardiol,* 78**,** 100-6.

BEVILACQUA, M. P., STENGELIN, S., GIMBRONE, M. A., JR. & SEED, B. 1989. Endothelial leukocyte adhesion molecule 1: an inducible receptor for neutrophils related to complement regulatory proteins and lectins. *Science,* 243**,** 1160-5.

BRADFIELD, J. W. & BORN, G. V. 1974. Lymphocytosis produced by heparin and other sulphated polysaccharides in mice and rats. *Cell Immunol,* 14**,** 22-32.

BRIFFA, T., HICKLING, S., KNUIMAN, M., HOBBS, M., HUNG, J., SANFILIPPO, F. M., JAMROZIK, K. & THOMPSON, P. L. 2009. Long term survival after evidence based treatment of acute myocardial infarction and revascularisation: follow-up of population based Perth MONICA cohort, 1984-2005. *BMJ,* 338**,** b36.

BROWN, R.A., LEUNG, E., KANKAANRANTA, H., MOILANEN, E., PAGE, C.P. 2012. Effects of heparin and related drugs on neutrophil function. *Pulm Pharmacol Ther*, 25, 185–192.

BOAG, S. E., ANDREANO, E. & SPYRIDOPOULOS, I. 2017. Lymphocyte Communication in Myocardial Ischemia/Reperfusion Injury. *Antioxid Redox Signal,* 26**,** 660-675.

BOLONGESE, L., CARRABBA, N., PARODI, G., SANTORO, G.M., BUONAMICI, P., CERISANO, G., ANTONIUCCI, D., 2004. Impact of microvascular dysfunction on left ventricular remodeling and long-term clinical outcome after primary coronary angioplasty for acute myocardial infarction. *Circulation*, 109, 1121-1126.

BONAVENTURA, A., MONTECUCCO, F. & DALLEGRI, F. 2016. Cellular recruitment in myocardial ischaemia/reperfusion injury. *Eur J Clin Invest,* 46**,** 590-601.

BOYLE, E.M., POHLMAN, T.H., CORBEJO, C.J., VERRIER, E.D., 1996. Endothelial cell injury in cardiovascular surgery: ischemia-reperfusion. *Ann Thorac Surg*, 62(6), 1868-75.

BULLUCK, H., DHARMAKUMAR, R., ARAI, A.E., BERRY, C., HAUSENLOY, D.J. 2018. Cardiovascular Magnetic Resonance in Acute ST-Segment-Elevation Myocardial Infarction: Recent Advances, Controversies, and Future Directions. *Circulation*, 137, 1949-1964.

BURNE, M. J., ELGHANDOUR, A., HAQ, M., SABA, S. R., NORMAN, J., CONDON, T., BENNETT, F. & RABB, H. 2001. IL-1 and TNF independent pathways mediate ICAM-1/VCAM-1 up-regulation in ischemia reperfusion injury. *J Leukoc Biol,* 70**,** 192-8.

BUSSER, H., NAJAR, M., RAICEVIC, G., PIETERS, K., VELEZ POMBO, R., PHILIPPART, P., MEULEMAN, N., BRON, D. & LAGNEAUX, L. 2015. Isolation and Characterization of Human Mesenchymal Stromal Cell Subpopulations: Comparison of Bone Marrow and Adipose Tissue. *Stem Cells Dev,* 24**,** 2142-57.

CADENAS, S. 2018. ROS and redox signaling in myocardial ischemia-reperfusion injury and cardioprotection. *Free Radic Biol Med,* 117**,** 76-89.

CALIO, M. L., MARINHO, D. S., KO, G. M., RIBEIRO, R. R., CARBONEL, A. F., OYAMA, L. M., ORMANJI, M., GUIRAO, T. P., CALIO, P. L., REIS, L. A., SIMOES MDE, J., LISBOA-NASCIMENTO, T., FERREIRA, A. T. & BERTONCINI, C. R. 2014. Transplantation of bone marrow mesenchymal stem cells decreases oxidative stress, apoptosis, and

hippocampal damage in brain of a spontaneous stroke model. *Free Radic Biol Med,* 70**,** 141-54.

CAMICI, P.G., CREA, F. 2007. Coronary microvascular dysfunction. *N Eng J Med*, 356, 830-840.

CARMAN, C. V. & SPRINGER, T. A. 2004. A transmigratory cup in leukocyte diapedesis both through individual vascular endothelial cells and between them. *J Cell Biol,* 167**,** 377-88.

CAO, J., HOU, S., DING, H., LIU, Z., SONG, M., QIN, X., WANG, X., YU, M., SUN, Z., LIU, J., SUN, S., XIAO, P., LV, Q. & FAN, H. 2016. In Vivo Tracking of Systemically Administered Allogeneic Bone Marrow Mesenchymal Stem Cells in Normal Rats through Bioluminescence Imaging. *Stem Cells Int,* 2016**,** 3970942.

CESARZ, Z. & TAMAMA, K. 2016. Spheroid Culture of Mesenchymal Stem Cells. *Stem Cells Int,* 2016**,** 9176357.

CAHILL, T.J., KHARBANDA, R.K. 2017. Heart failure after myocardial infarction in the era of primary percutaneous coronary intervention: Mechanisms, incidence and identification of patients at risk. *World journal of cardiology*, 9(5), 407–415.

CREA, F., CAMICI, P.G., BAIREY, C.N. 2014. Coronary microvascular dysfunction: an update. *Eur Heart J*, 35, 1101-1111.

CHEN, J., ROGERS, S. C. & KAVDIA, M. 2013. Analysis of kinetics of dihydroethidium fluorescence with superoxide using xanthine oxidase and hypoxanthine assay. *Ann Biomed Eng,* 41**,** 327-37.

CHENG, M., QIN, G. 2012. Progenitor cell mobilization and recruitment: SDF-1, CXCR4, α4-integrin, and c-kit. *Prog Mol Biol Transl Sci*, 111, 243-264.

CHENG, N. C., CHEN, S. Y., LI, J. R. & YOUNG, T. H. 2013. Short-term spheroid formation enhances the regenerative capacity of adipose-derived stem cells by promoting stemness, angiogenesis, and chemotaxis. *Stem Cells Transl Med,* 2**,** 584-94.

CHEN, W., HUANG, Y., HAN, J., YU, L., LI, Y., LU, Z., LI, H., LIU, Z., SHI, C., DUAN, F. & XIAO, Y. 2016. Immunomodulatory effects of mesenchymal stromal cells-derived exosome. *Immunol Res,* 64**,** 831-40.

CHOUDHERY, M. S., BADOWSKI, M., MUISE, A., PIERCE, J. & HARRIS, D. T. 2014. Donor age negatively impacts adipose tissue-derived mesenchymal stem cell expansion and differentiation. *J Transl Med,* 12**,** 8.

CHOI, E. Y., SANTOSO, S. & CHAVAKIS, T. 2009. Mechanisms of neutrophil transendothelial migration. *Front Biosci (Landmark Ed),* 14**,** 1596-605.

CLINICAL TRIAL.GOV, Mesenchymal stem cells, viewed 20 September 2020. https://clinicaltrials.gov/ct2/results?recrs=ab&cond=&term=Mesenchymal+stem+cells&cntry=&state=&city=&dist=

COLLARD, C. D. & GELMAN, S. 2001. Pathophysiology, clinical manifestations, and prevention of ischemia-reperfusion injury. *Anesthesiology,* 94**,** 1133-8.

COPPIN, L., SOKAL, E., STEPHENNE, X. 2019. Thrombogenic Risk induced by intravascular mesenchymal stem cell therapy: current status and future perspectives. *Cells*, 8, 1160.

COUFFINHAL, T., DUPLAA, C., LABAT, L., LAMAZIERE, J. M., MOREAU, C., PRINTSEVA, O. & BONNET, J. 1993. Tumor necrosis factor-alpha stimulates ICAM-1 expression in human vascular smooth muscle cells. *Arterioscler Thromb,* 13**,** 407-14.

COURTIES, G., HEIDT, T., SEBAS, M., IWAMOTO, Y., JEON, D., TRUELOVE, J., TRICOT, B., WOJTKIEWICZ, G., DUTTA, P., SAGER, H. B., BORODOVSKY, A., NOVOBRANTSEVA, T., KLEBANOV, B., FITZGERALD, K., ANDERSON, D. G., LIBBY, P., SWIRSKI, F. K., WEISSLEDER, R. & NAHRENDORF, M. 2014. In vivo silencing of the transcription factor IRF5 reprograms the macrophage phenotype and improves infarct healing. *J Am Coll Cardiol,* 63**,** 1556-66.

CURTIS, W. E., GILLINOV, A. M., WILSON, I. C., BATOR, J. M., BURCH, R. M., CAMERON, D. E. & GARDNER, T. J. 1993. Inhibition of neutrophil adhesion reduces myocardial infarct size. *Ann Thorac Surg,* 56**,** 1069-72; discussion 1072-3.

DA COSTA GONCALVES, F., GRINGS, M., NUNES, N. S., PINTO, F. O., GARCEZ, T. N., VISIOLI, F., LEIPNITZ, G. & PAZ, A. H. 2017. Antioxidant properties of mesenchymal stem cells against oxidative stress in a murine model of colitis. *Biotechnol Lett,* 39**,** 613-622.

DA, Q., DERRY, P. J., LAM, F. W. & RUMBAUT, R. E. 2018. Fluorescent labeling of endogenous platelets for intravital microscopy: Effects on platelet function. *Microcirculation,* 25**,** e12457.

DE BECKER, A. & RIET, I. V. 2016. Homing and migration of mesenchymal stromal cells: How to improve the efficacy of cell therapy? *World J Stem Cells,* 8**,** 73-87.

DE GODOY, M. A., SARAIVA, L. M., DE CARVALHO, L. R. P., VASCONCELOS-DOS-SANTOS, A., BEIRAL, H. J. V., RAMOS, A. B., SILVA, L. R. P., LEAL, R. B., MONTEIRO, V. H. S., BRAGA, C. V., DE ARAUJO-SILVA, C. A., SINIS, L. C., BODART-SANTOS, V., KASAI-BRUNSWICK, T. H., ALCANTARA, C. L., LIMA, A., DA CUNHA, E. S. N. L., GALINA, A., VIEYRA, A., DE FELICE, F. G., MENDEZ-OTERO, R. & FERREIRA, S. T. 2018. Mesenchymal stem cells and cell-derived extracellular vesicles protect hippocampal neurons from oxidative stress and synapse damage induced by amyloid-beta oligomers. *J Biol Chem,* 293**,** 1957-1975.

DE MARIS, G.L., CUCULI, F., PATEL, N., DAWKIN, S., FAHRNI, G., KASSIMIS, G., CHOUDHURY, R.P., FORFAR, J.C., PREDERGAST, B.D., CHANNON, K.M., KHARBANDA, R.K.,BANNIN, A.P. 2015. How does coronary stent implantation impact on the status of the microcirculation during primary percutaneous coronary intervention in patients with ST-elevation myocardial infarction? , 36, 3165-77.

DEYNOUX, M., SUNTER, N., DUCROCQ, E., DAKIK, H., GUIBON, R., BURLAUD-GAILLARD, J., BRISSON, L., ROULEUX-BONNIN, F., LE NAIL, L. R., HERAULT, O., DOMENECH, J., ROINGEARD, P., FROMONT, G. & MAZURIER, F. 2020. A comparative study of the capacity of mesenchymal stromal cell lines to form spheroids. *PLoS One,* 15**,** e0225485.

DOZZA, B., LESCI, I. G., DUCHI, S., DELLA BELLA, E., MARTINI, L., SALAMANNA, F., FALCONI, M., CINOTTI, S., FINI, M., LUCARELLI, E. & DONATI, D. 2017. When size matters: differences in demineralized bone matrix particles affect collagen structure, mesenchymal stem cell behavior, and osteogenic potential. *J Biomed Mater Res A,* 105**,** 1019-1033.

EGGER, D., TRIPISCIANO, C., WEBER, V., DOMINICI, M. & KASPER, C. 2018. Dynamic Cultivation of Mesenchymal Stem Cell Aggregates. *Bioengineering (Basel),* 5.

EGGENHOFER, E., LUK, F., DAHLKE, M. H. & HOOGDUIJN, M. J. 2014. The life and fate of mesenchymal stem cells. *Front Immunol,* 5**,** 148.

EISINGER, F., PATZELT, J. & LANGER, H. F. 2018. The Platelet Response to Tissue Injury. *Front Med (Lausanne),* 5**,** 317.

ELEUTERI, S. & FIERABRACCI, A. 2019. Insights into the Secretome of Mesenchymal Stem Cells and Its Potential Applications. *Int J Mol Sci,* 20.

FAULKNOR, R. A., OLEKSON, M. A., EKWUEME, E. C., KRZYSZCZYK, P., FREEMAN, J. W. & BERTHIAUME, F. 2017. Hypoxia Impairs Mesenchymal Stromal Cell-Induced Macrophage M1 to M2 Transition. *Technology (Singap World Sci),* 5**,** 81-86.

FEARON, W. F. & KOBAYASHI, Y. 2017. Invasive Assessment of the Coronary Microvasculature: The Index of Microcirculatory Resistance. *Circ Cardiovasc Interv,* 10.

FENG, J., MANTESSO, A., DE BARI, C., NISHIYAMA, A. & SHARPE, P. T. 2011. Dual origin of mesenchymal stem cells contributing to organ growth and repair. *Proc Natl Acad Sci U S A,* 108**,** 6503-8.

FERREIRA, J. R., TEIXEIRA, G. Q., SANTOS, S. G., BARBOSA, M. A., ALMEIDA-PORADA, G. & GONCALVES, R. M. 2018. Mesenchymal Stromal Cell Secretome: Influencing Therapeutic Potential by Cellular Pre-conditioning. *Front Immunol,* 9**,** 2837.

FISCHER, U. M., HARTING, M. T., JIMENEZ, F., MONZON-POSADAS, W. O., XUE, H., SAVITZ, S. I., LAINE, G. A. & COX, C. S., JR. 2009. Pulmonary passage is a major obstacle for intravenous stem cell delivery: the pulmonary first-pass effect. *Stem Cells Dev,* 18**,** 683-92.

FILIPPI, M. D. 2019. Neutrophil transendothelial migration: updates and new perspectives. *Blood,* 133**,** 2149-2158.

FLETCHER, D. A. & MULLINS, R. D. 2010. Cell mechanics and the cytoskeleton. *Nature,* 463**,** 485-92.

FONG, E. L., CHAN, C. K. & GOODMAN, S. B. 2011. Stem cell homing in musculoskeletal injury. *Biomaterials,* 32**,** 395-409.

FUSTER, V. Top 10 cardiovascular therapies and interventions for the next decade. 2014. *Nat Rev Cardiol*, 11, 671-683.

FONG, E. L., CHAN, C. K. & GOODMAN, S. B. 2011. Stem cell homing in musculoskeletal injury. *Biomaterials,* 32**,** 395-409.

FRIEDENSTEIN, A. J., PETRAKOVA, K. V., KUROLESOVA, A. I. & FROLOVA, G. P. 1968. Heterotopic of bone marrow. Analysis of precursor cells for osteogenic and hematopoietic tissues. *Transplantation,* 6**,** 230-47.

FRITH, J. E., THOMSON, B. & GENEVER, P. G. 2010. Dynamic three-dimensional culture methods enhance mesenchymal stem cell properties and increase therapeutic potential. *Tissue Eng Part C Methods,* 16**,** 735-49.

FROHLICH, G. M., MEIER, P., WHITE, S. K., YELLON, D. M. & HAUSENLOY, D. J. 2013. Myocardial reperfusion injury: looking beyond primary PCI. *Eur Heart J,* 34**,** 1714-22.

FU, X., LIU, G., HALIM, A., JU, Y., LUO, Q. & SONG, A. G. 2019. Mesenchymal Stem Cell Migration and Tissue Repair. *Cells,* 8.

GARCIA-DORADO, D., RUIZ-MEANA, M. & PIPER, H. M. 2009. Lethal reperfusion injury in acute myocardial infarction: facts and unresolved issues. *Cardiovasc Res,* 83**,** 165-8.

GAWAZ, M., LANGER, H. & MAY, A. E. 2005. Platelets in inflammation and atherogenesis. *J Clin Invest,* 115**,** 3378-84.

GAVINS, F. N. & CHATTERJEE, B. E. 2004. Intravital microscopy for the study of mouse microcirculation in anti-inflammatory drug research: focus on the mesentery and cremaster preparations. *J Pharmacol Toxicol Methods,* 49**,** 1-14.

GERSH, B. J., STONE, G. W., WHITE, H. D. & HOLMES, D. R., JR. 2005. Pharmacological facilitation of primary percutaneous coronary intervention for acute myocardial infarction: is the slope of the curve the shape of the future? *JAMA,* 293**,** 979-86.

GHADRDOOST, B., KHOSHRAVESH, R., ABOUTALEB, N., AMIRFARHANGI, A., DASHTI, S. & AZIZI, Y. 2018. Heparin Enhances the Effects of Mesenchymal Stem Cell Transplantation in a Rabbit Model of Acute Myocardial Infarction. *Niger J Physiol Sci,* 33**,** 9-15.

GLEESON, B. M., MARTIN, K., ALI, M. T., KUMAR, A. H., PILLAI, M. G., KUMAR, S. P., O'SULLIVAN, J. F., WHELAN, D., STOCCA, A., KHIDER, W., BARRY, F. P., O'BRIEN, T. & CAPLICE, N. M. 2015. Bone Marrow-Derived Mesenchymal Stem Cells Have Innate Procoagulant Activity and Cause Microvascular Obstruction Following Intracoronary Delivery: Amelioration by Antithrombin Therapy. *Stem Cells,* 33**,** 2726-37.

GÓMEZ-CONDE, I., CAETANO, S. S., TADOKORO, C. E. & OLIVIERI, D. N. 2015. Stabilizing 3D in vivo intravital microscopy images with an iteratively refined soft-tissue model for immunology experiments. *Computers in Biology and Medicine,* 64**,** 246-260.

GONZALEZ-APARICIO, M. & ALFARO, C. 2019. Influence of Interleukin-8 and Neutrophil Extracellular Trap (NET) Formation in the Tumor Microenvironment: Is There a Pathogenic Role? *J Immunol Res,* 2019**,** 6252138.

GORENEK, B., BLOMSTROM LUNDQVIST, C., BRUGADA TERRADELLAS, J., CAMM, A. J., HINDRICKS, G., HUBER, K., KIRCHHOF, P., KUCK, K. H., KUDAIBERDIEVA, G., LIN, T., RAVIELE, A., SANTINI, M., TILZ, R. R., VALGIMIGLI, M., VOS, M. A., VRINTS, C., ZEYMER, U., LIP, G. Y., POTPARA, T., FAUCHIER, L., STICHERLING, C., ROFFI, M., WIDIMSKY, P., MEHILLI, J., LETTINO, M., SCHIELE, F., SINNAEVE, P., BORIANI, G., LANE, D. & SAVELIEVA, I. 2014. Cardiac arrhythmias in acute coronary syndromes: position paper from the joint EHRA, ACCA, and EAPCI task force. *Europace,* 16**,** 1655-73.

GORENEK, B., LUNDQVIST, C. B., TERRADELLAS, J. B., CAMM, A. J., HINDRICKS, G., HUBER, K., KIRCHHOF, P., KUCK, K. H., KUDAIBERDIEVA, G., LIN, T., RAVIELE, A., SANTINI, M., TILZ, R. R., VALGIMIGLI, M., VOS, M. A., VRINTS, C. & ZEYMER, U. 2015. Cardiac arrhythmias in acute coronary syndromes: position paper from the joint EHRA, ACCA, and EAPCI task force. *Eur Heart J Acute Cardiovasc Care,* 4**,** 386.

GRANGER, D. N. 1988. Role of xanthine oxidase and granulocytes in ischemia-reperfusion injury. *Am J Physiol,* 255**,** H1269-75.

GRANGER, D. N., KVIETYS, P.R., 2015. Reperfusion injury and reactive oxygen species; the evolution of a concept. *Redox Biology*, 6, 524-551.

GRIENDLING, K. K., TOUYZ, R. M., ZWEIER, J. L., DIKALOV, S., CHILIAN, W., CHEN, Y. R., HARRISON, D. G., BHATNAGAR, A. & AMERICAN HEART ASSOCIATION COUNCIL ON BASIC CARDIOVASCULAR, S. 2016. Measurement of Reactive Oxygen Species, Reactive Nitrogen Species, and Redox-Dependent Signaling in the Cardiovascular System: A Scientific Statement From the American Heart Association. *Circ Res,* 119**,** e39-75.

GUO, L., GE, J., ZHOU, Y., WANG, S., ZHAO, R. C. & WU, Y. 2014. Three-dimensional spheroid-cultured mesenchymal stem cells devoid of embolism attenuate brain stroke injury after intra-arterial injection. *Stem Cells Dev,* 23**,** 978-89.

GUPTA, S. & GUPTA, M. M. 2016. No reflow phenomenon in percutaneous coronary interventions in ST-segment elevation myocardial infarction. *Indian Heart J,* 68**,** 539-51.

GUSTIN, J.K., DOUGLAS, J.L. 2013. BST-2/tetherin: viral tether, viral sensor or both?. *Future virology*, 8,11, 10.2217/fvl.13.96.

HAN, H., HU, J., YAN, Q., ZHU, J., ZHU, Z., CHEN, Y., SUN, J. & ZHANG, R. 2016. Bone marrow-derived mesenchymal stem cells rescue injured H9c2 cells via transferring intact mitochondria through tunneling nanotubes in an in vitro simulated ischemia/reperfusion model. *Mol Med Rep,* 13**,** 1517-24.

HARRELL, C. R., FELLABAUM, C., JOVICIC, N., DJONOV, V., ARSENIJEVIC, N. & VOLAREVIC, V. 2019. Molecular Mechanisms Responsible for Therapeutic Potential of Mesenchymal Stem Cell-Derived Secretome. *Cells,* 8.

HASENFUSS, G. & TEERLINK, J. R. 2011. Cardiac inotropes: current agents and future directions. *Eur Heart J,* 32**,** 1838-45.

HAUSENLOY, D. J. & YELLON, D. M. 2013. Myocardial ischemia-reperfusion injury: a neglected therapeutic target. *J Clin Invest,* 123**,** 92-100.

HAUSENLOY, D. J. & YELLON, D. M. 2016. Ischaemic conditioning and reperfusion injury. *Nat Rev Cardiol,* 13**,** 193-209.

HAUSENLOY, D. J., CHILLIAN, W., CREA, F., DAVIDSON, S.M., FERDINANDY, P., GARCIA-DORADO, D., VAN ROYEN, N., SCHULTZ, R., HEUSCH, G. 2019. The coronary circulation in acute myocardial ischaemia/reperfusion injury: a target for cardioprotection. *Cardiovasc Res,* 115, 1143-1155.

HMADCHA, A., MARTIN-MONTALVO, A., GAUTHIER, B. R., SORIA, B. & CAPILLA-GONZALEZ, V. 2020. Therapeutic Potential of Mesenchymal Stem Cells for Cancer Therapy. *Front Bioeng Biotechnol,* 8**,** 43.

HOCDE, S. A., HYRIEN, O. & WAUGH, R. E. 2009. Cell adhesion molecule distribution relative to neutrophil surface topography assessed by TIRFM. *Biophys J,* 97**,** 379-87.

HONCZARENKO, M., LE, Y., SWIERKOWSKI, M., GHIRAN, I., GLODEK, A. M. & SILBERSTEIN, L. E. 2006. Human bone marrow stromal cells express a distinct set of biologically functional chemokine receptors. *Stem Cells,* 24**,** 1030-41.

HORWITZ, E.M., LE BLANC, K., DOMINICI, M., MUELLER, I., SLAPER-CORTENBACH, I., MARINI, F.C., DEANS, R.J., KRAUSE, D.S., KEATING, A. 2005. Clarification of the nomenclature for MSC: The International Society for Cellular Therapy position statement. *Cytotherapy*, 7(5), 393-395.

HOWE, G.A., ADDISON, C.L. 2012. β1 integrin: an emerging player in the modulation of tumorigenesis and response to therapy. *Cell Adh Migr*, 6(2), 71-77.

HSU, P. J., LIU, K. J., CHAO, Y. Y., SYTWU, H. K. & YEN, B. L. 2015. Assessment of the Immunomodulatory Properties of Human Mesenchymal Stem Cells (MSCs). *J Vis Exp*, e53265.

HU, C. & LI, L. 2019. The immunoregulation of mesenchymal stem cells plays a critical role in improving the prognosis of liver transplantation. *J Transl Med,* 17**,** 412.

HUANG, P., WANG, L., LI, Q., XU, J., XU, J., XIONG, Y., CHEN, G., QIAN, H., JIN, C., YU, Y., LIU, J., QIAN, L. & YANG, Y. 2019. Combinatorial treatment of acute myocardial infarction using stem cells and their derived exosomes resulted in improved heart performance. *Stem Cell Res Ther,* 10**,** 300.

HUSAIN, S., ANDREWS, N. P., MULCAHY, D., PANZA, J. A. & QUYYUMI, A. A. 1998. Aspirin improves endothelial dysfunction in atherosclerosis. *Circulation,* 97**,** 716-20.

HUYGEN, S., GIET, O., ARTISIEN, V., DI STEFANO, I., BEGUIN, Y. & GOTHOT, A. 2002. Adhesion of synchronized human hematopoietic progenitor cells to fibronectin and vascular cell adhesion molecule-1 fluctuates reversibly during cell cycle transit in ex vivo culture. *Blood,* 100**,** 2744-52.

HYNES, R. O. 1992. Integrins: versatility, modulation, and signaling in cell adhesion. *Cell,* 69**,** 11-25.

IBANEZ, B., HEUSCH, G., OVIZE, M. & VAN DE WERF, F. 2015. Evolving therapies for myocardial ischemia/reperfusion injury. *J Am Coll Cardiol,* 65**,** 1454-71.

IKEDA, U., HOJO, Y., KATSUKI, T. & SHIMADA, K. 1999. Procoagulant and proinflammatory activity in acute coronary syndromes. *Cardiovasc Res,* 42**,** 823, author reply 825.

ISE, H., MATSUNAGA, K., SHINOHARA, M. & SAKAI, Y. 2019. Improved Isolation of Mesenchymal Stem Cells Based on Interactions between N-Acetylglucosamine-Bearing Polymers and Cell-Surface Vimentin. *Stem Cells Int,* 2019**,** 4341286.

ITO, H. 2006. No-reflow phenomenon and prognosis in patients with acute myocardial infarction. *Nat Clin Pract Cardiovasc Med,* 3**,** 499-506.

JAAKKOLA, K., JALKANEN, S., KAUNISMAKI, K., VANTTINEN, E., SAUKKO, P., ALANEN, K., KALLAJOKI, M., VOIPIO-PULKKI, L. M. & SALMI, M. 2000. Vascular adhesion protein-

1, intercellular adhesion molecule-1 and P-selectin mediate leukocyte binding to ischemic heart in humans. *J Am Coll Cardiol,* 36**,** 122-9.

JAFFE, R., CHARRON, T., PULEY, G., DICK, A. & STRAUSS, B. H. 2008. Microvascular obstruction and the no-reflow phenomenon after percutaneous coronary intervention. *Circulation,* 117**,** 3152-6.

JANSSENS, S., DUBOIS, C., BOGAERT, J., THEUNISSEN, K., DEROOSE, C., DESMET, W., KALANTZI, M., HERBOTS, L., SINNAEVE, P., DENS, J., MAERTENS, J., RADEMAKERS, F., DYMARKOWSKI, S., GHEYSENS, O., VAN CLEEMPUT, J., BORMANS, G., NUYTS, J., BELMANS, A., MORTELMANS, L., BOOGAERTS, M. & VAN DE WERF, F. 2006. Autologous bone marrow-derived stem-cell transfer in patients with ST-segment elevation myocardial infarction: double-blind, randomised controlled trial. *Lancet,* 367**,** 113-21.

JAMES, S., FOX, J., AFSARI, F., LEE, J., CLOUGH, S., KNIGHT, C., ASHMORE, J., ASHTON, P., PREHAM, O., HOOGDUIJN, M., PONZONI RDE, A., HANCOCK, Y., COLES, M. & GENEVER, P. 2015. Multiparameter Analysis of Human Bone Marrow Stromal Cells Identifies Distinct Immunomodulatory and Differentiation-Competent Subtypes. *Stem Cell Reports,* 4**,** 1004-15.

JAUKOVIC, A., ABADJIEVA, D., TRIVANOVIC, D., STOYANOVA, E., KOSTADINOVA, M., PASHOVA, S., KESTENDJIEVA, S., KUKOLJ, T., JESETA, M., KISTANOVA, E. & MOURDJEVA, M. 2020b. Specificity of 3D MSC Spheroids Microenvironment: Impact on MSC Behavior and Properties. *Stem Cell Rev Rep,* 16**,** 853-875.

JENNINGS, R.B., SOMMERS, H.M., SMYTH, G.A., FLACK, H.A. , LINN, H. 1960. Myocardial necrosis induced by temporary occlusion of a coronary artery in the dog. *Pathology*, 70, 68–78.

JIANG, W. & XU, J. 2020. Immune modulation by mesenchymal stem cells. *Cell Prolif,* 53**,** e12712.

JIMENEZ-PUERTA, G.J., MARCHAL, J.A., LOPEZ-RUIZ, E., GALVEZ-MARTIN, P.2020. Role of Mesenchymal Stromal Cells as Therapeutic Agents: Potential Mechanisms of Action and Implications in Their Clinical Use. *J Clin Med*, 9(2), 445.

JOEL, M. D. M., YUAN, J., WANG, J., YAN, Y., QIAN, H., ZHANG, X., XU, W. & MAO, F. 2019. MSC: immunoregulatory effects, roles on neutrophils and evolving clinical potentials. *Am J Transl Res,* 11**,** 3890-3904.

JONES, J. S., SMALL, D. M. & NISHIMURA, N. 2018. In Vivo Calcium Imaging of Cardiomyocytes in the Beating Mouse Heart With Multiphoton Microscopy. *Frontiers in Physiology,* 9.

JONG, W. M., TEN CATE, H., LINNENBANK, A. C., DE BOER, O. J., REITSMA, P. H., DE WINTER, R. J. & ZUURBIER, C. J. 2016. Reduced acute myocardial ischemia-reperfusion injury in IL-6-deficient mice employing a closed-chest model. *Inflamm Res,* 65**,** 489-99.

JUNG, K., KIM, P., LEUSCHNER, F., GORBATOV, R., KIM, J. K., UENO, T., NAHRENDORF, M. & YUN, S. H. 2013. Endoscopic time-lapse imaging of immune cells in infarcted mouse hearts. *Circ Res,* 112**,** 891-9.

JUNG, K.J., Lee, G.W., PARK, C.H., LEE, T.J., KIM, J.Y., SUNG, E.G., KIM, S.Y., JANG, B.I.,SONG, I.H. 2020. Mesenchymal Stem Cells Decrease Oxidative Stress in the Bowels of Interleukin-10 Knockout Mice. *Gut Liver*, 14, 100-107.

KAKIMOTO, Y., TSURUYAMA, T., MIYAO, M., ABIRU, H., SUMIYOSHI, S., KOTANI, H., HAGA, H. & TAMAKI, K. 2013. The effectiveness and limitations of triphenyltetrazolium chloride to detect acute myocardial infarction at forensic autopsy. *Am J Forensic Med Pathol,* 34**,** 242-7.

KALIA, N., POCKLEY, A. G., WOOD, R. F. & BROWN, N. J. 2002. Effects of hypothermia and rewarming on the mucosal villus microcirculation and survival after rat intestinal ischemia-reperfusion injury. *Ann Surg,* 236**,** 67-74.

KALOGERIS, T., BAINES, C. P., KRENZ, M. & KORTHUIS, R. J. 2012. Cell biology of ischemia/reperfusion injury. *Int Rev Cell Mol Biol,* 298**,** 229-317.

KALOGERIS, T., BAINES, C. P., KRENZ, M. & KORTHUIS, R. J. 2016. Ischemia/Reperfusion. *Compr Physiol,* 7**,** 113-170.

KANY, S., VOLLRATH, J. T. & RELJA, B. 2019. Cytokines in Inflammatory Disease. *Int J Mol Sci,* 20.

KARANTALIS, V. & HARE, J. M. 2015. Use of mesenchymal stem cells for therapy of cardiac disease. *Circ Res,* 116**,** 1413-30.

KAUKUA, N., SHAHIDI, M. K., KONSTANTINIDOU, C., DYACHUK, V., KAUCKA, M., FURLAN, A., AN, Z., WANG, L., HULTMAN, I., AHRLUND-RICHTER, L., BLOM, H., BRISMAR, H., LOPES, N. A., PACHNIS, V., SUTER, U., CLEVERS, H., THESLEFF, I., SHARPE, P., ERNFORS, P., FRIED, K. & ADAMEYKO, I. 2014. Glial origin of mesenchymal stem cells in a tooth model system. *Nature,* 513**,** 551-4.

KAVANAGH, D. P., DURANT, L. E., CROSBY, H. A., LALOR, P. F., FRAMPTON, J., ADAMS, D. H. & KALIA, N. 2010. Haematopoietic stem cell recruitment to injured murine liver sinusoids depends on (alpha)4(beta)1 integrin/VCAM-1 interactions. *Gut,* 59**,** 79-87.

KAVANAGH, D. P., SURESH, S., NEWSOME, P. N., FRAMPTON, J. & KALIA, N. 2015. Pretreatment of Mesenchymal Stem Cells Manipulates Their Vasculoprotective Potential While Not Altering Their Homing Within the Injured Gut. *Stem Cells,* 33**,** 2785-97.

KAVANAGH, D. P., YEMM, A. I., ALEXANDER, J. S., FRAMPTON, J. & KALIA, N. 2013. Enhancing the adhesion of hematopoietic precursor cell integrins with hydrogen peroxide increases recruitment within murine gut. *Cell Transplant,* 22**,** 1485-99.

KAVANAGH, D. P. J., GALLAGHER, M. T. & KALIA, N. 2019a. Tify: A quality-based frame selection tool for improving the output of unstable biomedical imaging. *PLOS ONE,* 14**,** e0213162.

KAVANAGH, D. P. J., LOKMAN, A. B., NEAG, G., COLLEY, A. & KALIA, N. 2019c. Imaging the injured beating heart intravitally and the vasculoprotection afforded by haematopoietic stem cells. *Cardiovasc Res,* 115**,** 1918-1932.

KAY, A.G., STONE, A., FOX, J.M., GENEVER, P.G. 2018. CD317 profiling distinguishes bone marrow stromal cell subtypes with distinct functional impact upon T cell proliferation and polarisation. *Osteoarthritis and Cartilage,* 26, 296-s297.

KEAN, T. J., LIN, P., CAPLAN, A. I. & DENNIS, J. E. 2013. MSCs: Delivery Routes and Engraftment, Cell-Targeting Strategies, and Immune Modulation. *Stem Cells Int,* 2013**,** 732742.

KIDD, S., SPAETH, E., DEMBINSKI, J. L., DIETRICH, M., WATSON, K., KLOPP, A., BATTULA, V. L., WEIL, M., ANDREEFF, M. & MARINI, F. C. 2009. Direct evidence of mesenchymal stem cell tropism for tumor and wounding microenvironments using in vivo bioluminescent imaging. *Stem Cells,* 27**,** 2614-23.

KIM, H., DARWISH, I., MONROY, M. F., PROCKOP, D. J., LILES, W. C. & KAIN, K. C. 2014. Mesenchymal stromal (stem) cells suppress pro-inflammatory cytokine production but fail to improve survival in experimental staphylococcal toxic shock syndrome. *BMC Immunol,* 15**,** 1.

KIM, Y. S., KIM, J. Y., SHIN, D. M., HUH, J. W., LEE, S. W. & OH, Y. M. 2014. Tracking intravenous adipose-derived mesenchymal stem cells in a model of elastase-induced emphysema. *Tuberc Respir Dis (Seoul),* 77**,** 116-23.

KLONER, R. A. 2020. Stunned and Hibernating Myocardium: Where Are We Nearly 4 Decades Later? *J Am Heart Assoc,* 9**,** e015502.

KLONER, R. A., BOLLI, R., MARBAN, E., REINLIB, L. & BRAUNWALD, E. 1998. Medical and cellular implications of stunning, hibernation, and preconditioning: an NHLBI workshop. *Circulation,* 97**,** 1848-67.

KLONER, R. A., RUDE, R. E., CARLSON, N., MAROKO, P. R., DEBOER, L. W. & BRAUNWALD, E. 1980. Ultrastructural evidence of microvascular damage and myocardial cell injury after coronary artery occlusion: which comes first? *Circulation,* 62**,** 945-52.

KONARI, N., NAGAISHI, K., KIKUCHI, S. & FUJIMIYA, M. 2019. Mitochondria transfer from mesenchymal stem cells structurally and functionally repairs renal proximal tubular epithelial cells in diabetic nephropathy in vivo. *Sci Rep,* 9**,** 5184.

KOTA, D. J., PRABHAKARA, K. S., TOLEDANO-FURMAN, N., BHATTARAI, D., CHEN, Q., DICARLO, B., SMITH, P., TRIOLO, F., WENZEL, P. L., COX, C. S., JR. & OLSON, S. D. 2017. Prostaglandin E2 Indicates Therapeutic Efficacy of Mesenchymal Stem Cells in Experimental Traumatic Brain Injury. *Stem Cells,* 35**,** 1416-1430.

KOZHURA, V. L., BASARAB, D. A., TIMKINA, M. I., GOLUBEV, A. M., RESHETNYAK, V. I. & MOROZ, V. V. 2005. Reperfusion injury after critical intestinal ischemia and its correction with perfluorochemical emulsion "perftoran". *World J Gastroenterol,* 11**,** 7084-90.

KRAMPERA, M., PASINI, A., RIGO, A., SCUPOLI, M. T., TECCHIO, C., MALPELI, G., SCARPA, A., DAZZI, F., PIZZOLO, G. & VINANTE, F. 2005. HB-EGF/HER-1 signaling in bone marrow mesenchymal stem cells: inducing cell expansion and reversibly preventing multilineage differentiation. *Blood,* 106**,** 59-66.

KRUEGER, T. E. G., THOREK, D. L. J., DENMEADE, S. R., ISAACS, J. T. & BRENNEN, W. N. 2018. Concise Review: Mesenchymal Stem Cell-Based Drug Delivery: The Good, the Bad, the Ugly, and the Promise. *Stem Cells Transl Med,* 7**,** 651-663.

KSIAZEK, K. 2009. A comprehensive review on mesenchymal stem cell growth and senescence. *Rejuvenation Res,* 12, 105-116.

KVIETYS, P. R. & GRANGER, D. N. 2012. Role of reactive oxygen and nitrogen species in the vascular responses to inflammation. *Free Radic Biol Med,* 52**,** 556-92.

KUCI, S., KUCI, Z., KREYENBERG, H., DEAK, E., PUTSCH, K., HUENECKE, S., AMARA, C., KOLLER, S., RETTINGER, E., GREZ, M., KOEHL, U., LATIFI-PUPOVCI, H., HENSCHLER, R., TONN, T., VON LAER, D., KLINGEBIEL, T. & BADER, P. 2010. CD271 antigen defines a subset of multipotent stromal cells with immunosuppressive and lymphohematopoietic engraftment-promoting properties. *Haematologica,* 95**,** 651-9.

LAM, F. W., VIJAYAN, K. V. & RUMBAUT, R. E. 2015. Platelets and Their Interactions with Other Immune Cells. *Compr Physiol,* 5**,** 1265-80.

LANGLEY, R. R., RAMIREZ, K. M., TSAN, R. Z., VAN ARSDALL, M., NILSSON, M. B. & FIDLER, I. J. 2003. Tissue-specific microvascular endothelial cell lines from H-2K(b)-tsA58 mice for studies of angiogenesis and metastasis. *Cancer Res,* 63**,** 2971-6.

LEE, C. Y., KIM, R., HAM, O., LEE, J., KIM, P., LEE, S., OH, S., LEE, H., LEE, M., KIM, J. & CHANG, W. 2016. Therapeutic Potential of Stem Cells Strategy for Cardiovascular Diseases. *Stem Cells Int,* 2016**,** 4285938.

LEE, S., VINEGONI, C., FERUGLIO, P. F., FEXON, L., GORBATOV, R., PIVORAVOV, M., SBARBATI, A., NAHRENDORF, M. & WEISSLEDER, R. 2012. Real-time in vivo imaging of the beating mouse heart at microscopic resolution. *Nat Commun,* 3**,** 1054.

LEMASTERS, J. J., BOND, J. M., CHACON, E., HARPER, I. S., KAPLAN, S. H., OHATA, H., TROLLINGER, D. R., HERMAN, B. & CASCIO, W. E. 1996. The pH paradox in ischemia-reperfusion injury to cardiac myocytes. *EXS,* 76**,** 99-114.

LEUCKER, T. M., GE, Z. D., PROCKNOW, J., LIU, Y., SHI, Y., BIENENGRAEBER, M., WARLTIER, D. C. & KERSTEN, J. R. 2013. Impairment of endothelial-myocardial interaction increases the susceptibility of cardiomyocytes to ischemia/reperfusion injury. *PLoS One,* 8**,** e70088.

LEVY, O., KUAI, R., SIREN, E. M. J., BHERE, D., MILTON, Y., NISSAR, N., DE BIASIO, M., HEINELT, M., REEVE, B., ABDI, R., ALTURKI, M., FALLATAH, M., ALMALIK, A., ALHASAN, A. H., SHAH, K. & KARP, J. M. 2020. Shattering barriers toward clinically meaningful MSC therapies. *Sci Adv,* 6**,** eaba6884.

LEY, K., LAUDANNA, C., CYBULSKY, M. I. & NOURSHARGH, S. 2007. Getting to the site of inflammation: the leukocyte adhesion cascade updated. *Nat Rev Immunol,* 7**,** 678-89.

LEY, K. 2017. M1 Means Kill; M2 Means Heal. *J Immunol,* 199**,** 2191-2193.

LI, L., CHU, L., FANG, Y., YANG, Y., QU, T., ZHANG, J., YIN, Y. & GU, J. 2017. Preconditioning of bone marrow-derived mesenchymal stromal cells by tetramethylpyrazine enhances cell migration and improves functional recovery after focal cerebral ischemia in rats. *Stem Cell Res Ther,* 8**,** 112.

LI, X., LIU, M., SUN, R., ZENG, Y., CHEN, S. & ZHANG, P. 2016. Protective approaches against myocardial ischemia reperfusion injury. *Exp Ther Med,* 12**,** 3823-3829.

LIAO, L., SHI, B., CHANG, H., SU, X., ZHANG, L., BI, C., SHUAI, Y., DU, X., DENG, Z. & JIN, Y. 2017. Heparin improves BMSC cell therapy: Anticoagulant treatment by heparin improves the safety and therapeutic effect of bone marrow-derived mesenchymal stem cell cytotherapy. *Theranostics,* 7**,** 106-116.

LIN, R. Z., CHOU, L. F., CHIEN, C. C. & CHANG, H. Y. 2006. Dynamic analysis of hepatoma spheroid formation: roles of E-cadherin and beta1-integrin. *Cell Tissue Res,* 324**,** 411-22.

LIN, W., XU, L., ZWINGENBERGER, S., GIBON, E., GOODMAN, S. B. & LI, G. 2017. Mesenchymal stem cells homing to improve bone healing. *J Orthop Translat,* 9**,** 19-27.

LINFERT, D., CHOWDHRY, T. & RABB, H. 2009. Lymphocytes and ischemia-reperfusion injury. *Transplant Rev (Orlando),* 23**,** 1-10.

LIU, J. H., WANN, H., CHEN, M. M., PAN, W. H., CHEN, Y. C., LIU, C. M., YEH, M. Y., TSAI, S. K., YOUNG, M. S., CHUANG, H. Y., CHAO, F. P. & CHAO, H. M. 2010. Baicalein significantly protects human retinal pigment epithelium cells against H(2)O(2)-induced oxidative stress by scavenging reactive oxygen species and downregulating the expression of matrix metalloproteinase-9 and vascular endothelial growth factor. *J Ocul Pharmacol Ther,* 26**,** 421-9.

LIU, Z., KASTIS, G. A., STEVENSON, G. D., BARRETT, H. H., FURENLID, L. R., KUPINSKI, M. A., PATTON, D. D. & WILSON, D. W. 2002. Quantitative analysis of acute myocardial infarct in rat hearts with ischemia-reperfusion using a high-resolution stationary SPECT system. *J Nucl Med,* 43**,** 933-9.

LUGRIN, J., PARAPANOV, R., ROSENBLATT-VELIN, N., RIGNAULT-CLERC, S., FEIHL, F., WAEBER, B., MULLER, O., VERGELY, C., ZELLER, M., TARDIVEL, A., SCHNEIDER, P., PACHER, P. & LIAUDET, L. 2015. Cutting edge: IL-1alpha is a crucial danger signal triggering acute myocardial inflammation during myocardial infarction. *J Immunol,* 194**,** 499-503.

LUO, B. H., CARMAN, C. V. & SPRINGER, T. A. 2007. Structural basis of integrin regulation and signaling. *Annu Rev Immunol,* 25**,** 619-47.

LUSCHER, T.F. 2017. From epicardial coronary arteries to the coronary microcirculation: novel insights into a neglected issue. *Eur Heart J*, 38, 461-464.

MABUCHI, Y., MORIKAWA, S., HARADA, S., NIIBE, K., SUZUKI, S., RENAULT-MIHARA, F., HOULIHAN, D. D., AKAZAWA, C., OKANO, H. & MATSUZAKI, Y. 2013. LNGFR(+)THY-1(+)VCAM-1(hi+) cells reveal functionally distinct subpopulations in mesenchymal stem cells. *Stem Cell Reports,* 1**,** 152-65.

MADIGAN, M. & ATOUI, R. 2018. Therapeutic Use of Stem Cells for Myocardial Infarction. *Bioengineering,* 5.

MAFFIA, P., ZINSELMEYER, B. H., IALENTI, A., KENNEDY, S., BAKER, A. H., MCINNES, I. B., BREWER, J. M. & GARSIDE, P. 2007. Images in cardiovascular medicine. Multiphoton microscopy for 3-dimensional imaging of lymphocyte recruitment into apolipoprotein-E-deficient mouse carotid artery. *Circulation,* 115**,** e326-8

MAHROUF-YORGOV, M., AUGEUL, L., DA SILVA, C. C., JOURDAN, M., RIGOLET, M., MANIN, S., FERRERA, R., OVIZE, M., HENRY, A., GUGUIN, A., MENINGAUD, J. P., DUBOIS-RANDE, J. L., MOTTERLINI, R., FORESTI, R. & RODRIGUEZ, A. M. 2017. Mesenchymal stem cells sense mitochondria released from damaged cells as danger signals to activate their rescue properties. *Cell Death Differ,* 24**,** 1224-1238.

MALARSTIG, A., ERIKSSON, P., HAMSTEN, A., LINDAHL, B., WALLENTIN, L. & SIEGBAHN, A. 2008. Raised interleukin-10 is an indicator of poor outcome and enhanced systemic inflammation in patients with acute coronary syndrome. *Heart,* 94**,** 724-9.

MASSBERG, S., ENDERS, G., MATOS, F. C., TOMIC, L. I., LEIDERER, R., EISENMENGER, S., MESSMER, K. & KROMBACH, F. 1999. Fibrinogen deposition at the postischemic vessel wall promotes platelet adhesion during ischemia-reperfusion in vivo. *Blood,* 94**,** 3829-38.

MASTERSON, C. H., TABUCHI, A., HOGAN, G., FITZPATRICK, G., KERRIGAN, S. W., JERKIC, M., KUEBLER, W. M., LAFFEY, J. G. & CURLEY, G. F. 2021. Intra-vital imaging of mesenchymal stromal cell kinetics in the pulmonary vasculature during infection. *Sci Rep,* 11**,** 5265.

MARTINEZ, F. O. & GORDON, S. 2014. The M1 and M2 paradigm of macrophage activation: time for reassessment. *F1000Prime Rep,* 6**,** 13.

MASTROLIA, I., FOPPIANI, E. M., MURGIA, A., CANDINI, O., SAMARELLI, A. V., GRISENDI, G., VERONESI, E., HORWITZ, E. M. & DOMINICI, M. 2019. Challenges in Clinical Development of Mesenchymal Stromal/Stem Cells: Concise Review. *Stem Cells Transl Med,* 8**,** 1135-1148.

MATSUURA, R., MIYAGAWA, S., FUKUSHIMA, S., GOTO, T., HARADA, A., SHIMOZAKI, Y., YAMAKI, K., SANAMI, S., KIKUTA, J., ISHII, M. & SAWA, Y. 2018. Intravital imaging with two-photon microscopy reveals cellular dynamics in the ischeamia-reperfused rat heart. *Sci Rep,* 8**,** 15991.

MENDELSON, A., STRAT, A. N., BAO, W., ROSSTON, P., FALLON, G., OHRN, S., ZHONG, H., LOBO, C., AN, X. & YAZDANBAKHSH, K. 2019. Mesenchymal stromal cells lower platelet activation and assist in platelet formation in vitro. *JCI Insight,* 4.

MCALINDON, E., PUFULETE, M., HARISS, J., LAWTON, C., JOHNSON, T., STRANGE, J., BAUMBACH, A., BUCCIARELLI-DUCCI, C., 2018. Microvascular dysfunction determines infarct characteristics in patients with reperfused ST-segment elevation myocardial infarction: MICROcirculation in Acute Myocardial Infarction (MICRO-AMI) study. PLoS One, 13, e0203750.

MCEVER, R. P. 1991. GMP-140: a receptor for neutrophils and monocytes on activated platelets and endothelium. *J Cell Biochem,* 45**,** 156-61.

MC NAMARA, K., ALZUBAIDI, H. & JACKSON, J. K. 2019. Cardiovascular disease as a leading cause of death: how are pharmacists getting involved? *Integr Pharm Res Pract,* 8**,** 1-11.

MANCHANDA, K., KOLAROVA, H., KERKENPASS, C., MOLLENHAUER, M., VITECEK, J., RUDOLPH, V., KUBALA, L., BALDUS, S., ADAM, M. & KLINKE, A. 2018. MPO

(Myeloperoxidase) Reduces Endothelial Glycocalyx Thickness Dependent on Its Cationic Charge. *Arterioscler Thromb Vasc Biol,* 38**,** 1859-1867.

MENDELSON, A., STRAT, A. N., BAO, W., ROSSTON, P., FALLON, G., OHRN, S., ZHONG, H., LOBO, C., AN, X. & YAZDANBAKHSH, K. 2019. Mesenchymal stromal cells lower platelet activation and assist in platelet formation in vitro. *JCI Insight,* 4.

MO, M., WANG, S., ZHOU, Y., LI, H. & WU, Y. 2016. Mesenchymal stem cell subpopulations: phenotype, property and therapeutic potential. *Cell Mol Life Sci,* 73**,** 3311-21.

MO, M., ZHOU, Y., LI, S. & WU, Y. 2018. Three-Dimensional Culture Reduces Cell Size By Increasing Vesicle Excretion. *Stem Cells,* 36**,** 286-292.

MOTEGI, S. I., SEKIGUCHI, A., UCHIYAMA, A., UEHARA, A., FUJIWARA, C., YAMAZAKI, S., PERERA, B., NAKAMURA, H., OGINO, S., YOKOYAMA, Y., AKAI, R., IWAWAKI, T. & ISHIKAWA, O. 2017. Protective effect of mesenchymal stem cells on the pressure ulcer formation by the regulation of oxidative and endoplasmic reticulum stress. *Sci Rep,* 7**,** 17186.

MOUISEDDINE, M., FRANCOIS, S., SEMONT, A., SACHE, A., ALLENET, B., MATHIEU, N., FRICK, J., THIERRY, D. & CHAPEL, A. 2007. Human mesenchymal stem cells home specifically to radiation-injured tissues in a non-obese diabetes/severe combined immunodeficiency mouse model. *Br J Radiol,* 80 Spec No 1**,** S49-55.

MULLER, P., LEMCKE, H. & DAVID, R. 2018. Stem Cell Therapy in Heart Diseases - Cell Types, Mechanisms and Improvement Strategies. *Cell Physiol Biochem,* 48**,** 2607-2655.

MULLER, W. A. 2013. Getting leukocytes to the site of inflammation. *Vet Pathol,* 50**,** 7-22.

MURPHY, M. P. 2009. How mitochondria produce reactive oxygen species. *Biochem J,* 417**,** 1-13.

MUTGAN, A. C., JANDL, K. & KWAPISZEWSKA, G. 2020. Endothelial Basement Membrane Components and Their Products, Matrikines: Active Drivers of Pulmonary Hypertension? *Cells,* 9.

MUSSBACHER, M., SALZMANN, M., BROSTJAN, C., HOESEL, B., SCHOERGENHOFER, C., DATLER, H., HOHENSINNER, P., BASILIO, J., PETZELBAUER, P., ASSINGER, A. & SCHMID, J. A. 2019. Cell Type-Specific Roles of NF-kappaB Linking Inflammation and Thrombosis. *Front Immunol,* 10**,** 85.

NAPODANO, M., PELUSO, D., MARRA, M. P., FRIGO, A. C., TARANTINI, G., BUJA, P., GASPARETTO, V., FRACCARO, C., ISABELLA, G., RAZZOLINI, R. & ILICETO, S. 2012. Time-dependent detrimental effects of distal embolization on myocardium and microvasculature during primary percutaneous coronary intervention. *JACC Cardiovasc Interv,* 5**,** 1170-7.

NASEF, A., ZHANG, Y. Z., MAZURIER, C., BOUCHET, S., BENSIDHOUM, M., FRANCOIS, S., GORIN, N. C., LOPEZ, M., THIERRY, D., FOUILLARD, L. & CHAPEL, A. 2009. Selected Stro-1-enriched bone marrow stromal cells display a major suppressive effect on lymphocyte proliferation. *Int J Lab Hematol,* 31**,** 9-19.

NETSCH, P., ELVERS-HORNUNG, S., UHLIG, S., KLUTER, H., HUCK, V., KIRSCHHOFER, F., BRENNER-WEISS, G., JANETZKO, K., SOLZ, H., WUCHTER, P., BUGERT, P. & BIEBACK, K. 2018. Human mesenchymal stromal cells inhibit platelet activation and aggregation involving CD73-converted adenosine. *Stem Cell Res Ther,* 9**,** 184.

NICCOLI, G., SCALONE, G., LERMAN, A. & CREA, F. 2016. Coronary microvascular obstruction in acute myocardial infarction. *Eur Heart J,* 37**,** 1024-33.

NITZSCHE, F., MULLER, C., LUKOMSKA, B., JOLKKONEN, J., DETEN, A. & BOLTZE, J. 2017. Concise Review: MSC Adhesion Cascade-Insights into Homing and Transendothelial Migration. *Stem Cells,* 35**,** 1446-1460.

NOIRI, E., YOKOMIZO, T., NAKAO, A., IZUMI, T., FUJITA, T., KIMURA, S. & SHIMIZU, T. 2000. An in vivo approach showing the chemotactic activity of leukotriene B(4) in acute renal ischemic-reperfusion injury. *Proc Natl Acad Sci U S A,* 97**,** 823-8.

NOURSHARGH, S. & ALON, R. 2014. Leukocyte migration into inflamed tissues. *Immunity,* 41**,** 694-707.

O'CONNOR, K. C. 2019. Molecular Profiles of Cell-to-Cell Variation in the Regenerative Potential of Mesenchymal Stromal Cells. *Stem Cells Int,* 2019**,** 5924878.

ORTIZ, L. A., DUTREIL, M., FATTMAN, C., PANDEY, A. C., TORRES, G., GO, K. & PHINNEY, D. G. 2007. Interleukin 1 receptor antagonist mediates the antiinflammatory and antifibrotic effect of mesenchymal stem cells during lung injury. *Proc Natl Acad Sci U S A,* 104**,** 11002-7.

OZ, M. C., LIAO, H., NAKA, Y., SELDOMRIDGE, A., BECKER, D. N., MICHLER, R. E., SMITH, C. R., ROSE, E. A., STERN, D. M. & PINSKY, D. J. 1995. Ischemia-induced interleukin-8 release after human heart transplantation. A potential role for endothelial cells. *Circulation,* 92**,** II428-32.

PAPADAKIS, E., KANAKIS, M., KATAKI, A. & SPANDIDOS, D. A. 2018. The spectrum of myocardial homeostasis mechanisms in the settings of cardiac surgery procedures (Review). *Mol Med Rep,* 17**,** 2089-2099.

PELED, A., KOLLET, O., PONOMARYOV, T., PETIT, I., FRANITZA, S., GRABOVSKY, V., SLAV, M. M., NAGLER, A., LIDER, O., ALON, R., ZIPORI, D. & LAPIDOT, T. 2000. The chemokine SDF-1 activates the integrins LFA-1, VLA-4, and VLA-5 on immature human CD34(+)

cells: role in transendothelial/stromal migration and engraftment of NOD/SCID mice. *Blood,* 95 **,** 3289-96.

PEREZ, J. R., YBARRA, N., CHAGNON, F., SERBAN, M., LEE, S., SEUNTJENS, J., LESUR, O. & EL NAQA, I. 2017. Tracking of Mesenchymal Stem Cells with Fluorescence Endomicroscopy Imaging in Radiotherapy-Induced Lung Injury. *Sci Rep,* 7**,** 40748.

PETRENKO, Y., SYKOVA, E. & KUBINOVA, S. 2017. The therapeutic potential of three-dimensional multipotent mesenchymal stromal cell spheroids. *Stem Cell Res Ther,* 8**,** 94.

PETRENKO, Y., VACKOVA, I., KEKULOVA, K., CHUDICKOVA, M., KOCI, Z., TURNOVCOVA, K., KUPCOVA SKALNIKOVA, H., VODICKA, P. & KUBINOVA, S. 2020. A Comparative Analysis of Multipotent Mesenchymal Stromal Cells derived from Different Sources, with a Focus on Neuroregenerative Potential. *Sci Rep,* 10**,** 4290.

PINTO DO, O. P., KOLTERUD, A. & CARLSSON, L. 1998. Expression of the LIM-homeobox gene LH2 generates immortalized steel factor-dependent multipotent hematopoietic precursors. *EMBO J,* 17**,** 5744-56.

POTAPOVA, I. A., GAUDETTE, G. R., BRINK, P. R., ROBINSON, R. B., ROSEN, M. R., COHEN, I. S. & DORONIN, S. V. 2007. Mesenchymal stem cells support migration, extracellular matrix invasion, proliferation, and survival of endothelial cells in vitro. *Stem Cells,* 25**,** 1761-8.

POTAPOVA, I. A., BRINK, P. R., COHEN, I. S. & DORONIN, S. V. 2008. Culturing of human mesenchymal stem cells as three-dimensional aggregates induces functional expression of CXCR4 that regulates adhesion to endothelial cells. *J Biol Chem,* 283**,** 13100-7.

PRIES, A. R. & REGLIN, B. 2017. Coronary microcirculatory pathophysiology: can we afford it to remain a black box? *Eur Heart J,* 38**,** 478-488.

QIU, Z., ZHOU, D. & SUN, D. 2014. Effects of human umbilical cord mesenchymal stem cells on renal ischaemia-reperfusion injury in rats. *Int Braz J Urol,* 40**,** 553-61.

QUEVEDO, H. C., HATZISTERGOS, K. E., OSKOUEI, B. N., FEIGENBAUM, G. S., RODRIGUEZ, J. E., VALDES, D., PATTANY, P. M., ZAMBRANO, J. P., HU, Q., MCNIECE, I., HELDMAN, A. W. & HARE, J. M. 2009. Allogeneic mesenchymal stem cells restore cardiac function in chronic ischemic cardiomyopathy via trilineage differentiating capacity. *Proc Natl Acad Sci U S A,* 106**,** 14022-7.

RAEDSCHELDERS, K., ANSLEY, D. M. & CHEN, D. D. 2012. The cellular and molecular origin of reactive oxygen species generation during myocardial ischemia and reperfusion. *Pharmacol Ther,* 133**,** 230-55.

RAHBARGHAZI, R., KEYHANMANESH, R., ASLANI, M. R., HASSANPOUR, M. & AHMADI, M. 2019. Bone marrow mesenchymal stem cells and condition media diminish

inflammatory adhesion molecules of pulmonary endothelial cells in an ovalbumin-induced asthmatic rat model. *Microvasc Res,* 121**,** 63-70.

REN, G., ROBERTS, A. I. & SHI, Y. 2011. Adhesion molecules: key players in Mesenchymal stem cell-mediated immunosuppression. *Cell Adh Migr,* 5**,** 20-2.

REN, G., ZHAO, X., ZHANG, L., ZHANG, J., L'HUILLIER, A., LING, W., ROBERTS, A. I., LE, A. D., SHI, S., SHAO, C. & SHI, Y. 2010. Inflammatory cytokine-induced intercellular adhesion molecule-1 and vascular cell adhesion molecule-1 in mesenchymal stem cells are critical for immunosuppression. *J Immunol,* 184**,** 2321-8.

RENNERT, R. C., SORKIN, M., GARG, R. K. & GURTNER, G. C. 2012. Stem cell recruitment after injury: lessons for regenerative medicine. *Regen Med,* 7**,** 833-50.

REZKALLA, S. H., STANKOWSKI, R. V., HANNA, J. & KLONER, R. A. 2017. Management of No-Reflow Phenomenon in the Catheterization Laboratory. *JACC Cardiovasc Interv,* 10**,** 215-223.

RIDKER, P. M., EVERETT, B. M., THUREN, T., MACFADYEN, J. G., CHANG, W. H., BALLANTYNE, C., FONSECA, F., NICOLAU, J., KOENIG, W., ANKER, S. D., KASTELEIN, J. J. P., CORNEL, J. H., PAIS, P., PELLA, D., GENEST, J., CIFKOVA, R., LORENZATTI, A., FORSTER, T., KOBALAVA, Z., VIDA-SIMITI, L., FLATHER, M., SHIMOKAWA, H., OGAWA, H., DELLBORG, M., ROSSI, P. R. F., TROQUAY, R. P. T., LIBBY, P., GLYNN, R. J. & GROUP, C. T. 2017. Antiinflammatory Therapy with Canakinumab for Atherosclerotic Disease. *N Engl J Med,* 377**,** 1119-1131.

RIFFO-VASQUEZ, Y., SOMANI, A., MAN, F., AMISON, R., PITCHFORD, S. & PAGE, C. P. 2016. A Non-Anticoagulant Fraction of Heparin Inhibits Leukocyte Diapedesis into the Lung by an Effect on Platelets. *Am J Respir Cell Mol Biol,* 55**,** 554-563.

RODRIGUES, S. F. & GRANGER, D. N. 2010. Role of blood cells in ischaemia-reperfusion induced endothelial barrier failure. *Cardiovasc Res,* 87**,** 291-9.

ROWART, P., ERPICUM, P., DETRY, O., WEEKERS, L., GREGOIRE, C., LECHANTEUR, C., BRIQUET, A., BEGUIN, Y., KRZESINSKI, J. M. & JOURET, F. 2015. Mesenchymal Stromal Cell Therapy in Ischemia/Reperfusion Injury. *J Immunol Res,* 2015**,** 602597.

RUSTER, B., GOTTIG, S., LUDWIG, R. J., BISTRIAN, R., MULLER, S., SEIFRIED, E., GILLE, J. & HENSCHLER, R. 2006. Mesenchymal stem cells display coordinated rolling and adhesion behavior on endothelial cells. *Blood,* 108**,** 3938-44.

RYU, N. E., LEE, S. H. & PARK, H. 2019. Spheroid Culture System Methods and Applications for Mesenchymal Stem Cells. *Cells,* 8.

SASAKI, S. 1967. Production of lymphocytosis by polysaccharide polysulphates (heparinoids). *Nature,* 214**,** 1041-2.

SACKSTEIN, R., MERZABAN, J. S., CAIN, D. W., DAGIA, N. M., SPENCER, J. A., LIN, C. P. & WOHLGEMUTH, R. 2008. Ex vivo glycan engineering of CD44 programs human multipotent mesenchymal stromal cell trafficking to bone. *Nat Med,* 14**,** 181-7.

SAITO, T., KUANG, J. Q., BITTIRA, B., AL-KHALDI, A. & CHIU, R. C. 2002. Xenotransplant cardiac chimera: immune tolerance of adult stem cells. *Ann Thorac Surg,* 74**,** 19-24; discussion 24.

SALVUCCI, O., BASIK, M., YAO, L., BIANCHI, R. & TOSATO, G. 2004. Evidence for the involvement of SDF-1 and CXCR4 in the disruption of endothelial cell-branching morphogenesis and angiogenesis by TNF-alpha and IFN-gamma. *J Leukoc Biol,* 76**,** 217-26.

SAMBUCETI, G., L'ABBATE, A., MARZILLI, M. 2002. Why should we study the coronary microcirculation?. *Am J Physiology - Heart Circ Phys*, 279, H2581-H2584.

SANADA, S., KOMURO, I. & KITAKAZE, M. 2011. Pathophysiology of myocardial reperfusion injury: preconditioning, postconditioning, and translational aspects of protective measures. *Am J Physiol Heart Circ Physiol,* 301**,** H1723-41.

SANINA, C., HARE, J.M. 2015. Mesenchymal Stem Cells as a Biological Drug for Heart Disease: Where Are We With Cardiac Cell-Based Therapy?. *Circ Res*, 2015, 117(3), 229-233.

SART, S., TSAI, A. C., LI, Y. & MA, T. 2014. Three-dimensional aggregates of mesenchymal stem cells: cellular mechanisms, biological properties, and applications. *Tissue Eng Part B Rev,* 20**,** 365-80.

SCARABELLI, T., STEPHANOU, A., RAYMENT, N., PASINI, E., COMINI, L., CURELLO, S., FERRARI, R., KNIGHT, R. & LATCHMAN, D. 2001. Apoptosis of endothelial cells precedes myocyte cell apoptosis in ischemia/reperfusion injury. *Circulation,* 104**,** 253-6.

SCHERSCHEL, J. A. & RUBART, M. 2008. Cardiovascular imaging using two-photon microscopy. *Microsc Microanal,* 14**,** 492-506.

SCHMAL, O., SEIFERT, J., SCHAFFER, T. E., WALTER, C. B., AICHER, W. K. & KLEIN, G. 2016. Hematopoietic Stem and Progenitor Cell Expansion in Contact with Mesenchymal Stromal Cells in a Hanging Drop Model Uncovers Disadvantages of 3D Culture. *Stem Cells Int,* 2016**,** 4148093.

SCHNOOR, M. 2015. Endothelial actin-binding proteins and actin dynamics in leukocyte transendothelial migration. *J Immunol,* 194**,** 3535-41.

SCHREPFER, S., DEUSE, T., REICHENSPURNER, H., FISCHBEIN, M. P., ROBBINS, R. C. & PELLETIER, M. P. 2007. Stem cell transplantation: the lung barrier. *Transplant Proc,* 39**,** 573-6.

SEGERS, V. F., VAN RIET, I., ANDRIES, L. J., LEMMENS, K., DEMOLDER, M. J., DE BECKER, A. J., KOCKX, M. M. & DE KEULENAER, G. W. 2006. Mesenchymal stem cell adhesion to cardiac microvascular endothelium: activators and mechanisms. *Am J Physiol Heart Circ Physiol,* 290**,** H1370-7.

SEZER, M., VAN ROYEN, N., UMMAN, B., BUGRA, Z., BULLUCK, H., HAUSENLOY, D. J. & UMMAN, S. 2018. Coronary Microvascular Injury in Reperfused Acute Myocardial Infarction: A View From an Integrative Perspective. *J Am Heart Assoc,* 7**,** e009949.

SHARMA, H. S. & DAS, D. K. 1997. Role of cytokines in myocardial ischemia and reperfusion. *Mediators Inflamm,* 6**,** 175-83.

SHAO, Y., ZHOU, F., HE, D., ZHANG, L. & SHEN, J. 2019. Overexpression of CXCR7 promotes mesenchymal stem cells to repair phosgene-induced acute lung injury in rats. *Biomed Pharmacother,* 109**,** 1233-1239.

SHEN, B., DELANEY, M. K. & DU, X. 2012. Inside-out, outside-in, and inside-outside-in: G protein signaling in integrin-mediated cell adhesion, spreading, and retraction. *Curr Opin Cell Biol,* 24**,** 600-6.

SHEN, H., KREISEL, D. & GOLDSTEIN, D. R. 2013. Processes of sterile inflammation. *J Immunol,* 191**,** 2857-63.

SHERIFF, L., ALANAZI, A., WARD, L. S. C., WARD, C., MUNIR, H., RAYES, J., ALASSIRI, M., WATSON, S. P., NEWSOME, P. N., RAINGER, G. E., KALIA, N., FRAMPTON, J., MCGETTRICK, H. M. & NASH, G. B. 2018. Origin-Specific Adhesive Interactions of Mesenchymal Stem Cells with Platelets Influence Their Behavior After Infusion. *Stem Cells,* 36**,** 1062-1074.

SCHIEBER, M. & CHANDEL, N. S. 2014. ROS function in redox signaling and oxidative stress. *Curr Biol,* 24**,** R453-62.

SILVA, L. H. A., ANTUNES, M. A., DOS SANTOS, C. C., WEISS, D. J., CRUZ, F. F. & ROCCO, P. R. M. 2018. Strategies to improve the therapeutic effects of mesenchymal stromal cells in respiratory diseases. *Stem Cell Res Ther,* 9**,** 45.

SINGHAL, A. K., SYMONS, J. D., BOUDINA, S., JAISHY, B. & SHIU, Y. T. 2010. Role of Endothelial Cells in Myocardial Ischemia-Reperfusion Injury. *Vasc Dis Prev,* 7**,** 1-14.

SIROTKOVIC-SKERLEV, M., PLESTINA, S., BILIC, I. & KOVAC, Z. 2006. [Pathophysiology of ischaemia-reperfusion injury]. *Lijec Vjesn,* 128**,** 87-95.

SKOVSTED, G. F., KRUSE, L. S., BERCHTOLD, L. A., GRELL, A. S., WARFVINGE, K. & EDVINSSON, L. 2017. Myocardial ischemia-reperfusion enhances transcriptional expression of endothelin-1 and vasoconstrictor ETB receptors via the protein kinase MEK-ERK1/2 signaling pathway in rat. *PLoS One,* 12**,** e0174119.

SLEGTENHORST, B. R., DOR, F. J., RODRIGUEZ, H., VOSKUIL, F. J. & TULLIUS, S. G. 2014. Ischemia/reperfusion Injury and its Consequences on Immunity and Inflammation. *Curr Transplant Rep,* 1**,** 147-154.

SOHNI, A. & VERFAILLIE, C. M. 2013. Mesenchymal stem cells migration homing and tracking. *Stem Cells Int,* 2013**,** 130763.

SOULET, D., PARÉ, A., COSTE, J. & LACROIX, S. 2013. Automated Filtering of Intrinsic Movement Artifacts during Two-Photon Intravital Microscopy. *PLOS ONE,* 8**,** e53942.

STAMPER, H. B., JR. & WOODRUFF, J. J. 1976. Lymphocyte homing into lymph nodes: in vitro demonstration of the selective affinity of recirculating lymphocytes for high-endothelial venules. *J Exp Med,* 144**,** 828-33.

STAVELY, R. & NURGALI, K. 2020. The emerging antioxidant paradigm of mesenchymal stem cell therapy. *Stem Cells Transl Med,* 9**,** 985-1006.

STANLEY, W. C. 2004. Myocardial energy metabolism during ischemia and the mechanisms of metabolic therapies. *J Cardiovasc Pharmacol Ther,* 9 Suppl 1**,** S31-45.

STICH, S., HAAG, M., HAUPL, T., SEZER, O., NOTTER, M., KAPS, C., SITTINGER, M. & RINGE, J. 2009. Gene expression profiling of human mesenchymal stem cells chemotactically induced with CXCL12. *Cell Tissue Res,* 336**,** 225-36.

STROBER, W. 2015. Trypan Blue Exclusion Test of Cell Viability. *Curr Protoc Immunol,* 111**,** A3 B 1-A3 B 3.

SUILA, H., HIRVONEN, T., KOTOVUORI, A., RITAMO, I., KERKELA, E., ANDERSON, H., NATUNEN, S., TUIMALA, J., LAITINEN, S., NYSTEDT, J., RABINA, J. & VALMU, L. 2014. Human umbilical cord blood-derived mesenchymal stromal cells display a novel interaction between P-selectin and galectin-1. *Scand J Immunol,* 80**,** 12-21.

SUN, R., LI, X., LIU, M., ZENG, Y., CHEN, S. & ZHANG, P. 2016. Advances in stem cell therapy for cardiovascular disease (Review). *Int J Mol Med,* 38**,** 23-9.

SUN, T., GAO, G. Z., LI, R. F., LI, X., LI, D. W., WU, S. S., YEO, A. E. & JIN, B. 2015. Bone marrow-derived mesenchymal stem cell transplantation ameliorates oxidative stress and restores intestinal mucosal permeability in chemically induced colitis in mice. *Am J Transl Res,* 7**,** 891-901.

SUN, Y., WANG, Y., ZHOU, L., ZOU, Y., HUANG, G., GAO, G., TING, S., LEI, X. & DING, X. 2018. Spheroid-cultured human umbilical cord-derived mesenchymal stem cells attenuate hepatic ischemia-reperfusion injury in rats. *Sci Rep,* 8**,** 2518.

TANG, B., LI, X., LIU, Y., CHEN, X., LI, X., CHU, Y., ZHU, H., LIU, W., XU, F., ZHOU, F. & ZHANG, Y. 2018. The Therapeutic Effect of ICAM-1-Overexpressing Mesenchymal Stem Cells on Acute Graft-Versus-Host Disease. *Cell Physiol Biochem,* 46**,** 2624-2635.

TANG, J. N., CORES, J., HUANG, K., CUI, X. L., LUO, L., ZHANG, J. Y., LI, T. S., QIAN, L. & CHENG, K. 2018. Concise Review: Is Cardiac Cell Therapy Dead? Embarrassing Trial Outcomes and New Directions for the Future. *Stem Cells Transl Med,* 7**,** 354-359.

TERASHVILI, M. & BOSNJAK, Z. J. 2019. Stem Cell Therapies in Cardiovascular Disease. *J Cardiothorac Vasc Anesth,* 33**,** 209-222.

THACKERAY, J. T., DERLIN, T., HAGHIKIA, A., NAPP, L. C., WANG, Y., ROSS, T. L., SCHAFER, A., TILLMANNS, J., WESTER, H. J., WOLLERT, K. C., BAUERSACHS, J. & BENGEL, F. M. 2015. Molecular Imaging of the Chemokine Receptor CXCR4 After Acute Myocardial Infarction. *JACC Cardiovasc Imaging,* 8**,** 1417-1426.

TOMA, C., WAGNER, W. R., BOWRY, S., SCHWARTZ, A. & VILLANUEVA, F. 2009. Fate of culture-expanded mesenchymal stem cells in the microvasculature: in vivo observations of cell kinetics. *Circ Res,* 104, 398-402.

TOMCHUCK, S. L., ZWEZDARYK, K. J., COFFELT, S. B., WATERMAN, R. S., DANKA, E. S. & SCANDURRO, A. B. 2008. Toll-like receptors on human mesenchymal stem cells drive their migration and immunomodulating responses. *Stem Cells,* 26**,** 99-107.

TOYOTA, E., FUJIMOTO, K., OGASAWARA, Y., KAJITA, T., SHIGETO, F., MATSUMOTO, T., GOTO, M. & KAJIYA, F. 2002. Dynamic changes in three-dimensional architecture and vascular volume of transmural coronary microvasculature between diastolic- and systolic-arrested rat hearts. *Circulation,* 105**,** 621-6.

TUNG, Y. C., HSIAO, A. Y., ALLEN, S. G., TORISAWA, Y. S., HO, M. & TAKAYAMA, S. 2011. High-throughput 3D spheroid culture and drug testing using a 384 hanging drop array. *Analyst,* 136**,** 473-8.

UCCELLI, A. & DE ROSBO, N. K. 2015. The immunomodulatory function of mesenchymal stem cells: mode of action and pathways. *Ann N Y Acad Sci,* 1351**,** 114-26.

ULBRICH, H., ERIKSSON, E. E. & LINDBOM, L. 2003. Leukocyte and endothelial cell adhesion molecules as targets for therapeutic interventions in inflammatory disease. *Trends Pharmacol Sci,* 24**,** 640-7.

ULLAH, M., LIU, D. D. & THAKOR, A. S. 2019. Mesenchymal Stromal Cell Homing: Mechanisms and Strategies for Improvement. *iScience,* 15**,** 421-438.

VALCARCEL, M., ARTETA, B., JAUREGUIBEITIA, A., LOPATEGI, A., MARTINEZ, I., MENDOZA, L., MURUZABAL, F. J., SALADO, C. & VIDAL-VANACLOCHA, F. 2008. Three-dimensional growth as multicellular spheroid activates the proangiogenic phenotype

of colorectal carcinoma cells via LFA-1-dependent VEGF: implications on hepatic micrometastasis. *J Transl Med,* 6**,** 57.

VALEN, G., YAN, Z. Q. & HANSSON, G. K. 2001. Nuclear factor kappa-B and the heart. *J Am Coll Cardiol,* 38**,** 307-14.

VALENSI, P., LORGIS, L. & COTTIN, Y. 2011. Prevalence, incidence, predictive factors and prognosis of silent myocardial infarction: a review of the literature. *Arch Cardiovasc Dis,* 104**,** 178-88.

VAN DEN AKKER, F., DE JAGER, S. C. & SLUIJTER, J. P. 2013. Mesenchymal stem cell therapy for cardiac inflammation: immunomodulatory properties and the influence of toll-like receptors. *Mediators Inflamm,* 2013**,** 181020.

VAN LINTHOUT, S., STAMM, C., SCHULTHEISS, H. P. & TSCHOPE, C. 2011. Mesenchymal stem cells and inflammatory cardiomyopathy: cardiac homing and beyond. *Cardiol Res Pract,* 2011**,** 757154.

VIGNAIS, M. L., CAICEDO, A., BRONDELLO, J. M. & JORGENSEN, C. 2017. Cell Connections by Tunneling Nanotubes: Effects of Mitochondrial Trafficking on Target Cell Metabolism, Homeostasis, and Response to Therapy. *Stem Cells Int,* 2017**,** 6917941.

VINEGONI, C., AGUIRRE, A. D., LEE, S. & WEISSLEDER, R. 2015. Imaging the beating heart in the mouse using intravital microscopy techniques. *Nat Protoc,* 10**,** 1802-19.

VINEGONI, C., LEE, S., GORBATOV, R. & WEISSLEDER, R. 2012. Motion compensation using a suctioning stabilizer for intravital microscopy. *Intravital,* 1**,** 115-121.

VIOLA, M., KAROUSOU, E., D'ANGELO, M. L., CAON, I., DE LUCA, G., PASSI, A. & VIGETTI, D. 2015. Regulated Hyaluronan Synthesis by Vascular Cells. *Int J Cell Biol,* 2015**,** 208303.

VISWANATHAN, S., SHI, Y., GALIPEAU, J., KRAMPERA, M., LEBLANC, K., MARTIN, I., NOLTA, J., PHINNEY, D. G. & SENSEBE, L. 2019. Mesenchymal stem versus stromal cells: International Society for Cell & Gene Therapy (ISCT(R)) Mesenchymal Stromal Cell committee position statement on nomenclature. *Cytotherapy,* 21**,** 1019-1024.

VLODAVSKY, I., IOZZO, R. V. & SANDERSON, R. D. 2013. Heparanase: multiple functions in inflammation, diabetes and atherosclerosis. *Matrix Biol,* 32**,** 220-2.

WANG, C. C., CHEN, C. H., HWANG, S. M., LIN, W. W., HUANG, C. H., LEE, W. Y., CHANG, Y. & SUNG, H. W. 2009. Spherically symmetric mesenchymal stromal cell bodies inherent with endogenous extracellular matrices for cellular cardiomyoplasty. *Stem Cells,* 27**,** 724-32.

WANG, J., HOSSAIN, M., THANABALASURIAR, A., GUNZER, M., MEININGER, C. & KUBES, P. 2017. Visualizing the function and fate of neutrophils in sterile injury and repair. *Science,* 358**,** 111-116.

WANG, X., JIANG, B., SUN, H., ZHENG, D., ZHANG, Z., YAN, L., LI, E., WU, Y. & XU, R. H. 2019. Noninvasive application of mesenchymal stem cell spheres derived from hESC accelerates wound healing in a CXCL12-CXCR4 axis-dependent manner. *Theranostics,* 9**,** 6112-6128.

WARD, M. R., ABADEH, A. & CONNELLY, K. A. 2018. Concise Review: Rational Use of Mesenchymal Stem Cells in the Treatment of Ischemic Heart Disease. *Stem Cells Transl Med,* 7**,** 543-550.

WEBSTER, K. A. 2012. Mitochondrial membrane permeabilization and cell death during myocardial infarction: roles of calcium and reactive oxygen species. *Future Cardiol,* 8**,** 863-84.

WEINBAUM, S., TARBELL, J. M. & DAMIANO, E. R. 2007. The structure and function of the endothelial glycocalyx layer. *Annu Rev Biomed Eng,* 9**,** 121-67.

WEISS, A. R. R. & DAHLKE, M. H. 2019. Immunomodulation by Mesenchymal Stem Cells (MSCs): Mechanisms of Action of Living, Apoptotic, and Dead MSCs. *Front Immunol,* 10**,** 1191.

WHITE, R. L., NASH, G., KAVANAGH, D. P., SAVAGE, C. O. & KALIA, N. 2013. Modulating the Adhesion of Haematopoietic Stem Cells with Chemokines to Enhance Their Recruitment to the Ischaemically Injured Murine Kidney. *PLoS One,* 8**,** e66489.

WILHELMI, M. H., LEYH, R. G., WILHELMI, M. & HAVERICH, A. 2005. Upregulation of endothelial adhesion molecules in hearts with congestive and ischemic cardiomyopathy: immunohistochemical evaluation of inflammatory endothelial cell activation. *Eur J Cardiothorac Surg,* 27**,** 122-7.

WILLIAMS, A. R., SUNCION, V. Y., MCCALL, F., GUERRA, D., MATHER, J., ZAMBRANO, J. P., HELDMAN, A. W. & HARE, J. M. 2013. Durable scar size reduction due to allogeneic mesenchymal stem cell therapy regulates whole-chamber remodeling. *J Am Heart Assoc,* 2**,** e000140.

WILSON, A., WEBSTER, A. & GENEVER, P. 2019. Nomenclature and heterogeneity: consequences for the use of mesenchymal stem cells in regenerative medicine. *Regen Med,* 14**,** 595-611.

WU, M. Y., YIANG, G. T., LIAO, W. T., TSAI, A. P., CHENG, Y. L., CHENG, P. W., LI, C. Y. & LI, C. J. 2018. Current Mechanistic Concepts in Ischemia and Reperfusion Injury. *Cell Physiol Biochem,* 46**,** 1650-1667.

WU, X., JIANG, J., GU, Z., ZHANG, J., CHEN, Y. & LIU, X. 2020. Mesenchymal stromal cell therapies: immunomodulatory properties and clinical progress. *Stem Cell Res Ther,* 11**,** 345.

WU, Z., RADEMAKERS, T., KIESSLING, F., VOGT, M., WESTEIN, E., WEBER, C., MEGENS, R. T. A. & VAN ZANDVOORT, M. 2017. Multi-photon microscopy in cardiovascular research. *Methods,* 130**,** 79-89.

VICENTE-MANZANARES, M. & SANCHEZ-MADRID, F. 2004. Role of the cytoskeleton during leukocyte responses. *Nat Rev Immunol,* 4**,** 110-22.

XIA, P., GAMBLE, J. R., RYE, K. A., WANG, L., HII, C. S., COCKERILL, P., KHEW-GOODALL, Y., BERT, A. G., BARTER, P. J. & VADAS, M. A. 1998. Tumor necrosis factor-alpha induces adhesion molecule expression through the sphingosine kinase pathway. *Proc Natl Acad Sci U S A,* 95**,** 14196-201.

XIE, C., JIN, J., LV, X., TAO, J., WANG, R. & MIAO, D. 2015. Anti-aging Effect of Transplanted Amniotic Membrane Mesenchymal Stem Cells in a Premature Aging Model of Bmi-1 Deficiency. *Sci Rep,* 5**,** 13975.

YADA, T., HIRAMATSU, O., KIMURA, A., GOTO, M., OGASAWARA, Y., TSUJIOKA, K., YAMAMORI, S., OHNO, K., HOSAKA, H. & KAJIYA, F. 1993. In vivo observation of subendocardial microvessels of the beating porcine heart using a needle-probe videomicroscope with a CCD camera. *Circ Res,* 72**,** 939-46.

YAGO, T., PETRICH, B. G., ZHANG, N., LIU, Z., SHAO, B., GINSBERG, M. H. & MCEVER, R. P. 2015. Blocking neutrophil integrin activation prevents ischemia-reperfusion injury. *J Exp Med,* 212**,** 1267-81.

YANG, C. F. 2018. Clinical manifestations and basic mechanisms of myocardial ischemia/reperfusion injury. *Ci Ji Yi Xue Za Zhi,* 30**,** 209-215.

YANG, Q., HE, G. W., UNDERWOOD, M. J. & YU, C. M. 2016. Cellular and molecular mechanisms of endothelial ischemia/reperfusion injury: perspectives and implications for postischemic myocardial protection. *Am J Transl Res,* 8**,** 765-77.

YANG, Y., JIANG, G., ZHANG, P. & FAN, J. 2015. Programmed cell death and its role in inflammation. *Mil Med Res,* 2**,** 12.

YANG, Z., ZINGARELLI, B. & SZABO, C. 2000. Crucial role of endogenous interleukin-10 production in myocardial ischemia/reperfusion injury. *Circulation,* 101**,** 1019-26.

YANG, Z. X., HAN, Z. B., JI, Y. R., WANG, Y. W., LIANG, L., CHI, Y., YANG, S. G., LI, L. N., LUO, W. F., LI, J. P., CHEN, D. D., DU, W. J., CAO, X. C., ZHUO, G. S., WANG, T. & HAN, Z. C. 2013. CD106 identifies a subpopulation of mesenchymal stem cells with unique immunomodulatory properties. *PLoS One,* 8**,** e59354.

YAO, L., XUE, X., YU, P., NI, Y. & CHEN, F. 2018. Evans Blue Dye: A Revisit of Its Applications in Biomedicine. *Contrast Media Mol Imaging,* 2018**,** 7628037.

YELLON, D. M. & HAUSENLOY, D. J. 2007. Myocardial reperfusion injury. *N Engl J Med,* 357**,** 1121-35.

YLOSTALO, J. H., BARTOSH, T. J., COBLE, K. & PROCKOP, D. J. 2012. Human mesenchymal stem/stromal cells cultured as spheroids are self-activated to produce prostaglandin E2 that directs stimulated macrophages into an anti-inflammatory phenotype. *Stem Cells,* 30**,** 2283-96.

YOSHIDA, K., KONDO, R., WANG, Q. & DOERSCHUK, C. M. 2006. Neutrophil cytoskeletal rearrangements during capillary sequestration in bacterial pneumonia in rats. *Am J Respir Crit Care Med,* 174**,** 689-98.

ZANOTTI, L., ANGIONI, R., CALI, B., SOLDANI, C., PLOIA, C., MOALLI, F., GARGESHA, M., D'AMICO, G., ELLIMAN, S., TEDESCHI, G., MAFFIOLI, E., NEGRI, A., ZACCHIGNA, S., SARUKHAN, A., STEIN, J. V. & VIOLA, A. 2016. Mouse mesenchymal stem cells inhibit high endothelial cell activation and lymphocyte homing to lymph nodes by releasing TIMP-1. *Leukemia,* 30**,** 1143-54.

ZARYCHTA-WISNIEWSKA, W., BURDZINSKA, A., ZIELNIOK, K., KOBLOWSKA, M., GALA, K., PEDZISZ, P., IWANICKA-NOWICKA, R., FOGTMAN, A., AKSAMIT, A., KULESZA, A., ZOLOCINSKA, A. & PACZEK, L. 2019. The Influence of Cell Source and Donor Age on the Tenogenic Potential and Chemokine Secretion of Human Mesenchymal Stromal Cells. *Stem Cells Int,* 2019**,** 1613701.

ZHANG, J. M. & AN, J. 2007. Cytokines, inflammation, and pain. *Int Anesthesiol Clin,* 45**,** 27-37.

ZHANG, S., CONDAC, E., QIU, H., JIANG, J., GUTIERREZ-SANCHEZ, G., BERGMANN, C., HANDEL, T. & WANG, L. 2012. Heparin-induced leukocytosis requires 6-O-sulfation and is caused by blockade of selectin- and CXCL12 protein-mediated leukocyte trafficking in mice. *J Biol Chem,* 287**,** 5542-53.

ZHAO, W., PHINNEY, D. G., BONNET, D., DOMINICI, M. & KRAMPERA, M. 2014. Mesenchymal stem cell biodistribution, migration, and homing in vivo. *Stem Cells Int,* 2014**,** 292109.

ZHOU, Y., CHEN, H., LI, H. & WU, Y. 2017. 3D culture increases pluripotent gene expression in mesenchymal stem cells through relaxation of cytoskeleton tension. *J Cell Mol Med,* 21**,** 1073-1084.

ZHU, J., HUANG, J., DAI, D., WANG, X., GAO, J., HAN, W. & ZHANG, R. 2019. Recombinant human interleukin-1 receptor antagonist treatment protects rats from myocardial ischemia-reperfusion injury. *Biomed Pharmacother,* 111**,** 1-5.

ZIEGLER, M., WANG, X. & PETER, K. 2019. Platelets in cardiac ischaemia/reperfusion injury: a promising therapeutic target. *Cardiovasc Res,* 115**,** 1178-1188.

ZIMMERMANN, J. A. & MCDEVITT, T. C. 2014. Pre-conditioning mesenchymal stromal cell spheroids for immunomodulatory paracrine factor secretion. *Cytotherapy,* 16**,** 331-45.